CLOSED-LOOP ACTUATOR AND SENSOR LOCATION SELECTION STRATEGIES FOR FLEXIBLE STRUCTURES

by

Murat Güney

B.S., in M.E., Istanbul Technical University, 2000

M.S., in M.E., Boğaziçi University, 2002

Submitted to the Institute for Graduate Studies in
Science and Engineering in partial fulfillment of
the requirements for the degree of
Doctor of Philosophy

Graduate Program in Mechanical Engineering

Boğaziçi University

2008

CLOSED-LOOP ACTUATOR AND SENSOR LOCATION SELECTION STRATEGIES FOR FLEXIBLE STRUCTURES

APPROVED BY:

Prof. Eşref Eşkinat (Thesis Supervisor)	.....
Prof. Günay Anlaş	.....
Assoc. Prof. İ. Emre Köse	.....
Assist. Prof. Hilmi Luş	.....
Dr. Âli Yurdun Orbak	.....

DATE OF APPROVAL: 12.June.2008

ACKNOWLEDGEMENTS

I would like to express my sincere gratitude to Professor Eşref Eşkinat for his invaluable guidance and help during the preparation of this dissertation. I would like to thank the members of my thesis committee; Assoc. Prof. Emre Köse for his valuable comments about mathematical notations, and Assist. Prof. Âli Yurdun Orbak for his suggestions, corrections and coming all the way from Bursa to İstanbul every time when necessary. I will also like to thank Prof. Günay Anlaş and Assist. Prof. Hilmi Luş for participating in the jury.

I thank all of my colleagues, the research assistants and the staff at the mechanical engineering department. I am indebted to Utku Ünlü, for during his assistantship he had worked a lot to maintain the computers in the department, which alleviated my responsibilities and left me more time to worry about my thesis.

Finally, I am deeply grateful to my family for their unending support.

ABSTRACT

CLOSED-LOOP ACTUATOR AND SENSOR LOCATION SELECTION STRATEGIES FOR FLEXIBLE STRUCTURES

Vibration suppression in flexible structures such as beams and plates, space shuttles, large antennas is a common engineering problem studied by many researchers. Exposed to periodic external disturbances, a flexible structure vibrates. These vibrations need to be eliminated or reduced to a certain level through control forces applied by the actuators. The control forces are determined by a controller using the feedback of the vibrations measured via the sensors. Most often the number of actuators and sensors is limited. Hence, one has to find the best actuator and sensor locations to achieve the maximum vibration suppression.

In this thesis, the problem of finding the optimal actuator and sensor locations for vibration control of a flexible structure is studied. An iterative search strategy is used, where the closed-loop criteria are selected as the optimization metric. During each iteration a controller (an approximate $\mathcal{H}_\infty$-coprime controller or a low-authority $\mathcal{H}_\infty$-controller) is designed or alternatively a quasi-controller method (the residual deformations norm minimization) is used, which does not directly calculate a controller but obtains some norms that instead approximate the closed-loop behavior well.

In the case of applications with controllers, the controller design is simplified by introducing simple approximate Algebraic Riccati Equation (ARE) solutions and their derivatives, which are obtained by converting the state space descriptions of the physical system with signal weights into state space representations with decoupled block diagonal state matrices. Hence, based on such approximate solutions, it is possible to design computationally less complex coprime controllers and low-authority

$\mathcal{H}_\infty$-controllers with less computational effort.

Since for a gradient based search technique, the partial derivatives of the closed-loop criteria are required, Finite Element sensitivity analysis is utilized. First, the partial derivatives of the mass, stiffness and electromechanical coupling matrices are defined. Then, the partial derivatives of the open-loop and controller matrices are introduced.

For plates with piezoelectric actuator and sensor pairs, the minimization procedure is enriched with constrained techniques, where Finite Element discretization is done automatically at each iteration regarding the constraints. The modified constrained optimization technique is based on Zoutendijk's method of feasible directions and introduces constraints to avoid a mesh generation of badly scaled finite elements.

ÖZET

ESNEK YAPILARDA UYGULAYICI VE ALGILAYICILARIN EN İYİ YERLEŞİMİ İÇİN KAPALI ÇEVRİM STRATEJİLERİ

Kirişler, plaklar, uzay mekikleri, büyük boyutlu antenler gibi esnek yapıların titreşimlerinin sönümlenmesi pek çok araştırmacının üzerinde yoğunlaştığı bir konudur. Peryodik zorlamalara maruz kalan bu tür esnek yapılar titreşirler ve bu titreşimler uygulayıcılar tarafından tatbik edilen kontrol kuvvetleri ile ya tamamen ya da kısmen sönümlenmek istenir. Sensörler tarafından ölçülen titreşimler denetimciye geri beslenir. Denetimci de kontrol girdilerini tayin eder. Çoğunlukla uygulayıcı ve sensörlerin sayısı sınırlıdır ve mevcut uygulayıcı ile sensörlerin yerleri değiştikçe sönümlenen titreşim düzeyi de farklılılık gösterir. Bu yüzden maksimum titreşim sönümlenmesi için uygulayıcı ve sensörlerin olabilecek en iyi yerleşimi bulunmalıdır.

Bu tezde, esnek yapıların titreşim kontrolü için uygulayıcı ve sensörlerin en ideal yerleşimi problemi incelenmektedir. Optimizasyon kriteri olarak kapalı çevrim kriterlerin uygulandığı iteratif bir arama stratejisi geliştirilmiştir. İterasyonlar sırasında ya bir $\mathcal{H}_\infty$ coprime denetimci ya da düşük otorite $\mathcal{H}_\infty$ denetimci veyahut kapalı çevrime alternatif olarak kontrolcü eşdeğeri bir yapı (artık gerilmelerin normlarının minimizasyonu metodunda) kullanılır. Bu eşdeğer kontrolcü tam olarak bir denetimci tasarımını ve hesaplanmasını gerektirmemesine rağmen kapalı çevrim sistemin normlarına yakın sayılabilecek bir bilgi verebilmektedir.

Kapalı çevrim optimizasyon uygulamalarında denetimci dizaynından önce fiziksel sistemin sinyal filtrelerini içeren durum uzayı modelleri, kipsel (modal) durum uzayı formlarına sokulur. Bu formlara dönüşüm için uygun kordinat transformasyon vektörleri bulunmuştur. Böylece yaklaşık ama daha basit Cebirsel Riccati Denklemi

(ARE) çözümleri ve de çözümlere ait türevleri geliştirmek mümkün olmuştur. Basit yaklaşık çözümler kullanılması ile ise daha az kompleks coprime ve düşük otoriteli $\mathcal{H}_\infty$ denetimcilerinin hem de daha az bilgisayar performansına ihtiyaç duyarak tasarlanması sağlanmıştır.

Düşüm (gradyen) bilgisine dayalı en iyiyi arama tekniklerinde kapalı çevrim kriterlerin kısmi türevleri gerekmektedir. Bu türevler Sonlu Elemanlar Yönteminde Hassasiyet (Sensitivite) Analizi kullanılarak hesaplanmıştır. Önce kütle, rijitlik ve elektomekanik bağlaşım matrislerinin kısmi türevleri tanımlanır. Sonra da açık çevrim sistem ve kontolcü matrislerine ait türevler bulunur.

Piezoelektrik uygulayıcı ve sensörlerlere sahip plaklar için de her iterasyonda otomatik olarak tatbik edilen Sonlu Elemanlar Tekniği ile uyumlu, "sınırlı" optimizasyon metodu geliştirilmiştir. Söz konusu sınırlı optimizasyon yöntemi Zoutendijk'in olası yönler metoduna dayanmaktadır ve kötü ölçekli sonlu elemanlardan oluşan ağları (mesh) engelleyen kısıtlamaları her iterasyon için ayrı ayrı hesaplayabilmektedir.

TABLE OF CONTENTS

LIST OF FIGURES

LIST OF TABLES

LIST OF SYMBOLS/ABBREVIATIONS

A	Cross-sectional area
$\mathbf{A}$	Global state matrix
$\mathcal{A}$	Electromechanical derivative operator
a	Length of a finite element in x-direction
$\hat{\mathbf{A}}$	Global state matrix of the nodal form
$\mathbf{A_c}$	Closed-loop state matrix
$\mathbf{A_{cl}}$	General closed-loop state matrix
$\mathbf{A_g}$	Non-diagonalized global state matrix
$\mathbf{A_K}$	State matrix of the controller
$\tilde{\mathbf{A}}_\mathbf{K}$	State matrix of the controller for the scaled plant
$\mathbf{A_{K_a}}$	State matrix of the controller $\mathbf{K_a}$
$\mathbf{A_l}$	State matrix of leaved states
$\mathbf{A_m}$	Modal state matrix
$\mathbf{A_{mi}}$	i^{th} mode's state matrix
a_{PZT}	Length of a piezoelectric finite element in x-direction
$\mathbf{A_r}$	State matrix of retained state
$\mathbf{B}$	Global input matrix
$\mathcal{B}$	Strain derivative operator
b	Length of a finite element in y-direction
$\hat{\mathbf{B}}$	Global input matrix of the nodal form
$\mathbf{B_c}$	Closed-loop input matrix
$\mathbf{B_{cl}}$	General closed-loop input matrix
$\mathbf{B_g}$	Non-diagonalized global input matrix
$\mathbf{B_K}$	Input matrix of the controller
$\tilde{\mathbf{B}}_\mathbf{K}$	Input matrix of the controller for the scaled plant
$\mathbf{B_{K_a}}$	Input matrix of the controller $\mathbf{K_a}$
$\mathbf{B_l}$	Input matrix of leaved states
$\mathbf{B_m}$	Modal input matrix
$\mathbf{B_{mi}}$	i^{th} mode's input matrix

b_{PZT}	Length of a piezoelectric finite element in y-direction
$\mathbf{B_r}$	Input matrix of retained state
$\mathbf{b_w}$	Modal transformation vector for $\mathbf{f_w}$
b_{wi}	i^{th} modal transformation vector of $\mathbf{b_w}$
$\mathbf{C}$	Global output matrix
c	Elastic stiffness constant
$\boldsymbol{c}$	Elastic stiffness constant (in matrix notation)
$\hat{\mathbf{C}}$	Global output matrix of the nodal form
$\mathbf{C_c}$	Closed-loop output matrix
$\mathbf{C_{cl}}$	General closed-loop output matrix
$\mathbf{C^d}$	Damping matrix
c^D	Elastic stiffness for constant D
$\mathbf{C_m^d}$	Diagonalized damping datrix
c^E	Elastic stiffness for constant E
c_{ijkl}^E	Elastic stiffness constant tensor
$\mathbf{C_g}$	Non-diagonalized global output matrix
$\mathbf{C_K}$	Output matrix of the controller
$\tilde{\mathbf{C}}_\mathbf{K}$	Output matrix of the controller for the scaled plant
$\mathbf{C_{K_a}}$	Output matrix of the controller $\mathbf{K_a}$
$\mathbf{C_l}$	Output matrix of leaved states
$\mathbf{C_m}$	Modal output matrix
$\mathbf{C_{mi}}$	i^{th} mode's output matrix
$\mathbf{C_r}$	Output matrix of retained state
$\mathbf{C_{yq}}$	Measured output displacement matrix
$\mathbf{C_{yq,m}}$	Modal measured output displacement matrix
$\mathbf{C_{yv}}$	Measured output velocity matrix
$\mathbf{C_{yv,m}}$	Modal measured output velocity matrix
$\mathbf{C_{zq}}$	Performance output displacement matrix
$\mathbf{C_{zq,m}}$	Modal performance output displacement matrix
$\mathbf{C_{zv}}$	Performance output velocity matrix
$\mathbf{C_{zv,m}}$	Modal performance output velocity matrix

c_{11}, c_{12}, c_{21}, c_{22}, c_{66}	Components of elastic stiffness constant tensor c^E_{ijkl}
$\mathbf{D}$	Global static gain matrix
$\mathfrak{D}$	Material constant matrix
d	The piezoelectric coupling constant for (T, E)-type relation
$\mathbf{d}$	Disturbance input vector
$\hat{\mathbf{D}}$	Global static gain matrix of the nodal form
$\mathbf{D_{cl}}$	General closed-loop static gain matrix
D_i	Electrical displacement tensor
$\widehat{\mathbf{D}}_\mathbf{i}$	Destination vector for summing the finite element matrices
D_1, D_2 D_3	Electrical displacement in the X, Y, Z-directions
E	Young modulus
e	The piezoelectric coupling constant for (S, E)-type relation
$\boldsymbol{e}$	The piezoelectric coupling coefficient (in matrix notation)
E_l, $\mathbf{E}$	Electrical Field
e_{lij}	The piezoelectric coupling coefficient
$\mathbf{e_m}$	Filtered deflections
E_1, E_2, E_3	Electrical Field in the X, Y and Z-directions
e_{31}, e_{32}	Components of the piezoelectric coupling coefficient tensor
$\boldsymbol{\nabla} f$	Gradient of f
$\mathcal{F}_l$	Lower Linear Fractional Transformation
$\mathbf{f_q}$	Electrical charge input vector
$\mathbf{f_{q_s}}$	Sensor electrical charge input vector
$\mathbf{f_u}$	Control input vector
$\mathbf{f_{u}}_{bc}$	Control input vector with boundary conditions
$\mathbf{f_w}$	Disturbance input vector
$\mathbf{f_{w}}_{bc}$	Disturbance input vector with boundary conditions
g	Piezoelectric coupling constant for (T, D)-type relation
g_i^b	i^{th} bound constraint
g_i^o	Third type of conditional constraints
g_i^p	Second type of conditional constraints
$g_{k_i}^d$	First type of conditional constraints

g_j	j^{th} constraint evaluated at the point
$\boldsymbol{\nabla} g_j$	Gradient of g_j
$\mathbf{G_{12}^{-L}}$	Left inverse of the state space representation $\mathbf{G_{12}}$
$\mathbf{G_{21}^{-R}}$	Right inverse of the state space representation $\mathbf{G_{21}}$
$\mathbf{G_{21}^{+}}$, $\mathbf{G_{12}^{+}}$	Pseudo inverse of the state space representation $\mathbf{G_{21}}$ and $\mathbf{G_{12}}$
h	The piezoelectric coupling constant for (S, D)-type relation
h_{PZT}	Thickness of a piezoelectric finite element in z-direction
$\mathcal{H}_2$	H-2
$\mathcal{H}_\infty$	H-infinity
I_z	Moment of inertia about z-axis
J	Objective function
$\mathbf{K}$	Stiffness matrix
$\mathbf{K}_{bc}$	Global stiffness matrix with boundary conditions
$\mathbf{K}_c$	General $\mathcal{H}_\infty$ controller
K_{d_i,d_j}	$(d_i, d_j)^{\text{th}}$ element of the global stiffness matrix
$\mathbf{K}_e$	Element stiffness matrix
$\mathbf{K_I}$	Internal model controller
$k_{i,j}$	$(i, j)^{\text{th}}$ element of the element stiffness matrix
$\mathbf{K_m}$	Diagonalized stiffness matrix
$\mathbf{K_p}$	General coprime controller
$\mathbf{K_{Q}}_c$	Central $\mathcal{H}_\infty$ controller
$\mathbf{K_{uu}}$	Finite element non piezoelectric stiffness matrix
$\mathbf{K_{u\phi}}$	Finite element electrical mechanical coupling stiffness matrix
$\mathbf{K_{u\phi_s}}$	Finite element electrical mechanical coupling stiffness matrix for sensor equation
$\mathbf{K_{u\phi}}_{bc}$	Finite element electrical mechanical coupling stiffness matrix for sensor equation with boundary conditions
$\mathbf{K_{\phi u}}$	Finite element mechanical electrical coupling stiffness matrix
$\mathbf{K_{\phi\phi}}$	Finite element dielectric stiffness matrix
$\mathbf{K}^*$	Stiffness matrix after condensing
$\mathbf{K}_{bc}^*$	Stiffness matrix after condensing with boundary conditions

$\mathbf{K}_\infty$	Coprime controller
$\mathbf{L}$	Modal reduction matrix
L	Length of the whole structure
$\mathbf{L_c}$, $\mathbf{L_o}$	Controllability and observability Gramians
l_{ci}, l_{oi}	i^{th} (physical) mode's of the Controllability and Observability Gramians
l^w_{ci}, l^w_{oi}	i^{th} (filter) mode's of the Controllability and Observability Gramians
l_i	Length of the i^{th} element
$\mathbf{L_p}$	Piezoelectric actuator input transformation matrix
$\mathbf{L}^p$	Partial derivatives vector
$\mathbf{L_u}$	Control input transformation matrix
$\mathbf{L_{u,m}}$	Modal control input transformation matrix
$\mathbf{L_w}$	Disturbance input transformation matrix
$\mathbf{L_{w,m}}$	Modal disturbance input transformation matrix
$\mathbf{M}$	Global mass matrix
$\mathbf{M}_{bc}$	Global mass matrix with boundary conditions
M_{d_i,d_j}	$(d_i, d_j)^{\text{th}}$ element of the global mass matrix
$\mathbf{M}_e$	Element mass matrix
$m_{i,j}$	$(i, j)^{\text{th}}$ element of the element mass matrix
$\mathbf{M_m}$	Diagonalized mass matrix
$\mathbf{M_{\boldsymbol{p}}}$	First part from left coprime factor of $\mathbf{P}$
$\mathbf{M_{uu}}$	Finite element non piezoelectric mass matrix
$\mathbf{M_{uu}}_{bc}$	Finite element non piezoelectric mass matrix with boundary conditions
$\mathbf{n}$	Measurement noise vector
$\mathbf{N_b}$	Finite Element shape function vector for beams
N_i	i^{th} component of the Finite Element Shape function for beams
$\mathbf{N_p}$	Finite Element shape function vector for plates
$\mathbf{N_{\boldsymbol{p}}}$	Second part from left coprime factor of $\mathbf{P}$
N_u	Number of actuators

N_w	Number of disturbance inputs
$\mathbf{P_{12}^{-L}}$	Left inverse of the state space representation $\mathbf{P_{12}}$
$\mathbf{P_{21}^{-R}}$	Right inverse of the state space representation $\mathbf{P_{21}}$
$\mathbf{Q}$	IMC parameter (not stabilizing)
$\mathbf{q}$	Nodal displacement vector
$\mathbf{\hat{Q}}$	IMC parameter (stabilizing)
$\mathbf{q_m}$	Modal displacement vector
q_{mi}	i^{th} Modal displacement vector
$\mathbf{R}$	Coordinate transformation from nodal to the third modal state space form
$\mathbf{\hat{R}}$	Coordinate transformation from the nodal to the the third modal state space form
Re	Real part of number
$\mathbf{R}_{31}$	Coordinate transformation from the first to the third modal state space form
$\mathbf{S}$	Approximate FARE solution
s^D	The elastic compliance coefficient for constant dielectric displacement
s^E	The elastic compliance coefficient for constant electric field
$\mathbf{s}^{(k)}$	Search direction of the k^{th} iteration
$\mathbf{S_u}$, $\mathbf{S_y}$	Transformation vectors for input $\mathbf{u}$ and output $\mathbf{y}$
S_1	Strain in the X-direction
$\mathbf{T}$	Approximate CARE solution
T_e	Kinetic Energy of the beam or plate element
$t^{(k)}$	k^{th} iteration step size
$t_{optimistic}$	Optimistic closed-loop $\mathcal{H}_\infty$ norm
$\mathbf{T_w}$, $\mathbf{T_z}$	Transformation vectors for input $\mathbf{w}$ and output $\mathbf{z}$
$\mathbf{T_{zw}}$	Transfer function from inputs $\mathbf{w}$ to disturbances $\mathbf{z}$
$\mathbf{T_{zw}^*}$	Conjugate transpose of the transfer function $\mathbf{T_{zw}}$
T_1	Stress in the X-direction
$\mathbf{t_1}$, $\mathbf{t_2}$	First and second part of $\mathbf{R}$

$\mathbf{u}$	Outputs vector
$\tilde{\mathbf{u}}$	Scaled outputs vector
U_e	Potential Energy of the beam or plate element
$\mathbf{u}_i$, $\mathbf{u}_r$	The i^{th} and r^{th} mode shape vector
$\mathbf{u_m}$	Filtered outputs vector
$\mathbf{u_{12}}$, $\mathbf{u_{21}}$	Left Eigenvector associated with zero singular values of the matrices $\mathbf{G_{12}}$ and $\mathbf{G_{21}}$
$\mathbf{U_{12}}$, $\mathbf{U_{21}}$	Left Eigenvector associated with zero non-singular values of the matrices $\mathbf{G_{12}}$ and $\mathbf{G_{12}}$
V	Voltage
v_1	Vertical displacement of the first node of the beam element
v_2	Vertical displacement of the second node of the beam element
$\mathbf{v_{12}}$, $\mathbf{v_{21}}$	Right Eigenvector associated with zero singular values of the matrices $\mathbf{G_{12}}$ and $\mathbf{G_{21}}$
$\mathbf{V_{12}}$, $\mathbf{V_{21}}$	Right Eigenvector associated with zero non-singular values of the matrices $\mathbf{G_{12}}$ and $\mathbf{G_{12}}$
w	Displacement in z-direction
$\mathbf{w}$	Disturbance input vector
$\tilde{\mathbf{w}}$	Scaled disturbance vector
$\mathbf{W_c(t)}$, $\mathbf{W_o(t)}$	Controllability and Observability Gramians
$\mathbf{W_{dist}}$	Disturbance weight
$\mathbf{w}_e$	Vector of element displacements
$\mathbf{W_{er}}$	Error output weight
w_i	Displacement of the i^{th} node in z-direction
$\mathbf{W_{in}}$	Control input voltage weight
$\mathbf{W_{sn}}$	Sensor noise weight
$\mathbf{X}$	Eigenvector of $\mathbf{A}$
$\mathbf{x}$	State vector for the state space realization of the generalized plant
$\boldsymbol{x}$	Coordinate vector of elements
$\hat{\mathbf{X}}$	Eigenvector of $\mathbf{A}$

$\hat{\mathbf{x}}$	State vector of the nodal state space form
x_A, x_B	x-coordinates of the left lower node of the element A and B
$\mathbf{x_c}$	Closed-loop state vector
$\mathbf{X_g}$	Eigenvector of $\mathbf{A_g}$
$\mathbf{x_g}$	State vector for the state space realization of the generalized plant in non-diagonalized coordinates
$\mathbf{x_{K_a}}$	Controller (K_a) state vector
$\mathbf{x}^{(k)}$	k^{th} iteration point
$\mathbf{\Delta x}^{(k)}$	Search direction of the k^{th} iteration
$\mathbf{x_r}$	State vector of retained states
$\mathbf{x_t}$	State vector of truncated
x_1, x_2	x-coordinates of the left lower node of the first and second piezoelectric finite element
$\mathbf{x_1}$, $\mathbf{x_3}$	State vector for the first and third modal state space form
$\mathbf{X}_\infty$	Exact solution of CARE
$\mathbf{Y}$	Exact solution of Lyapunov Equation
$\mathbf{y}$	Measured outputs vector
$\tilde{\mathbf{y}}$	Scaled measured outputs vector
$\mathbf{y_m}$	Noised measured outputs vector
y_1, y_2	y-coordinates of the left lower node of the first and second piezoelectric finite element
$\mathbf{Y}_\infty$	Exact solution of FARE
$\mathbf{Z}$	Coordinate Transformation between global and diagonalized state matrices
z	Thickness of a finite element in z-direction
$\mathbf{z}$	Performance outputs vector
$\tilde{\mathbf{z}}$	Scaled performance outputs vector
z^*	Optimistic lower limit of deformation
α	Coprime Contoller Design Parameter

$\hat{\alpha}$	Parameter for backtracking step size selection
$\bar{\alpha}$	Minimized variable in the line search procedure
β	Coprime Contoller Sub-design Parameter
$\hat{\beta}$	Parameter for decreasing step size
$\mathbf{\Gamma}$	Hankel Singular Value Gramian
γ	Disturbance attenuation factor
$\boldsymbol{\delta}$	Vector of generalized displacements
$\boldsymbol{\delta_s}$	Vector of sensed generalized displacements
$\boldsymbol{\epsilon}$	Permittivity (in matrix notation)
ϵ^T	The dielectric constant
ϵ_{11}, ϵ_{22}, ϵ_{33}	Permittivity componenents
$\boldsymbol{\varepsilon}$	Strain (in matrix notation)
ε_{ij}	Strain Tensor
ε_1, ε_2, ε_6	Strain componenents
ζ_i	i^{th} Damping Coefficient
η	Second coordinate of the plate element
θ_x	Rotation of a plate element about x-axis
$\theta_{x\,i}$	Rotation of the i^{th} node of the plate element about x-axis
θ_y	Rotation of a plate element about y-axis
$\theta_{y\,i}$	Rotation of the i^{th} node of the plate element about y-axis
$\theta_{z\,i}$	Rotation at the i^{th} node of the beam element about z-axis
$\mathbf{\Lambda}$	Eigenvalue matrix
$\bar{\lambda}$	Maximum eigenvalue
λ_i	i^{th} eigenvalue
ν	Poisson's Ration
ξ	First local coordinate of the beam or plate element
ρ	Density
$\boldsymbol{\sigma}$	Stress (in matrix notation)
$\bar{\sigma}$	Maximum singular value
σ_{ij}	Stress tensor
σ_1, σ_2, σ_6	Stress component

$\mathbf{\Sigma_{12}}$, $\mathbf{\Sigma_{21}}$	Non-zero singular values of $\mathbf{G_{12}}$ and $\mathbf{G_{21}}$
$\mathbf{\Upsilon}$	Matrix of damping coefficients
Φ	Vertical displacements of a beam or plate
$\mathbf{\Phi}$	Matrix of mode shapes
$\boldsymbol{\phi}_i$	i^{th} mode shape
$\boldsymbol{\phi}$	Vector of electrical potentials
$\boldsymbol{\phi_a}$	Vector of actuating electrical potentials
$\boldsymbol{\phi_s}$	Vector of sensed electrical potentials
$\mathbf{\Omega}$	Matrix of natural frequencies
ω	Natural frequency
ω_i	i^{th} Natural frequency

ARE	Algebraic Riccati Equation
CARE	Control Algebraic Riccati Equation
DOF	Degree of Freedom
dom (.)	Domain of (.)
FARE	Fare Algebraic Riccati Equation
FE	Finite Element
FEM	Finite Element Method
IMC	Internal Model Control
I/O	Input/Output
LQG	Linear Quadratic Gaussian
max, min	Maximum, minimum
MFD	Method of Feasible Directions
MNRD	Norm Minimization of Residual Deformations
PZT	Piezoelectric
RGA	Relative Gain Array
r.m.s	root mean square
sup	Supremum
SVD	Singular Value Decomposition

1. INTRODUCTION

Beams and plates vibrate under periodic loading and the levels of motions are strongly amplified at resonance frequencies. The vibrations can be suppressed by passive methods, where the system is redesigned and sometimes passive absorbers are added. Another possibility is to apply control forces through an actuator which is determined by a controller. The information about how much the structure displaces is fed back to the controller by a sensor. The latter approach, called active control or closed-loop control, raises another question about the locations for the actuators and sensors. Since the vibration suppression levels vary at different locations of actuators and sensors, finding the best locations invokes interest of many researchers of different disciplines. This thesis deals mainly with closed-loop optimal actuator and sensor placement for flexible structures. Specifically, examples are given on beams and plates.

Beams and plates belong to a special type of structures called *flexible structures*. Exposed to external uncontrolled forces flexible structures deform in such a way that the structure can become afunctional or hazardous for other neighboring parts. Sensing the deformations and applying the control forces it is possible to eliminate these deformations to a certain limit. However, since limited number of actuators is available in most applications, it is rarely possible to eliminate the deformations produced by the external disturbances. Hence, the resulting deformations are called residual deformations [2].

The amount of the residual deformations depends on type, number and locations of actuators/sensors. If the type and the number of actuators and sensors are given, the main purpose is to find the optimal actuator and sensor locations, where the residual deformations are at minimum. Generally, the determination of the number, the type and the location of actuators and sensors is a stage of the control system design. This step is called input and output selection.

If a system is exposed to external disturbances **w** and there are certain restrictions on the performance outputs **z**, input/output selection problem becomes selecting suitable plant inputs **u** and suitable measured output **y** (see Figure 1.1). Every combination of **u** and **y** is an input/output set. For different types of plants ranging from

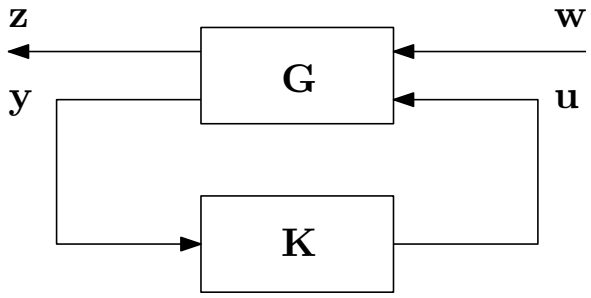

Figure 1.1. General control configuration

the chemical distillation columns to the acoustic noise cancelation systems in airplanes, this problem has a wide application field in both industry and academia. Hence, the problem of finding the best suitable combinations of inputs and outputs is given different names such as best allocation problem, optimal location selections or simple input/output selection.

Since people of different specialization areas have different attitudes towards the optimal location selection problem, the problem can be categorized in many different ways. One may group according to the optimization methods, whereas another one may prefer to group according to the selection criteria.

However, since the scientists who deal with the vibration suppression problem have a control engineering background, they simply divide the method according to whether the selection criterion includes a controller synthesis or not. The approaches in which a controller is designed are called methods with closed-loop criteria. On the other hand, if the method does not require a controller design or does not give any information about the closed-loop behavior of the system, it is said to be an open-loop one.

Best location selection strategies without any controller design may achieve the results much faster. However, if the system of concern is to be combined with a

controller, its results can deviate too much from the real case. Conversely, methods with controllers do not reflect the phenomenon of lack of information about the closed-loop behavior, though they might take longer computation times. Hence, different input/output selection approaches have different advantages. Generally, a placement method may not have all the desired properties. A designer has to decide which optimization criteria best fit the needs and has to select the most useful criteria for his or her purposes.

Selecting a suitable optimization metric depends heavily on the physical system. The more information about the system is known, the more appropriate optimal actuator and sensor location selection approach can be chosen. Hence, an investigation about the physical system may bring certain advantages in optimization part. If the system possesses some certain characteristics, they might involved in any stage of the minimization procedure to simplify calculations, to decrease computation cost, to reduce the complexity of the controller, to increase the accuracy in results, etc. Some properties of flexible structures (e.g. diagonally dominant Gramians) can make a simple controller design and modal reduction possible.

The modelling of the physical structure is another issue one cannot neglect in an optimization procedure since the model might impose limitations on the optimization method. For some modelling methods, the optimization techniques can be easily implemented, whereas for some other modelling types the desired optimization technique might be totally useless. For instance, if it requires too much effort to take the analytical gradient of the objective function or the numerical gradient that is obtained by finite differentiating is not accurate enough, one should probably prefer a heuristic method without gradient such as simulated annealing or genetic algorithms.

1.1. Problem Statement

The problem of I/O selection can be applied to many structures. However, the main goal in this thesis is to locate the optimal locations of collocated actuators and sensor pairs for a given structure combined with a set of piezoelectric patches.

For finding the best location, closed-loop criteria are preferred since in most applications there is need for a controller. However, not all types of controllers are searched. For the given structure and disturbances, which act at fixed points, a certain class of controllers (e.g. $\mathcal{H}_\infty$-controllers) is chosen before initiating the optimization procedure.

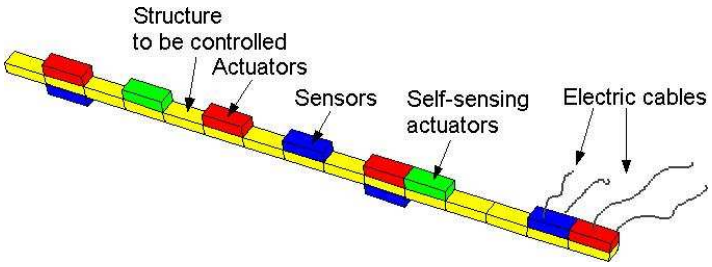

Figure 1.2. Beam with piezoelectric actuator and sensors

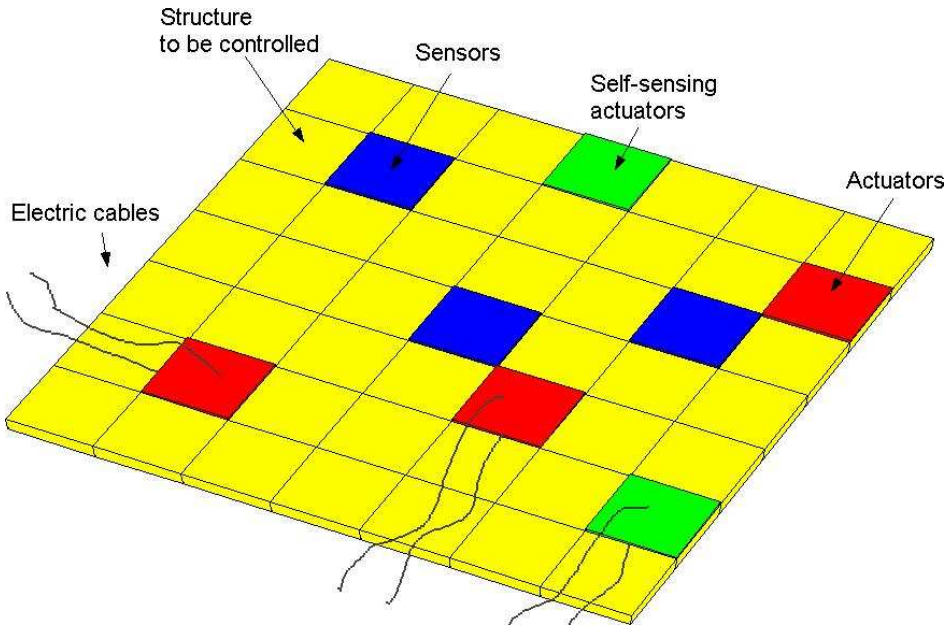

Figure 1.3. Plate with piezoelectric actuator and sensors

1.2. Approaches

In this thesis, two types of optimization algorithms are used for the minimization of an objective function:

- Unconstrained gradient based minimization (in cases with only limitations on the bounds of design variables).
- Method of feasible directions, shortly MFD, (in cases of more complicated constraints such as multiple piezoelectric (PZT) actuators which may not overlap each other).

Both techniques use the backtracking line search for step size selection. In MFD, the backtracking is modified such that constraints are also checked.

Both open- and closed-loop objective functions are selected as the optimization criteria as follows:

- Some sort of $\mathcal{H}_\infty$-norm in the method of minimization of the norm of the residual deformations (MNRD). This norm is calculated without designing a controller, hence, can be regarded as the open-loop criterion. In fact, it gives enough information about the closed-loop behavior of the generalized plant without calculating a stable controller.
- Closed-loop $\mathcal{H}_2$-norm with the design of a coprime controller.
- Closed-loop $\mathcal{H}_2$-norm with the design of a low-authority $\mathcal{H}_\infty$-controller.

For modelling of the flexible structures, the following steps are taken:

- Finite Element Method (FEM) is used to discretize the structures with actuator and sensor pairs.
- Sensitivity analysis is utilized for taking the partial derivatives of the FEM mass, stiffness, and electromechanical coupling (in cases of PZT patches) matrices, the partial derivatives of resonance frequencies and mode shapes.
- The generalized plant is obtained. If required, it is converted into the first modal state space representation with the introduced coordinate transformation.

Controller design strategies can be the following ones:

- The normalized coprime controller for the right lower part of the generalized plant.
- The low-authority $\mathcal{H}_\infty$-controller.

1.3. Research Objectives and Contributions

The main goal of this thesis is to design a gradient based optimal location selection method for flexible structures, which improves upon the currently available closed-loop criteria based techniques. The work is motivated by the following facts:

- In a gradient based technique, mostly open-loop criteria are selected to avoid taking the gradient of the controller matrices.
- Most of the current closed-loop criteria based techniques use simple continuous models of the structures, which render their methods applicable to structures of resulting from a finite element discretization, since for discrete models it is more complicated to find analytical gradients of the objective function.
- The state space form of flexible structures can be converted into modal models where the modes are decoupled. For such cases, the controller matrices can be obtained much simpler with introducing diagonally dominant ARE solutions.

To begin with, one of the contributions of this thesis is the modal models with use of frequency weights in the controller design stage. Although the physical systems show certain characteristics of flexible structures, their model becomes not decoupled if their physical plant is augmented with the signal weightings. In the current work, a useful but simple idea is introduced to convert the augmented generalized plant into a state space representation with a block diagonal state matrix. Theorem 2.6.1 states that the state space representation of the generalized plant of a flexible structure can be converted to a modal state space realization.

Gawronski [3] augments the plants only with smooth filters, the slope of the transfer function of which is small when compared with the slope of the transfer function of the structure at resonance frequencies. In fact, the plant is not augmented, but

scaled to have the same system norms with that of the generalized plant. However, a different technique is applied without any restriction on the filters. Unlike the other modal representation techniques given in [3], the approach in this thesis does not give any limitation for the signal weights.

The new modal form of the generalized plant leads to further simplifications in the controller design stage. With block diagonal modal form of the augmented plant, a coprime controller design strategy is introduced in the thesis. Theorem 4.2.4 provides ARE solutions for this new coprime controller design. This controller design method is inspired by the work of Hiramoto et al. [1]. They design their coprime controller in the same fashion as done in the current thesis. However, they have obtained a controller for the un-augmented plant and assumed zero-damping, whereas the controller that is implemented in this study considers the damping, and is augmented with weightings.

Additionally, not only coprime controllers but also low-authority $\mathcal{H}_\infty$-controllers are designed with the ARE solutions (Lemma 4.3.1 and Theorem 4.3.2). The results with this $\mathcal{H}_\infty$-controller are again promising. It should be emphasized that this controller is also for the generalized plant. According to the introduced Theorem 2.6.1, the state space representation of the generalized plant of a flexible is converted to one of the modal forms so that the individual physical and signal modes can be dealt separately. Lemma 4.2.1 and Lemma 4.2.2 give the physical and filter entries of the controllability and observability Gramians, which are diagonal for flexible structures. Corollary 4.2.3 restates that the Gramians can be split into physical and filter parts.

The $\mathcal{H}_2$-norm is smooth and has some nice definitions in terms of frequency-independent functions such that their partial derivatives are not rare in literature. However, the closed-loop $\mathcal{H}_2$-norm is not much preferred since it may be difficult and cumbersome to take the partial derivatives of controller matrices. In this thesis, partial derivatives of controller matrices are introduced. For this purpose, the partial derivatives of element matrices are defined, which result from Finite Element discretezation. Then, Lemmas 5.7.1 and 5.8.1 are introduced, which state how to compute the partial derivatives ARE solutions.

For beams and plates with point and piezoelectric actuator/sensor pairs a gradient based optimization technique is developed, which uses the closed-loop $\mathcal{H}_2$-norm as the objective function. Conditional constraints are introduced through Definitions 3.4.2, 3.4.3 and 3.4.4 so that overlapping of piezoelectric patches and badly scaled finite elements are prevented.

1.4. Thesis Overview

Chapter 2 starts with a literature survey and preliminaries on different topics such as flexible structures, piezoelectric material, finite element modelling. In Section 2.1, the flexible structures are explained in detail. In Section 2.2, the basic constitutive theory of the piezoelectricity and piezoelectric equations are given since flexible structures with piezoelectric actuator and sensor pairs are dealt with throughout the thesis. Section 2.3 introduces the Finite Element Method. In the remaining part of Chapter 2, the principles that are used to convert the generalized plant into the first modal state space form are introduced. Section 2.4 covers the first modal state space representation of the physical structure. In Section 2.5, the signal weightings are explained. In Section 2.6, the generalized plant with weightings is put into the modal state space form.

Chapter 3 provides a detailed literature review on different input/output selection criteria. Different methods for various types of plants such as chemical, mechanical, etc. are grouped in Section 3.1. Section 3.2 introduces some preliminaries for a gradient-based optimization. Sections 3.3 and 3.5 briefly explains the steps for the unconstrained and constrained minimization. Section 3.4 describes constraints which are necessary for optimization with piezoelectric actuator and sensor pairs.

In Chapter 4, the developed controller design strategies are introduced. In Section 4.1 different controller design strategies such as Hiramoto's coprime controllers, $\mathcal{H}_\infty$-controllers, MNRD-controllers are mentioned. In Subsection 4.1.5 the calculation of the MNRD-value is explained. Section 4.2 deals with the improved coprime controller design. In Section 4.3, the new low-authority controller is given.

Chapter 5 gives how the partial derivatives of finite element matrices, ARE solutions, open-loop generalized plant and control matrices are obtained. Sections 5.1 and 5.3 explain the partial derivatives of the mass, stiffness and piezoelectric coupling matrices. Sections 5.2 and 5.4 introduce remeshing strategies for structures combined with point and piezoelectric actuator and sensor pairs, respectively. Section 5.5 gives the mode shape and eigenvector derivatives. In Section 5.6, the partial derivatives of open-loop generalized plants are mentioned. Sections 5.7 and 5.8 provide the partial derivatives of the ARE solutions for the coprime and low-authority controllers, respectively. Section 5.11 describes how to obtain the derivative of the MNRD-value. Section 5.9 gives the partial derivative of the disturbance attenuation factor γ_{min} for the modified coprime controllers. In Sections 5.6 and 5.10, the partial derivatives of state space description of the generalized plant and of the closed-loop matrices are defined, which result from Finite Element discretezation.

In Chapter 6, design examples are presented to illustrate the proposed optimal locations selection techniques. Section 6.1 gives a comprehensive example of a beam with collocated point actuator and sensor pairs. Sections 6.2 through 6.5 deal with different examples of beams and plates with both point and piezoelectric actuator and sensor pairs.

2. MODELLING OF FLEXIBLE STRUCTURES

2.1. Flexible Structures

A linear system, which is excited by periodic forces and has low resonance frequencies as its significant vibration modes, is called a flexible structure. This is the definition mostly used in mechanical and civil engineering [3].

Whereas in control engineering, linear systems, which are exposed to harmonic signal at certain frequencies, amplify the input signals strongly and have nearly uncorrelated modes are referred to as flexible structures.

According to Gawronski [3], a flexible structure is defined to posses the following specific properties:

- It has to be a linear system.
- It has to be finite-dimensional.
- It has to be controllable and observable.
- Its poles have to be complex with small real parts.
- Its poles have to be non-clustered.

Considering the structures based on this set of descriptions, Gawronski [3] derived many useful modal properties of flexible structures such as modal controllability and observability Gramians, modal norms, low-authority modal LQG, $\mathcal{H}_2$ and $\mathcal{H}_\infty$-controllers, etc.

Aerospace structures, active earthquake-damping devices of sky scrapers, active vibrations suppression devices, most machinery with beam-plate-like parts can be examples of flexible structures.

Even though some of the restrictions for flexible structures are violated, the modal

approach developed by Gawronski [3] can be applied to many linear systems.

The linear second order differential equations are preferred by structural engineers, whereas the first order state space models are used in control engineering. In state space representation, the states describe the dynamics, which is represented by the system degrees of freedom, and the velocities.

For both equations of motion and state space representation the most common coordinates are the nodal and the modal coordinates. Nodal coordinates are described by displacements and velocities of selected points on the structures. These locations are referred to as nodes. Modal coordinates are given in terms of displacements and velocities of natural modes.

2.1.1. Nodal Models for Second-Order Structural Models

In engineering, one starts an analysis of a physical system most often by modeling them in physical coordinates. These models are described as *nodal models* since they are derived in nodal coordinates, in terms of nodal quantities such as displacements and velocities. A structure in nodal model is given as

$$\mathbf{M}\ddot{\mathbf{q}} + \mathbf{C^d}\dot{\mathbf{q}} + \mathbf{K}\mathbf{q} = \mathbf{f_w}. \tag{2.1}$$

Equation (2.1) is a second order matrix differential equation, which is obtained from a discretizetion method such as Finite Element Method. In (2.1), $\mathbf{M}$, $\mathbf{C^d}$, $\mathbf{K}$, $\mathbf{q}$ and $\mathbf{f_w}$ denote the mass matrix, the damping matrix, the stiffness matrix, the vector of displacements at the nodes and the applied force vector, respectively.

2.1.2. Modal Models for Second-Order Structural Models

If a second order nodal model is at hand, a corresponding modal model can be obtained by a coordinate transformation. The system given by Equation (2.1) is exposed to a harmonic force and its resulting solution is hence harmonic also: $\mathbf{q} =$

$\boldsymbol{\phi} e^{j\omega t}$. Applying this harmonic solution to Equation (2.1) without damping ($\mathbf{C} = \mathbf{0}$) and in free vibration case (no force, $\mathbf{f_w} = \mathbf{0}$), will give the frequency equation

$$\det\left(\mathbf{K} - \omega^2\mathbf{M}\right) = 0. \tag{2.2}$$

Equation (2.2) is satisfied for the set $\omega_1, \omega_2, \ldots, \omega_i, \ldots, \omega_N$, where ω_i is referred to as the *natural frequency of the i^{th} mode*. Since Equation (2.2) dates back to a eigenvalue problem, there exists a corresponding set of eigenfunctions such as $\boldsymbol{\phi}_1, \boldsymbol{\phi}_2, \ldots, \boldsymbol{\phi}_i, \ldots, \boldsymbol{\phi}_N$, where $\boldsymbol{\phi}_i$ is called the i^{th} mode shape. Using the natural frequencies and the mode shapes, the following matrices are defined:

$$\boldsymbol{\Omega} := \begin{bmatrix} \omega_1 & 0 & \ldots & \ldots & 0 \\ 0 & \omega_2 & 0 & \ldots & 0 \\ 0 & 0 & \omega_3 & \ldots & 0 \\ \vdots & & & & \vdots \\ 0 & \ldots & 0 & \omega_{N-1} & 0 \\ 0 & \ldots & \ldots & 0 & \omega_N \end{bmatrix}, \tag{2.3}$$

$$\boldsymbol{\Phi} := [\boldsymbol{\phi_1}\, \boldsymbol{\phi_2}\, \ldots\, \boldsymbol{\phi_N}]\,. \tag{2.4}$$

The matrices in Equations (2.3) and (2.4) are called matrix of natural frequencies and modal matrix, respectively. The modal matrix $\boldsymbol{\Phi}$ diagonalizes the mass matrix $\mathbf{M}$ and the stiffness matrix $\mathbf{K}$ as

$$\begin{aligned} \mathbf{M_m} &= \boldsymbol{\Phi}^{\mathrm{T}}\mathbf{M}\boldsymbol{\Phi}, \\ \mathbf{K_m} &= \boldsymbol{\Phi}^{\mathrm{T}}\mathbf{K}\boldsymbol{\Phi}. \end{aligned}$$

Furthermore, if proportional damping is assumed, the damping matrix can also be diagonalized as

$$\mathbf{C_m^d} = \boldsymbol{\Phi}^{\mathrm{T}}\mathbf{C^d}\boldsymbol{\Phi}.$$

Defining the modal coordinate $\mathbf{q_m}$ as

$$\mathbf{q} := \mathbf{\Phi q_m}, \tag{2.5}$$

one needs to left-multiply Equation (2.1) by $\mathbf{\Phi}^{\mathrm{T}}$ to obtain

$$\mathbf{\Phi}^{\mathrm{T}}\mathbf{M\Phi\ddot{q}_m} + \mathbf{\Phi}^{\mathrm{T}}\mathbf{C^d\Phi\dot{q}_m} + \mathbf{\Phi}^{\mathrm{T}}\mathbf{K\Phi q_m} = \mathbf{\Phi}^{\mathrm{T}}\mathbf{f_w},$$

which is multiplied by the inverse of the modal mass matrix $\mathbf{M_m}$ so that the modal model is achieved in the form

$$\mathbf{\ddot{q}_m} + 2\mathbf{\Upsilon\Omega}\,\mathbf{\dot{q}_m} + \mathbf{\Omega}^2\,\mathbf{q_m} = \mathbf{b_w f_w}, \tag{2.6}$$

where

$$\begin{aligned}
\mathbf{\Omega}^2 &:= \mathbf{M_m}^{-1}\mathbf{K_m}, \\
\mathbf{\Upsilon} &:= 1/2\mathbf{M_m}^{-1/2}\mathbf{K_m}^{-1/2}\mathbf{C_m}, \\
\mathbf{b_w} &:= \mathbf{M_m}^{-1}\mathbf{\Phi}.
\end{aligned}$$

Equation (2.6) gives the N modes in matrix form. Each mode can be represented independently since they are uncoupled as

$$\ddot{q}_{mi} + 2\zeta_i\omega_i\,\dot{q}_{mi} + \omega_i^2\,q_{mi} = b_{wi}f_{wi}, \quad \forall\, i = 1:N.$$

2.1.3. State Space Modal Models

The modal state space representation of a flexible structure is given by the triple $(\mathbf{A_m}, \mathbf{B_m}, \mathbf{C_m})$ and the state vector $\mathbf{x}$, which are

$$\mathbf{A_m} = \mathrm{diag}\left(\mathbf{A_{mi}}\right),$$

$$\mathbf{B_m} = \begin{bmatrix} \mathbf{B_{m1}^T} & \mathbf{B_{m1}^T} & \dots & \mathbf{B_{mn}^T} \end{bmatrix}^{\mathrm{T}},$$
$$\mathbf{C_m} = \begin{bmatrix} \mathbf{C_{m1}} & \mathbf{C_{m2}} & \dots & \mathbf{C_{mn}} \end{bmatrix},$$
$$\mathbf{x} = \begin{bmatrix} \mathbf{x_1} & \mathbf{x_2} & \dots & \mathbf{x_n} \end{bmatrix}^{\mathrm{T}}.$$

Each block $\mathbf{A_{mi}}$, $\mathbf{B_{mi}}$ and $\mathbf{C_{mi}}$ has the dimensions 2×2, $2\times N_u$ and $N_s\times 2$, respectively. The number of actuators in the system is given by N_u, and N_s denotes the number of sensors. The state vector is given by $\mathbf{x}$. The $\mathbf{A_{mi}}$ blocks and the corresponding state vectors can be given in four different forms as in [3]

$$\mathbf{A_{mi}} = \begin{bmatrix} 0 & \omega_i \\ -\omega_i & -2\zeta_i\omega_i \end{bmatrix}, \tag{2.7}$$
$$\mathbf{A_{mi}} = \begin{bmatrix} -\zeta_i\omega_i & \omega_i \\ -\omega_i & -\zeta_i\omega_i \end{bmatrix}, \tag{2.8}$$
$$\mathbf{A_{mi}} = \begin{bmatrix} 0 & 1 \\ -\omega_i^2 & -2\zeta_i\omega_i \end{bmatrix}, \tag{2.9}$$
$$\mathbf{A_{mi}} = \begin{bmatrix} -\zeta_i\omega_i + j\omega_i\sqrt{1-\zeta_i^2} & 0 \\ 0 & -\zeta_i\omega_i - j\omega_i\sqrt{1-\zeta_i^2} \end{bmatrix}, \tag{2.10}$$

$$\mathbf{x_i} = \begin{bmatrix} q_{mi} \\ \dot{q}_{mi}/\omega_i \end{bmatrix}, \tag{2.11}$$
$$\mathbf{x_i} = \begin{bmatrix} q_{mi} \\ q_{moi} \end{bmatrix}, \tag{2.12}$$
$$\mathbf{x_i} = \begin{bmatrix} q_{mi} \\ \dot{q}_{mi} \end{bmatrix}, \tag{2.13}$$
$$\mathbf{x_i} = \begin{bmatrix} q_{mi} - jq_{moi} \\ q_{mi} + jq_{moi} \end{bmatrix}, \quad \text{where } q_{moi} = \zeta_i q_{mi} + \dot{q}_{mi}/\omega_i. \tag{2.14}$$

Since the triple $(\mathbf{A_m}, \mathbf{B_m}, \mathbf{C_m})$ is decoupled, each mode's state space representation

can be given by the corresponding i^{th} block $(\mathbf{A_{mi}}, \mathbf{B_{mi}}, \mathbf{C_{mi}})$ as

$$\begin{aligned} \dot{\mathbf{x}}_\mathbf{i} &= \mathbf{A_{mi}}\,\mathbf{x_i} + \mathbf{B_{mi}}\,\mathbf{u}, \\ \mathbf{y} &= \mathbf{C_{mi}}\,\mathbf{x_i}. \end{aligned}$$

2.2. Piezoelectricity

Piezoelectricity has been frequently studied for control and disturbance sensing of flexible structures in different areas such as aerospace engineering, electrical engineering, precision engineering and mechatronics [4]. Piezoelectric materials are widely preferred as electromechanical converter parts of devices such as ultrasonic generators, filters, sensors and actuators. In this study, piezoelectric materials are used as actuators and sensors for active vibration control of beams and plates.

The piezoelectric materials can be incorporated into a structure, either by embedding them as laminates, or mounting them onto the surface of the structure. The piezoelectric actuators and sensors are assumed to be perfectly bonded to the structure. The actuators and sensors can be continuous over the entire structure or can be placed on some specific locations.

First, constitutive theory of piezoelectricity and piezoelectric equations are given. Then, Finite Element models of piezoelectric materials are derived, when basic FEM concepts are introduced for non-piezoelectric media.

2.2.1. Constitutive Theory of Piezoelectricity

Piezoelectricity is the linear interaction between mechanical and electrical systems [5]. It is first discovered by Curie brothers in 1880. Their studies on thermal-electrical effects of crystal symmetry have led them to further investigate the electromechanical interaction.

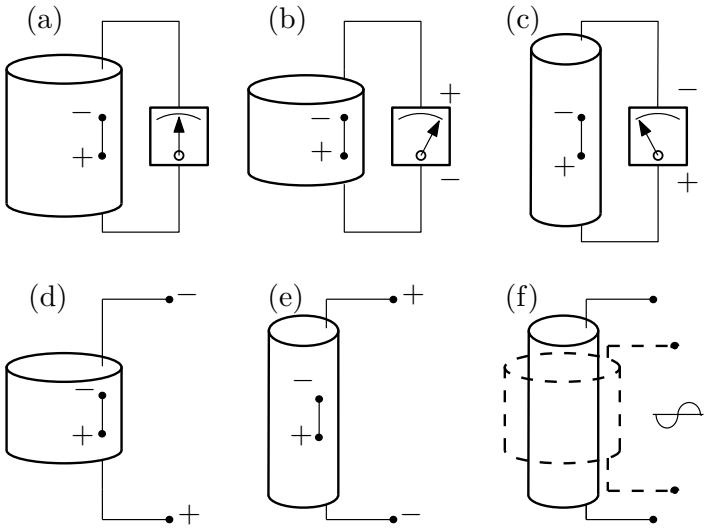

Figure 2.1. The piezoelectric effect on a single piezo disc

To illustrate the piezoelectric effect, consider a cylinder made of a piezoelectric material of a certain length without any voltage or stress applied initially as shown in Figure 2.1 (a). Whenever a force is applied to the ends of the cylinder, the resulting deformation produces a voltage at the two electrodes placed at the two surfaces of the cylinder. The polarity of the resulting voltage depends on the loading mode. If the forces act in a way such that there is a tension on the cylinder, the resulting voltage is of the same magnitude but of a different sign than in the case when a pressure is applied as shown in Figure 2.1 (b) and (c). Since this effect is discovered first, it is called the direct piezoelectric effect. The piezoelectric materials exhibit also the reverse piezoelectric effect. If a DC voltage is applied to the electrodes, the cylinder contracts (Figure 2.1 (d)). When the same voltage is applied to the opposite electrodes of the piezoelectric material, the cylinder will extend (Figure 2.1 (e)). When an AC voltage is applied to the electrodes, the piezo cylinder will extend and contract at the frequency of the AC voltage.

Some examples of materials which show high piezoelectric properties are quartz (see Figure 2.2), Rochelle salt, tourmaline and lithium sulphate. These naturally piezoelectric materials have specific directions, the so-called *Polar Axis*, at which they show the piezoelectric effect.

Piezoelectric effect can also be added to some ferroelectric substances such as

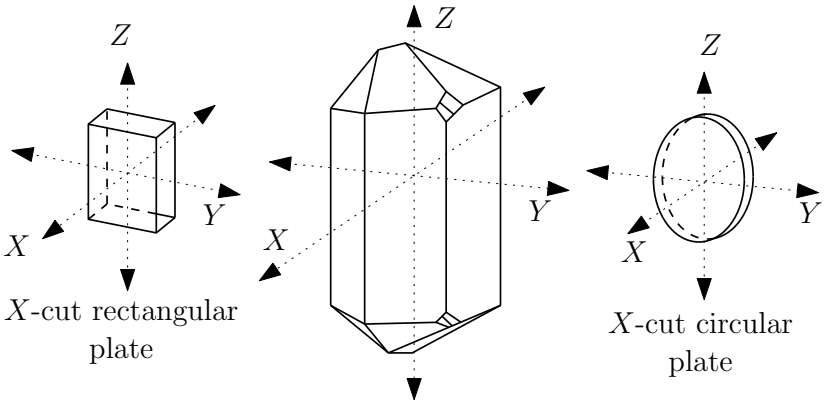

Figure 2.2. Natural quartz

barium titanate, lead meta-niobate and lead zirconate titanate through sintering from crystalline powder, which are made of cells consisting of dipoles. As shown in Figure 2.3 (a), the dipoles in the ceramic are of arbitrary direction when no voltage is applied. In the presence of an electric field, the dipoles are aligned (Figure 2.3 (b)). Keeping the ferroelectric material in the electric field, the ceramic is heated to a temperature higher than the Curie point and cooled slowly down to the room temperature (Figure 2.3 (c)). So the ferroelectric material becomes a piezoelectric one [6].

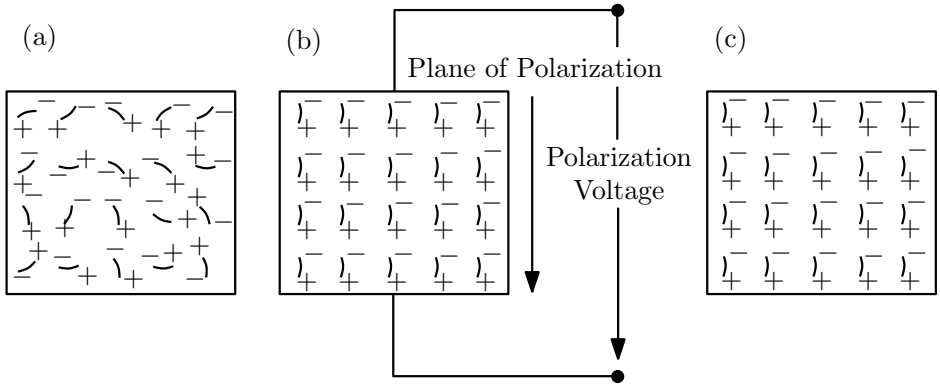

Figure 2.3. Schematic representation of electric dipole elements

2.2.2. Piezoelectric Equations

Consider a piezoelectric X-cut circular plate of cross sectional area A, and thickness l in Figure 2.2. When V is the voltage applied through the electrodes on the two surfaces of the piezo disc, V is the integral of the electric field E_1

$$V = \int_{x=0}^{l} E_1 \, \mathrm{d}x,$$

where the subindex "1" denotes the X-direction in Figure 2.2. For such a disc, T_1 and S_1 are the resultant stress and strain in the X-direction, respectively. Since both the applied electric field and the resultant deformation are directed perpendicular to the faces, this type of vibration mode is known as the *Longitudinal Effect*. The piezoelectric constitutive relation for the disc is given by a pair of equations

$$S_1 = s^E T_1 + d\, E_1, \tag{2.15}$$

$$D_1 = \epsilon^T E_1 + d\, T_1, \tag{2.16}$$

where D_1 is the electric displacement, s^E is the elastic compliance coefficient, d is the piezoelectric constant and ϵ^T is the dielectric constant. The suffix E in s^E means that the elastic compliance s^E gives the relationship between the strain S_1 and the stress T_1, while the electric field E_1 is kept constant. Similarly, the superscript T in the dielectric constant ϵ^T means that T_1 is kept constant. The same notation and approach is valid for all other constants in the coupled piezoelectric equations, which will follow. In Equations (2.15) and (2.16) the strain S_1 and the electric displacement D_1 are both functions of the stress T_1 and the electric field E_1, which are the independent variables in the equations. Hence, this type of piezoelectric relation is called (T, E) type. The piezoelectric equations can be expressed in terms of other independent variables as well as in Table 2.1. From Equations (2.15), (2.16) and Table 2.1 it can be easily seen that

Table 2.1. Other types of fundamental piezoelectric relations

Independent Variables	**Piezoelectric Relation**
S, D	$T = c^D S - hD$ $E = -hS + \beta^s D$
T, D	$S = s^D T + gD$ $E = -gT + \beta^T D$
S, E	$T = c^E S - eE$ $D = eS + \epsilon^s E$

the coefficients d, h, g and e are the *coupling coefficients*, which relate the electrical properties such as electric field and electric displacement to the mechanical properties such as stress and strain and vice versa. For example, d gives the strain caused by the applied electric field in the reverse piezoelectric effect or in the direct piezoelectricity it gives the electric displacement resulting from the stress. The coupling coefficient d has the unit m/V. Another example is the piezoelectric pressure constant g. It represents the electric field produced by the unit stress applied to a piezoelectric material or the strain caused by a unit electric displacement. The pressure constant g has the unit Vm/N.

The other coefficients with suffixes, c^D, s^D, c^E, are the *primary constants*. They relate the properties of the same group, e.g. elastic stiffness coefficient c^D gives the relationship between strain and stress. All of the constants, whether they are primary or coupling coefficients, can be expressed in terms of others [5, 7, 8, 9, 10, 11].

2.3. Finite Element Method

The Finite Element Method (FEM) is a widely used approximate solution technique to solve boundary value problems. The method is based on the idea of dividing the solution domain into smaller subregions, the finite elements, and of obtaining an approximate solution for the overall domain. With the advances in computer technology, the method is been used successfully in many areas of engineering ranging from deformation and stress analysis of automotive, aircraft, aerospace, and building to field analysis of heat flux, fluid mechanics, and magnetic flux problems.

In FEM, the approximate solution is obtained in steps. First, the solution region, that corresponds a geometry of a structure in vibration analysis, is discretized into smaller subregions. These smaller subregions, the finite elements, are assigned nodes, in terms of which the displacement field of the structure will be expressed. The number of nodes, the degree of freedom (DOF) at nodes is selected according to the general suggestions for finite elements and according to the experience of the engineer who solves the problem. To give an example, for flexural vibrations of thin plates, each

node is assigned three DOFs, whereas two DOFs are enough for in plane vibrations of structures. Although a finite element assigned two nodes for its starting and ending points, the numbers of nodes can be increased for more accurate results if the engineer wishes. The functions which are used to approximate the solution in the finite elements, the shape functions, are generated. This initial procedure is called mesh generation.

In the second step, the element stiffness and mass matrices are calculated. These matrices arise when the governing equations, which describe the physical system's dynamic equilibrium in vibration analysis, are reformulated by using approximate solutions in terms of the nodes and the shape functions. The unknown quantities are the values of the displacements and rotations at the nodes.

In the third step, the element matrices are assembled to obtain the global mass and stiffness matrices. When boundary conditions are applied and the constraints are taken into account, the contribution of some of the nodes needs to be eliminated from the global matrices.

In the remaining steps, the values of the variables at the nodes can be determined, strains and stresses may be calculated, or an error estimation might be done [12, 13].

According to the goals of this thesis, modelling of the flexible structures and their state space equations are necessary. Before introducing them, global mass, stiffness and electromechanical coupling matrices have to be defined. In the following sections, finite element mass, stiffness and piezoelectric coupling matrices, the shape functions for beam and plate elements are derived based on the information given in literature [14, 15, 16, 17, 13, 18].

2.3.1. Finite Element Matrices of Beams

To derive the interpolation functions and the finite element matrices for beam elements a finite element with dimensions shown in Figure 2.4 is taken. The element has two nodes at its ends and each node has two degrees of freedom (DOFs) v and

$\partial v/\partial x$. The node at $\xi = -1$ has the DOFs v_1 and $(\partial v/\partial x)_1$. Similarly, the translational DOF and the rotational DOF at the node at $\xi = 1$ are v_2 and $(\partial v/\partial x)_2$, respectively.

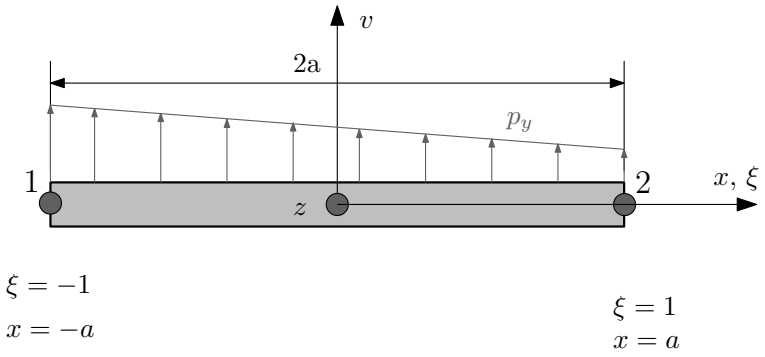

Figure 2.4. Geometry of a single beam element

Using standard finite element procedure, the hermite displacement functions are derived as

$$\mathbf{N_b}(\xi) := \left[\begin{array}{cccc} N_1(\xi) & aN_2(\xi) & N_3(\xi) & aN_4(\xi) \end{array} \right], \tag{2.17}$$

where

$$\begin{aligned} N_1(\xi) &:= \frac{1}{4}\left(2 - 3\xi + \xi^3\right), \\ N_2(\xi) &:= \frac{1}{4}\left(1 - \xi - \xi^2 + \xi^3\right), \\ N_3(\xi) &:= \frac{1}{4}\left(2 + 3\xi - \xi^3\right), \\ N_4(\xi) &:= \frac{1}{4}\left(-1 - \xi + \xi^2 + \xi^3\right). \end{aligned} \tag{2.18}$$

By describing

$$\mathbf{w}_e := \left[\begin{array}{cccc} v_1 & \theta_{z1} & v_2 & \theta_{z2} \end{array} \right],$$

and letting $\theta_{z1} := \left(\dfrac{dv}{dx}\right)_1$ and $\theta_{z2} := \left(\dfrac{dv}{dx}\right)_2$, the kinetic energy of the beam finite element is given by

$$T_e = \frac{1}{2}\, \dot{\mathbf{w}}_e\, \mathbf{M}_e\, \dot{\mathbf{w}}_e\,,$$

and the element inertia or mass matrix is expressed as

$$\mathbf{M}_e := \rho A a \int_{-1}^{+1} \mathbf{N_b}(\xi)^{\mathrm{T}}\, \mathbf{N_b}(\xi)\ \mathrm{d}\xi. \tag{2.19}$$

The potential energy of the beam element is given as

$$U_e = \frac{1}{2}\, \mathbf{w}_e\, \mathbf{K}_e\, \mathbf{w}_e\,. \tag{2.20}$$

The element stiffness matrix is defined as

$$\mathbf{K}_e := \frac{EI_z}{a^3} \int_{-1}^{+1} \mathbf{N_b}''(\xi)^{\mathrm{T}}\, \mathbf{N_b}''(\xi)\ \mathrm{d}\xi. \tag{2.21}$$

2.3.2. Finite Element Matrices of Plates

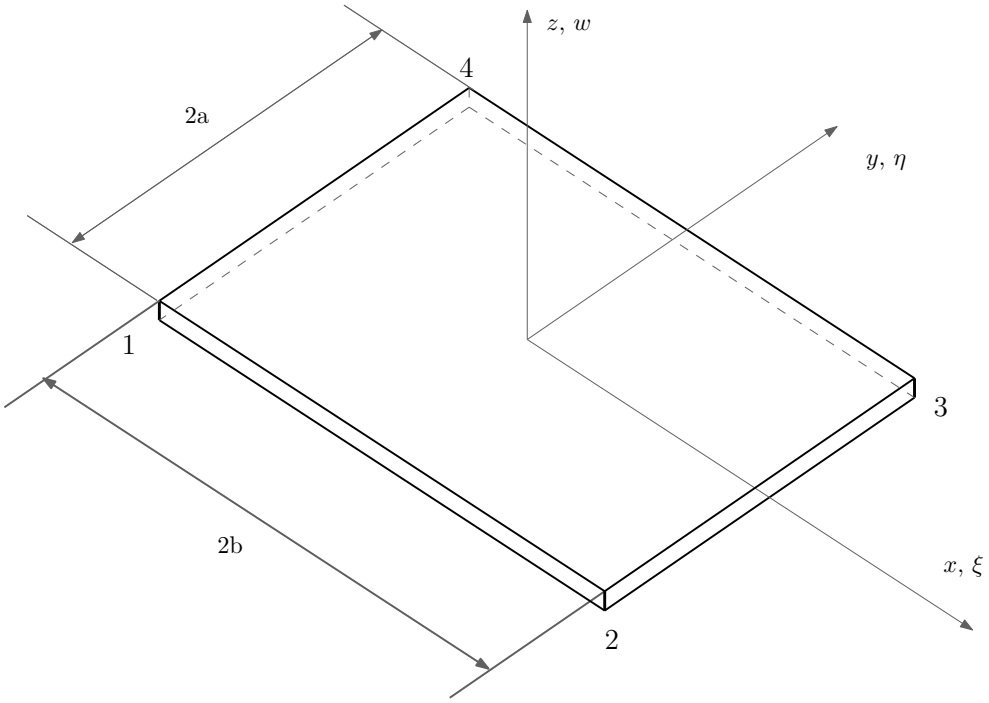

Figure 2.5. Geometry of a rectangular element. $\xi = x/a$, $\eta = y/b$

Figure 2.5 shows a rectangular element with four nodal points 1, 2, 3 and 4 at each corner. At each node the component of displacement normal to the plane of the plate, w, and the two rotations $\theta_x := \partial w/\partial y$ and $\theta_y := -\partial w/\partial x$ are set as degrees of

freedom. In terms of the local coordinates (ξ, η), the nodal rotational displacements are expressed as

$$\theta_x = \frac{1}{b}\frac{\partial w}{\partial \eta}, \qquad \theta_y = -\frac{1}{a}\frac{\partial w}{\partial \xi}. \tag{2.22}$$

Similar to the beam element calculations, one tries to obtain a shape function to express the displacements and the DOFs at the four nodes, which are given by

$$\mathbf{w}_e := \begin{bmatrix} w_1 & \theta_{x1} & \theta_{y1} & \cdots & w_4 & \theta_{x4} & \theta_{y4} \end{bmatrix}^{\mathrm{T}}. \tag{2.23}$$

The displacement of the plate element can be given in terms of nodal DOFs as

$$w = \mathbf{N_p}(\xi, \eta)\ \mathbf{w}_e\ , \tag{2.24}$$

where

$$\mathbf{N_p} := \begin{bmatrix} \mathbf{N}_1(\xi,\eta) & \mathbf{N}_2(\xi,\eta) & \mathbf{N}_3(\xi,\eta) & \mathbf{N}_4(\xi,\eta) \end{bmatrix} \mathbf{w}_e$$

and

$$\mathbf{N}_i(\xi,\eta) := \begin{bmatrix} \frac{1}{8}(1+\xi_i\xi)(1+\eta_i\eta)(2+\xi_i\xi+\eta_i\eta-\xi^2-\eta^2) \\ \frac{b}{8}(1+\xi_i\xi)(\eta_i+\eta)(\eta^2-1) \\ \frac{a}{8}(\xi_i+\xi)(\xi^2-1)(1+\eta_i\eta) \end{bmatrix}^{\mathrm{T}}, \forall\ i = 1:4. \tag{2.25}$$

In Equation (2.25) (ξ_i, η_i) are the coordinates of the node i. This element is commonly referred to as the ACM element [14], since it is given the initials of the researches who successfully used it. Here

$$\begin{aligned} &\xi_1 = -1, && \xi_2 = 1, && \xi_3 = 1, && \xi_4 = -1, \\ &\eta_1 = -1, && \eta_2 = -1, && \eta_3 = 1, && \eta_4 = 1 \end{aligned}$$

as can easily be seen from Figure 2.5.

The kinetic energy of the plate element can be expressed as

$$T_e = \frac{1}{2}\,\dot{\mathbf{w}}_e{}^{\mathrm{T}}\,\mathbf{M}_e\,\dot{\mathbf{w}}_e\,, \tag{2.26}$$

where

$$\begin{aligned}\mathbf{M}_e &:= \int_{A_e} \rho h\,\mathbf{N_p}{}^{\mathrm{T}}\,\mathbf{N_p}\;\mathrm{d}A \\ &= \rho h a b \int_{-1}^{+1}\int_{-1}^{+1} \mathbf{N_p}(\xi,\eta)^{\mathrm{T}}\,\mathbf{N_p}(\xi,\eta)\;\mathrm{d}\xi\,\mathrm{d}\eta \end{aligned} \tag{2.27}$$

is the element inertia matrix. The potential energy of the plate element is given as

$$U_e = \frac{1}{2}\,\mathbf{w}_e^{\mathrm{T}}\,\mathbf{K}_e\,\mathbf{w}_e\,.$$

The element stiffness matrix $\mathbf{K}_e$ is given by

$$\mathbf{K}_e := ab\int_{-1}^{1}\int_{-1}^{1}\frac{h^3}{12}\,\mathcal{B}^{\mathrm{T}}\,\mathfrak{D}\;\mathcal{B}\;\mathrm{d}\xi\,\mathrm{d}\eta,$$

where

$$\mathcal{B} := \begin{bmatrix} \dfrac{\partial^2}{\partial x^2} & \dfrac{\partial^2}{\partial y^2} & 2\dfrac{\partial^2}{\partial x\partial y}\end{bmatrix}^{\mathrm{T}}\mathbf{N_p} = \begin{bmatrix} \dfrac{1}{a^2}\dfrac{\partial^2}{\partial \xi^2} & \dfrac{1}{b^2}\dfrac{\partial^2}{\partial \eta^2} & \dfrac{2}{ab}\dfrac{\partial^2}{\partial \xi\partial \eta}\end{bmatrix}^{\mathrm{T}}\mathbf{N_p} \tag{2.28}$$

and

$$\mathfrak{D} = E\begin{bmatrix} \dfrac{1}{1-\nu^2} & \dfrac{\nu}{1-\nu^2} & 0 \\ \dfrac{\nu}{1-\nu^2} & \dfrac{1}{1-\nu^2} & 0 \\ 0 & 0 & \dfrac{1}{2\,(1+\nu)}\end{bmatrix}. \tag{2.29}$$

In Equation (2.29) E and ν are Young modulus and Poisson's ratio, respectively.

2.3.3. Finite Element Matrices of Piezoelectric Materials

For finite element discretization of piezoelectric materials, the (ε, E)-type piezoelectric constitutive equations

$$\sigma_{ij} = c^E_{ijkl}\varepsilon_{kl} + e_{lij}E_l, \tag{2.30}$$

$$D_i = e_{ikl}\varepsilon_{kl} + \epsilon^{\varepsilon}_{il}E_l \tag{2.31}$$

are used, where the definitions of the variables are given in Table 2.2.

Table 2.2. The definition of the variables of Equations (2.30) and (2.31)

Tensor notation	Matrix notation	Definition
σ_{ij}	$\boldsymbol{\sigma}$	stress
ε_{kl}	$\boldsymbol{\varepsilon}$	strain
c^E_{ijkl}	$\boldsymbol{c}$	the elastic stiffness constant
e_{lji}	$\boldsymbol{e}$	the piezoelectric coupling coefficient
E_l	$\mathbf{E}$	the electric field
D_i	$\mathcal{D}$	the electric displacement
$\epsilon^{\varepsilon}_{il}$	$\boldsymbol{\epsilon}$	permittivity

When performing finite element discretization of a structure with piezoelectric materials, the coupling matrices and the electrical stiffness matrix come out in addition to the usual mass and stiffness matrices due to the coupled electrical and mechanical behavior of piezoelectric material.

The coupling terms are the element electrical-mechanical coupling stiffness matrix $\mathbf{K}_{\mathbf{u}\phi}$ and the element mechanical-electrical coupling stiffness matrix $\mathbf{K}_{\phi\mathbf{u}}$. The electrical stiffness term is the element dielectric stiffness matrix $\mathbf{K}_{\phi\phi}$. They are given by

$$\mathbf{K}_{\mathbf{u}\phi} := \int_V \mathcal{B}^{\mathrm{T}}\boldsymbol{e}^{\mathrm{T}}\mathcal{A}\,\mathrm{d}V, \tag{2.32}$$

$$\mathbf{K}_{\phi\mathbf{u}} := \int_V \mathcal{A}^{\mathrm{T}}\boldsymbol{e}\,\mathcal{B}\,\mathrm{d}V, \tag{2.33}$$

$$\mathbf{K}_{\phi\phi} := \int_V \mathcal{A}^{\mathrm{T}} \boldsymbol{\epsilon}\, \mathcal{A}\, \mathrm{d}V, \tag{2.34}$$

where V is the volume of the element, $\mathcal{A} := \begin{bmatrix} -\partial/\partial x & -\partial/\partial y & -\partial/\partial z \end{bmatrix}^{\mathrm{T}}$ is the derivative operator between electrical charge and electric potential, $\mathcal{B}$ is the derivative operator between strain and the generalized nodal displacements given by Equation (2.28). It can be seen from Equation (2.32) and Equation (2.33) that $\mathbf{K_{u\phi}} = \mathbf{K_{\phi u}}^{\mathrm{T}}$ [18].

The element mass matrix $\mathbf{M_{uu}}$ and the element mechanical stiffness matrix $\mathbf{K_{uu}}$ are the same as those of beams and plates. For calculating $\mathbf{M_{uu}}$ and $\mathbf{K_{uu}}$, the element is treated as if it were not an electromechanically coupled element and had only mechanical behavior.

As piezoelectric materials have two coupled equations, the finite element equations for them will also consist of two coupled equations, one for mechanical and one for electrical behavior of the element [19]. Their coupled equations of motions are

$$\mathbf{M_{uu}}\, \ddot{\boldsymbol{\delta}} + \mathbf{K_{uu}}\, \boldsymbol{\delta} - \mathbf{K_{u\phi}}\, \boldsymbol{\phi} = \mathbf{f_w}, \tag{2.35}$$

$$\mathbf{K_{\phi u}}\ \boldsymbol{\delta} + \mathbf{K_{\phi\phi}}\, \boldsymbol{\phi} = -\mathbf{f_q}, \tag{2.36}$$

where $\mathbf{f_w}$ is the vector of applied mechanical forces, $\mathbf{f_q}$ is the vector of applied electrical charges, $\boldsymbol{\delta}$ is the vector of generalized nodal displacements, $\boldsymbol{\phi}$ is the vector of electrical potentials. After substituting Equation (2.36) into Equation (2.35), one obtains

$$\mathbf{M_{uu}}\, \ddot{\boldsymbol{\delta}} + \mathbf{K}^*\, \boldsymbol{\delta} = \mathbf{f_w} - \mathbf{K_{u\phi}}\mathbf{K_{\phi\phi}}^{-1}\mathbf{f_q}, \tag{2.37}$$

where

$$\mathbf{K}^* := \mathbf{K_{uu}} + \mathbf{K_{u\phi}}\mathbf{K_{\phi\phi}}^{-1}\mathbf{K_{\phi u}}. \tag{2.38}$$

Since the internal DOFs, $\boldsymbol{\phi}$, of the system are eliminated, this substitution operation

is called static condensation of $\boldsymbol{\phi}$.

For sensors one assumes that the converse piezoelectric effect, shown in Figure 2.1 (d), is negligible, the voltage and the electrical charge sensed from the piezoelectric sensor are

$$\boldsymbol{\phi}_s = -\mathbf{K}_{\phi\phi}{}^{-1}\mathbf{K}_{\phi\mathbf{u}_s}\boldsymbol{\delta}_s, \tag{2.39}$$

$$\mathbf{f}_{\mathbf{q}\,s} = -\mathbf{K}_{\phi\mathbf{u}_s}\boldsymbol{\delta}_s. \tag{2.40}$$

Once Equations (2.39) and (2.40) are at hand, one can use electric potential as an input to the element rather than electrical charge using the equation

$$\mathbf{M}_{\mathbf{uu}}\,\ddot{\boldsymbol{\delta}} + \mathbf{K}^*\,\boldsymbol{\delta} = \mathbf{f}_{\mathbf{w}} - \mathbf{K}_{\mathbf{u}\phi}\,\boldsymbol{\phi}_{\boldsymbol{a}}, \tag{2.41}$$

since electrical charge can be measured only indirectly. In Equations (2.39) to (2.41), subscript s denotes sensors and a denotes actuators.

In the following subsections Equations (2.32) to (2.34) are solved for their open forms for piezoelectric beam and piezoelectric plate elements. Since Equation (2.41) can be used for any type of finite element of piezoelectric material, the solved electromechanical matrices can be inserted into that equation.

2.3.4. Piezoelectric Beam Element

The (S, E)-type piezoelectric constitutive equations were given by (2.30) and (2.31). The open form of Equations (2.30) and (2.31) for the piezoelectric beam are

$$\sigma_1 = c_{11}\varepsilon_1 - e_{31}E_3, \tag{2.42}$$

$$D_1 = e_{31}\varepsilon_1 - \epsilon_{33}E_3. \tag{2.43}$$

For the piezoelectric beam element, the open forms of Equations (2.32) to (2.34) are

solved to give

$$\begin{aligned}
\mathbf{K}_{\mathbf{u}\phi} &= \begin{bmatrix} 0 \\ e_{31}b_{pzt} \\ 0 \\ -e_{31}b_{pzt} \end{bmatrix}, \\
\mathbf{K}_{\phi\mathbf{u}} &= \begin{bmatrix} 0 & e_{31}b_{pzt} & 0 & -e_{31}b_{pzt} \end{bmatrix}, \\
\mathbf{K}_{\phi\phi} &= \frac{2ab_{pzt}\epsilon_{33}}{h_{pzt}},
\end{aligned}$$

where b_{pzt} is the thickness of the piezoelectric beam element along the y-direction.

2.3.5. Piezoelectric Plate Element

For the piezoelectric plate, the open form of Equations (2.30) and (2.31) are

$$\begin{aligned}
\begin{Bmatrix} \sigma_1 \\ \sigma_2 \\ \sigma_6 \end{Bmatrix} &= \begin{bmatrix} c_{11} & c_{12} & 0 \\ c_{12} & c_{22} & 0 \\ 0 & 0 & c_{66} \end{bmatrix} \begin{Bmatrix} \varepsilon_1 \\ \varepsilon_2 \\ \varepsilon_6 \end{Bmatrix} - \begin{bmatrix} 0 & 0 & e_{31} \\ 0 & 0 & e_{32} \\ 0 & 0 & 0 \end{bmatrix} \begin{Bmatrix} E_1 \\ E_2 \\ E_3 \end{Bmatrix}, \\
\begin{Bmatrix} D_1 \\ D_2 \\ D_6 \end{Bmatrix} &= \begin{bmatrix} 0 & 0 & 0 \\ 0 & 0 & 0 \\ e_{31} & e_{32} & 0 \end{bmatrix} \begin{Bmatrix} \varepsilon_1 \\ \varepsilon_2 \\ \varepsilon_6 \end{Bmatrix} - \begin{bmatrix} \epsilon_{11} & 0 & 0 \\ 0 & \epsilon_{22} & 0 \\ 0 & 0 & \epsilon_{33} \end{bmatrix} \begin{Bmatrix} E_1 \\ E_2 \\ E_3 \end{Bmatrix}.
\end{aligned}$$

For the piezoelectric plate element, the open forms of Equations (2.32) to (2.34) are solved to be give

$$\begin{aligned}
\mathbf{K}_{\mathbf{u}\phi} &= \Big[0 \quad a_{pzt}e_{32} \quad b_{pzt}e_{31} \quad 0 \quad a_{pzt}e_{32} \quad -b_{pzt}e_{31} \quad \cdots \\
&\qquad \cdots \quad 0 \quad -a_{pzt}e_{32} \quad -b_{pzt}e_{31} \quad 0 \quad -a_{pzt}e_{32} \quad b_{pzt}e_{31} \Big]^{\mathrm{T}}, \\
\mathbf{K}_{\phi\mathbf{u}} &= \Big[0 \quad a_{pzt}e_{32} \quad b_{pzt}e_{31} \quad 0 \quad a_{pzt}e_{32} \quad -b_{pzt}e_{31} \quad \cdots \\
&\qquad \cdots \quad 0 \quad -a_{pzt}e_{32} \quad -b_{pzt}e_{31} \quad 0 \quad -a_{pzt}e_{32} \quad b_{pzt}e_{31} \Big], \\
\mathbf{K}_{\phi\phi} &= \frac{4a_{pzt}b_{pzt}\epsilon_{33}}{h_{pzt}},
\end{aligned}$$

where a_{pzt} and b_{pzt} are half of the element length of the piezoelectric plate element along the x- and the y-directions, respectively.

2.3.6. Assembly and Application of Boundary Conditions

After the element matrices are calculated, they need to be assembled to obtain the global finite element mass and stiffness matrices. The assembly procedure can be done with the aid of computer for any number of elements. However, it must be done on a systematic basis since the assembly affects the condition number of the global finite element matrices. In most cases, the assembled finite element matrices are sparse matrices with its entries on the diagonal bands. The correct order of numbering of the nodes, the DOFs and the elements gives the banded structure of these matrices. For beams, the assembly process is much simpler than that for plates. Beams are one-dimensional and 4×4 element matrices are just added considering the fact that each neighboring element has one vertical and one rotational DOFs as common. For plates, the assembly process is more complicated.

For a 2D plate, each node has three DOFs, namely w, θ_x and θ_y. Hence, each node is represented by three numbers. The numbering of nodes is started at the left lower corner, and the nodes to the right are numbered first. The same strategy is used for element numbering.

The global matrices of the plate model have to reflect the contributions of individual DOFs each element matrix has. When the finite element matrices are assembled, the contribution of the DOFs must be preserved. For this purpose, a *destination vector* for each element is created. The destination vector consists simply of the DOF numbers of each element.

DOF numbers of the local element nodes in the order $1, 2, 3$, and 4 in Figure 2.6 are selected as the destination vector

$$\widehat{\mathbf{D}}_\mathbf{i} = \begin{bmatrix} \text{DOFs of Local Node 1} \\ \text{DOFs of Local Node 2} \\ \text{DOFs of Local Node 3} \\ \text{DOFs of Local Node 4} \end{bmatrix}^{\mathrm{T}}.$$

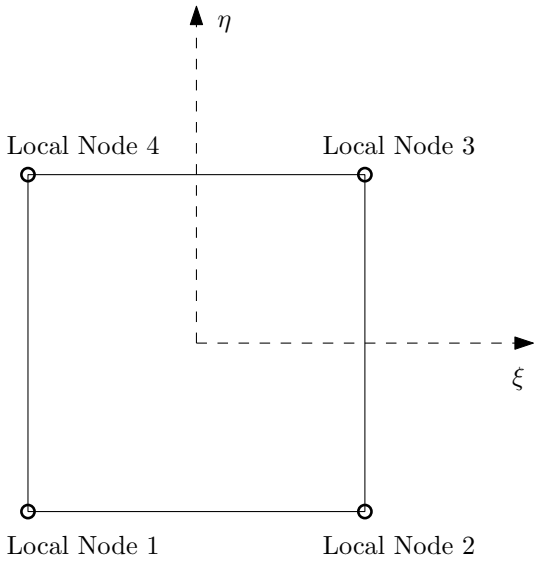

Figure 2.6. Local element

Using the destination vectors, the local element matrices are added to the global matrices as

$$\begin{aligned} M_{d_i,d_j} &= M_{d_i,d_j} + m_{i,j}, \\ K_{d_i,d_j} &= K_{d_i,d_j} + k_{i,j}, \end{aligned}$$

where $i, j = 1, 2, \ldots, 12$. The entries of the global matrices $\mathbf{M}$ and $\mathbf{K}$ at the d_i^{th} row and d_j^{th} column are described by M_{d_i,d_j} and K_{d_i,d_j}, respectively. The entries of the local finite element matrices $\mathbf{M}_e$ and $\mathbf{K}_e$ at row i and column j are denoted by $m_{i,j}$ and $k_{i,j}$, respectively. The i^{th} and j^{th} entries of the destination vector $\widehat{\mathbf{D}}_\mathbf{i}$ for the local element are given by d_i and d_j, respectively.

When the procedure is completed for all of the elements of the structure, the

global matrices $\mathbf{M}$ and $\mathbf{K}$ are obtained as banded matrices. If there are other global matrices such as those arising from the piezoelectric materials in the structure, they can be calculated in a similar way. After the global matrices are obtained, the next step is the application of the boundary conditions.

Using the global matrices, the equation of motion of the structure can be written as

$$\mathbf{M}_{bc}\ \ddot{\boldsymbol{\delta}} + \mathbf{K}_{bc}\ \boldsymbol{\delta} = \mathbf{f}_{\mathbf{w}\,bc} + \mathbf{f}_{\mathbf{u}\,bc}\,, \tag{2.44}$$

where $\mathbf{M}_{bc}$, $\mathbf{K}_{bc}$, $\mathbf{f}_{\mathbf{w}\,bc}$ and $\mathbf{f}_{\mathbf{u}\,bc}$ are the global matrices obtained after applying the boundary conditions.

2.4. Model of the Structure

Before incorporating the signal weights into the generalized plant, the state space representation of the flexible structure in Figure 2.7 needs to be obtained. The state space model of the physical plant can be given in one of the four modal forms (2.7) through (2.10) [3]. In this thesis, the first modal form is preferred. Since one of the objectives of this thesis is to obtain approximate ARE solutions in the coprime and $\mathcal{H}_\infty$-controller design parts and the first modal state space representation is the most suitable for this purpose, the physical plant is converted to that form.

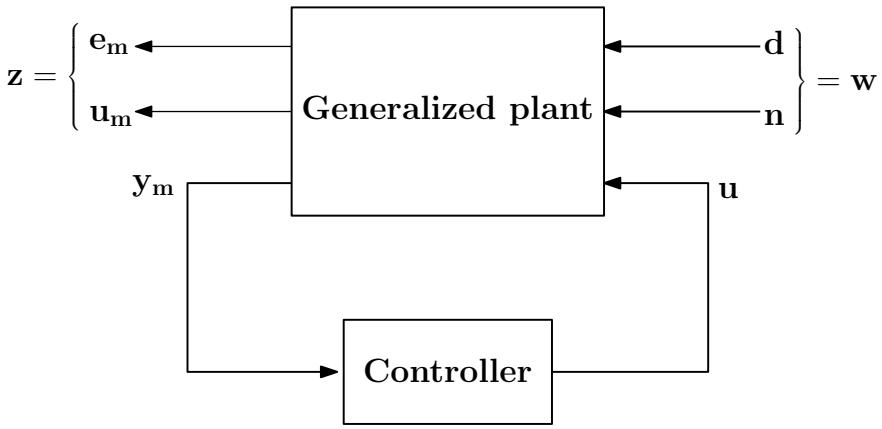

Figure 2.7. The generalized control configuration

To obtain a state space representation like in Equation (2.7), first, the equation of motion of the flexible structure with point actuators and sensors must be given in nodal form as

$$\begin{aligned} \mathbf{M}\ddot{\mathbf{q}} + \mathbf{C}^{\mathbf{d}}\dot{\mathbf{q}} + \mathbf{K}\mathbf{q} &= \mathbf{L}_{\mathbf{w}}\mathbf{d} + \mathbf{L}_{\mathbf{u}}\mathbf{u}, \\ \mathbf{z} &= \mathbf{C}_{\mathbf{zq}}\mathbf{q} + \mathbf{C}_{\mathbf{zv}}\dot{\mathbf{q}}, \\ \mathbf{y} &= \mathbf{C}_{\mathbf{yq}}\mathbf{q} + \mathbf{C}_{\mathbf{yv}}\dot{\mathbf{q}}, \end{aligned} \tag{2.45}$$

where $\mathbf{q}$ is the vector of displacements, $\mathbf{d}$ and $\mathbf{u}$ are the vectors of disturbances and control inputs acting on the nodes, respectively. The $N_y \times 1$ output vector is denoted by $\mathbf{y}$. The matrix $\mathbf{L_u}$ of dimensions $N \times N_u$, is a function of the point actuators where N and N_u denote the degree of freedom of the structure and the number of point actuators, respectively.

The measured output displacement matrix $\mathbf{C_{yq}}$ has the dimensions $N_r \times N$, and $\mathbf{C_{yv}}$ is the $N_r \times N$ measured output velocity matrix. The performance output vector of dimensions $N_z \times 1$ is denoted by $\mathbf{z}$, where $\mathbf{C_{zq}}$ and $\mathbf{C_{zv}}$ are performance output displacement and performance output velocity matrices, respectively.

If only rate sensors are installed and are collocated with actuators, no displacement is measured, $\mathbf{C_{yq}} = 0$, and $\mathbf{C_{yv}}$ becomes

$$\mathbf{C_{yv}} = \mathbf{L}_u^{\mathrm{T}}\,.$$

Assuming proportional damping and following the procedure in [3], Equation (2.45) can be transformed to the equation of motion in the modal coordinates as

$$\begin{aligned} \ddot{\mathbf{q}}_{\mathbf{m}} + 2\boldsymbol{\Upsilon}\boldsymbol{\Omega}\dot{\mathbf{q}}_{\mathbf{m}} + \boldsymbol{\Omega}^2\mathbf{q}_{\mathbf{m}} &= \mathbf{L}_{\mathbf{w,m}}\mathbf{d} + \mathbf{L}_{\mathbf{u,m}}\mathbf{u}, \\ \mathbf{z} &= \mathbf{C}_{\mathbf{zq,m}}\mathbf{q}_{\mathbf{m}} + \mathbf{C}_{\mathbf{zv,m}}\dot{\mathbf{q}}_{\mathbf{m}}, \\ \mathbf{y} &= \mathbf{C}_{\mathbf{yv,m}}\dot{\mathbf{q}}_{\mathbf{m}}. \end{aligned} \tag{2.46}$$

In Equations (2.46), the newly defined variables are $\mathbf{L_{w,m}} := \mathbf{\Phi}^{\mathrm{T}}\mathbf{L_w}$, $\mathbf{L_{u,m}} := \mathbf{\Phi}^{\mathrm{T}}\mathbf{L_u}$, $\mathbf{C_{zv,m}} := \mathbf{C_{zv}}\mathbf{\Phi}$, $\mathbf{C_{zq,m}} := \mathbf{C_{zq}}\mathbf{\Phi}$, $\mathbf{C_{yv,m}} := \mathbf{C_{yv}}\mathbf{\Phi}$ and $\mathbf{\Upsilon} := \mathrm{diag}\left(\zeta_1, \zeta_2, \ldots \zeta_N\right)$, where $\mathbf{\Omega}$, $\mathbf{\Phi}$ and $\mathbf{q_m}$ are the matrix of natural frequencies in (2.3), the mode shape matrix in (2.4) and the modal displacement vector in (2.5), respectively.

Equation (2.46) is obtained from the modal Equation (2.45) for point actuator and sensor pairs. Since throughout the thesis the piezoelectric patches are also used for actuating and sensing purposes, their nodal equations need to be converted to Equation (2.45). This is done easily by defining new variables for Equation (2.44) and by adding a proportional damping matrix $\mathbf{C}$ to Equation (2.44). Letting $\mathbf{M} := \mathbf{M_{uu}}_{bc}$, $\mathbf{K} := \mathbf{K}^*_{bc}$, $\mathbf{q} := \boldsymbol{\delta}$, $\mathbf{f_{w}}_{bc} = \mathbf{L_w d}$, and $\mathbf{L_u} := -\mathbf{K_{u}}_{\phi bc}\mathbf{L_p}$, where $\mathbf{L_p}$ transforms the actuator and sensor input to inputs at the corresponding DOFs, one may have the second order ordinary differential equation for structures with piezoelectric patches.

The state space realization of Equations (2.46) is

$$\begin{aligned} \dot{\hat{\mathbf{x}}} &= \hat{\mathbf{A}}\hat{\mathbf{x}} + \hat{\mathbf{B}}_{\mathbf{1}}\mathbf{d} + \hat{\mathbf{B}}_{\mathbf{2}}\mathbf{u}, \\ \mathbf{z} &= \hat{\mathbf{C}}_{\mathbf{1}}\hat{\mathbf{x}}, \\ \mathbf{y} &= \hat{\mathbf{C}}_{\mathbf{2}}\hat{\mathbf{x}}, \end{aligned} \tag{2.47}$$

where $\hat{\mathbf{x}} := \begin{bmatrix} \mathbf{q_m}^{\mathrm{T}} & \dot{\mathbf{q}}_{\mathbf{m}}^{\mathrm{T}} \end{bmatrix}^{\mathrm{T}}$,

$$\hat{\mathbf{A}} := \begin{bmatrix} \mathbf{0} & \mathbf{I} \\ \mathbf{\Omega}^2 & 2\mathbf{\Upsilon\Omega} \end{bmatrix}, \qquad \hat{\mathbf{B}}_{\mathbf{1}} := \begin{bmatrix} \mathbf{0} \\ \mathbf{L_{w,m}} \end{bmatrix}, \qquad \hat{\mathbf{B}}_{\mathbf{2}} := \begin{bmatrix} \mathbf{0} \\ \mathbf{L_{u,m}} \end{bmatrix},$$

$$\hat{\mathbf{C}}_{\mathbf{1}} := \begin{bmatrix} \mathbf{C_{zq,m}} & \mathbf{0} \\ \mathbf{0} & \mathbf{C_{zv,m}} \end{bmatrix}, \quad \hat{\mathbf{C}}_{\mathbf{2}} := \begin{bmatrix} \mathbf{0} & \mathbf{C_{yv,m}} \end{bmatrix}.$$

The state space representation in (2.47) can be converted to the third modal form in Equation (2.9) by the coordinate transformation $\mathbf{x_3} = \mathbf{R}\hat{\mathbf{x}}$, where

$$\mathbf{R} := \begin{bmatrix} \mathbf{t_1} & \mathbf{t_2} \end{bmatrix}. \tag{2.48}$$

In Expression (2.48) $\mathbf{t_1}$ and $\mathbf{t_2}$ are

$$\mathbf{t_1} := \begin{bmatrix} 1 & 0 & \cdots & 0 \\ 0 & 0 & \cdots & 0 \\ 0 & 1 & 0 & \cdots & 0 \\ 0 & 0 & 0 & \cdots & 0 \\ \vdots & & & & \vdots \\ 0 & \cdots & 0 & 1 & 0 \\ 0 & \cdots & 0 & 0 & 0 \\ 0 & \cdots & 0 & 1 \\ 0 & \cdots & 0 & 0 \end{bmatrix}, \quad \mathbf{t_2} := \begin{bmatrix} 0 & 0 & \cdots & 0 \\ 1 & 0 & \cdots & 0 \\ 0 & 0 & 0 & \cdots & 0 \\ 0 & 1 & 0 & \cdots & 0 \\ \vdots & & & & \vdots \\ 0 & \cdots & 0 & 0 & 0 \\ 0 & \cdots & 0 & 1 & 0 \\ 0 & \cdots & 0 & 0 \\ 0 & \cdots & 0 & 1 \end{bmatrix}.$$

The coordinate transformation which is used to obtain the state space realization of the structure in the first modal form is $\mathbf{x_1} = \mathbf{R_{31}}\mathbf{x_3}$, where

$$\mathbf{R_{31}} := \operatorname{diag}\left(\begin{pmatrix} 1 & 0 \\ 0 & \omega_1 \end{pmatrix}, \begin{pmatrix} 1 & 0 \\ 0 & \omega_2 \end{pmatrix}, \cdots, \begin{pmatrix} 1 & 0 \\ 0 & \omega_N \end{pmatrix}\right). \tag{2.49}$$

The total coordinate transformation $\mathbf{x_m} = \mathbf{R_{31}}\mathbf{R}\hat{\mathbf{x}}$ can be used to convert the state space realization in Equation (2.47) to the first modal form

$$\left(\begin{array}{c|c|c} \hat{\mathbf{R}}^{-1}\hat{\mathbf{A}}\hat{\mathbf{R}} & \hat{\mathbf{B}}_1\hat{\mathbf{R}} & \hat{\mathbf{B}}_2\hat{\mathbf{R}} \\ \hline \hat{\mathbf{R}}^{-1}\hat{\mathbf{C}}_1 & \mathbf{0} & \mathbf{0} \\ \hline \hat{\mathbf{R}}^{-1}\hat{\mathbf{C}}_2 & \mathbf{0} & \mathbf{0} \end{array}\right) =: \left(\begin{array}{c|c|c} \mathbf{A_m} & \mathbf{B_{m1}} & \mathbf{B_{m2}} \\ \hline \mathbf{C_{m1}} & \mathbf{0} & \mathbf{0} \\ \hline \mathbf{C_{m2}} & \mathbf{0} & \mathbf{0} \end{array}\right),$$

where $\hat{\mathbf{R}} := \mathbf{R_{31}}\,\mathbf{R}$ and the state matrix

$$\mathbf{A_m} = \operatorname{diag}\left(\begin{pmatrix} 0 & \omega_1 \\ -\omega_1 & -2\zeta_1\omega_1 \end{pmatrix}, \cdots, \begin{pmatrix} 0 & \omega_N \\ -\omega_N & -2\zeta_N\omega_N \end{pmatrix}\right). \tag{2.50}$$

2.5. Signal Weightings

Most often in control engineering, it is necessary to emphasize some of the desired control objectives, and also some re-scalings of the inputs and outputs are required. This is done by using the signal weightings as shown in Figure 2.8. Some measurement noise may also be modeled by signal weights.

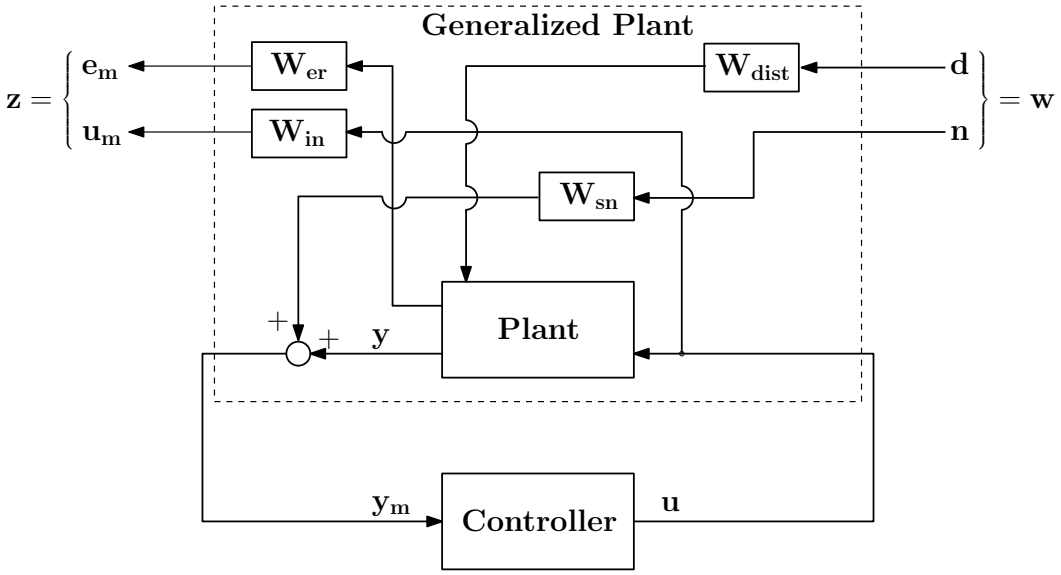

Figure 2.8. The weighted generalized plant with the controller

In Figure 2.8, each system ($\mathbf{W_{dist}}$,$\mathbf{W_{sn}}$,$\mathbf{W_{er}}$,$\mathbf{W_{in}}$ and **Plant**) has its own state space realization. If these subsystems are interconnected, the generalized plant in Figure 2.8 has the state space representation

$$\begin{aligned} \dot{\mathbf{x}}_\mathbf{g} &= \mathbf{A_g x_g} + \mathbf{B_{g_1} w} + \mathbf{B_{g_2} u}, \\ \mathbf{z} &= \mathbf{C_{g_1} x_g} + \mathbf{D_{g_{11}} w} + \mathbf{D_{g_{12}} u}, \\ \mathbf{y} &= \mathbf{C_{g_2} x_g} + \mathbf{D_{g_{21}} w} + \mathbf{D_{g_{22}} u}, \end{aligned} \tag{2.51}$$

where $\mathbf{w}$, $\mathbf{z}$ and $\mathbf{y}$ are $[\mathbf{d}^{\mathrm{T}} \quad \mathbf{n}^{\mathrm{T}}]^{\mathrm{T}}$, $[\mathbf{e_m}^{\mathrm{T}} \quad \mathbf{u_m}^{\mathrm{T}}]^{\mathrm{T}}$ and $\mathbf{y_m}$, respectively.

In Equation (2.51), $\mathbf{A_g}$, $\mathbf{B_{g1}}$, $\mathbf{B_{g2}}$, $\mathbf{C_{g1}}$, $\mathbf{C_{g2}}$, $\mathbf{D_{g11}}$, $\mathbf{D_{g12}}$, $\mathbf{D_{g21}}$ and $\mathbf{D_{g22}}$ are

$$\mathbf{A_g} = \begin{bmatrix} \mathbf{A_m} & \mathbf{B_{m1}C_w} & \mathbf{0} & \mathbf{0} & \mathbf{0} \\ \mathbf{0} & \mathbf{A_w} & \mathbf{0} & \mathbf{0} & \mathbf{0} \\ \mathbf{B_zC_{m1}} & \mathbf{B_zD_{m11}C_w} & \mathbf{A_z} & \mathbf{0} & \mathbf{0} \\ \mathbf{0} & \mathbf{0} & \mathbf{0} & \mathbf{A_u} & \mathbf{0} \\ \mathbf{0} & \mathbf{0} & \mathbf{0} & \mathbf{0} & \mathbf{A_s} \end{bmatrix}, \tag{2.52}$$

$$\mathbf{B_{g_1}} = \begin{bmatrix} (\mathbf{B_{m1}D_w})^{\mathrm{T}} & \mathbf{0} & \mathbf{B_w}^{\mathrm{T}} & \mathbf{0} & (\mathbf{B_zD_{m11}D_w})^{\mathrm{T}} \\ \mathbf{0} & \mathbf{0} & \mathbf{0} & \mathbf{0} & \mathbf{B_s}^{\mathrm{T}} \end{bmatrix}^{\mathrm{T}}, \tag{2.53}$$

$$\mathbf{B_{g_2}} = \begin{bmatrix} \mathbf{B_{m2}}^{\mathrm{T}} & \mathbf{0} & (\mathbf{B_zD_{m12}})^{\mathrm{T}} & \mathbf{B_u}^{\mathrm{T}} & \mathbf{0} \end{bmatrix}^{\mathrm{T}}, \tag{2.54}$$

$$\mathbf{C_{g_1}} = \begin{bmatrix} \mathbf{0} & \mathbf{0} & \mathbf{0} & \mathbf{C_u} & \mathbf{0} \\ \mathbf{D_zC_{m1}} & \mathbf{D_zD_{m11}C_w} & \mathbf{C_z} & \mathbf{0} & \mathbf{0} \end{bmatrix}, \tag{2.55}$$

$$\mathbf{C_{g_2}} = -\begin{bmatrix} \mathbf{C_{m2}} & \mathbf{D_{m21}C_w} & \mathbf{0} & \mathbf{0} & \mathbf{C_s} \end{bmatrix}, \tag{2.56}$$

$$\mathbf{D_{g_{11}}} = \begin{bmatrix} \mathbf{0} & \mathbf{0} \\ \mathbf{D_zD_{m11}D_w} & \mathbf{0} \end{bmatrix}, \tag{2.57}$$

$$\mathbf{D_{g_{12}}} = \begin{bmatrix} \mathbf{D_u} \\ \mathbf{D_zD_{m12}} \end{bmatrix}, \tag{2.58}$$

$$\mathbf{D_{g_{21}}} = -\begin{bmatrix} \mathbf{D_{m21}D_w} & \mathbf{D_s} \end{bmatrix}, \tag{2.59}$$

$$\mathbf{D_{g_{22}}} = -\mathbf{D_{m22}}. \tag{2.60}$$

2.6. Obtaining Modal Models of the Generalized Plant

Hiramoto et al. [1] design their controller for the physical plant and neglect damping. Since the aim is to design a coprime controller for the shaped plant without neglecting the modal damping, it is necessary to put the generalized plant into a modal state space form, where the state matrix is block diagonal and each mode can be dealt individually.

Theorem 2.6.1. *By the coordinate transformation* $\mathbf{x} = \mathbf{Z}\mathbf{x_g}$*, the state space representation of the generalized plant in Equation* (2.51)*, in which the physical system is*

given in one of the four modal forms (2.7) *through* (2.10)*, can be converted to the space realization*

$$\begin{array}{lll} \mathbf{A} := \mathbf{Z^{-1}A_gZ}, & \mathbf{B_1} := \mathbf{B_{g_1}Z}, & \mathbf{B_2} := \mathbf{B_{g_2}Z}, \\ \mathbf{C_1} := \mathbf{Z^{-1}C_{g_1}}, & \mathbf{D_{11}} := \mathbf{D_{g_{11}}}, & \mathbf{D_{12}} := \mathbf{D_{g_{12}}}, \\ \mathbf{C_2} := \mathbf{Z^{-1}C_{g_2}}, & \mathbf{D_{21}} := \mathbf{D_{g_{21}}}, & \mathbf{D_{22}} := \mathbf{D_{g_{22}}}, \end{array} \tag{2.61}$$

where

$$\mathbf{A} := \text{blockdiag}\left(\begin{array}{ccccc} \mathbf{A_m}, & \mathbf{A_w}, & \mathbf{A_z}, & \mathbf{A_u}, & \mathbf{A_s} \end{array} \right), \tag{2.62}$$

and $\mathbf{Z} := \mathbf{X}^{-1}\mathbf{X_g}$*,* $\mathbf{X}$ *and* $\mathbf{X_g}$ *being the eigenvectors of the state matrices* $\mathbf{A}$ *and* $\mathbf{A_g}$*, respectively.*

Proof. Since the eigenvalues of the global state matrices in Equations (2.52) and (2.62) are equal, there exists a single diagonal eigenvalue matrix $\mathbf{\Lambda}$ for both of the state matrices in Equations (2.52) and (2.62) which obey

$$\begin{aligned} \mathbf{A_g} &= \mathbf{X_g \Lambda {X_g}^{-1}}, \\ \mathbf{A} &= \mathbf{X \Lambda X^{-1}}, \end{aligned}$$

where

$$\mathbf{\Lambda} = \text{diag}\left(\lambda_1, \lambda_2, \ldots \lambda_i, \ldots \lambda_n\right).$$

Using the coordinate transformation $\mathbf{Z}$ the global state matrix $\mathbf{A_g}$ can be put into a block diagonal form in (2.62). □

The block diagonal form of the state matrix in (2.62) will make it possible to obtain simple and diagonally dominant solutions of the Algebraic Riccati Equations (ARE's) in the controller synthesis step.

2.7. Model Reduction

As the DOFs of a physical system increase, the dynamic analysis of that system becomes numerically more difficult and takes more computation time. Also the order of the controller is dependent on the order of the structure. In fact, the order of the controller is higher than the order of the physical plant since most controllers are designed using signal weights to scale inputs and outputs of the plant and to emphasize the control objectives. Hence, to reduce computation costs, some of the states (modes) can be left whose contribution are small (in terms of system norms such as $\mathcal{H}_2$ or $\mathcal{H}_\infty$) in comparison to others.

Mainly, the methods are categorized into two groups of truncation and residualization techniques. These methods for order reduction can be found in various books [3, 20, 21, 22, 23]. Among the methods described in these references, the reduction through truncation will be applied for model reduction purposes throughout the thesis.

2.7.1. Modal Truncation

Let

$$\mathbf{P} := \left[\begin{array}{c|c} \mathbf{A} & \mathbf{B} \\ \hline \mathbf{C} & \mathbf{D} \end{array}\right]$$

be a state space representation of a stable system. For n modes, the corresponding modal state vector $\mathbf{x}$ with the dimensions $N = 2n \times 1$ can be partitioned into the retained states $\mathbf{x_r}$ and the truncated states $\mathbf{x_t}$. If k modes are truncated, then $r = 2k$ and $l = 2(n-k)$. The state vector $\mathbf{x}$ and the corresponding modal state space matrices $\mathbf{A}$, $\mathbf{B}$, $\mathbf{C}$ can be given in the partitioned form as

$$\mathbf{x} = \begin{bmatrix} \mathbf{x_r} \\ \mathbf{x_t} \end{bmatrix}, \quad \mathbf{A} = \begin{bmatrix} \mathbf{A_r} & \mathbf{0} \\ \mathbf{0} & \mathbf{A_t} \end{bmatrix}, \quad \mathbf{B} = \begin{bmatrix} \mathbf{B_r} \\ \mathbf{B_t} \end{bmatrix}, \quad \mathbf{C} = \begin{bmatrix} \mathbf{C_r} & \mathbf{C_t} \end{bmatrix}, \qquad (2.63)$$

where $\mathbf{A}$ is in one of the modal forms as (2.7) through (2.10). The truncated model has the state space realization as

$$\mathbf{P_r} = \left[\begin{array}{c|c} \mathbf{A_r} & \mathbf{B_r} \\ \hline \mathbf{C_r} & \mathbf{D} \end{array}\right].$$

The state space matrices $\mathbf{A_r}$, $\mathbf{B_r}$ and $\mathbf{C_r}$ can also be achieved by the operation

$$\mathbf{A_r} = \mathbf{LAL}^{\mathrm{T}}, \quad \mathbf{B_r} = \mathbf{LB}, \quad \mathbf{C_r} = \mathbf{CL}^{\mathrm{T}},$$

where $\mathbf{L} = \left[\begin{array}{cc} \mathbf{I_{2k}} & \mathbf{0} \end{array}\right]$. This reduction is said to be modal model reduction since the state matrix $\mathbf{A}$ is one of the four modal forms [3, 24].

Theorem 2.7.1 (Skogestad and Postlethwaite [20])**.** *The difference between the full- and reduced-order models is*

$$\mathbf{P} - \mathbf{P_r} = \sum_{i=r+1}^{n} \frac{\mathbf{C}_i \, \mathbf{B}_i}{s - \omega_i^2}, \tag{2.64}$$

where r is the number of truncated states, ω_i is the i^{th} natural frequency of the system $\mathbf{P}$. The i^{th} modal input and output matrices $\mathbf{B}_i$ and $\mathbf{C}_i$ are of dimensions $2 \times N_u$ and $N_s \times 2$, respectively. The number of inputs and outputs are described by N_u and N_s, respectively.

Proof. If the state space realization $\mathbf{P}$ is given in one of the modal forms (2.7) through (2.10), the state matrix $\mathbf{A}$ can be diagonalized such that

$$\begin{aligned} \mathbf{A} &= \mathrm{diag}\left(\begin{array}{cccc} \omega_1^2, & \omega_1^2, & \ldots & \omega_n^2, \quad \omega_n^2 \end{array} \right), \\ \mathbf{B} &= \left[\begin{array}{cccc} \mathbf{B}_1^{\mathrm{T}} & \mathbf{B}_1^{\mathrm{T}} & \ldots & \mathbf{B}_n^{\mathrm{T}} \end{array} \right]^{\mathrm{T}}, \\ \mathbf{C} &= \left[\begin{array}{cccc} \mathbf{C}_1 & \mathbf{C}_2 & \ldots & \mathbf{C}_n \end{array} \right], \end{aligned}$$

If the natural frequencies are ordered as $\omega_1^2 < \omega_2^2 < \ldots$ and first r states are retained,

then the truncated system in (2.63) has the state space realization

$$\begin{aligned}
\mathbf{A_t} &= \text{diag}\left(\begin{array}{cccc} \omega_{r+1}^2, & \omega_{r+1}^2, & \ldots & \omega_n^2, \quad \omega_n^2 \end{array} \right), \\
\mathbf{B}_t &= \left[\begin{array}{cccc} \mathbf{B}_{r+1}^{\mathrm{T}} & \mathbf{B}_{r+2}^{\mathrm{T}} & \ldots & \mathbf{B}_n^{\mathrm{T}} \end{array} \right]^{\mathrm{T}}, \\
\mathbf{C}_t &= \left[\begin{array}{cccc} \mathbf{C}_{r+1} & \mathbf{C}_{r+2} & \ldots & \mathbf{C}_n \end{array} \right],
\end{aligned}$$

for which the transfer function is given by Equation (2.64). □

Remark. Note that the difference (the error between the full-order and truncated models) depends on both the residues $\mathbf{C}_i\mathbf{B}_i$ and the distance of ω_i^2 from the imaginary axis. For flexible structures, however, the error of the mode decreases monotonically as the index i increases. That is, the faster the mode is, the smaller is ratio between $\mathbf{C}_i\mathbf{B}_i$ and ω_i^2 [3, 20, 24].

3. OPTIMIZATION AND I/O SELECTION

3.1. Review on Different I/O Selection Criteria

The optimal location selection techniques can be roughly grouped into two main categories. First type of methods uses closed-loop objective criteria, whereas second group selects open-loop optimization metric without designing a feedback controller. The latter can be preferred in some cases where a controller design stage takes much computation time. However, open-loop criteria based approach may exhibit great deviations, when the controller is added to the system.

Beside this simple categorization of the actuator and sensor location selection methods, all of the methods are desired to posses some certain properties for a successful optimal placement.

3.1.1. Desired Properties of Input/Output Selection Methods

According to the review paper [25], an input/output selection method should have the following desired properties.

Well-founded: The selection technique must give the relation between the measured outputs $\mathbf{y}$ and the control inputs $\mathbf{u}$ clearly. If one applies the method to a physical application, the change in both the system input variables $\mathbf{u}$ and the controller input variables $\mathbf{y}$ should affect the control goals.

Efficient: As the number of the inputs $\mathbf{u}$ and the outputs $\mathbf{y}$ increases, the number of the candidate input/output sets increases more rapidly. Hence, the selection method is desired to solve the best location selection problems quickly.

Effective: An input/output selection method is said to be effective if the combinations, for which the control goals cannot be obtained, are eliminated. These com-

binations are called nonviable input/output sets.

Generally Applicable: An input/output selection method is desired to be applicable to every control problem which can be put into the general control configuration in Figure 1.1.

Rigorous: Viable input/output sets must be determined rigorously. The more rigorous the selection method is, the less is the number of available viable sets. For instance, a selection technique for choosing robustly stable candidates is said to be more rigorous than a method for obtaining nominal stable plants.

Quantitative: A qualitative input/output method gives only a binary answer about viability of an input/output set. It says only "yes, the configuration is viable" or "no, this set is not viable" whereas a quantitative approach can include information about the strength of a corresponding candidate set. This property is extremely desired since otherwise one cannot compare the candidate input/output sets.

Controller independent: The input/output selection method can identify some sets as viable for which, however, there is not any controller meeting the initial control specifications. Such methods require a check for the existence of controllers and are therefore controller dependent.

Direct: For the selection of the optimal location of actuators and sensors there could be an infinite number of combinations. In such problems an exhaustive candidate by candidate search becomes not doable. Therefore, the search method is desired to be direct so that it obtains the best location directly without dealing with each candidate.

3.1.2. Different I/O Selection Criteria

In the review paper [25], many input/output selection methods are discussed and grouped in different ways.

3.1.2.1. State Controllability and State Observability. Consider Figure 1.1, in which the plant $\mathbf{G}$ consists of four blocks as

$$\mathbf{G} := \begin{pmatrix} \mathbf{G_{zw}} & \mathbf{G_{zu}} \\ \mathbf{G_{yw}} & \mathbf{G_{yu}} \end{pmatrix}.$$

The plant $\mathbf{G}$ is finite-dimensional, linear, time-invariant and continuous time. The lower right part of the plant $\mathbf{G}$ is denoted by $\mathbf{G_{yu}}$ and has the state space description

$$\dot{\mathbf{x}} = \mathbf{A}\mathbf{x} + \mathbf{B}\mathbf{u}, \tag{3.1}$$

$$\mathbf{y} = \mathbf{C}\mathbf{x} + \mathbf{D}\mathbf{u}. \tag{3.2}$$

The dynamic system (3.1) or the pair $(\mathbf{A}, \mathbf{B})$ is state controllable if, for any given initial state $\mathbf{x}_0$, any time $t_e > 0$, any final state $\mathbf{x}_e$ there exists an input $\mathbf{u}(t)$ such that $\mathbf{x}(t_e) = \mathbf{x_e}$.

The dynamic system (3.1) and (3.2) or the pair $(\mathbf{C}, \mathbf{A})$ is state observable if, for any time $t_e > 0$, the initial state $\mathbf{x}_0$ can be determined from the time history of the input $\mathbf{u}(t)$ and the output $\mathbf{y}(t)$ in the interval $[0, t_e]$.

These are basic definitions of state controllability and state observability. Although some modified versions are also introduced which exhibit a quantitative nature, the state controllability and the state observability are both "binary" properties of a physical system. That is, a system is state controllable or not. These properties of a system can be checked in various ways such as controllability/observability Gramians, matrices, etc. [20, 21].

A naive and simple approach for input/output selection is to accept configurations which are both state controllable and state observable. However, in literature there are few optimal selection methods based on this simple idea. Quantitative measures of controllability and observability are preferred since they can give more information for comparing the different combinations of actuator and sensor locations.

Among the techniques, which are used for checking controllability and observability, Gramians can serve as a more rigorous quantitative measure.

For optimal actuator and sensor location selection, Georges [26] defines transient controllability and observability Gramians at a time T as

$$\mathbf{W_c}(\mathbf{C}, T) = \int_0^T \mathbf{e}^{\mathbf{A}t}\mathbf{B}\mathbf{B}^{\mathrm{T}}\mathbf{e}^{\mathbf{A}^{\mathrm{T}}t}\,\mathrm{d}t,$$
$$\mathbf{W_o}(\mathbf{C}, T) = \int_0^T \mathbf{e}^{\mathbf{A}^{\mathrm{T}}t}\mathbf{C}^{\mathrm{T}}\mathbf{C}\mathbf{e}^{\mathbf{A}t}\,\mathrm{d}t.$$

Optimal sensor location is the solution of a integer programming problem of the form

$$\max_{c_{i,j}\in\{0,1\},\forall\, i=1:p, j\in\{S\}} \underline{\lambda}(\mathbf{W_o}(\mathbf{C}, T)) \tag{3.3}$$
$$\text{subject to } \sum_{j\in S} c_{i,j} = 1, \quad \forall\, i = 1:p, \tag{3.4}$$

where $\underline{\lambda}(\mathbf{W_o}(\mathbf{C}, T))$ is the minimum eigenvalue of the transient observability Gramian $\mathbf{W_o}(\mathbf{C}, T)$ at a time T. The $(i,j)^{\text{th}}$ element of the output matrix $\mathbf{C}$ is denoted by $c_{i,j}$. The configuration of sensor locations is given by $c_{i,j}$. The number of sensors is p, and S is the set of indices corresponding to states which can be measured.

According to Equation (3.3) the best sensor location is the configuration which maximizes the minimum eigenvalue of $\mathbf{W_o}(\mathbf{C}, T)$ at the time T. This configuration corresponds to the case where the output energy is at maximum for the given state.

For optimal actuator location selection a similar Gramian based technique is introduced. The energy to reach a given state has to be minimized by minimizing the maximum eigenvalue of $\mathbf{W_c}(\mathbf{C}, T)^{-1}$, the inverse of the controllability Gramian at a time T.

$$\min_{b_{i,j}\in\{0,1\}, i\in\{A\}, \forall\, j=1:m} \overline{\lambda}\left(\mathbf{W_c}(\mathbf{B}, T)^{-1}\right) \tag{3.5}$$

$$\Leftrightarrow$$

$$\max_{b_{i,j}\in\{0,1\},i\in\{A\},\forall\ j=1:m} \underline{\lambda}\left(\mathbf{W_c}(\mathbf{B},T)\right) \tag{3.6}$$

$$\text{subject to} \sum_{i\in A} b_{i,j} = 1, \quad \forall\ j = 1:m \tag{3.7}$$

In (3.5), $\overline{\lambda}(\mathbf{W_c}(\mathbf{B},T))$ is the maximum eigenvalue of the inverse of the transient controllability Gramian $\mathbf{W_c}(\mathbf{B},T)$ at a time T. The $(i,j)^{\text{th}}$ element of the input matrix $\mathbf{B}$ is denoted by $b_{i,j}$, which gives configuration of the actuator locations. The number of actuators is given by m, and A is the set of indices corresponding to states which can be actuated.

Hać and Liu [27] have dealt with optimal placement of actuators and sensors of flexible structures which are exposed to external transient and persistent disturbances. They have developed certain criteria which contain some measures of controllability and observability Gramians. They provide some Gramian based energy expressions which are result of their criteria designed to obtain a balance between the global response of the system and response of the weakest controlled/observed mode.

Hać and Liu [27] model continuous systems by the general wave equation [28]

$$M(P)\frac{\partial^2 w(P,t)}{\partial t^2} + 2\zeta[M(P)L]^{1/2}\left[\frac{\partial w(P,t)}{\partial t}\right] + L[w(P,t)] = F(P,t), \tag{3.8}$$

where $w(P,t)$ is the displacement of the structure as a function of spatial variable $P \in D$ and time t. The domain over which the wave equation is valid is denoted by D and $F(P,t)$ describes the external forces. The linear differential operator for the spatial variable P is L, and $M(P)$ gives the mass distribution. There are p point force actuators located at points P_j $(j = 1, 2, \ldots, p)$.

Introducing the modal coordinates, Equation (3.8) can be replaced by the set of ordinary differential equations

$$\ddot{\eta}_i + 2\zeta\omega_i\dot{\eta}_i + \omega_i^2\eta_i = \sum_{j=1}^{p}\phi_i(P_j)f_j(t), \quad \forall\ i = 1:n. \tag{3.9}$$

The state space representation of Equation (3.9) reads as

$$\begin{aligned}\dot{\mathbf{x}} &= \mathbf{A}\mathbf{x} + \mathbf{B}\mathbf{u},\\ \mathbf{y_d} &= \mathbf{C_d}\mathbf{x}, \quad \text{or}\\ \mathbf{y}_v &= \mathbf{C}_v\mathbf{x},\end{aligned}$$

where the state vector $\mathbf{x}$, the input vector $\mathbf{u}$, the state matrix $\mathbf{A}$, the input matrix $\mathbf{B}$, the displacement output matrix $\mathbf{C_d}$ and the velocity output matrix $\mathbf{C}_v$ are

$$\begin{aligned}
\mathbf{x} &= \begin{bmatrix} \dot{\eta}_1 & \omega_1\eta_1 & \dots & \dot{\eta}_n & \omega_n\eta_n \end{bmatrix}^{\mathrm{T}},\\
\mathbf{u} &= \begin{bmatrix} f_1 & f_2 & \dots & f_p \end{bmatrix}^{\mathrm{T}},\\
\mathbf{A} &= \operatorname{diag}(\mathbf{A_i}), \quad \mathbf{A_i} = \begin{bmatrix} -2\zeta_i\omega_i & -\omega_i \\ \omega_i & 0 \end{bmatrix},\\
\mathbf{B} &= \begin{bmatrix} \Phi_1(P_1) & \dots & \Phi_1(P_p) \\ 0 & \dots & 0 \\ \vdots & \vdots & \vdots \\ \Phi_n(P_1) & \dots & \Phi_n(P_p) \\ 0 & \dots & 0 \end{bmatrix},\\
\mathbf{C_d} &= \begin{bmatrix} 0 & \Phi_1(P_1)/\omega_1 & \dots & 0 & \Phi_n(P_1)\omega \\ 0 & \Phi_1(P_2)/\omega_1 & \dots & 0 & \Phi_n(P_2)\omega \\ \vdots & \vdots & & \vdots & \vdots \\ 0 & \Phi_1(P_r)/\omega_1 & \dots & 0 & \Phi_n(P_r)\omega \end{bmatrix},\\
\mathbf{C}_v &= \begin{bmatrix} 0 & \Phi_1(P_1)/\omega_1 & \dots & 0 & \Phi_n(P_1)\omega \\ 0 & \Phi_1(P_2)/\omega_1 & \dots & 0 & \Phi_n(P_2)\omega \\ \vdots & \vdots & & \vdots & \vdots \\ 0 & \Phi_1(P_r)/\omega_1 & \dots & 0 & \Phi_n(P_r)\omega \end{bmatrix},
\end{aligned}$$

respectively.

Using the state space model, Hać and Liu [27] discuss transient and persistent disturbance cases. In both of them the control energy to bring the system to the

desired states can be expressed in terms of controllability Gramian $\mathbf{L_c}$. Since the flexible structures exhibit small damping rations ($\zeta_i << 1 \; \forall \; i = 1 : n$) and have well separated resonance frequencies, the controllability Gramian has a simple diagonal form. "Well separated natural frequencies" means that the frequency response of the i^{th} mode at the i^{th} resonance frequency is always much higher than the frequency responses of other modes at the i^{th} resonance frequency [3]. In this case, the diagonal blocks of $\mathbf{L_c}$ become

$$L_{ii} = \text{diag}\left(\frac{\beta_{ii}}{4\zeta_i\omega_i}, \frac{\beta_{ii}}{4\zeta_i\omega_i}\right), \quad \text{where} \quad \beta_{ij} = \sum_{q=1}^{p} \Phi_i(P_q)\Phi_j(P_q).$$

Since the same or similar controllability and energy expressions appear for flexible structures exposed to both persistent and transient disturbances, a single actuator placement criterion can be proposed as

$$PI' = \left(2\sum_{i=1}^{n} E_i\right) \sqrt[n]{\prod_{i=1}^{n}(E_i)}, \quad \text{where} \quad E_i = \beta_{ii}/4\zeta_i\omega_i. \tag{3.10}$$

The performance index (3.10) is chosen according to simulations the authors [27] have made and is said to give a good balance between the importance of all modes. The first term of the optimization index (3.10) describes the total energy of the system, which is dominated by lower order modes. As the order of modes gets higher, the energy decreases. The second term in Equation (3.10) under the root sign gives a ellipsoid volume in an n dimensional space. This term vanishes when some high frequency modes become uncontrollable.

For sensor location selection a similar approach is used where observability Gramian is considered. Diagonally dominant observability Gramians are obtained for both transient and persistent disturbance cases. Finally a global optimal sensor location selection index, similar to that in Equation (3.10), is introduced.

Another study about optimal actuator and sensor location selection, which uses

controllability and observability Gramians, is the paper of Gawronski and Lim [29]. According to their definition, a flexible structure is a finite dimensional, controllable and observable linear system with small damping and complex poles. They derive some structural properties of flexible structures in modal and balanced coordinates. In balanced representation, the controllability and observability Gramians are equal, and diagonal entries of them are Hankel singular values which give a measure for controllability and observability.

The controllability Gramian $\mathbf{L_c}$ and observability Gramian $\mathbf{L_o}$ are the results of the Lyapunov equations

$$\mathbf{A}\mathbf{L_c} + \mathbf{L_c}\mathbf{A}^{\mathrm{T}} + \mathbf{B}\mathbf{B}^{\mathrm{T}} = \mathbf{0},$$
$$\mathbf{A}^{\mathrm{T}}\mathbf{L_o} + \mathbf{L_o}\mathbf{A} + \mathbf{C}^{\mathrm{T}}\mathbf{C} = \mathbf{0}.$$

If the state matrix $\mathbf{A}$ is stable, the resulting Gramians are positive definite. The state space realization of the system is said to be balanced if the controllability Gramian and the observability Gramian are equal and digonal, where the diagonal entries are the square of the Hankel singular values as

$$\mathbf{L_c} = \mathbf{L_o} = \mathbf{\Gamma}^2, \quad \mathbf{\Gamma} = \mathrm{diag}(\gamma_1, \gamma_2, \ldots, \gamma_n), \quad \gamma_i \geq 1, \quad \forall\, i = 1 : n,$$

where γ_i is the i^{th} Hankel singular value of the system.

If the system of concern fulfils the requirements of being a flexible structure, the following assumptions can be made which are used in the optimal actuator and sensor selection by means of Gramians:

In modal coordinates the controllability and observability Gramians are diagonally dominant such that off-diagonal terms can be neglected. Hence, they become

$$\mathbf{L_c} \cong \mathrm{diag}(\mathbf{L_{ci}}), \quad \mathbf{L_{ci}} \cong l_{ci}\mathbf{I_2}, \quad \mathbf{L_o} \cong \mathrm{diag}(\mathbf{L_{oi}}), \quad \mathbf{L_{oi}} \cong l_{oi}\mathbf{I_2},$$

where the product of the Gramians ($\mathbf{L_c}$ and $\mathbf{L_o}$) gives the Hankel singular values

$$\mathbf{L_c L_o} \cong \mathbf{\Gamma}^4 = \text{diag}(\gamma_1^4, \gamma_2^4, \ldots, \gamma_n^4). \tag{3.11}$$

Given a modal state space representation with matrices $(\mathbf{A_m}, \mathbf{B_m}, \mathbf{C_m})$, the balanced representation with matrices $(\mathbf{A_b}, \mathbf{B_b}, \mathbf{C_b})$ can be obtained as

$$(\mathbf{A_b}, \mathbf{B_b}, \mathbf{C_b}) \cong (\mathbf{A_m}, \mathbf{R_{mb}^{-1}} \mathbf{B_m}, \mathbf{C_m R_{mb}}),$$

where

$$\begin{aligned}
&\mathbf{R_{mb}} = \text{diag}(\mathbf{R_{mb}}_i), \\
&\mathbf{R_{mb}}_i = r_i \mathbf{I_2}, \quad \forall\, i = 1 : n_2, \\
&r_i = \left(\frac{l_{ci}}{l_{oi}} \right)^{1/4}.
\end{aligned}$$

Given the natural modes ϕ_i ($\forall\, i = 1 : n_2$) of a flexible structure in modal coordinates, the balanced modes ϕ_{bi} are obtained as

$$\phi_{bi} \cong r_i \phi_i, \quad \forall\, i = 1 : n_2.$$

The balanced state matrix for a flexible structure has the form

$$\begin{aligned}
\mathbf{A_b} &\cong \text{diag}(\mathbf{A_{bi}}), \quad \forall\, i = 1 : n_2, \\
\mathbf{A_{bi}} &= \begin{bmatrix} -\zeta_i & \omega_i \\ -\omega_i & -\zeta_i \omega_i \end{bmatrix}.
\end{aligned}$$

The actuator and sensor placement technique is developed according to balanced realizations of flexible structures. Gawronski and Lim [29] obtain a relationship between Hankel singular values and actuator/sensor locations in balanced coordinates. Using the balanced representation of flexible structures they define root mean square (r.m.s) law of Hankel singular values, which says that the squares of the Hankel singular values

of a structure with multiple actuator and sensors are approximately the r.m.s sum of squares of Hankel singular values of structures with a single actuator and sensor pair as

$$\gamma_k^2 \cong \left(\sum_{i=1}^{p} \sum_{j=1}^{q} \gamma_k^4(i,j) \right)^{1/2}, \quad \forall\, k = 1 : n_2, \tag{3.12}$$

where p, q and $\gamma_k(i,j)$ are the number of actuators, the number of sensors and the Hankel singular value of k^{th} balanced mode for the i^{th} actuator and j^{th} sensor, respectively.

The next step is to derive a placement strategy. Since actuator location selection, sensor location selection and joint actuator and sensor selection problems are similar, for simplicity the authors [29] handle the actuator placement only. Equation (3.12) becomes then

$$\gamma_k^4 \cong \sum_{i=1}^{p} \gamma_k^4(i).$$

The placement index $\sigma_k^2(i)$ of the i^{th} actuator at the k^{th} mode is defined as

$$\sigma_k^2(i) = \frac{\gamma_k^4(i)}{\gamma^4(N)}, \quad \sigma_k^2(i) \leq 1, \quad \text{where} \quad \gamma^4(N) = \sum_{k=1}^{n_2} \sum_{i=1}^{N} \gamma_k^4(i).$$

The global coefficient for N candidate locations is denoted by $\gamma_k^4(i)$. It gives the contribution of each Hankel singular value $\gamma_k(i)$ for all candidates of actuators and all modes.

The controllability and observability of the k^{th} mode is measured in terms of k^{th} modal index σ_{mk}^2, which equals to

$$\sigma_{mk}^2(p) = \sum_{i=1}^{p} \sigma_k^2(i), \quad \sigma_{mk}^2 \leq 1, \quad \forall\, k = 1 : n_2.$$

The i^{th} actuator index is defined to give the controllability and observability properties of the i^{th} actuator as

$$\sigma_a^2(i) = \sum_{k=1}^{n_2} \sigma_k^2(i), \quad \sigma_a^2 \leq 1, \quad \forall\, i = 1 : p.$$

The actuators with small index $\sigma_a^2(i)$ are to be removed. The controllability and observability of modes with small index σ_{mk}^2 should be eliminated or improved by changing the position of the actuator and the sensor location.

3.1.2.2. Right Half Plane Zeros. A multi-variable system with the transfer function $G(s)$ has its zeros z_i as the values of s where $G(s)$ loses rank. For SISO systems, $G(s)$ has the rank one, and at zeros z_i the rank of the system reduces to zero. Hence, for a SISO system $G(z_i) = 0$. The general definition of zeros is given by Skogestad and Postlethwaite [20] as follows:

If the rank of the system $G(s)$ at z_i is less than the normal rank of $G(s)$, z_i is a zero of $G(s)$. For n_z zeros of the system $G(s)$, the associated zero polynomial is expressed as $z(s) = \sum_{i=2}^{n_z}(s - z_i)$.

Multivariable zeros are called *transmission zeros* in literature [30, 31]. Zeros can be computed either from transfer functions or state space realizations. In the former, the transfer function which corresponds to a minimal realization of the system is obtained. The minors of the order r are generated, where r is the nominal rank of the transfer function $G(s)$. The greatest common divisor of all the numerators of the minors is the zero polynomial $z(s)$. If one needs to compute zeros from state space description of the system, the following state space equations must be achieved:

$$P(s) \begin{bmatrix} \mathbf{x} \\ \mathbf{u} \end{bmatrix} = \begin{bmatrix} \mathbf{0} \\ \mathbf{y} \end{bmatrix}, \text{ where } P(s) = \begin{bmatrix} s\mathbf{I} - \mathbf{A} & -\mathbf{B} \\ \mathbf{C} & \mathbf{D} \end{bmatrix}. \tag{3.13}$$

The zeros are the values of s at which the matrix $P(s)$ in Equation (3.13) has zero output for some non-zero input. At zeros the rank of $P(s)$ is smaller than the normal

rank of $P(s)$. Zeros are the non-trivial solutions of the problem

$$(z_i \mathbf{I_g} - \mathbf{M}) \begin{bmatrix} x_{z_i} \\ u_{z_i} \end{bmatrix} = 0, \tag{3.14}$$

$$\mathbf{M} = \begin{bmatrix} \mathbf{A} & \mathbf{B} \\ \mathbf{C} & \mathbf{D} \end{bmatrix}, \quad \mathbf{I_g} = \begin{bmatrix} \mathbf{I} & \mathbf{0} \\ \mathbf{0} & \mathbf{0} \end{bmatrix}.$$

Right Half Plane zeros limit the closed-loop performance for both SISO and MIMO control systems. For a SISO single DOF control system setup, the performance measure is given in terms of magnitude bounds on the sensitivity function $S(s) = 1/(1+P(s)K(s))$. That is, $|S(s)|$ needs to be small at low frequencies for good enough disturbance rejection properties, and the bandwidth should be as large as possible. However, the presence of RHP-zeros causes the bandwidth to be smaller. For MIMO systems, the phenomena of RHP-zeros are similar and even more severe. Skogestad and Postlethwaite [20], Zhou et al. [21], Freudenberg and Looze [32], Sidi [33], Havre and Skogestad[34] study the performance limitations because of RHP-zeros by using different performance specifications. Holt and Morari [35], Morari et al. [36] discuss the effect of RHP-zeros on the achievable closed-loop performance by introducing a new tool called *zero directions*, which can be used to evaluate the feasibility of different decouplers, inverse-based controllers of the form $C(s) = P^{-1}(s)K(s)$. (See [31] for more details.)

Since the open-loop RHP-zeros of a system play an important role in the performance of the closed-loop system, a simple input/output selection criterion would reject the actuator and sensor configurations where RHP-zeros cause the performance limitations to decrease under a desired level. Hovd and Skogestad [37] use this principal as a part of their selection criteria of the manipulated and measured variables for their chemical plant.

Maghami and Joshi [38] develop an optimal actuator and sensor location selection

technique for large-order flexible space structure, where the placement of actuators and sensors is optimized in order to move the zeros in right-half-plane to the left-half-plane.

3.1.2.3. Input-Output Controllability. A plant P is said to be input/output controllable if a desired performance level can be obtained. That is, the performance outputs, which consist of both physical deformations of the system and outputs, can be kept under certain limits, in the presence of bounded uncertainties, references, disturbances and measurement and sensor noises.

There are different measures of input/output controllability of a plant. Most of them are based on singular value decomposition (SVD). Given a complex $l \times m$ matrix P, the singular value decomposition of P has the form

$$P = \underbrace{\begin{bmatrix} U_1 & U_2 \end{bmatrix}}_{U} \underbrace{\begin{bmatrix} \Sigma_1 & 0 \\ 0 & 0 \end{bmatrix}}_{\Sigma} \underbrace{\begin{bmatrix} V_1^{\mathrm{H}} \\ V_2^{\mathrm{H}} \end{bmatrix}}_{V^{\mathrm{H}}}, \tag{3.15}$$

where U and V are the unitary matrices of dimensions of $l \times l$ and $m \times m$, which form orthonormal bases for the column space of P and the row space of P, respectively. Σ_1 is diagonal matrix of the dimension $k = min(l, m)$ and consists of real nonnegative singular values σ_i, which are found as

$$\sigma_i(P) = \sqrt{\lambda_i(P^{\mathrm{H}}P)}, \quad \forall\, i = 1 : k. \tag{3.16}$$

The input direction U_1 and the output direction V_1 are related to nonzero singular values and are therefore described as the most important directions.

Using the general definition of singular value decomposition, Euclidean condition number κ and pseudo inverse $P^{\dagger}$ of a complex matrix P are given as

$$\kappa(P) = \frac{\overline{\sigma}(P)}{\underline{\sigma}(P)},$$

$$P^{\dagger} = \sum_{i=1}^{r} \frac{1}{\sigma_i(P)} V_i U_i^{\mathrm{H}}.$$

3.1.2.4. The Minimum Singular Value. The frequency dependent minimum singular value $\underline{\sigma}(P)$ of a plant P can be used for input/output selection purposes. Generally, actuator and sensor configurations with a large $\underline{\sigma}(P)$ are preferred. The reasons can be summarized as follows:

- According to [20], a MIMO system which has as many inputs as outputs is input/output uncontrollable if $\underline{\sigma}(P(j\omega)) = 0 \quad \forall\, \omega$. In case of $\underline{\sigma}(P) = 0$, not all of the outputs of the plant can be controlled independently.
- Another reason is the presence of input magnitude limitations. In such cases, Morari [39] suggests to choose combinations with large $\underline{\sigma}(P)$ to improve the tracking following (r) and disturbance rejection (d) properties of a plant.

3.1.2.5. The Maximum Singular Value. Most of the input/output controllability measures are applied to physical plants such as P in Figure 3.1. However, the maximum singular value $\overline{\sigma}$ may be used as a measure for a generalized plant G in general control configurations (see Figure 1.1).

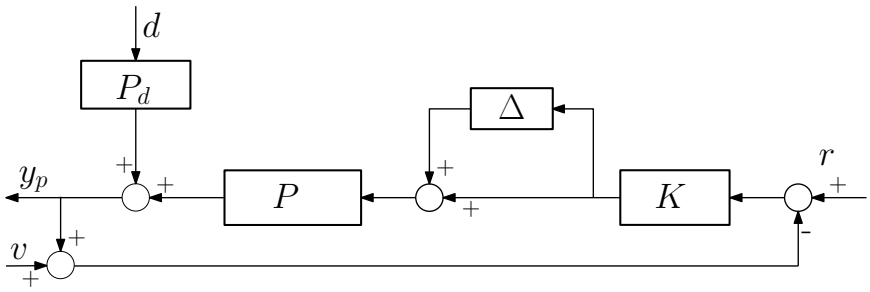

Figure 3.1. Input/output Controllability

The transfer function $P(s)$ in Figure 3.1 gives the contribution of the control inputs to the outputs of the system. The other transfer function $P_d(s)$ describes the effect of disturbances on the system. The deformations or the outputs become $y_P = Pu + P_d d$. For perfect control, $u = P^{\dagger} P d$. So, the closed error $e = r - y_P = M_d d + M_v v$. Generally it is desired to select control inputs and sensor measurements in such a

combination that $\overline{\sigma}(M_d)$ and $\overline{\sigma}(M_v)$ are kept as small as possible in the frequency range of concern. This idea can also be applied to the general control configuration in Figure 1.1.

Arabyan et al. [2] deal with the physical plant $P(s)$. They obtain an expression for the residual deformation of the system. Maximum singular value of this expression needs to be kept small according to their best location selection criteria. The actuator and sensor location with the smallest residual deformation is the best place for the point actuators.

3.1.2.6. The Condition Number. The condition number is defined as the ratio between the maximum singular value and the minimum singular value

$$\kappa(P) = \frac{\overline{\sigma}(P)}{\underline{\sigma}(P)}.$$

General idea for optimal input/output selection is to choose the actuator sensor configuration which results in the smallest condition number of the corresponding plant or system.

Morari [39] deals with plants which are shown in Figure 3.1 and finds out that plants with smaller condition numbers are more robust to unstructured multiplicative uncertainty. Similar statements can be found in the book of Skogestad and Postlethwaite [20].

Modified types of condition numbers also appear in different papers of scientists. Skogestad and Morari [40] define the following expression as the disturbance condition number

$$\kappa_{d_k}(P, P_d) = \frac{\|P^{-1}P_{d_k}\|_2}{\|P_{d_k}\|_2}\overline{\sigma}(P),$$

where $1 \leqslant \kappa_{d_k}(P, P_d) \leqslant \kappa(P)$, d_k is the k^{th} disturbance in Figure 3.1, P_{d_k} is the k^{th}

column of P_d and $\|.\|_2$ denotes the Euclidean 2-norm. Input/output sets with smaller disturbance condition numbers ($\kappa_{d_k}(P, P_d)$'s) are preferred due to less input magnitude required to reject the disturbance in the desired k^{th} direction.

Another type of condition number, which is very similar to the input disturbance number $\kappa_{d_k}(P, P_d)$, is the input disturbance alignment introduced by Cao and Rossiter [41] and is given as

$$\eta_{d_k}(P, P_d) = \frac{\|PP^{\dagger}P_{d_k}\|_2}{\|P_{d_k}\|_2},$$

where $0 \leqslant \eta_{d_k}(P, P_d) \leqslant 1$. Input/output configurations, the input disturbance alignments of which are close to one, have good disturbance rejection properties.

3.1.2.7. The Relative Gain Array. Another well known input/output controllability measure is the relative gain array (RGA), which is defined as

$$\Lambda(P(j\omega)) = P(j\omega).*(P^{-1}(j\omega))^{\mathrm{T}}, \tag{3.17}$$

where "$.*$" describes element by element matrix multiplication. Equation (3.17) is defined for square matrices. For nonsquare plants, the ordinary inverse can be replaced with preudo inverse. RGA is firstly used by Bristol [42]. He introduced this quantity to measure the interactions in decentralized control systems.

The general selection criterion is to reject plants with large RGA elements, since RGA is a measure of interactions in decentralized control systems, and such plants are difficult to be controlled.

Furthermore, studies of Hovd and Skogestad [43] and Skogestad and Morari [44] propose that systems with large RGA are sensitive to input multiplicative uncertainties if a plant-inverting controller is applied to the plant.

3.1.2.8. Efficiency of Manipulation and Estimation. In input/output selection the objective is to find the best position of actuators and sensors. In fact, the location selection of actuators and sensors can be dealt with separately. The problem of actuator positioning is to find the configuration of actuators at which the actuators, with limited energy, can manipulate the system as desired. In efficiency of manipulation, an input set dependent cost function is minimized in terms of the input energy. Similar to that for sensor location selection, an output set dependent cost function is minimized (efficiency of estimation). If the cost function, which is to be minimized, depends on both input and output sets, the two objectives, (optimum actuator location selection and optimum sensor location selection), can be considered as a single one. This is the joint efficiency of manipulation and estimation.

3.1.2.9. Efficiency of Manipulation. Al-Sulaiman and Zaman [45] design a full state feedback controller by pole placement for each actuator combination and then evaluate the cost function

$$J_u = \int_0^{t_e} \left(x(t)^{\mathrm{T}} Q x(t) + u(t)^{\mathrm{T}} R u(t) \right) \, \mathrm{d}t$$

for the time interval $[0, t_e]$, where $Q = Q^{\mathrm{T}} \geq 0$ and $R = R^{\mathrm{T}} \geq 0$ are weights. The actuator combination, which results in the smallest J_u, is the best placement for a specified input set.

Cao, Biss and Perkins [46] deal with bonded input selection for nonlinear systems. In their work the cost function takes the form

$$J_u = \int_0^{t_e} \left((z(t) - z_r)^{\mathrm{T}} Q (z(t) - z_r) \right) \, \mathrm{d}t, \tag{3.18}$$

where z_r is the reference value set for the controlled variables z, and Q is the positive definite weighting matrix that consists of diagonal entries only.

3.1.2.10. Efficiency of Estimation. In the efficiency of estimation, the cost function J_y to be minimized is an integral which includes some functions of measurements (sensor outputs). Morari and Stephanopoulos [47] want to minimize errors in the measurements.

3.1.2.11. Joint Efficiency of Manipulation and Estimation. For joint efficiency of manipulation and estimation Norris and Skelton [48] use a cost function in the linear quadratic Gaussian control form as

$$J_{uy} = E\left(\int_0^\infty \left(z(t)^{\mathrm{T}} Q z(t) + u(t)^{\mathrm{T}} R u(t)\right)\, \mathrm{d}t\right), \tag{3.19}$$

where $z = Fx$ and $E(.)$ is the expectation operator. Mellefont and Sargent [49] use a cost function similar to LQG cost function (3.19) for online switching between actuator configurations.

3.2. Gradient Based Optimization Techniques

Generally, in descent methods, one tries to produce a minimizing sequence $\mathbf{x}^{(k)}$, $k = 1, 2, 3, \ldots$ such that

$$\mathbf{x}^{(k+1)} = \mathbf{x}^{(k)} + t^{(k)} \boldsymbol{\Delta}\mathbf{x}^{(k)},$$

where $t^{(k)} > 0$ is a scalar quantity that is called *step size* or *step length* at the k^{th} iteration, and $\boldsymbol{\Delta}\mathbf{x}^{(k)} \in \mathbf{R}^n$ is *search direction*. Since $f(\mathbf{x}^{(k+1)}) < f(\mathbf{x}^{(k)})$ is always valid except the optimal location $\mathbf{x}_{opt}^{(k)}$, these techniques are called descent methods. In a general descent method, a starting point $\mathbf{x}^{(0)} \in \mathbf{dom}\, f$ (which means that the initial point lies in the domain of the objective function) is chosen and the following steps are repeated for each iteration until the desired optimal point is reached.

1. Determine the descent direction $\boldsymbol{\Delta}\mathbf{x}^{(k)}$ for the k^{th} iteration.
2. Choose a positive step size $t^{(k)}$ (Line search step).

3. Obtain the next iteration's point $\mathbf{x}^{(k+1)} = \mathbf{x}^{(k)} + t^{(k)}\boldsymbol{\Delta}\mathbf{x}^{(k)}$.

If the negative gradient of the objective function $f(\mathbf{x}^{(k)})$ is selected as the search direction $\boldsymbol{\Delta}\mathbf{x}^{(k)} = -\boldsymbol{\nabla} f(\mathbf{x}^{(k)})$, the corresponding unconstrained minimization technique is called *gradient descent method*.

In the second step of an descent method (line search), there are two options available for step size selection:

- Exact line search: Step length t (dropping the superscript (k) for a simpler notation) is determined such that

$$t = \text{argmin}_{(s\geq 0)} f\left(\mathbf{x}^{(k)} + s\,\boldsymbol{\Delta}\mathbf{x}^{(k)}\right).$$

- Backtracking line search: Step size is chosen inexact, but "enough" to minimize f. Step size t is selected by the following way: Given a descent direction $\boldsymbol{\Delta}\mathbf{x}^{(k)}$, with $\hat{\alpha} \in (0, 0.5)$, $\hat{\beta} \in (0, 1)$ and $t := 1$. Take the step size $t := \hat{\beta}t$ as long as $f(\mathbf{x}^{(k)} + \boldsymbol{\Delta}\mathbf{x}^{(k)}) > f(\mathbf{x}^{(k)}) + \hat{\alpha}\, t\, \boldsymbol{\nabla} f(\mathbf{x}^{(k)})^{\mathrm{T}}\, \boldsymbol{\Delta}\mathbf{x}^{(k)}$ [50].

3.2.1. Constraints on Optimization Variables

In structural optimization it is common to formulate a minimization problem with constraints. The constraints may be functions of the design variables since there are physical limitations for these quantities (e.g. the dimensions of the strucutre may not exceed some value) or some specifications which are desired for certain engineering purposes.

Basically, an optimization problem with n_e numbers of equality constraints and n_g numbers of inequality constraints can be given as

$$\begin{aligned} &\text{minimize } f(\boldsymbol{x}) \\ &\text{subject to } h_i(\boldsymbol{x}) \;=\; 0, \quad \forall\, i = 1 : n_e, \end{aligned}$$

$$g_j(\boldsymbol{x}) \;\geq\; 0, \quad \forall\, j = 1 : n_g,$$

where $\boldsymbol{x}$ describes the design variables such as the x- or/and y-coordinates of the actuator and sensor pairs [51, 52]. In cases with point actuator and sensors, the constraints may become simple bound limitations. That is, the actuator coordinate must be positive (lower limit) or less than the total length of the structure (upper limit). In these situations, the constraints may be eliminated since one can select a shorter step size not to exceed the limits.

However, if one uses piezoelectric pathes for actuating and sensing purposes, the need for constraints may become inevitable.

3.2.2. Zoutendik's Method of Feasible Directions

For unconstrained minimization it is usually enough to take the negative of the gradient of the optimization function as the search direction. Even in the presence of upper and lower bound constraints, taking shorter step sizes will allow the use of the gradient of the optimization metric. Whenever there are more complicated constraints, the gradient based search methods must be modified in such a way that their search direction is always feasible. That is, a small move in that direction may not violate any of the constraints.

Zoutendik's Method of Feasible Directions is one of the simplest approaches for constrained nonlinear programming. The basic idea of the technique is to make the current direction feasible by solving another direction-finding problem [51]:

$$\begin{aligned}
\min \quad & -\bar{\alpha} \\
\text{subject to} \quad & \mathbf{S}^{\mathrm{T}} \boldsymbol{\nabla} g_j(\boldsymbol{x}) + \theta_j \bar{\alpha} \leq 0, \quad \forall\, j = 1 : p, \\
& \mathbf{S}^{\mathrm{T}} \boldsymbol{\nabla} f(\boldsymbol{x}) + \bar{\alpha} \leq 0, \\
& -1 \leq s_i \leq 1, \qquad\qquad \forall\, i = 1 : n,
\end{aligned}$$

where $\mathbf{S}$, $\boldsymbol{\nabla} g_i$, $\boldsymbol{\nabla} f$, p and θ_j are the search direction, the gradient of i^{th} constraint, the gradient of the objective function, the number of active constraints and the weight for j^{th} constraint, respectively. If at the end of the current iteration a constraint is hit, that constraint is said to be active, and the search direction in the next iteration must be decided as the solution of the direction-finding problem.

3.2.3. Closed-loop $\mathcal{H}_2$-norm as Optimization Function

Let

$$P_c := \left[\begin{array}{c|c} \mathbf{A_c} & \mathbf{B_c} \\ \hline \mathbf{C_c} & \mathbf{D_c} \end{array}\right] \tag{3.20}$$

be the state space realization of the closed-loop system, where $\mathbf{A_c}$ is Hurwitz. That means, the real parts of all the eigenvalues of state matrix $\mathbf{A_c}$ is in the left half-plane ($\mathcal{R}(s) < 0$) so that P_c is stable.

For the optimal location selection, the square of the $\mathcal{H}_2$-norm of the closed-loop system is selected as the optimization criterion J, which can be given as

$$J = \|\mathbf{G_{zw}}\|_2^2 = \text{trace}\left(\mathbf{C_c L_c C_c^{\mathrm{T}}}\right). \tag{3.21}$$

In Equation (3.21) $\mathbf{L_c}$ is the Controllability Gramian of the closed-loop system and satisfies the Lyapunov equation

$$\mathbf{A_c L_c} + \mathbf{L_c A_c^{\mathrm{T}}} + \mathbf{B_c B_c^{\mathrm{T}}} = 0. \tag{3.22}$$

Denoting the location of the i^{th} actuator/sensor pair by the coordinate ξ_a^i, the partial derivatives of Equation (3.21) can be obtained as

$$\frac{\partial J}{\partial \xi_a^i} = \text{trace}\left(\frac{\partial \mathbf{C_c}}{\partial \xi_a^i}\mathbf{L_c C c^{\mathrm{T}}} + \mathbf{C_c}\frac{\partial \mathbf{L_c}}{\partial \xi_a^i}\mathbf{C c^{\mathrm{T}}} + \mathbf{C_c L_c}\frac{\partial \mathbf{C c^{\mathrm{T}}}}{\partial \xi_a^i}\right), \tag{3.23}$$

where $\partial \mathbf{A_c}/\partial \xi_a^i$ and $\partial \mathbf{C_c}/\partial \xi_a^i$ are the derivatives of the state matrix and the performance output matrix of the closed-loop system with respect to ξ_a^i, respectively.

By differentiating (3.22) with respect to the actuator/sensor locations ξ_a^i from $i = 1$ to N_u, $\partial \mathbf{L_c}/\partial \xi_a^i$ is achieved from

$$\mathbf{A_c Y} + \mathbf{Y A_c}^{\mathrm{T}} + \mathbf{Q_c} = \mathbf{0},$$

where $\mathbf{Y} := \dfrac{\partial \mathbf{L_c}}{\partial \xi_a^i}$ and $\mathbf{Q_c} := \dfrac{\partial \mathbf{A_c}}{\partial \xi_a^i}\mathbf{L_c} + \mathbf{L_c}\dfrac{\partial \mathbf{A_c}^{\mathrm{T}}}{\partial \xi_a^i} + \dfrac{\partial \mathbf{B_c}}{\partial \xi_a^i}\mathbf{B_c}^{\mathrm{T}} + \mathbf{B_c}\dfrac{\partial \mathbf{B_c}^{\mathrm{T}}}{\partial \xi_a^i}$.

Since the optimization function J is partially differentiable with respect to the locations ξ_a^i, different gradient based techniques can be applied for the optimal placement problem. Among these techniques gradient descent method can be easily applied to obtain the optimal locations [50, 53, 54].

In calculation of the derivative of the optimization metric J, one needs the partial derivatives of the state matrices $\mathbf{A}_c, \mathbf{B}_c, \mathbf{C}_c$ of the closed-loop system with respect to actuator/sensor locations ξ_a^i. Since these partial derivatives require open forms of controller matrices, which are introduced in upcoming chapters, the closed-loop state space matrix derivatives will be given in a separate chapter later in this thesi.

3.3. Steps of Unconstrained Optimization Procedure

A gradient based unconstrained optimization is utilized for the closed-loop optimal location selection of point actuator and sensor pairs. Although there are lower and upper bounds for the coordinates of actuator and sensor locations, violation of these constraints can be prevented by simply selecting smaller step sizes. The optimization procedure is made up of the following steps:

1. *Required Data*: The disturbance locations, the boundary conditions and the dimensions of the structure are given.
2. *Initial Guess*: The initial guesses $(\xi_a^1 \dots \xi_a^{N_u})$ are selected, where the objective

function and its gradient will be evaluated. To be used in step size selection, some optimization parameters are chosen.

3. *The physical structure modeling*: The structure is modeled and put into the first modal state space form with the matrices $\mathbf{A_m}$, $\mathbf{B_{m1}}$, $\mathbf{B_{m2}}$, $\mathbf{C_{m1}}$, $\mathbf{C_{m2}}$, $\mathbf{D_{m11}}$, $\mathbf{D_{m12}}$, $\mathbf{D_{m21}}$, $\mathbf{D_{m22}}$. The partial derivatives of the state space matrices are taken with respect to the current actuator and sensor locations.
4. *The generalized plant*: For the given signal weightings the state space matrices of the shaped plant are obtained. If the improved coprime controller or the improved low-authority $\mathcal{H}_\infty$-controller is selected, using the coordinate transformation the generalized plant is put into the first modal form with block diagonal state matrix. The state space matrices are $\mathbf{A}$, $\mathbf{B_1}$, $\mathbf{B_2}$, $\mathbf{C_1}$, $\mathbf{C_2}$, $\mathbf{D_{11}}$, $\mathbf{D_{12}}$, $\mathbf{D_{21}}$, $\mathbf{D_{22}}$. However, if MNRD approach is used, the generalized plant is not diagonalized since MNRD does not require ARE solutions.
5. *Controller Synthesis and Closed-loop System*: This step is skipped if MNRD-value is selected as the optimization metric. In the case of the improved coprime controller or the improved low-authority $\mathcal{H}_\infty$-controller, the corresponding ARE's are solved. Then, the closed-loop state space matrices $\mathbf{A_c}$, $\mathbf{B_c}$, $\mathbf{C_c}$, $\mathbf{D_c}$ are calculated.
6. *Objective Function and its Gradient*: In the case of MNRD-controller, the square of the optimistic $\mathcal{H}_2$-norm is set as the objective function J. The function value and the gradient of J with respect to actuator and sensor locations are calculated at the current point. If a controller is used, the square of the closed-loop $\mathcal{H}_2$-norm is selected as J.
7. *The New Actuator and Sensor Locations*: Using gradient of J, the search direction of the k^{th} iteration is established as $\mathbf{s}^{(k)} = \boldsymbol{\Delta}\mathbf{x}^{(k)}/\|\boldsymbol{\Delta}\mathbf{x}^{(k)}\|$, where $\boldsymbol{\Delta}\mathbf{x}^{(k)}$ is given in Equation (3.24). The next iteration's points become $\mathbf{x}^{(k+1)} = \mathbf{x}^{(k)} + t\,\mathbf{s}^{(k)}$, with t being the step size. The step size t is chosen according to the backtracking line search technique in [50]. If the difference $\|\mathbf{x}^{(k+1)} - \mathbf{x}^{(k)}\| < \epsilon$, the optimization procedure is stopped. Otherwise, the procedure is returned to the second step with the next actuator and sensor points.

The negative gradient of the objective function J is defined as

$$\mathbf{\Delta x}^{(k)} := -\left[\begin{array}{ccc} \dfrac{\partial J}{\partial \xi_a^1} & , \cdots , & \dfrac{\partial J}{\partial \xi_a^{N_u}} \end{array}\right]^{\mathrm{T}}, \tag{3.24}$$

where $\dfrac{\partial J}{\partial \xi_a^i}$ is the partial derivative of the objective function J with respect to i^{th} actuator and sensor pair.

3.4. Constraints for the Multiple Piezoelectric Actuator and Sensor Pairs

In the case of point actuator and sensor pairs, there exist only lower and upper bounds for the actuator and sensor locations. That is, the coordinates of the actuator/sensor locations must be greater than zero (lower bound) and less than the length of the beam or the plate (upper bound). Whenever these constraints are violated, decreasing step size will enable to avoid these types of constraints.

However in the case of the PZT actuator and sensor pairs, expressing the constraints in linear inequalities will simplify the optimization formulation.

In this study two groups of constraints are given. The constraints of the first group are bound constraints, which are used to limit the optimization variable to a range between a lower and an upper value. For instance, the x-coordinate of PZT pair must between $0 \times L$ and $(L - 2a) \times L$, where $2a$ and L are the length of the PZT pair and the length of the plate, respectively.

The bound constraints may not be violated in any case. All of them are given as $g_j^b(\boldsymbol{x}) < 0$, for $j = 1 : 2 \times n_c \times n_a$, where n_a are and the number of actuator and sensor pairs, respectively. The number n_c describes the coordinates a single pair has. For beams, n_c becomes one, and for plates two.

However, there is a need for another group of constraints, which will be valid only for some predefined conditions. To give an example, if two adjacent piezoelectric actuator and sensor pair become too close, the finite element between them might have unwanted dimensions. That is, its length can be much larger than its width (see Figure

3.4). If the second actuator is on the right of the first actuator (i.e., the x-coordinate of the actuator B is greater than the x-coordinate of the actuator A), the constraint

$$x_B - x_A > \frac{2a}{3},$$

where $2a$ is the length of the actuators A and B, may be utilized to avoid unwanted dimensions. This constraint prevents the length of any finite element to be less than $\frac{2a}{3}$. If the second actuator is on the left of the first actuator (i.e., the x-coordinate of the actuator B is less than the x-coordinate of the actuator A), the constraint changes to

$$x_A - x_B > \frac{2a}{3}.$$

Such a group of constraints, which are implemented in the optimization algorithm for multiple of PZT patches, are called *conditional constraints*.

Three types of conditional constraints are defined. The first type is required for preventing the disturbances acting on an unwanted location, i.e. too close to a side or corner of a PZT pair. The second type of conditional constraints is used to prevent distorted, badly scaled finite elements between two PZT pairs, whereas the third type is required for preventing PZT pairs to overlap each other.

3.4.1. Lower and Upper Bound Constraints

For a plate with two actuator and sensor pairs, the lower and upper bounds on the coordinates of the PZT patches are given by the definition below:

Definition 3.4.1 (Bound type constraints)**.** *The constraints, which must be satisfied so that the PZT patches are inside the feasible domain, are*

$$g_1^b(\boldsymbol{x}) = -x_1 + \epsilon < 0, \tag{3.25}$$

$$g_2^b(\boldsymbol{x}) = x_1 + 2a - \epsilon < 0, \tag{3.26}$$

$$g_3^b(\boldsymbol{x}) = -y_1 + \epsilon < 0, \tag{3.27}$$

$$g_4^b(\boldsymbol{x}) = y_1 + 2b - \epsilon < 0, \tag{3.28}$$

$$g_5^b(\boldsymbol{x}) = -x_2 + \epsilon < 0, \tag{3.29}$$

$$g_6^b(\boldsymbol{x}) = x_2 + 2a - \epsilon < 0, \tag{3.30}$$

$$g_7^b(\boldsymbol{x}) = -y_2 + \epsilon < 0, \tag{3.31}$$

$$g_8^b(\boldsymbol{x}) = y_2 + 2b - \epsilon < 0, \tag{3.32}$$

where $2a$ *and* $2b$ *are the length and width of the piezoelectric patches, respectively. As* ϵ *a small number may be selected such as* 0.01*. The coordinates of the left lower node of the PZT pairs are given by* $\boldsymbol{x} = [x_1, y_1, x_2, y_2]^{\mathrm{T}}$*. The inequalities on* $g_1^b(\boldsymbol{x})$*,* $g_3^b(\boldsymbol{x})$*,* $g_5^b(\boldsymbol{x})$ *and* $g_7^b(\boldsymbol{x})$ *are lower bounds on* x_1*,* y_1*,* x_2 *and* y_2*, respectively. The inequalities* $g_2^b(\boldsymbol{x})$*,* $g_4^b(\boldsymbol{x})$*,* $g_6^b(\boldsymbol{x})$ *and* $g_8^b(\boldsymbol{x})$ *are upper bounds on* x_1*,* y_1*,* x_2 *and* y_2*, respectively.*

3.4.2. First Type of Conditional Constraints

These constraints are necessary to prevent configurations of badly scaled finite elements such as those in Figures 3.2 and 3.3. The constraints are given by the following definition:

Definition 3.4.2 (First type of conditional constraints)**.** *First type of conditional constraints, which must be satisfied so that the disturbance does not become too close to the corners or sides of a PZT pair, are given by*

$$g_{k_1}^d(\boldsymbol{x}) = c_j - d_j + \frac{l_j}{p_j} < 0, \tag{3.33}$$

$$g_{k_2}^d(\boldsymbol{x}) = -c_j + d_j - \frac{l_j}{p_j} < 0, \tag{3.34}$$

$$g_{k_2}^d(\boldsymbol{x}) = c_j - d_j + \frac{l_j}{p_j} + l_j < 0, \tag{3.35}$$

$$g_{k_4}^d(\boldsymbol{x}) = -c_j + d_j + \frac{l_j}{p_j} < 0, \tag{3.36}$$

where d_j *and* l_j *denote the* x*-coordinate or the* y*-coordinate of the disturbance and the length* $2a$ *or the width* $2b$*, respectively. The term* p_j *is a constant such as* 2 *or* 3*, and* c_j *describes the* x*- or* y*-coordinate of the first or second PZT patch.*

The values of quantities in (3.33) *through* (3.36) *are given in Table 3.1 for the four possible combinations, and Table 3.2 shows how the indices of* $g^d_{k_j}$ *change for the combinations shown in Table 3.1.*

Table 3.1. Values of c_j, d_j, l_j, p_j

j	c_j	d_j	l_j	p_j
1	x_1	x_d	$2a$	p_x
2	y_1	y_d	$2b$	p_y
3	x_2	x_d	$2a$	p_x
4	y_2	y_d	$2b$	p_y

Table 3.2. Indices j and k_j for constraints $g^d_{k_j}$

j	1	2	3	4
k_j	$4j-3$	$4j-2$	$4j-1$	$4j$

The conditional statement (i.e. the conditions at which the constraints are required) can be expressed mathematically as follows:

If $d_j - \dfrac{l_j}{p_j} < c_j$ and $c_j < d_j$,
  then $g^d_{k_1}$ and $g^d_{k_2}$ must be valid,
else if $c_j + \dfrac{l_j}{p_j} < d_j$,
  then g^p_2 must be valid.
else if $c_j > d_j$,
  the constraint $g^d_{k_4}$ must be valid.

For the case shown in Figure 3.2, where the disturbance acts on a PZT actuator and sensor pair, the constraints $g^d_{k_1}$ and $g^d_{k_2}$ must be satisfied, otherwise the disturbance may act at a point too close to the sides or corners of the PZT pair. Figure 3.3 gives the case where there is a disturbance close to the lower right side of a PZT pair and the constraint $g^d_{k_3}$ must be valid.

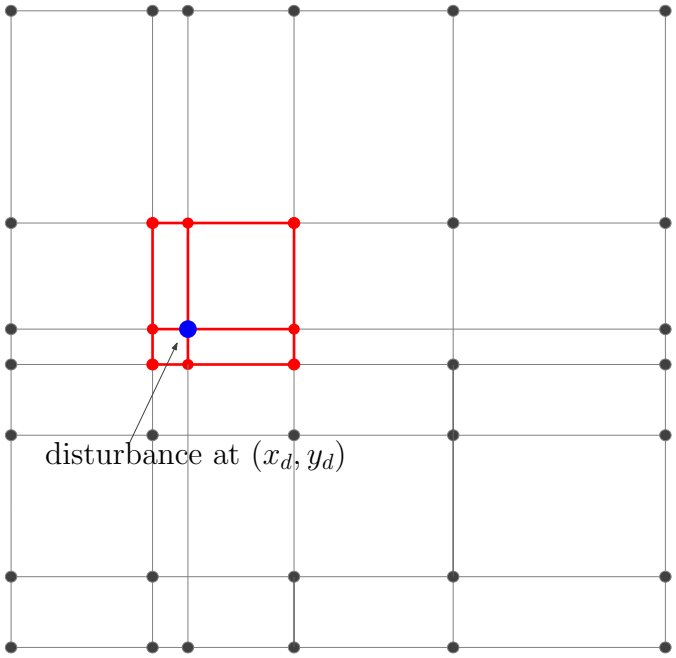

Figure 3.2. Example for the first type of conditional constraints (disturbance on the actuator and sensor)

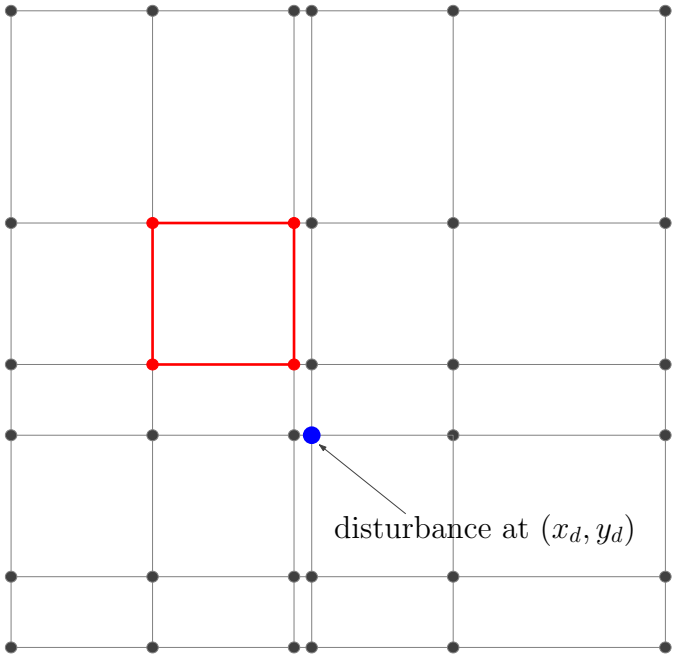

Figure 3.3. Example for the first type of conditional constraints (disturbance outside the actuator and sensor)

3.4.3. Second Type of Conditional Constraints

These constraints are used to prevent combinations at which there are finite elements of bad aspect ratios if two PZT pairs become too close to each other as in Figure 3.4.

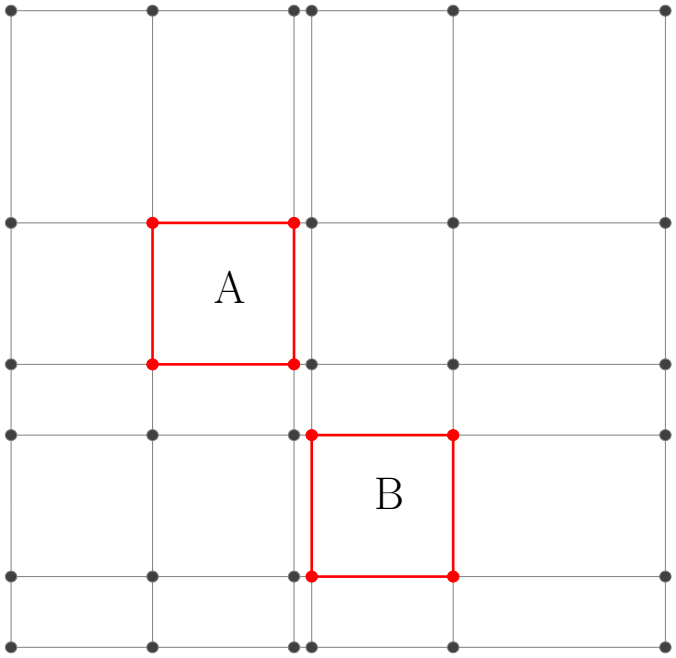

Figure 3.4. Example for the second type of conditional constraints

Definition 3.4.3 (Second type of constraint)**.** *The conditional constraints, which are required to prevent one PZT pair to get too close to another one, are expressed as*

$$g_1^p(\boldsymbol{x}) = -x_2 + (x_1 + 2a) + \frac{2a}{p_x} < 0, \tag{3.37}$$

$$g_2^p(\boldsymbol{x}) = -x_1 + (x_2 + 2a) + \frac{2a}{p_x} < 0, \tag{3.38}$$

$$g_3^p(\boldsymbol{x}) = -y_2 + (y_1 + 2b) + \frac{2b}{p_y} < 0, \tag{3.39}$$

$$g_4^p(\boldsymbol{x}) = -y_1 + (y_2 + 2b) + \frac{2b}{p_y} < 0, \tag{3.40}$$

where the PZT pairs are of dimensions $2a \times 2b$*, and the terms* $\frac{2a}{p_x}$ *and* $\frac{2n}{p_y}$ *are used to limit the difference between two PZT pairs in the* x*- and* y*-directions, respectively. As* p_x *and* p_y *constants such as* 2 *or* 3 *may be selected.*

If the left lower corner of the PZT pair labeled as B in Figure 3.4 has the coordinates (x_2, y_2) and the PZT pair A is the first actuator and sensor pair with the coordinates (x_1, y_1), then the constraints g_1^p must be satisfied. However, if A is the second PZT pair, g_2^p must be valid. That is the convention used in the constrained optimization part of the thesis. In the same manner, the conditional constraints g_3^p and g_4^p are defined for the y-directions.

The conditional statement can be expressed mathematically as follows:

If $x_2 - (x_1 + 2a) \neq 0$ and $x_1 + 2a < x_2$,

g_1^p must be satisfied,

else if $x_1 - (x_2 + 2a) \neq 0$ and $x_2 + 2a < x_1$,

then g_2^p must be valid.

Similarly, if $y_2 - (y_1 + 2b) \neq 0$ and $y_1 + 2b < y_2$,

g_3^p must be satisfied,

else if $y_1 - (y_2 + 2b) \neq 0$ and $y_2 + 2b < y_1$,

then g_4^p must be satisfied.

3.4.4. Third Type of Conditional Constraints

To avoid overlapping of PZT pairs, which are shown in Figures 3.5(a) through 3.5(d), some constraints must be used, which are given by the Definition 3.4.4.

Definition 3.4.4 (Third type constraints)**.** *If* $(x_1 < x_2 < x_1 + 2a$ *or* $x_2 < x_1 < x_2 + 2a)$ *and* $(y_1 < y_2 < y_1 + 2b$ *or* $y_2 < y_1 < y_2 + 2b)$*, then there is a collocation of PZT patches, and at least one of the constraints given in* (3.41) *through* (3.44) *must be satisfied.*

Third type conditional constraints are

$$g_1^o(\boldsymbol{x}) = -x_2 + x_1 + 2a + \frac{2a}{n_x} < 0, \tag{3.41}$$

$$g_2^o(\boldsymbol{x}) = x_2 + 2a - x_1 + \frac{2a}{n_x} < 0, \tag{3.42}$$

$$g_3^o(\boldsymbol{x}) = -y_2 + y_1 + 2b + \frac{2b}{n_y} < 0, \tag{3.43}$$

$$g_4^o(\boldsymbol{x}) = y_2 + 2b - y_1 + \frac{2b}{n_y} < 0, \tag{3.44}$$

where n_x and n_y are some constants such as 2, 3 and 4, which are used to determine how far the x- and y- coordinates of the two PZT pairs should be.

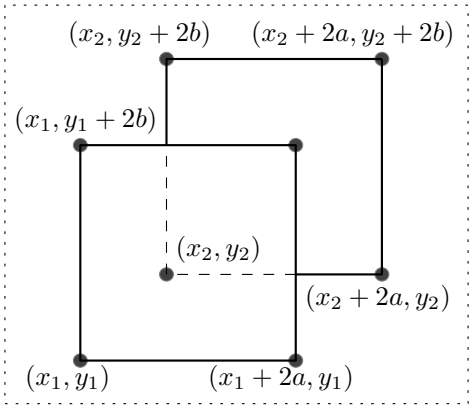

(a) Overlap case one:
$x_1 < x_2 < x_1 + 2a$ and
$y_1 < y_2 < y_1 + 2b$

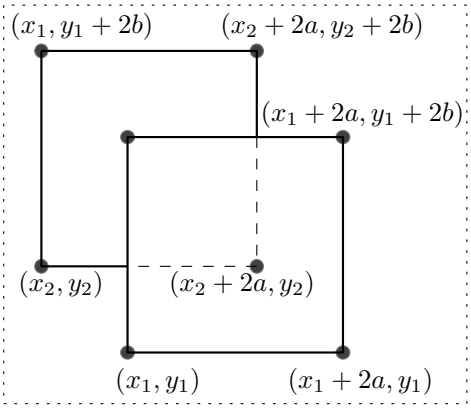

(b) Overlap case two:
$x_2 < x_1 < x_2 + 2a$ and
$y_1 < y_2 < y_1 + 2b$

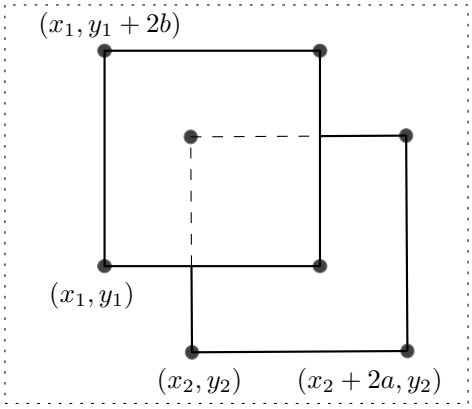

(c) Overlap case three:
$x_1 < x_2 < x_1 + 2a$ and
$y_2 < y_1 < y_2 + 2b$

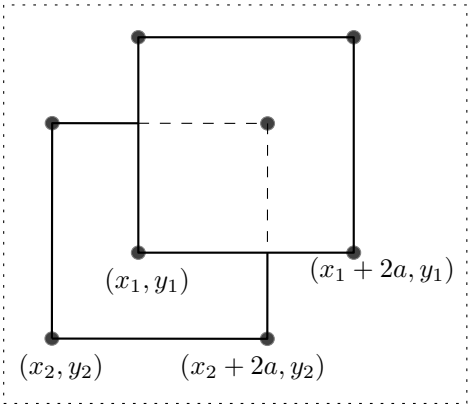

(d) Overlap case four:
$x_2 < x_1 < x_2 + 2a$ and
$y_2 < y_1 < y_2 + 2b$

Figure 3.5. Overlap cases

3.5. Steps of Constrained Optimization

If there exist only lower and upper limits for the design variables, an unconstrained optimization may be utilized. (Simply taking shorter step size will prevent

violation of constraints if the optimal solution lies always interior the design space.) However, if the optimum is allowed to be on the constraint boundaries or the constraints are too complicated and cannot be expressed simply; a constrained minimization procedure is required which considers the constraints in the direction selection part of the optimization. Hence, a constrained minimization procedure must be utilized. In this study, Zoutendijk's method of feasible directions is used for problems with complicated constraints.

The constrained minimization procedure is performed using the following steps:

1. *Required Data*: The disturbance locations, the boundary conditions and the dimensions of the structure are given. Constraints are obtained to prevent of overlapping of actuators and sensors or to prevent badly scaled elements from finite element discretization. Some optimization parameters are chosen to be used in step size selection, in controller design stage, in the determination of active constraints.
2. *Initial Guess*: The initial locations of PZT pairs ($\mathbf{x}^{(1)} = \left[\xi_x^1 \dots \xi_x^{N_u}, \xi_y^1 \dots \xi_y^{N_u}\right]$) are selected. For the first iteration $k = 1$, the constraints $g_j(\mathbf{x}^{(k)}), \quad \forall\, j = 1 : m$ are evaluated. If any of them is violated, then another point is selected until all of the constraints are satisfied.
3. (a) *The physical structure modeling*: The structure is modeled and put into the first modal state space form with matrices $\mathbf{A_m}$, $\mathbf{B_{m1}}$, $\mathbf{B_{m2}}$, $\mathbf{C_{m1}}$, $\mathbf{C_{m2}}$, $\mathbf{D_{m11}}$, $\mathbf{D_{m12}}$, $\mathbf{D_{m21}}$, $\mathbf{D_{m22}}$. The partial derivatives of them are taken with respect to the current actuator and sensor locations.

   (b) *The generalized plant*: For the given signal weightings the state space matrices of the shaped plant are obtained. If the improved coprime controller or the low-authority $\mathcal{H}_\infty$-controller is selected, using the coordinate transformation the generalized plant is put into the first modal form with block diagonal state matrix. The obtained state space matrices are $\mathbf{A}$, $\mathbf{B_1}$, $\mathbf{B_2}$, $\mathbf{C_1}$, $\mathbf{C_2}$, $\mathbf{D_{11}}$, $\mathbf{D_{12}}$, $\mathbf{D_{21}}$, $\mathbf{D_{22}}$. However, if MNRD approach is used, the generalized plant is not diagonalized since MNRD does not require ARE solutions.

(c) *Controller Synthesis and Closed-loop System*: This step is skipped if MNRD-value is selected as the optimization metric. In the case of the improved coprime controller or the improved low-authority $\mathcal{H}_\infty$-controller, the corresponding ARE's are solved. Then, the closed-loop state space matrices $\mathbf{A_c}$, $\mathbf{B_c}$, $\mathbf{C_c}$, $\mathbf{D_c}$ are calculated.

(d) *Objective Function and its Gradient*: In the case of MNRD-controller, the square of the optimistic $\mathcal{H}_2$-norm is set as the objective function J. The function value and the gradient of J with respect to actuator and sensor locations are calculated at the current point. If a controller is used, the square of the closed-loop $\mathcal{H}_2$-norm is selected as J.

4. *Constraint Check*: For the k^{th} iteration all of the constraints are evaluated to test whether any constraint is active or not. That is, if for the constraints $j = 1 : p$, $g_j\left(\mathbf{x}^{(k)}\right) < \epsilon_z$ (ϵ_z being a small number), these p constraints are said to be active. If none of them is active, and the current point is an interior feasible location, then the gradient of the objective function is selected as the search direction and is normalized as $\mathbf{s}^{(k)} = \mathbf{\Delta x}^{(k)}/\|\mathbf{\Delta x}^{(k)}\|$, where $\mathbf{\Delta x}^{(k)}$ is given in Equation (3.24). Otherwise the search direction is obtained in Step 5.

5. (a) *Making the search direction feasible*: If there are active constraints in the iteration k, then the search direction is selected as the solution of the following sub-optimization problem:

$$\begin{aligned} \min \quad & -\bar{\alpha} \\ \text{subject to} \quad & {\mathbf{s}^{(k)}}^{\mathrm{T}} \boldsymbol{\nabla} \mathbf{g}_j\left(\mathbf{x}^{(k)}\right) + \theta_j \bar{\alpha} \leq 0, \quad \forall\, j = 1 : p, \\ & {\mathbf{s}^{(k)}}^{\mathrm{T}} \boldsymbol{\nabla} \mathbf{f}\left(\mathbf{x}^{(k)}\right) + \bar{\alpha} \leq 0, \\ & -1 \leq s_i^{(k)} \leq 1, \qquad\qquad \forall\, i = 1 : n, \end{aligned}$$

where $s_i^{(k)}$ is the i^{th} component of $\mathbf{s}^{(k)}$, p is the number of active constraints.

(b) *Termination due to α^**: If $\bar{\alpha}^* \leq \epsilon_1$, then the optimization is terminated at this point. Otherwise, the search direction is selected as the solution of the previous sub-optimization problem.

6. *Next Point Check and New Locations Selection*: If the next point $\mathbf{x}^{(k+1)}$ is ob-

tained as $\mathbf{x}^{(k+1)} = \mathbf{x}^{(k)} + t\,\mathbf{s}^{(k)}$, with t being the step size, the next point must be both feasible and "better". The term "better" describes a point, the function value of which is less than that of the previous iteration.

Hence, for the k^{th} iteration all of the constraints are evaluated $g_j\left(\mathbf{x}^{(k)}\right)$ for $j = 1 : n_g$, n_g being the number of constraints. If any constraint is not satisfied, the step size must be reduced until none of the constraints is violated. On the other hand, to minimize the objective function "enough" (to obtain a "better" next point), the step size must reduced as well. Therefore, the ordinary backtracking line search given in [50] is modified to select a proper step size t, which fulfills both the feasibility requirement and the requirement that $f\left(\mathbf{x}^{(k+1)}\right) < f\left(\mathbf{x}^{(k)}\right)$, as follows:

Initially $\hat{\alpha} \in (0, 0.5)$ and $\hat{\beta} \in (0, 1)$ are selected, and the iterations start with $t := 1$. The step size is taken $t := \hat{\beta}t$ as long as there are any constraint violations or $f\left(\mathbf{x}^{(k+1)}\right) > f\left(\mathbf{x}^{(k)}\right) + \hat{\alpha}\,t\,\boldsymbol{\nabla} f\left(\mathbf{x}^{(k)}\right)^{\mathrm{T}} \mathbf{s}^{(k)}$. However, during the step size reduction, care must be taken to avoid combinations shown in Figure 3.6. Any combinations similar to those given in Figures 3.7 are acceptable. In other words, step size must be reduced in such a way that the number of finite elements of a PZT pair shall not change in any iteration due to finite element discretization.

7. *Termination of the optimization*: If $\left|\frac{f\left(\mathbf{x}^{(k+1)}\right) - f\left(\mathbf{x}^{(k)}\right)}{f\left(\mathbf{x}^{(k)}\right)}\right| \leq \epsilon_2$ and $\left\|\mathbf{x}^{(k+1)} - \mathbf{x}^{(k)}\right\| \leq \epsilon_3$, the optimization procedure is stopped. Otherwise, the procedure is returned to the second step with the next actuator and sensor points.
8. *Next Point Selection*: If the step size t achieved in the iteration k is not too small (e.g. $t > 10^{-8}$), then it is jumped to the next iteration with $k = k + 1$.

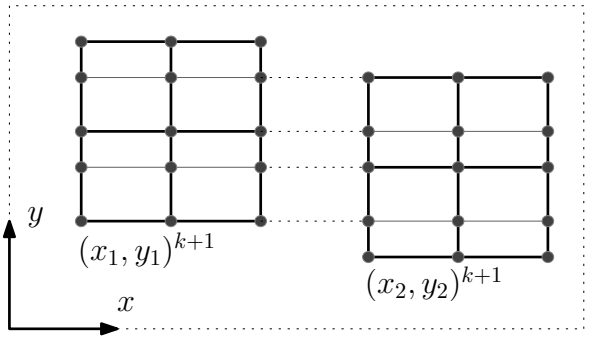

Figure 3.6. Case: $y_2^{(k+1)} < y_1^{(k+1)} < y_2^{(k+1)} + 2b$

In Figure 3.6, the next actuator sensor location $\mathbf{x}^{(k+1)}$ results in a finite element

mesh, due to which the PZT groups need to be divided into more elements. The PZT groups are aimed to consist of the same number of finite elements in each iteration. Hence, such combinations must be avoided by simply calculating values of step sizes at which the configurations similar to those depicted in Figures 3.7 are obtained. As an example, the values

$$t_0 = \frac{y_2^{(k+1)} - y_1^{(k+1)} + 2b}{s_2^{(k)} - s_4^{(k)}}, \qquad t_1 = \frac{y_2^{(k+1)} - y_1^{(k+1)} + b}{s_2^{(k)} - s_4^{(k)}}, \qquad t_2 = \frac{y_2^{(k+1)} - y_1^{(k+1)}}{s_2^{(k)} - s_4^{(k)}}$$

enable one to obtain configurations in Figures 3.7.

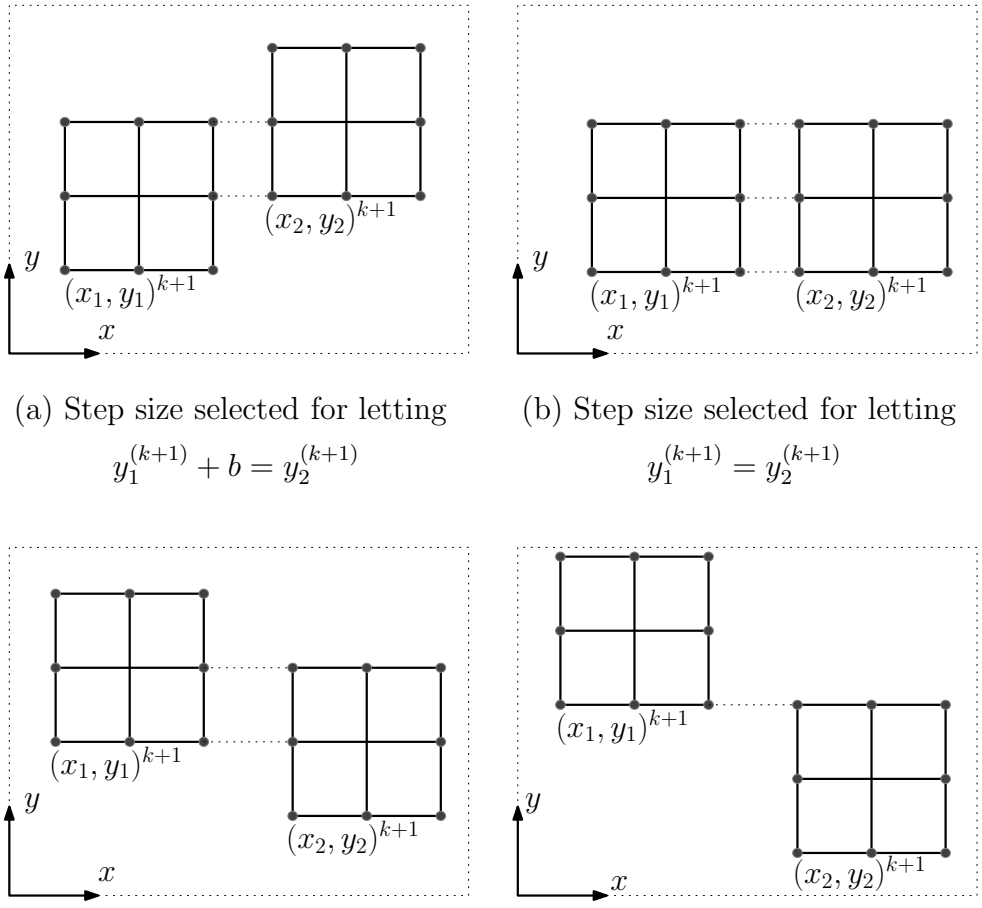

(a) Step size selected for letting $y_1^{(k+1)} + b = y_2^{(k+1)}$

(b) Step size selected for letting $y_1^{(k+1)} = y_2^{(k+1)}$

(c) Step size selected for letting $y_1^{(k+1)} - b = y_2^{(k+1)}$

(d) Step size selected for letting $y_1^{(k+1)} - 2b = y_2^{(k+1)}$

Figure 3.7. Correct step size selection

4. CLOSED-LOOP I/O SELECTION

4.1. Existing Controller Design Strategies for I/O Selection

Since most controller design methods are time consuming, the closed-loop location selection problem becomes computationally complex. Therefore, most optimal location selection methods try to bypass the controller design step. Hence, if one desires to apply a closed-loop location selection method, the controller design part should not take much computation time.

For this purpose Hiramoto et al. [1] have suggested a simple controller design procedure. They obtain a coprime controller for the right lower part of the physical plant by manipulating the corresponding generalized ARE's such that they have a predefined simple solution. The robust coprime controller design Hiramoto et al. [1] have developed is a modified version of the robust stabilization of coprime factors [20, 22].

A second choice for a less time consuming controller might be a low-authority $\mathcal{H}_\infty$-controller for a flexible structe [3].

Another possibility to overcome the time consuming nature of the controller synthesis is the MNRD approach given by Arabyan et al. [55]. They design a $\mathcal{H}_\infty$-controller for which the stability is not required.

All of these three controllers have certain disadvantages. The controller given by Hiramoto et al. [1] is designed for a plant without any signal weights and assumes zero-damping. The $\mathcal{H}_\infty$-controller given in [3] is applicable to plants only with simple input/output filters. For MNRD-controller the partial derivatives of MNRD-values are not defined so that a gradient-based search is not utilized [55].

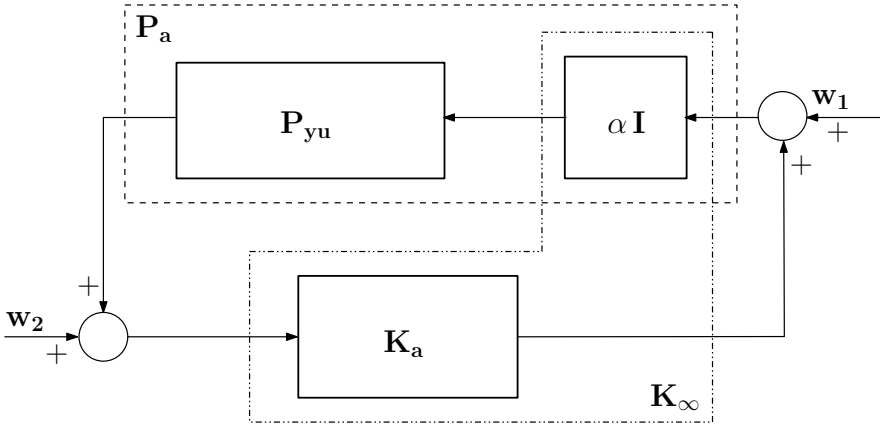

Figure 4.1. Closed-loop System with $\mathbf{P_{yu}}$ and $\mathcal{H}_\infty$ Controller [1]

4.1.1. The Controller Used by Hiramoto et al. [1]

The robust coprime controller Hiramoto et al. [1] have developed in their work is a modified version of the robust stabilization of coprime factors [20, 22].

Definition 4.1.1 (Mcfarlane and Glover [56])**.** *For a state space realization*

$$\mathbf{P} := \left[\begin{array}{c|c} \mathbf{A} & \mathbf{B} \\ \hline \mathbf{C} & \mathbf{D} \end{array}\right],$$

there exists a controller $\mathbf{K_p}$ *which guarantees the inequality*

$$\left\| \begin{bmatrix} \mathbf{K_p} \\ \mathbf{I} \end{bmatrix} (\mathbf{I} - \mathbf{P}\mathbf{K_p})^{-1} \mathbf{M_p^{-1}} \right\|_\infty \leq \gamma, \tag{4.1}$$

where $\mathbf{M_p}$ *comes from the normalized left coprime of the plant* $\mathbf{P} = \mathbf{M_p^{-1}}\mathbf{N_p}$*. The state space representation of the controller* $\mathbf{K_p}$ *reads as*

$$\mathbf{A_{K_p}} := \mathbf{A} + \mathbf{B}\mathbf{F_p} + \gamma^2(\mathbf{G_p^{\mathrm{T}}})^{-1}\mathbf{T}\mathbf{C}^{\mathrm{T}}(\mathbf{C} + \mathbf{D}\mathbf{F_p}), \tag{4.2}$$

$$\mathbf{B_{K_p}} := \gamma^2(\mathbf{G_p^{\mathrm{T}}})^{-1}\mathbf{T}\mathbf{C}^{\mathrm{T}}, \tag{4.3}$$

$$\mathbf{C_{K_p}} := \mathbf{B}^{\mathrm{T}}\mathbf{S}, \tag{4.4}$$

$$\mathbf{D_{K_p}} := -\mathbf{D}^{\mathrm{T}}, \tag{4.5}$$

where $\mathbf{F_p}$ *and* $\mathbf{G_p}$ *are*

$$\mathbf{F_p} := -\mathbf{U}^{-1}(\mathbf{D}^{\mathrm{T}}\mathbf{C} + \mathbf{B}^{\mathrm{T}}\mathbf{S}), \tag{4.6}$$

$$\mathbf{G_p} := (1-\gamma^2)\mathbf{I} + \mathbf{ST}. \tag{4.7}$$

In (4.6) *and* (4.7), $\mathbf{S}$ *and* $\mathbf{T}$ *are the unique positive definite solutions of the ARE's*

$$(\mathbf{A} - \mathbf{B}\mathbf{U}^{-1}\mathbf{D}^{\mathrm{T}}\mathbf{C})^{\mathrm{T}}\mathbf{S} + \mathbf{S}(\mathbf{A} - \mathbf{B}\mathbf{U}^{-1}\mathbf{D}^{\mathrm{T}}\mathbf{C}) - \mathbf{S}\mathbf{B}\mathbf{U}^{-1}\mathbf{B}^{\mathrm{T}}\mathbf{S} + \mathbf{C}^{\mathrm{T}}\mathbf{R}^{-1}\mathbf{C} = 0,$$

$$(\mathbf{A} - \mathbf{B}\mathbf{U}^{-1}\mathbf{D}^{\mathrm{T}}\mathbf{C})\mathbf{T} + \mathbf{T}(\mathbf{A} - \mathbf{B}\mathbf{U}^{-1}\mathbf{D}^{\mathrm{T}}\mathbf{C})^{\mathrm{T}} - \mathbf{T}\mathbf{C}^{\mathrm{T}}\mathbf{R}^{-1}\mathbf{C}\mathbf{T} + \mathbf{B}\mathbf{U}^{-1}\mathbf{B}^{\mathrm{T}} = 0,$$

respectively, where

$$\mathbf{R} := \mathbf{I} + \mathbf{D}\mathbf{D}^{\mathrm{T}},$$

$$\mathbf{U} := \mathbf{I} + \mathbf{D}^{\mathrm{T}}\mathbf{D}.$$

Hiramoto et al. [1] augment the plant $\mathbf{P_{yu}}$ as $\mathbf{P_a} = \alpha\mathbf{P_{yu}}$ and obtain a feedback controller $\mathbf{K_a}$ (see Figure 4.1), where α serves as a design parameter, and β is used to obtain suboptimal controller by selecting β slightly greater than one. For improving disturbance rejection properties of the controller, one should increase α. However, to obtain the robustness of the closed-loop system, α should be kept as small as possible. Hence, there is a tradeoff for this parameter as discussed detailed in Hiramoto et al. [1]. In Figure 4.1, $\mathbf{P_{yu}}$ has the state space realization

$$\mathbf{P_{yu}} = \left[\begin{array}{c|c} \mathbf{A} & \mathbf{B_2} \\ \hline \mathbf{C_2} & \mathbf{0} \end{array}\right]. \tag{4.8}$$

The controller that is used in the optimization part of [1] is $\mathbf{K}_\infty = \alpha\mathbf{K_a}$, and $\mathbf{K_a}$ is obtained by solving the ARE's of the augmented plant $\mathbf{P_a}$

$$\mathbf{A}^{\mathrm{T}}\mathbf{S} + \mathbf{S}\mathbf{A} - \alpha^2\mathbf{S}\mathbf{B_2}\mathbf{B_2}^{\mathrm{T}}\mathbf{S} + \mathbf{C_2}^{\mathrm{T}}\mathbf{C_2} = \mathbf{0}, \tag{4.9}$$

$$\mathbf{AT} + \mathbf{TA}^{\mathrm{T}} - \mathbf{TC_2}^{\mathrm{T}}\mathbf{C_2T} + \alpha^2\mathbf{B_2}\mathbf{B_2}^{\mathrm{T}} = \mathbf{0}. \tag{4.10}$$

Lemma 4.1.2 (Hiramoto et al. [1])**.** *If the damping of the system in* (4.8) *is neglected and the rate sensors are collocated by the actuators, then ARE's in* (4.9) *and* (4.10) *have the solutions*

$$\mathbf{S} := \frac{\mathbf{\Omega}^2}{\alpha}, \tag{4.11}$$

$$\mathbf{T} := \alpha\mathbf{\Omega}^{-2}, \tag{4.12}$$

where $\mathbf{\Omega}$ *is given by Equation* (2.3) *and its square consists of the squares of the natural frequencies as*

$$\mathbf{\Omega}^2 = \operatorname{diag}\left(\omega_1^2, \omega_1^2, \omega_2^2, \omega_2^2, \ldots, \omega_N^2, \omega_N^2\right).$$

Proof. In Equations (4.9) and (4.10), $\mathbf{A}$ is in the first modal form as in Equation (2.7). If $\zeta_i = 0$ from $i = 1$ to $i = N$, the terms $\mathbf{AT} + \mathbf{TA}^{\mathrm{T}}$ and $\mathbf{A}^{\mathrm{T}}\mathbf{S} + \mathbf{SA}$ become zero. Since sensors are collocated with actuators and measure rates, the output matrix becomes $\mathbf{C_2} = \mathbf{B_2}^{\mathrm{T}}\mathbf{\Omega}^2$. Therefore, the diagonal positive-definite matrices

$$\mathbf{S} = \operatorname{diag}\left(s_1, s_1, s_2, s_2, \ldots, s_N, s_N\right), \tag{4.13}$$

$$\mathbf{T} = \operatorname{diag}\left(t_1, t_1, t_2, t_2, \ldots, t_N, t_N\right), \tag{4.14}$$

can be assumed as the solutions of (4.9) and (4.10), which are equal to (4.11) and (4.12), respectively. □

If the new defined variables are inserted, the state space representation of the controller $\mathbf{K_a}$ in Equation (4.2) takes the following form:

$$\mathbf{A_{K_a}} := \mathbf{A} + \frac{\alpha(2\beta^2 - 1)}{1 - \beta^2}\mathbf{B_2}\mathbf{B_2}^{\mathrm{T}}\mathbf{\Omega}^2, \tag{4.15}$$

$$\mathbf{B_{K_a}} := \frac{\alpha\beta^2}{1 - \beta^2}\mathbf{B_2}, \tag{4.16}$$

$$\mathbf{C_{K_a}} := \mathbf{B_2}^{\mathrm{T}}\mathbf{\Omega}^2. \tag{4.17}$$

The controller $\mathbf{K}_\infty$ in Figure 4.1 is obtained by choosing the parameters $\alpha > 0$ and $\beta > 1$. With the controller $\mathbf{K}_\infty$, the state space realization of the closed-loop system $\mathbf{G_{zw}}$ can be given as

$$\dot{\mathbf{x}}_\mathbf{c} = \mathbf{A_c x_c} + \mathbf{B_c w}, \tag{4.18}$$

$$\mathbf{z_c} = \mathbf{C_c x_c}, \tag{4.19}$$

with

$$\mathbf{x_c} = \begin{bmatrix} \mathbf{x} \\ \mathbf{x_c} \end{bmatrix}, \quad \mathbf{A_c} = \begin{bmatrix} \mathbf{A} & \alpha\mathbf{B_2 C_{K_a}} \\ \mathbf{B_{K_a} C_2} & \mathbf{A_{K_a}} \end{bmatrix},$$
$$\mathbf{B_c} = \begin{bmatrix} \mathbf{B_2} \\ \mathbf{0} \end{bmatrix}, \quad \mathbf{C_c} = \begin{bmatrix} \mathbf{C_1} & \alpha\mathbf{D_{12} C_{K_a}} \end{bmatrix}.$$

The closed-loop system $\mathbf{G_{zw}}$ includes open-loop plant and controller matrices which are functions of the configuration of the actuators and sensors ($\mathbf{L_u}$).

To obtain (4.13) and (4.14), Hiramoto et al. [1] neglect the modal damping for all modes and solve the simplified ARE's (4.9) and (4.10) for zero-damping state space matrices. However, in this study the damping is kept, new signal weights are added to the generalized plant, and it is still possible to obtain diagonal ARE solutions, which lead to simple but more efficient coprime controller design. The developed approach is given in Section 4.2.

4.1.2. $\mathcal{H}_\infty$-Controller

In $\mathcal{H}_\infty$-control, the overall control objective is to minimize the $\mathcal{H}_\infty$-norm of the transfer function from the inputs $\mathbf{w}$ to the outputs $\mathbf{z}$, which are shown in Figure 4.2. In other words, the controller design problem is to find a stabilizing controller $\mathbf{K}_c$ which

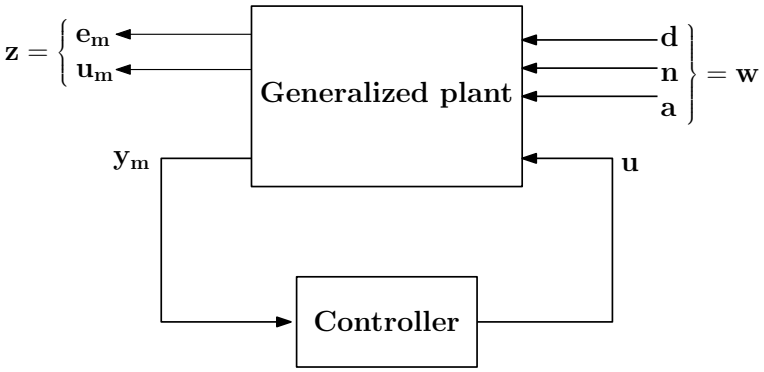

(a) General control configuration

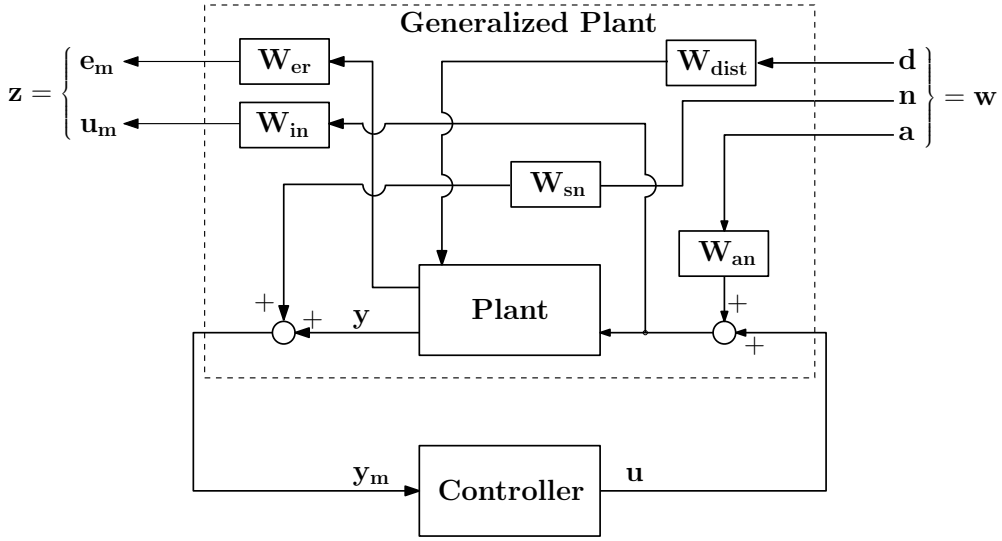

(b) Signal weights in the general control configuration

Figure 4.2. The generalized control configuration and the weighted generalized plant with the controller

minimizes

$$\|\mathcal{F}_l(\mathbf{P},\mathbf{K}_c)\|_\infty = \sup_\omega \overline{\sigma}\left(\mathcal{F}_l(\mathbf{P},\mathbf{K}_c)(j\omega)\right), \tag{4.20}$$

where $\overline{\sigma}$ denotes the maximum singular value, $\mathcal{F}_l(\mathbf{P},\mathbf{K}_c)$ is the lower linear fractional transformation of $\mathbf{P}$ and $\mathbf{K}_c$. The transformation $\mathcal{F}_l(\mathbf{P},\mathbf{K}_c)$ is a closed-loop transfer function from $\mathbf{w}$ to $\mathbf{z}$ which is

$$\mathcal{F}_l(\mathbf{P},\mathbf{K}_c) = \mathbf{P_{11}} + \mathbf{P_{12}}\mathbf{K}_c(\mathbf{I} - \mathbf{P_{22}}\mathbf{K}_c)^{-1}\mathbf{P_{21}}.$$

In Figure 4.2, $\mathbf{K}_c$ is the controller, $\mathbf{P}$ is the generalized plant (including the weighting transfer functions), which is shown in the dashed box in Figure 4.2. The generalized plant $\mathbf{P}$ has the state-space realization

$$\mathbf{P} = \left[\begin{array}{c|c:c} \mathbf{A} & \mathbf{B_1} & \mathbf{B_2} \\ \hline \mathbf{C_1} & \mathbf{D_{11}} & \mathbf{D_{12}} \\ \hdashline \mathbf{C_2} & \mathbf{D_{21}} & \mathbf{D_{22}} \end{array}\right]. \tag{4.21}$$

In practice, it is usually not necessary to obtain an optimal controller for the $\mathcal{H}_\infty$-problem, and it is often computationally and theoretically simpler to design a suboptimal one. Let γ_{min} be the minimum value of $\|\mathcal{F}_l(\mathbf{P}, \mathbf{K}_c)\|_\infty$ over a stabilizing controller $\mathbf{K}_c$. Then, the $\mathcal{H}_\infty$-suboptimal control problem becomes: given a $\gamma > \gamma_{min}$, find all stabilizing controllers $\mathbf{K}_c$ such that

$$\|\mathcal{F}_l(\mathbf{P}, \mathbf{K}_c)\|_\infty < \gamma. \tag{4.22}$$

In Figure 4.2, $\mathbf{d}$ is the force disturbance acting on some of the DOFs of the model given in the problem configuration, $\mathbf{e_m}$ is the error output of the system, $\mathbf{a}$ is the actuator noise, $\mathbf{n}$ is the sensor noise, $\mathbf{u}$ is the controller output, $\mathbf{u_m}$ is the actual control input to the plant, $\mathbf{y}$ is the piezoelectric sensor output from the plant, and $\mathbf{y_m}$ is the actual piezoelectric sensor output fed back into the controller which includes some noise [20].

The following assumptions must hold in order to be able to design an $\mathcal{H}_\infty$-controller [20]:

1. $(\mathbf{A}, \mathbf{B}_2)$ is stabilizable, and $(\mathbf{C}_2, \mathbf{A})$ is detectable.
2. $\mathbf{D}_{12}$ and $\mathbf{D}_{21}$ have full rank.
3. $\begin{bmatrix} \mathbf{A} - j\omega\mathbf{I} & \mathbf{B}_2 \\ \mathbf{C_1} & \mathbf{D}_{12} \end{bmatrix}$ has full column rank for all ω.
4. $\begin{bmatrix} \mathbf{A} - j\omega\mathbf{I} & \mathbf{B}_1 \\ \mathbf{C}_2 & \mathbf{D}_{21} \end{bmatrix}$ has full row rank for all ω.

5. $\mathbf{D}_{11} = 0$ and $\mathbf{D}_{22} = 0$.

The third and fourth assumptions may be replaced with the following ones, if one finds them more convenient:

3. $\mathbf{D}_{\mathbf{12}}^{\mathrm{T}}\mathbf{C} = 0$ and $\mathbf{B_1}\mathbf{D}_{\mathbf{12}}^{\mathrm{T}} = 0$
4. $(\mathbf{A}, \mathbf{B_1})$ is stabilizable, and $(\mathbf{C_1}, \mathbf{A})$ is detectable.

With these assumptions, for the generalized plant in Figure 4.2 there exists a stabilizing controller $\mathbf{K_c}(s)$ such that $\|\mathcal{F}_l(\mathbf{P}, \mathbf{K}_c)\|_\infty < \gamma$ if and only if [20]

(i) $\mathbf{X}_\infty \geq 0$ is a solution to the algebraic Riccati equation

$$\mathbf{A}^{\mathrm{T}}\mathbf{X}_\infty + \mathbf{X}_\infty\mathbf{A} + \mathbf{C}_1^{\mathrm{T}}\mathbf{C}_1 + \mathbf{X}_\infty\left(\gamma^{-2}\mathbf{B}_1\mathbf{B}_1^{\mathrm{T}} - \mathbf{B}_2\mathbf{B}_2^{\mathrm{T}}\right)\mathbf{X}_\infty = \mathbf{0} \tag{4.23}$$

such that Re $\lambda_i\left[\mathbf{A} + \left(\gamma^{-2}\mathbf{B}_1\mathbf{B}_1^{\mathrm{T}} - \mathbf{B}_2\mathbf{B}_2^{\mathrm{T}}\right)\mathbf{X}_\infty\right] < 0, \forall i$; and

(ii) $\mathbf{Y}_\infty \geq 0$ is a solution to the algebraic Riccati equation

$$\mathbf{A}\mathbf{Y}_\infty + \mathbf{Y}_\infty\mathbf{A}^{\mathrm{T}} + \mathbf{B}_1\mathbf{B_1}^{\mathrm{T}} + \mathbf{Y}_\infty\left(\gamma^{-2}\mathbf{C}_1^{\mathrm{T}}\mathbf{C}_1 - \mathbf{C}_2^{\mathrm{T}}\mathbf{C}_2\right)\mathbf{Y}_\infty = \mathbf{0} \tag{4.24}$$

such that Re $\lambda_i\left[\mathbf{A} + \mathbf{Y}_\infty\left(\gamma^{-2}\mathbf{C}_1^{\mathrm{T}}\mathbf{C}_1 - \mathbf{C}_2^{\mathrm{T}}\mathbf{C}_2\right)\right] < 0, \forall i$; and

(iii) $\rho\left(\mathbf{X}_\infty\mathbf{Y}_\infty\right) < \gamma^2$.

All such controllers are then given by $\mathbf{K}_c = \mathcal{F}_l(\mathbf{K}_{\mathbf{Q}_c}, \mathbf{Q}_c)$, where

$$\begin{aligned}
\mathbf{K}_{\mathbf{Q}_c}(s) &= \left[\begin{array}{c|cc} \mathbf{A}_\infty & -\mathbf{Z}_\infty\mathbf{L}_\infty & \mathbf{Z}_\infty\mathbf{B}_2 \\ \hline \mathbf{F}_\infty & \mathbf{0} & \mathbf{I} \\ -\mathbf{C}_2 & \mathbf{I} & \mathbf{0} \end{array}\right], \\
\mathbf{F}_\infty &= -\mathbf{B}_2^{\mathrm{T}}\mathbf{X}_\infty, \\
\mathbf{L}_\infty &= -\mathbf{Y}_\infty, \mathbf{C}_2^{\mathrm{T}}, \\
\mathbf{Z}_\infty &= \left(\mathbf{I} - \gamma^{-2}\mathbf{Y}_\infty\mathbf{X}_\infty\right)^{-1},
\end{aligned} \tag{4.25}$$

$$\mathbf{A}_\infty \;=\; \mathbf{A} + \gamma^{-2}\mathbf{B}_1\mathbf{B}_1^{\mathrm{T}}\mathbf{X}_\infty + \mathbf{B}_2\mathbf{F}_\infty + \mathbf{Z}_\infty\mathbf{L}_\infty\mathbf{C}_2$$

and $\mathbf{Q}_c(s)$ is any stable proper transfer function such that $\|\mathbf{Q}_c\|_\infty < \gamma$. If $\mathbf{Q}_c(s) = 0$, the resulting controller is the central controller.

4.1.3. The Low-Authority $\mathcal{H}_\infty$-Controller

The control forces which act on structures can be categorized into tracking forces and damping forces. The tracking forces are of high amplitude and used to track a reference input whereas damping forces suppress vibrations of the structures and have limited magnitude. Hence, controllers can be divided into high-authority and low-authority controllers [24].

When a low-authority $\mathcal{H}_\infty$-controller is to be designed for a flexible structure, some of the properties of flexible structures can be used to obtain diagonal solutions for the ARE's. With these diagonal ARE solutions, it is possible to obtain a low-authority $\mathcal{H}_\infty$-controller. Below, a methodology is given which is developed by Gawronski [3, 24] to derive diagonal ARE solutions for Equations (4.23) and (4.24).

For a state space realization

$$P := \left[\begin{array}{c|c} \mathbf{A} & \mathbf{B} \\ \hline \mathbf{C} & \mathbf{D} \end{array}\right],$$

the Gramians are used to express the controllability and observability properties of a system P qualitatively and are defined as [57]

$$\begin{aligned} \mathbf{W_c}(t) &= \int_0^t \mathbf{e}^{\mathbf{A}t}\mathbf{B}\mathbf{B}^{\mathrm{T}}\mathbf{e}^{\mathbf{A}^{\mathrm{T}}t}\,\mathrm{d}t, \\ \mathbf{W_o}(t) &= \int_0^t \mathbf{e}^{\mathbf{A}t}\mathbf{C}^{\mathrm{T}}\mathbf{C}\mathbf{e}^{\mathbf{A}^{\mathrm{T}}t}\,\mathrm{d}t. \end{aligned}$$

The exact (full) controllability and observability Gramians are obtained alternatively

from the Lyapunov equations

$$\mathbf{A}\mathbf{L_c} + \mathbf{L_c}\mathbf{A}^{\mathrm{T}} + \mathbf{B}\mathbf{B}^{\mathrm{T}} = \mathbf{0}, \tag{4.26}$$

$$\mathbf{A}^{\mathrm{T}}\mathbf{L_o} + \mathbf{L_o}\mathbf{A} + \mathbf{C}^{\mathrm{T}}\mathbf{C} = \mathbf{0}, \tag{4.27}$$

where $\mathbf{A}$ is Hurwitz.

Lemma 4.1.3 (Gawronski [3])**.** *If P is given in one of the modal coordinates (such as expressions* (2.7)*,* (2.8) *or* (2.9)*), the controllability and observability Gramians can be approximated by*

$$\mathbf{L_c} \cong \mathrm{diag}\left(l_{ci}\,\mathbf{I_2}\right), \quad l_{ci} > 0, \quad \forall\, i = N, \tag{4.28}$$

$$\mathbf{L_c} \cong \mathrm{diag}\left(l_{ci}\,\mathbf{I_2}\right), \quad l_{ci} > 0, \quad \forall\, i = N, \tag{4.29}$$

where $\mathbf{I_2}$, $2 \times N$, l_{ci} and l_{oi} are the 2×2 identity matrix, the number of states P has, the i^{th} mode's controllability and observability Gramians, respectively.

Proof. If P is given in the first modal coordinate (2.7) and is inserted into Equations (4.26) and (4.27), one can inspect that

$$\lim_{\zeta \to 0} \; l_{cij} < \infty, \quad \text{for } i \neq j,$$
$$\lim_{\zeta \to 0} \; l_{oij} < \infty, \quad \text{for } i \neq j,$$

while

$$\lim_{\zeta \to 0} \; l_{cii} \to \infty,$$
$$\lim_{\zeta \to 0} \; l_{oii} \to \infty.$$

Thus, for small damping the controllability and observability Gramians in modal coordinates are diagonally dominant. □

The diagonally dominant Gramians (4.28) and (4.29) are very useful for solving ARE's approximately. Further properties are introduced to simplify some terms in Equations (4.23) and (4.24).

Lemma 4.1.4 (Gawronski [3]). *If for a controllable and observable flexible structure there exists $r_0 > 0$ such that*

$$\|\mathbf{X}_\infty\|_2 \leq r_0, \tag{4.30}$$

$$\|\mathbf{Y}_\infty\|_2 \leq r_0, \tag{4.31}$$

where $\mathbf{X}_\infty$ and $\mathbf{Y}_\infty$ are solutions of ARE's (4.23) and (4.24), then the resulting controller is said to be of low-authority.

If the state space representation P of a flexible structure is converted into the first or second modal form (Equation (2.7) or (2.8)), the controllability and observability Gramians are diagonally dominant, and off-diagonal terms are negligibly small according to Lemma 4.1.3. Hence, the terms $\mathbf{B}\mathbf{B}^{\mathrm{T}}$ and $\mathbf{C}^{\mathrm{T}}\mathbf{C}$ become

$$\mathbf{B}\mathbf{B}^{\mathrm{T}} \cong -\mathbf{L_c}\left(\mathbf{A} + \mathbf{A}^{\mathrm{T}}\right), \tag{4.32}$$

$$\mathbf{C}^{\mathrm{T}}\mathbf{C} \cong -\mathbf{L_o}\left(\mathbf{A} + \mathbf{A}^{\mathrm{T}}\right). \tag{4.33}$$

If only i^{th} mode is considered and the state matrix $\mathbf{A}$ is in the second modal form, Equations (4.32) and (4.33) become

$$\mathbf{B}_i\mathbf{B}_i^{\mathrm{T}} \cong -l_{ci}\left(\mathbf{A}_i + \mathbf{A}_i^{\mathrm{T}}\right) = l_{ci}\, 2\zeta_i\omega_i\, \mathbf{I_2}, \quad \forall\, i = 1:N, \tag{4.34}$$

$$\mathbf{C}_i^{\mathrm{T}}\mathbf{C}_i \cong -l_{oi}\left(\mathbf{A}_i + \mathbf{A}_i^{\mathrm{T}}\right) = l_{oi}\, 2\zeta_i\omega_i\, \mathbf{I_2}, \quad \forall\, i = 1:N, \tag{4.35}$$

where ζ_i, ω_i and $\mathbf{I_2}$ are the modal damping coefficient for the i^{th} mode, the i^{th} natural frequency and the 2×2 identity matrix, respectively. In Equations (4.34) and (4.35), $\mathbf{B}_i$ and $\mathbf{C}_i$ are the i^{th} two-row block of $\mathbf{B}$ and the i^{th} two-column block of $\mathbf{C}$, respectively.

Proof. If expressions in (4.28) and (4.29) are inserted into (4.26) and (4.27), Equations (4.32) and (4.33) are obtained.

For the positive semidefinite $\mathbf{B}\mathbf{B}^{\mathrm{T}}$ and $\mathbf{C}^{\mathrm{T}}\mathbf{C}$ one may obtain that

$$\left(b_i b_j^{\mathrm{T}}\right)^2 \leq \left(b_i b_i^{\mathrm{T}}\right)\,\left(b_j b_j^{\mathrm{T}}\right), \tag{4.36}$$

$$\left(c_i^{\mathrm{T}} c_j\right)^2 \leq \left(c_i^{\mathrm{T}} c_i\right)\,\left(c_j^{\mathrm{T}} c_j\right), \tag{4.37}$$

which means that off-diagonal terms are always less than the geometric means of the corresponding diagonal entries. Hence, if the state matrix is in the first or second modal form, and there exists a value r_0 such that $\|\mathbf{X}_\infty\|_2 \leq r_0$ and $\|\mathbf{Y}_\infty\|_2 \leq r_0$, then the off-diagonal terms of $\mathbf{B}\mathbf{B}^{\mathrm{T}}$ and $\mathbf{C}^{\mathrm{T}}\mathbf{C}$ do not affect the closed-loop eigenvalues. So, the off-diagonal terms can be set equal to zero, and the diagonal terms can be calculated from Gramians as in (4.34) and (4.35). □

Lemma 4.1.5 (Gawronski [3])**.** *If the state space matrices are expressed in terms of modal coordinates, for a low-authority $\mathcal{H}_\infty$-controller design case the solutions of ARE's in Equations* (4.23) *and* (4.24) *become diagonally dominant as*

$$\mathbf{X}_\infty \cong \mathrm{diag}\left(x_{\infty i}\,\mathbf{I_2}\right), \quad \forall\, i = 1:N, \tag{4.38}$$

$$\mathbf{Y}_\infty \cong \mathrm{diag}\left(y_{\infty i}\,\mathbf{I_2}\right), \quad \forall\, i = 1:N. \tag{4.39}$$

Proof. If the state space realization of the structure is in one of the modal forms, the solutions of Equations (4.23) and (4.24) tend to be diagonally dominant (similar to Lemma 4.1.3). □

Lemma 4.1.6 (Gawronski [3])**.** *If the state space realization P of a flexible structure is in one of the modal coordinates, then ARE's* (4.23) *and* (4.24) *reduce to the quadratic equations*

$$\kappa_{ci} x_{i\infty}^2 + x_{\infty i} - w_{o1i} \;\cong\; 0, \quad \forall\, i = 1:N, \tag{4.40}$$

$$\kappa_{ei} y_{i\infty}^2 + y_{\infty i} - w_{c1i} \;\cong\; 0, \quad \forall\, i = 1:N, \tag{4.41}$$

where

$$\kappa_{ci} = l_{c2i} - \frac{l_{c1i}}{\gamma^2}, \tag{4.42}$$

$$\kappa_{ei} = l_{o2i} - \frac{l_{o1i}}{\gamma^2} \tag{4.43}$$

and l_{c1i}, l_{c2i} *are the* i^{th} *diagonal components of the controllability Gramians of the pair* $(\mathbf{A}, \mathbf{B_1})$ *and of the pair* $(\mathbf{A}, \mathbf{B_2})$*, respectively. Similarly,* l_{o1i} *and* l_{o2i} *are the* i^{th} *diagonal components of the observability Gramians of the pair* $(\mathbf{C_1}, \mathbf{A})$ *and of the pair* $(\mathbf{C_2}, \mathbf{A})$*, respectively.*

Proof. Since $\mathbf{A}$ is in the first or second modal form, $\mathbf{B}\mathbf{B}^{\mathrm{T}}$ and $\mathbf{C}^{\mathrm{T}}\mathbf{C}$ in Equations (4.23) and (4.24) are replaced by the expressions in (4.34) and (4.35). Then, Equations (4.23) and (4.24) reduce to Equations (4.40) and (4.41), respectively, if the solutions of ARE's (4.23) and (4.24) are assumed to be diagonally dominant as in (4.38) and (4.39). □

Gawronski [3, 24] makes use of properties of flexible structures and low-authority controllers. He decouples the ARE's in (4.23) and (4.24) into their modes and converts them to simple quadratic equations. These simple quadratic equations provide diagonal solutions for ARE's. However, they are valid only for physical plants in modal coordinates but not for the state space representations of the generalized plant since the state matrices are no longer in modal forms after the filters are incorporated into the physical model.

4.1.4. Norm Minimization of Residual Deformations (MNRD)

Arabyan and Chemiskian [58, 55, 59] obtain an "optimistic value" for the lower limit of deformation suppression instead of the exact level of residual deformation that is obtained as the disturbance attenuation factor in $\mathcal{H}_\infty$-control. By introducing the optimistic value they perform investigation of each individual input/output set much faster, since the $\mathcal{H}_\infty$-design computation takes much more time. Although the

calculation of $t_{optimistic}$ does not include any closed-loop stability requirement, they use it as a best location selection criterion. They denote the optimistic value as the residual deformation and their method as the minimization of residual deformations (MNRD).

Theorem 4.1.7 (Arabyan et al. [2]). *Let*

$$\mathbf{G} = \left(\begin{array}{c|c} \mathbf{G_{11}} & \mathbf{G_{12}} \\ \hline \mathbf{G_{21}} & \mathbf{G_{22}} \end{array}\right) \tag{4.44}$$

be a stable state space realization which is shown in Figure 4.3. For $\mathbf{G}$*, a controller* $\mathbf{K}$ *can be designed. If closed-loop stability is not required, then the optimistic lower limit is a lower bound for the actual residual deformation and is defined as*

$$t_{optimistic} \;=\; \sup_{\omega} \overline{\sigma}\left(\mathbf{G_{11}} - \mathbf{G_{12}}\mathbf{G_{12}}^{-\mathrm{L}}\mathbf{G_{11}}\mathbf{G_{21}}^{-\mathrm{R}}\mathbf{G_{21}}\right). \tag{4.45}$$

Proof. Consider the closed-loop transfer function $\mathbf{T_{zw}}$ between $\mathbf{w}$ and $\mathbf{z}$ in Figure 4.3, which can be given as

$$\|\mathbf{T_{zw}}\|_\infty = \|\mathcal{F}_l\left(\mathbf{P}, \mathbf{K_I}\right)\|_\infty = \sup_{\omega} \overline{\sigma}\left(\mathcal{F}_l\left(\mathbf{P}, \mathbf{K_I}\right)(j\omega)\right). \tag{4.46}$$

The feedback controller $\mathbf{K_I}$ in Figure 4.3 is given in the form of Youla parametrization as

$$\mathbf{K_I} = \mathbf{Q}\left[\mathbf{I} + \mathbf{Q}\mathbf{G}_{\mathbf{22}}^{'}\right]^{-1}. \tag{4.47}$$

In Figure 4.3, if $\mathbf{G}_{\mathbf{22}}^{'} = \mathbf{G_{22}}$, the signal that is fed back to the controller parameter $\mathbf{Q}$ is $-\mathbf{G_{21}}\mathbf{w}$. Since one wants to minimize the performance outputs $\mathbf{z}$, the control input $\mathbf{u}$ is required to be $\mathbf{u} = -\mathbf{G_{12}}^{-\mathrm{L}}\mathbf{G_{11}}\mathbf{w}$. In the case of no model mismatch ($\mathbf{G}_{\mathbf{22}}^{'} = \mathbf{G_{22}}$), this can be achieved if the controller parameter $\mathbf{Q}$ in Figure 4.3 has the expression

$$\mathbf{Q} = \mathbf{G_{12}}^{-\mathrm{L}}\mathbf{G_{11}}\mathbf{G_{21}}^{-\mathrm{R}}, \tag{4.48}$$

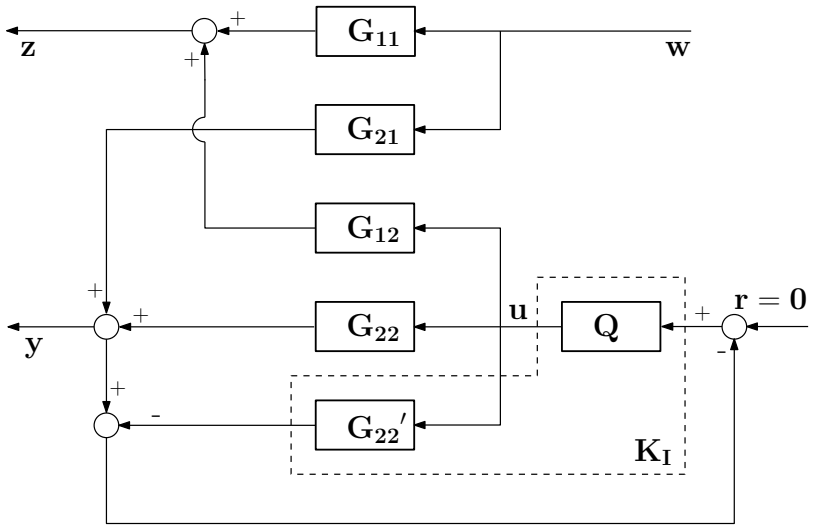

Figure 4.3. Internal Model Control Configuration

where $\mathbf{G}^{-\mathrm{L}}$, $\mathbf{G}^{-\mathrm{R}}$ are the left inverse and the right inverse of the system $\mathbf{G}$, respectively. If (4.47) and (4.48) are inserted into (4.46), Equation (4.45) is obtained. □

Definition 4.1.8 (Arabyan and Chemiskian [55]). *The controller which is required to obtain the optimistic value in* (4.45) *can be given as*

$$\mathbf{K_I} = \mathbf{Q}\left[\mathbf{I} + \mathbf{Q}\mathbf{G_{22}}\right]^{-1}, \tag{4.49}$$

where $\mathbf{Q} = \mathbf{G_{12}^{-L}}\mathbf{G_{11}}\mathbf{G_{21}^{-R}}$.

Remark. According to [55, 58, 59] the parameter $\mathbf{Q}$ in the expression of the controller $\mathbf{K_I}$ may not always be real rational and stable. To achieve a stabilizing controller $\mathbf{K_I}$, $\mathbf{Q}$ needs to be replaced by $\hat{\mathbf{Q}} \in RH_\infty$. So, the difference between the actual vibration suppression level and the optimistic lower limit can be given as the approximation

$$\min_{\hat{\mathbf{Q}} \in RH_\infty} \left\| \mathbf{G_{12}} \left(\mathbf{Q} - \hat{\mathbf{Q}} \right) \mathbf{G_{21}} \right\|_\infty. \tag{4.50}$$

The approximation (4.50) is solved according to Nehari's theorem [21, 30, 23]. However, it takes more time than solving the Riccati equations resulting from $\mathcal{H}_\infty$-control problem.

Theorem 4.1.9 (Arabyan and Chemiskian [55]). *The minimum norm of residual de-*

formations (MNRD), given by (4.45)*, can be computed alternatively by the theorem in* [2] *as*

$$t_{optimistic} = z^* = \sup_{\omega} \overline{\sigma} \left(\mathbf{G_{11}} - \mathbf{U_{12}} \mathbf{U_{12}^{H}} \mathbf{G_{11}} \mathbf{V_{21}} \mathbf{V_{21}^{H}} \right), \tag{4.51}$$

where $\mathbf{U_{12}}$ *and* $\mathbf{V_{12}}$ *result from the singular value decomposition of* $\mathbf{G_{12}}(j\omega)$ *and* $\mathbf{G_{21}}(j\omega)$

$$\mathbf{G_{12}}(j\omega) = [\mathbf{U_{12}}(j\omega)\ \mathbf{u_{12}}(j\omega)] \begin{bmatrix} \mathbf{\Sigma_{12}}(\omega) & \mathbf{0} \\ \mathbf{0} & \mathbf{0} \end{bmatrix} [\mathbf{V_{12}}(j\omega)\ \mathbf{v_{12}}(j\omega)]^{\mathrm{H}}, \tag{4.52}$$

$$\mathbf{G_{21}}(j\omega) = [\mathbf{U_{21}}(j\omega)\ \mathbf{u_{21}}(j\omega)] \begin{bmatrix} \mathbf{\Sigma_{21}}(\omega) & \mathbf{0} \\ \mathbf{0} & \mathbf{0} \end{bmatrix} [\mathbf{V_{21}}(j\omega)\ \mathbf{v_{21}}(j\omega)]^{\mathrm{H}}. \tag{4.53}$$

Proof. Consider the performance outputs in Figure 4.3, which are

$$\mathbf{z} = \mathbf{G_{11}}\mathbf{w} + \mathbf{G_{12}}\mathbf{u}, \tag{4.54}$$

where $\mathbf{u} = -\mathbf{Q}\mathbf{G_{12}}\mathbf{w}$. To minimize $\mathbf{z}$, $\mathbf{Q}$ can be selected as $\mathbf{Q} = \mathbf{G_{12}^{+}}\mathbf{G_{11}}\mathbf{G_{21}^{+}}$. Using singular value decomposition (4.52) and (4.53), the pseudo inverses of $\mathbf{G_{12}}$ and $\mathbf{G_{21}}$ become

$$\mathbf{G_{12}^{+}} = \mathbf{V_{12}}\mathbf{\Sigma_{12}^{-1}}\mathbf{U_{12}^{H}}, \tag{4.55}$$

$$\mathbf{G_{21}^{+}} = \mathbf{V_{21}}\mathbf{\Sigma_{21}^{-1}}\mathbf{U_{21}^{H}}. \tag{4.56}$$

Hence, $\mathbf{z}$ becomes

$$\begin{aligned} \mathbf{z} &= \mathbf{G_{11}}\mathbf{w} - \mathbf{G_{12}}\mathbf{G_{12}}\mathbf{G_{12}^{+}}\mathbf{G_{11}}\mathbf{G_{21}^{+}}\mathbf{G_{21}}\mathbf{w} \\ &= \left(\mathbf{G_{11}} - \mathbf{U_{12}}\mathbf{U_{12}^{H}}\mathbf{G_{11}}\mathbf{V_{21}}\mathbf{V_{21}^{H}} \right) \mathbf{w}. \end{aligned}$$

So, the transfer function from $\mathbf{w}$ to $\mathbf{z}$ becomes $\mathbf{G_{11}} - \mathbf{U_{12}}\mathbf{U_{12}^{H}}\mathbf{G_{11}}\mathbf{V_{21}}\mathbf{V_{21}^{H}}$, the $\mathcal{H}_\infty$-norm of which can be given by (4.51). □

To find the optimal actuator and sensor location using MNRD-technique, the performance outputs $\mathbf{z}$ of the general plant in Figure 4.3 can be given in terms of transfer functions $\mathbf{G_{12}}$ and $\mathbf{G_{11}}$ as

$$\mathbf{z} = \mathbf{G_{11}}\mathbf{w} + \mathbf{G_{12}}(\mathbf{L_u})\mathbf{u}, \tag{4.57}$$

where $\mathbf{G_{12}}$ is the transfer function which gives the contribution of the point or piezo-electric actuators to $\mathbf{z}$, and $\mathbf{G_{11}}$ gives the contribution of external disturbances $\mathbf{w}$.

The objective is to minimize $\mathbf{z}$ in terms of $\mathbf{L_u}$, which gives the best combination of actuator and sensor pairs as

$$z^*\left(\mathbf{L_u^*}\right) = \min_{\mathbf{L_u}} \|z^*\left(\mathbf{L_u}\right)\|_2.$$

For the configuration $\mathbf{L_u}$, the residual deformation is given as

$$\begin{aligned} z^*\left(\mathbf{L_u}\right) &= \min_{\mathbf{u}} \|\mathbf{G_{11}}\mathbf{w} + \mathbf{G_{12}}\mathbf{u}\|_2, \\ &= \|\mathbf{G_{11}}\mathbf{w} + z_u^*\|_2, \end{aligned}$$

where $z_u^* = \min_{\mathbf{u}} \|\mathbf{G_{12}}\mathbf{u}\|_2$. Since $\mathbf{u} = -\mathbf{Q}\,\mathbf{G_{21}}\,\mathbf{w}$ and $\mathbf{Q} = \mathbf{G_{12}^{-L}}\mathbf{G_{11}}\mathbf{G_{21}^{-R}}$, z_u^* becomes

$$z_u^* = \|\mathbf{G_{12}}\mathbf{G_{12}^{-L}}\mathbf{G_{11}}\mathbf{G_{21}^{-R}}\mathbf{G_{21}}\mathbf{w}\|_2.$$

Hence, the residual deformation for the configuration $\mathbf{L_u}$ can be stated as

$$\begin{aligned} z^*\left(\mathbf{L_u}\right) &= \left\| \left(\mathbf{G_{11}} - \mathbf{G_{12}}\mathbf{G_{12}^{-L}}\,\mathbf{G_{11}}\,\mathbf{G_{21}^{-R}}\mathbf{G_{21}}\right)\mathbf{w} \right\|_2 \\ &= \overline{\sigma}\left(\mathbf{G_{11}} - \mathbf{G_{12}}\mathbf{G_{12}^{-L}}\,\mathbf{G_{11}}\,\mathbf{G_{21}^{-R}}\mathbf{G_{21}}\right)\|\mathbf{w}\|_2 \\ &\leq \overline{\sigma}\left(\mathbf{G_{11}} - \mathbf{G_{12}}\mathbf{G_{12}^{-L}}\,\mathbf{G_{11}}\,\mathbf{G_{21}^{-R}}\mathbf{G_{21}}\right), \end{aligned}$$

which is equal to the optimistic deformation in Equation (4.45).

The location $\mathbf{L}_{\mathbf{u}}^{*}$ where the MNRD is at minimum can be taken as the best locations for actuator placement [60].

Remark. If there is no restriction on the inputs, $\mathbf{z}$ consists of only deformations. Generally, it is not possible to eliminate deformations comprised of m DOFs completely by means of a relatively small number of actuators. The deformations that cannot be eliminated are called residual deformations.

4.1.5. Calculation of MNRD-value

One can choose the optimistic value for the lower limit of deformation suppression (MNRD-value) as the closed-loop optimization metric. Usually, it is very close to the real disturbance attenuation factor γ of an $\mathcal{H}_\infty$-control problem, but its computation time is shorter. For this purpose state space representation in Equation (2.51) can be partitioned, without converting the global plant into modal form, as

$$\left[\begin{array}{c|c:c} \mathbf{A_g} & \mathbf{B_{g1}} & \mathbf{B_{g2}} \\ \hline \mathbf{C_{g1}} & \mathbf{D_{g11}} & \mathbf{B_{g12}} \\ \hdashline \mathbf{C_{g2}} & \mathbf{D_{g21}} & \mathbf{B_{g22}} \end{array}\right] =: \left(\begin{array}{c:c} \mathbf{P_{g11}} & \mathbf{P_{g12}} \\ \hdashline \mathbf{P_{g21}} & \mathbf{P_{g22}} \end{array}\right).$$

Hence, MNRD-value can be calculated as

$$t_{optimistic} = \sup_{\omega} \overline{\sigma}\left(\mathbf{T_{zw}}(j\omega)\right), \tag{4.58}$$

where $\overline{\sigma}\left(\mathbf{T_{zw}}\right)$ is defined as

$$\overline{\sigma}\left(\mathbf{T_{zw}}\right) = \sqrt{\lambda_{max}\left(\mathbf{T}_{\mathbf{zw}}^{*}\ \mathbf{T_{zw}}\right)}$$

and

$$\mathbf{T_{zw}} = \mathbf{P_{g11}} - \mathbf{P_{g12}}\,\mathbf{P}_{\mathbf{g12}}^{-\mathrm{L}}\,\mathbf{P_{g11}}\,\mathbf{P}_{\mathbf{g21}}^{-\mathrm{R}}\,\mathbf{P_{g21}}.$$

The transfer functions $\mathbf{P}_{\mathbf{g12}}^{-\mathrm{L}}$ and $\mathbf{P}_{\mathbf{g21}}^{-\mathrm{R}}$ are defined as

$$\begin{aligned}\mathbf{P}_{\mathbf{g12}}^{-\mathrm{L}} &= \left(\mathbf{P}_{\mathbf{g12}}^{\sim}\mathbf{P_{g12}}\right)^{-1}\mathbf{P}_{\mathbf{g12}}^{\sim},\\ \mathbf{P}_{\mathbf{g21}}^{-\mathrm{R}} &= \mathbf{P}_{\mathbf{g21}}^{\sim}\left(\mathbf{P_{g21}}\mathbf{P}_{\mathbf{g21}}^{\sim}\right)^{-1},\end{aligned}$$

where conjugate system of $\mathbf{P_{g12}}$ and $\mathbf{P_{g21}}$ are given as

$$\begin{aligned}\mathbf{P}_{\mathbf{g12}}^{\sim} &= -\mathbf{B}_{\mathbf{g2}}^{\mathrm{T}}\left(j\omega\mathbf{I}+\mathbf{A}_{\mathbf{g}}^{\mathrm{T}}\right)^{-1}\mathbf{C}_{\mathbf{g2}}^{\mathrm{T}}+\mathbf{D}_{\mathbf{g12}}^{\mathrm{T}},\\ \mathbf{P}_{\mathbf{g21}}^{\sim} &= -\mathbf{B}_{\mathbf{g1}}^{\mathrm{T}}\left(j\omega\mathbf{I}+\mathbf{A}_{\mathbf{g}}^{\mathrm{T}}\right)^{-1}\mathbf{C}_{\mathbf{g2}}^{\mathrm{T}}+\mathbf{D}_{\mathbf{g21}}^{\mathrm{T}},\end{aligned}$$

respectively.

The calculation of the MNRD-value in Equation (4.58) requires a selection of the supremum out of infinitely many frequencies. However, since the static gain is expected to be zero at infinity and the maximum singular values at very high frequency do not contribute, a ω-vector of frequencies which ranges from 10^{-1} to 10^{4} including the resonance frequencies of the physical system can be used to determine the frequency at which the maximum singular value is the supremum. Mostly this range is divided into 300 to 1000 number of frequency points. This gives fairly well resolution for optimization purposes. If simply dividing this range from 10^{-1} to 10^{4} does not provide a good resolution, the interval halving method [51] can be utilized for that purpose.

Using MNRD-controller principle, it is also possible to calculate the closed-loop $\mathcal{H}_2$-norm square approximately. The definition of the $\mathcal{H}_2$-norm of the transfer function $\mathbf{T_{zw}}$ is as

$$\left\|\mathbf{T_{zw}}\right\|_2^2 = \frac{1}{2\pi}\int_{-\infty}^{\infty}\mathrm{trace}\left(\mathbf{T}_{\mathbf{zw}}^{*}\left(\omega\right)\mathbf{T_{zw}}\left(\omega\right)\right)\,\mathrm{d}\omega, \tag{4.59}$$

$$= \frac{1}{2\pi}\int_{-\infty}^{\infty}\sum_{i=1}^{n}\sigma_i^2\left(\mathbf{T_{zw}}\left(\omega\right)\right)\,\mathrm{d}\omega. \tag{4.60}$$

The integrals in (4.59) and (4.60) can be computed by the MATLAB commands QUADL and QUADGK numerically, which are written based on some adaptive quadrature integration techniques [61, 62].

4.2. The Improved Coprime Controller

In this section, a controller design method is proposed which improves over Hiramoto et al. [1]'s design. The approximate solutions of Equations (4.9) and (4.10) can be determined using the following property: The controllability and observability Gramians of diagonally dominant state matrices are also diagonally dominant and their off-diagonal terms can be neglected [3]. Hence, for state space realizations in one of the modal forms [3], one can solve the generalized ARE in Equations (4.9) and (4.10) approximately.

Lemma 4.2.1. *Assuming that the controllability and observability Gramians* $\mathbf{L_c}$ *and* $\mathbf{L_o}$ *of the stable generalized plant in* (2.61) *are diagonally dominant, their diagonal entries for "physical modes" are*

$$l_{ci} \cong \frac{\|\mathbf{B}_i\|_2^2}{4\zeta_i\omega_i}, \quad \forall i = 1 : N_p, \tag{4.61}$$

$$l_{oi} \cong \frac{\|\mathbf{C}_i\|_2^2}{4\zeta_i\omega_i}, \quad \forall i = 1 : N_p, \tag{4.62}$$

where $\mathbf{B}_i$ *and* $\mathbf{C}_i$ *are the* i^{th} *mode's contribution of the input matrix* $\mathbf{B_1}$ *or* $\mathbf{B_2}$ *and of the output matrix* $\mathbf{C_1}$ *or* $\mathbf{C_2}$*, respectively.*

Proof. The generalized plant has N modes. The first N_p modes are the physical modes and the remaining N_w modes relate to the signal weights. For the i^{th} mode (from $i = 1$ to N), the Lyapunov equations simplify to

$$l_{ci}\left(\mathbf{A}_i + \mathbf{A}_i^{\mathrm{T}}\right) + \mathbf{B}_i\mathbf{B}_i^{\mathrm{T}} = \mathbf{0}, \tag{4.63}$$

$$l_{oi}\left(\mathbf{A}_i + \mathbf{A}_i^{\mathrm{T}}\right) + \mathbf{C}_i^{\mathrm{T}}\mathbf{C}_i = \mathbf{0}, \tag{4.64}$$

where

$$\begin{aligned}
\mathbf{A}_i &= \begin{bmatrix} 0 & \omega_i \\ -\omega_i & -2\zeta_i\omega_i \end{bmatrix}, \\
\mathbf{B}_i\mathbf{B}_i^{\mathrm{T}} &= \begin{bmatrix} 0 & 0 \\ 0 & \|\mathbf{B}_i\|_2^2 \end{bmatrix}, \|\mathbf{B}_i\|_2^2 = \left(b_{i,1}^2 + b_{i,2}^2 + \ldots + b_{i,N_u}^2\right), \\
\mathbf{C}_i^{\mathrm{T}}\mathbf{C}_i &= \begin{bmatrix} 0 & 0 \\ 0 & \|\mathbf{C}_i\|_2^2 \end{bmatrix}, \|\mathbf{C}_i\|_2^2 = \left(c_{i,1}^2 + c_{i,2}^2 + \ldots + c_{i,N_s}^2\right).
\end{aligned}$$

In (4.63) and (4.64), $\mathbf{B}_i$ is the i^{th} mode's contribution to the input matrix $\mathbf{B}$, which is

$$\mathbf{B} = \left[\begin{array}{ccccc:cc:ccc} 0 & b_{1,1} & 0 & b_{2,1} & \cdots & 0 & b_{i,1} & \cdots & 0 & b_{N_p,1} & \cdots \\ 0 & b_{1,2} & 0 & b_{2,2} & \cdots & 0 & b_{i,2} & \cdots & 0 & b_{N_p,2} & \cdots \\ \vdots & & & & & \vdots & \vdots & & & \vdots & \\ 0 & b_{1,N_u} & 0 & b_{2,N_u} & \cdots & 0 & b_{i,N_u} & \cdots & 0 & b_{N_p,N_u} & \cdots \end{array}\right]^{\mathrm{T}}, \tag{4.65}$$

and $\mathbf{C}_i$ is the i^{th} mode's contribution to the output matrix $\mathbf{C}$, which is given as

$$\mathbf{C} = \left[\begin{array}{ccccc:cc:ccc} 0 & c_{1,1} & 0 & c_{2,1} & \cdots & 0 & c_{i,1} & \cdots & 0 & c_{N,1} & \cdots \\ 0 & c_{1,2} & 0 & c_{2,2} & \cdots & 0 & c_{i,2} & \cdots & 0 & c_{N,2} & \cdots \\ \vdots & & & & & \vdots & \vdots & & & \vdots & \\ 0 & c_{1,N_s} & 0 & c_{2,N_s} & \cdots & 0 & c_{i,N_s} & \cdots & 0 & c_{N_p,N_s} & \cdots \end{array}\right]. \tag{4.66}$$

So, if $\mathbf{A}_i$, $\mathbf{B}_i$ and $\mathbf{C}_i$ are inserted into Equations (4.63) and (4.64), the approximate controllability and observability Gramians for the i^{th} mode become (4.61) and (4.62).

□

Lemma 4.2.2. *Assuming that the controllability and observability Gramians* $\mathbf{L_c}$ *and* $\mathbf{L_o}$ *of the stable generalized plant in* (2.61) *are diagonally dominant, their diagonal entries for* N_w *"weighting modes" from* $i = N_p + 1$ *to* $N_p + N_w$ *are*

$$l_{ci}^w \cong -\frac{\mathbf{b}_i\mathbf{b}_i^{\mathrm{T}}}{2a_i}, \quad \forall\, i = N_p + 1 : N,$$

$$l_{oi}^{w} \cong -\frac{\mathbf{c}_i^{\mathrm{T}}\mathbf{c}_i}{2a_i}, \quad \forall\, i = N_p + 1 : N,$$

where $\mathbf{b}_i$ *and* $\mathbf{c}_i$ *are the* i^{th} *mode's contribution of the input matrix* $\mathbf{B_1}$ *or* $\mathbf{B_2}$ *and of the output matrix* $\mathbf{C_1}$ *or* $\mathbf{C_2}$*, respectively.*

Proof. For each of the N_w modes from $i = N_p + 1$ to N, which are concerned with signal weights, the Lyapunov equations simplify to

$$l_{ci}^{w}\left(a_i + a_i^{\mathrm{T}}\right) + \mathbf{b}_i\mathbf{b}_i^{\mathrm{T}} = 0, \tag{4.67}$$

$$l_{oi}^{w}\left(a_i + a_i^{\mathrm{T}}\right) + \mathbf{c}_i^{\mathrm{T}}\mathbf{c}_i = 0, \tag{4.68}$$

where a_i is scalar and is the i^{th} mode's contribution to the global block diagonalized state matrix $\mathbf{A}$. In (4.67) and (4.68), $\mathbf{b}_i\mathbf{b}_i^{\mathrm{T}}$ and $\mathbf{c}_i^{\mathrm{T}}\mathbf{c}_i$ are

$$\begin{aligned} \mathbf{b}_i\mathbf{b}_i^{\mathrm{T}} &= \|\mathbf{b}_i\|_2^2 = \left(b_{i1}^2 + b_{i2}^2 + \ldots + b_{iN_u}^2\right), \\ \mathbf{c}_i^{\mathrm{T}}\mathbf{c}_i &= \|\mathbf{c}_i\|_2^2 = \left(c_{i1}^2 + c_{i2}^2 + \ldots + c_{iN_s}^2\right), \end{aligned}$$

and $\mathbf{b}_i$ is the i^{th} mode's contribution to the input matrix

$$\mathbf{B} = \left[\begin{array}{ccc:c:c} \cdots & b_{N_p+1,1} & b_{N_p+2,1} & \cdots & b_{i,1} & \cdots & b_{N_p+N_w,1} \\ \cdots & b_{N_p+1,2} & b_{N_p+2,2} & \cdots & b_{i,2} & \cdots & b_{N_p+N_w,2} \\ & \vdots & \vdots & & \vdots & & \vdots \\ \cdots & b_{N_p+1,N_u} & b_{N_p+2,N_u} & \cdots & b_{i,N_u} & \cdots & b_{N_p+N_w,N_s} \end{array}\right]^{\mathrm{T}},$$

and $\mathbf{c}_i$ is the i^{th} mode's contribution to the output matrix

$$\mathbf{C} = \left[\begin{array}{ccc:c:c} \cdots & c_{N_p+1,1} & c_{N_p+2,1} & \cdots & c_{i,1} & \cdots & c_{N_p+N_w,1} \\ \cdots & c_{N_p+1,2} & c_{N_p+2,2} & \cdots & c_{i,2} & \cdots & c_{N_p+N_w,2} \\ & \vdots & \vdots & & \vdots & & \vdots \\ \cdots & c_{N_p+1,N_s} & c_{N_p+2,N_s} & \cdots & c_{i,N_s} & \cdots & c_{N_p+N_w,N_s} \end{array}\right].$$

The first $2 \times N_p$ entries of the diagonal approximate Gramians are calculated from Equations (4.61) and (4.62). The remaining N_w entries of the Gramians are calculated from Equations (4.67) and (4.68). □

Corollary 4.2.3. *The controllability and observability Gramians of the weighted generalized plant, which is stable, can be approximately given as*

$$\mathbf{L_c} = \operatorname{diag}\left(l_{c1}, l_{c1}, l_{c2}, l_{c2}, \ldots, l_{cN_p}, l_{cN_p}, l^w_{c1}, l^w_{c2}, \ldots, l^w_{cN_w}\right), \tag{4.69}$$

$$\mathbf{L_o} = \operatorname{diag}\left(l_{o1}, l_{o1}, l_{o2}, l_{o2}, \ldots, l_{oN_p}, l_{oN_p}, l^w_{o1}, l^w_{o2}, \ldots, l^w_{oN_w}\right). \tag{4.70}$$

Proof. Proofs of Lemmas 4.2.1 and 4.2.2 give how the approximate Gramians are calculated for physical and weighting modes, respectively. The controllability and observability Gramians of the generalized plant are simply

$$\mathbf{L_c} = \begin{bmatrix} \mathbf{L_c^p} & \mathbf{L_c^w} \end{bmatrix},$$
$$\mathbf{L_o} = \begin{bmatrix} \mathbf{L_o^p} & \mathbf{L_o^w} \end{bmatrix},$$

where

$$\mathbf{L_c^p} = \operatorname{diag}\left(l_{ci}, l_{ci}\right), \quad \mathbf{L_c^w} = \operatorname{diag}\left(l^w_{ci}\right),$$
$$\mathbf{L_o^p} = \operatorname{diag}\left(l_{oi}, l_{oi}\right), \quad \mathbf{L_o^w} = \operatorname{diag}\left(l^w_{oi}\right),$$

since the state space matrices in (2.61) can be partitioned as

$$\mathbf{A} =: \begin{bmatrix} \mathbf{A_m} & \mathbf{0} \\ \mathbf{0} & \hat{\mathbf{A}}_\mathbf{w} \end{bmatrix},$$
$$\mathbf{B_1} =: \begin{bmatrix} \hat{\mathbf{B}}^{\mathrm{T}}_{\mathbf{m1}} & \hat{\mathbf{B}}^{\mathrm{T}}_{\mathbf{w1}} \end{bmatrix}^{\mathrm{T}},$$
$$\mathbf{B_2} =: \begin{bmatrix} \hat{\mathbf{B}}^{\mathrm{T}}_{\mathbf{m2}} & \hat{\mathbf{B}}^{\mathrm{T}}_{\mathbf{w2}} \end{bmatrix}^{\mathrm{T}},$$
$$\mathbf{C_1} =: \begin{bmatrix} \hat{\mathbf{C}}_{\mathbf{m1}} & \hat{\mathbf{C}}_{\mathbf{w1}} \end{bmatrix},$$
$$\mathbf{C_2} =: \begin{bmatrix} \hat{\mathbf{C}}_{\mathbf{m2}} & \hat{\mathbf{C}}_{\mathbf{w2}} \end{bmatrix},$$

where

$$\hat{\mathbf{A}}_{\mathbf{w}} := \text{blockdiag}\left(\mathbf{A_w}, \ \mathbf{A_z}, \ \mathbf{A_u}, \ \mathbf{A_s} \right).$$

□

Theorem 4.2.4. *If the solutions of ARE's* (4.9) *and* (4.10) *are assumed to be of the form*

$$\mathbf{S} = \text{diag}\left(s_1, s_1, s_2, s_2, \ldots, s_N, s_N\right),$$
$$\mathbf{T} = \text{diag}\left(t_1, t_1, t_2, t_2, \ldots, t_N, t_N\right),$$

then the i^{th} entries can be calculated from equations

$$s_i^2 \alpha^2 l_{ci} + s_i - l_{oi} = 0,$$
$$t_i^2 l_{oi} + t_i - \alpha^2 l_{ci} = 0.$$

Since the solutions of Equations (4.9) *and* (4.10) *must be positive definite ($s_i > 0$ and $t_i > 0$), the positive solutions of the scalar quadratic equations*

$$s_i = \frac{-1 + \sqrt{1 + 4\alpha^2 l_{ci} l_{oi}}}{2\alpha^2 l_{ci}}, \tag{4.71}$$
$$t_i = \frac{-1 + \sqrt{1 + 4\alpha^2 l_{ci} l_{oi}}}{2 l_{oi}}, \tag{4.72}$$

are taken as the diagonally dominant solutions of the control and filter ARE's.

Proof. If only i^{th} mode is considered and indices of $\mathbf{B_2}$ and $\mathbf{C_2}$ are leaved by letting $\mathbf{B} := \mathbf{B_2}$ and $\mathbf{C} := \mathbf{C_2}$, ARE's (4.9) and (4.10) become

$$\mathbf{A}_i^{\mathrm{T}} s_i \mathbf{I_2} + s_i \mathbf{I_2} \mathbf{A}_i - \alpha^2 s_i \mathbf{I_2} \mathbf{B}_i \mathbf{B}_i^{\mathrm{T}} s_i \mathbf{I_2} + \mathbf{C}_i^{\mathrm{T}} \mathbf{C}_i = \mathbf{0},$$
$$\mathbf{A}_i t_i \mathbf{I_2} + t_i \mathbf{I_2} \mathbf{A}_i^{\mathrm{T}} - t_i \mathbf{I_2} \mathbf{C}_i^{\mathrm{T}} \mathbf{C}_i t_i \mathbf{I_2} + \alpha^2 \mathbf{B}_i \mathbf{B}_i^{\mathrm{T}} = \mathbf{0},$$

which can be expressed as

$$s_i\left(\mathbf{A}_i^{\mathrm{T}}+\mathbf{A}_i\right)-\alpha^2 s_i^2\mathbf{B}_i\mathbf{B}_i^{\mathrm{T}}+\mathbf{C}_i^{\mathrm{T}}\mathbf{C}_i = \mathbf{0}, \tag{4.73}$$

$$t_i\left(\mathbf{A}_i+\mathbf{A}_i^{\mathrm{T}}\right)-t_i^2\mathbf{C}_i^{\mathrm{T}}\mathbf{C}_i+\alpha^2\mathbf{B}_i\mathbf{B}_i^{\mathrm{T}} = \mathbf{0}. \tag{4.74}$$

Since it is clear from Equations (4.63) and (4.64) that

$$\begin{aligned}\mathbf{B}_i\mathbf{B}_i^{\mathrm{T}} &= -l_{ci}\left(\mathbf{A}_i+\mathbf{A}_i^{\mathrm{T}}\right),\\ \mathbf{C}_i^{\mathrm{T}}\mathbf{C}_i &= -l_{oi}\left(\mathbf{A}_i+\mathbf{A}_i^{\mathrm{T}}\right),\end{aligned}$$

where

$$\mathbf{A}_i+\mathbf{A}_i^{\mathrm{T}}=\begin{bmatrix}0 & 0\\ 0 & -4\zeta_i\omega_i\end{bmatrix},$$

Equations (4.73) and (4.74) become scalar quadratic equations of s_i and t_i. □

Remark. The solutions of Equations (4.73) and (4.74) for the weighting modes from N_p+1 to $N=N_p+N_w$ have the same expressions as s_i and t_i in Equations (4.71) and (4.72). Hence, once the Gramians in Equations (4.69) and (4.70) are calculated, the solutions of ARE's for the generalized plant can be obtained directly from Equations (4.71) and (4.72).

The controller K_∞ in Figure 4.1 is obtained by solving the ARE's (4.9) and (4.10) approximately and by choosing the parameters $\alpha>0$, $\beta>1$. With the controller K_∞, the state space realization of the closed-loop system $\mathbf{G_{zw}}$ is

$$\dot{\mathbf{x}}_\mathbf{c} = \mathbf{A_c}\mathbf{x_c}+\mathbf{B_c}\mathbf{w}, \tag{4.75}$$

$$\mathbf{z_c} = \mathbf{C_c}\mathbf{x_c}, \tag{4.76}$$

where

$$\mathbf{x_c} := \begin{bmatrix} \mathbf{x}^{\mathrm{T}} & \mathbf{x_{K_a}}^{\mathrm{T}} \end{bmatrix}^{\mathrm{T}}, \qquad \mathbf{A_c} := \begin{bmatrix} \mathbf{A} & \mathbf{B_2 C_{K_a}} \\ \mathbf{B_{K_a} C_2} & \mathbf{A_{K_a}} \end{bmatrix},$$
$$\mathbf{B_c} := \begin{bmatrix} \mathbf{B_1}^{\mathrm{T}} & \mathbf{B_{K_a} D_{21}} \end{bmatrix}^{\mathrm{T}}, \mathbf{C_c} := \begin{bmatrix} \mathbf{C_1} & \mathbf{D_{12} C_{K_a}} \end{bmatrix}.$$

The state space matrices $\mathbf{A_{K_a}}$, $\mathbf{B_{K_a}}$ and $\mathbf{C_{K_a}}$ of the controller in Figure 4.1 can be given as

$$\begin{aligned} \mathbf{A_{K_a}} &:= \mathbf{A} - \alpha^2 \mathbf{B_2 B_2}^{\mathrm{T}} \mathbf{S} + (\beta\gamma_{min})^2 \left(\mathbf{W}^{-1}\right)^{\mathrm{T}} \mathbf{T C_2}^{\mathrm{T}} \mathbf{C_2}, \\ \mathbf{B_{K_a}} &:= (\beta\gamma_{min})^2 \left(\mathbf{W}^{-1}\right)^{\mathrm{T}} \mathbf{T C_2}^{\mathrm{T}}, \\ \mathbf{C_{K_a}} &:= \alpha^2 \mathbf{B_2}^{\mathrm{T}} \mathbf{S}, \\ \text{with} \quad \mathbf{W} &:= \left(1 - (\beta\gamma_{min})^2\right) \mathbf{I} + \mathbf{ST}, \quad \gamma_{min} := \left(\mathbf{I} + \lambda_{max}\left(\mathbf{ST}\right)\right)^{1/2}. \end{aligned} \tag{4.77}$$

In (4.77), $\lambda_{max}(.)$ is the maximum eigenvalue. The closed-loop system $\mathbf{G_{zw}}$ includes open-loop plant and controller matrices which are functions of the configuration of the actuators and sensors [63].

4.3. The Improved Low-Authority $\mathcal{H}_\infty$-Controller

In Subsection 4.1.2, the general $\mathcal{H}_\infty$-control design framework was mentioned. This controller design strategy can be applied to any physical system in nature ranging from an highly maneuverable war plane to a simple spring mass system.

For the flexible structures another $\mathcal{H}_\infty$-control design (the low-authority $\mathcal{H}_\infty$-control design) given in Subsection 4.1.3 can be preferred if it takes less computation time without any significant changes in the values of the objective functions, but the design of a low-authority $\mathcal{H}_\infty$-controller given in [3] is limited to certain types of frequency weights.

In Section 4.2, a useful and simpler coprime controller design strategy is intro-

duced, which handles a more general class of systems and frequency weights. Using the principles given in [3], the improved coprime controller design method mentioned in Section 4.2 will be extended to the general $\mathcal{H}_\infty$-control design framework.

For this purpose, first, the signal weights in Figures 2.7 and 2.8 are added to the physical system which is given in the first modal state space form. The obtained generalized plant is diagonalized by the procedure introduced in Section 2.6 and converted to the block diagonal form as in (2.61).

4.3.1. Low-Authority $\mathcal{H}_\infty$-Controllers for Generalized Plants

The assumptions given in Subsection 4.1.2 must be valid before designing the improved low-authority $\mathcal{H}_\infty$-controller. Furthermore, although $\mathbf{D_{12}}$ and $\mathbf{D_{21}}$ are

$$\begin{aligned} \mathbf{D_{12}} &= \begin{bmatrix} \mathbf{D_u} \\ \mathbf{D_z D_{m12}} \end{bmatrix}, \\ \mathbf{D_{21}} &= -\begin{bmatrix} \mathbf{D_{m21} D_w} & \mathbf{D_s} \end{bmatrix}, \end{aligned}$$

where $\mathbf{D_{m12}} = \mathbf{0}$ and $\mathbf{D_{m21}} = \mathbf{0}$, $\mathbf{D_{12}}$ and $\mathbf{D_{21}}$ matrices are assumed to be $\mathbf{D_{12}^T} = \mathbf{D_{21}} = \begin{bmatrix} \mathbf{0} & \mathbf{I} \end{bmatrix}$ for simplicity [30, 64]. These assumptions can be achieved by scaling of $\mathbf{u}$ and $\mathbf{y}$ as

$$\tilde{\mathbf{u}} := \mathbf{S_u u}, \tag{4.78}$$

$$\tilde{\mathbf{y}} := \mathbf{S_y y}, \tag{4.79}$$

and by nonsingular unitary transformations of $\mathbf{w}$ and $\mathbf{z}$ as

$$\tilde{\mathbf{w}} := \mathbf{T_w w}, \tag{4.80}$$

$$\tilde{\mathbf{z}} := \mathbf{T_z z}. \tag{4.81}$$

The resulting generalized plant has the state space representation

$$
\begin{aligned}
\tilde{\mathbf{A}} &:= \mathbf{A}, & \tilde{\mathbf{B}}_{\mathbf{1}} &:= \mathbf{B}_{\mathbf{1}}\mathbf{T}_{\mathbf{w}}^{\mathrm{H}}, & \tilde{\mathbf{B}}_{\mathbf{2}} &:= \mathbf{B}_{\mathbf{2}}{\mathbf{S}_{\mathbf{u}}}^{-1}, \\
\tilde{\mathbf{C}}_{\mathbf{1}} &:= \mathbf{T}_{\mathbf{z}}\mathbf{C}_{\mathbf{1}}, & \tilde{\mathbf{D}}_{\mathbf{11}} &:= \mathbf{T}_{\mathbf{z}}\mathbf{D}_{\mathbf{11}}\mathbf{T}_{\mathbf{w}}^{\mathrm{H}}, & \tilde{\mathbf{D}}_{\mathbf{12}} &:= \mathbf{T}_{\mathbf{z}}\mathbf{D}_{\mathbf{12}}{\mathbf{S}_{\mathbf{u}}}^{-1}, \\
\tilde{\mathbf{C}}_{\mathbf{2}} &:= \mathbf{S}_{\mathbf{y}}\mathbf{C}_{\mathbf{2}}, & \tilde{\mathbf{D}}_{\mathbf{21}} &:= \mathbf{S}_{\mathbf{y}}\mathbf{D}_{\mathbf{21}}\mathbf{T}_{\mathbf{w}}^{\mathrm{H}}, & \tilde{\mathbf{D}}_{\mathbf{22}} &:= \mathbf{S}_{\mathbf{y}}\mathbf{D}_{\mathbf{22}}{\mathbf{S}_{\mathbf{u}}}^{-1}.
\end{aligned}
\tag{4.82}
$$

Lemma 4.3.1. *For the generalized plant* (4.82)*, the ARE's* (4.23) *and* (4.24) *associated with the $\mathcal{H}_\infty$-controller design can be reduced to simple quadratic equations* (4.40) *and* (4.41)*, which are introduced by Gawronski* [3] *for the physical plant of a flexible structure.*

Proof. The transformations $\mathbf{T_w}$, $\mathbf{T_z}$, $\mathbf{S_u}$ and $\mathbf{S_y}$ are diagonal and scale only the input and output matrices. The state matrix is still block diagonal, since $\tilde{\mathbf{A}} = \mathbf{A}$. Therefore, as stated in Corollary 4.2.3, the approximate Gramians (4.69) and (4.70) are obtained for the realization in Equation (4.82) such that (4.40) and (4.41) become valid for state space representation of the generalized plant. □

Remark. Lemma 4.3.1 states that Equations (4.40) and (4.41), which are derived only for the physical plant [3], are also valid for a generalized plant with signal weightings so that the low-authority assumption given by Gawronski [3] is applicable to the plant in (4.82). Therefore, the diagonal versions of the Control Algebraic Riccati Equation (CARE) and the Filter Algebraic Riccati Equation (FARE) in (4.40) and (4.41) are allowed to be used, which have diagonal solutions

$$x_{\infty i} = \frac{\beta_c - 1}{2\kappa_c}, \tag{4.83}$$

$$y_{\infty i} = \frac{\beta_e - 1}{2\kappa_e}, \tag{4.84}$$

where

$$\beta_c = \sqrt{1 + 4l_{o1}\kappa_c},$$

$$\beta_e = \sqrt{1 + 4l_{c1}\kappa_e}$$

and κ_c and κ_e are defined in Equations (4.42) and (4.43). In (4.83) and (4.84) $x_{\infty i}$ and $y_{\infty i}$ are i^{th} diagonal component of $\mathbf{X}_\infty$ and $\mathbf{Y}_\infty$, respectively.

4.3.2. Controller Matrices for Generalized Plants

Theorem 4.3.2. *The low-authority controller design which is introduced by Gawronski* [3] *for a physical plant of a flexible structure is also applicable to a generalized plant with signal filtering if the state space representation of the generalized plant is converted to one of the modal forms using Theorem 2.6.1.*

Proof. In the $\mathcal{H}_\infty$-controller design given by [30, 64], $\mathbf{D_{m12}} = \mathbf{0}$ and $\mathbf{D_{m21}} = \mathbf{0}$. That can be achieved by the transformations (4.78) through (4.81), and the generalized plant can be converted to the scaled generalized plant in (4.82). According Lemma 4.3.1, ARE's for the plant (4.82) can be solved as quadratic equations. Using again the transformations (4.78) through (4.81), the controller (4.85) can be given for the generalized plant. □

The $\mathcal{H}_\infty$-norm can be computed by a simple bisection algorithm. In the bisection method, disturbance attenuation factor γ is minimized in successive iterations at each of which all of the assumptions are checked. If γ_{min} is achieved, then this value and the corresponding approximate CARE and FARE solutions are used to obtain the central $\mathcal{H}_\infty$-controller that is given by Equation (4.25). Using ARE solutions (4.83) and (4.84), a low-authority $\mathcal{H}_\infty$ controller is designed for the scaled plant in Equation (4.82). The controller matrices are

$$\begin{aligned}
\tilde{\mathbf{A}}_\mathbf{K} &= \tilde{\mathbf{A}}_\infty, \\
\tilde{\mathbf{B}}_\mathbf{K} &= \begin{bmatrix} -\tilde{\mathbf{Z}}_\infty \tilde{\mathbf{L}}_\infty & \tilde{\mathbf{Z}}_\infty \tilde{\mathbf{B}}_\mathbf{2} \end{bmatrix}, \\
\tilde{\mathbf{C}}_\mathbf{K} &= \begin{bmatrix} \tilde{\mathbf{F}}_\infty \\ -\tilde{\mathbf{C}}_\mathbf{2} \end{bmatrix},
\end{aligned}$$

where

$$\begin{aligned}
\tilde{\mathbf{A}}_\infty &= \tilde{\mathbf{A}} + \gamma^{-2}\tilde{\mathbf{B}}_\mathbf{1}\tilde{\mathbf{B}}_\mathbf{1}^{\mathrm{T}}\mathbf{X}_\infty + \tilde{\mathbf{B}}_\mathbf{2}\tilde{\mathbf{F}}_\infty + \tilde{\mathbf{Z}}_\infty\tilde{\mathbf{L}}_\infty\tilde{\mathbf{C}}_\mathbf{2}, \\
\tilde{\mathbf{F}}_\infty &= -\tilde{\mathbf{B}}_\mathbf{2}^{\mathrm{T}}\mathbf{X}_\infty, \\
\tilde{\mathbf{L}}_\infty &= -\mathbf{Y}_\infty, \tilde{\mathbf{C}}_\mathbf{2}^{\mathrm{T}}, \\
\tilde{\mathbf{Z}}_\infty &= \left(\mathbf{I} - \gamma^{-2}\mathbf{Y}_\infty\mathbf{X}_\infty\right)^{-1}.
\end{aligned}$$

The designed controller can be converted to the coordinates, in terms of which the generalized plant is expressed, as

$$\begin{aligned}
\mathbf{A_K} &= \tilde{\mathbf{A}}_\mathbf{K}, \\
\mathbf{B_K} &= \tilde{\mathbf{B}}_\mathbf{K}\mathbf{S_y}, \\
\mathbf{C_K} &= \mathbf{S_u}^{-1}\tilde{\mathbf{C}}_\mathbf{K}.
\end{aligned} \tag{4.85}$$

5. PARTIAL DERIVATIVES OF CLOSED-LOOP STATE SPACE MATRICES

For an optimization using gradient of closed-loop criteria, partial derivatives of both open-loop state space matrices and controller matrices are required. For this purpose, partial derivatives of finite element matrices are defined in this chapter.

5.1. Partial Derivatives of FE Matrices for Point Actuator/Sensor Pairs

If FEM is applied, the optimization function J for optimal location selection becomes a function of the global mass and stiffness matrices, the natural frequencies and the modes shapes. The natural frequencies and mode shapes are not differentiable. In order to overcome this limitation, the discrete nature of eigenvalues (natural frequencies) and eigenvectors (mode shapes) one may employ sensitivity analysis [52].

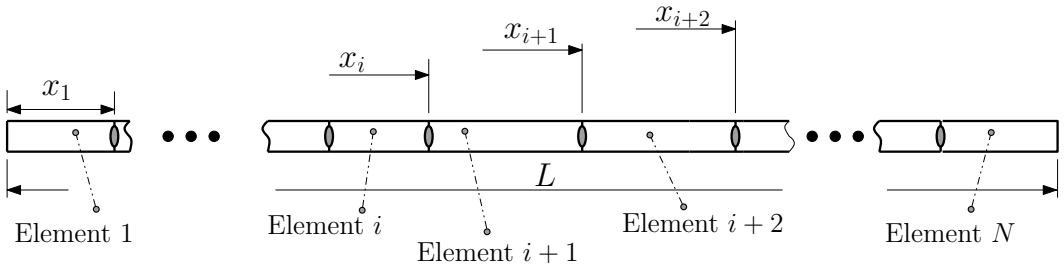

Figure 5.1. Typical beam with finite elements

For the sensitivity analysis the derivatives of the global Finite Element mass and stiffness matrices with respect to the design variables must be defined. In our case, the design parameter can be selected as the distance of the point actuator and sensor pair from the left end of the beam. When FEM is applied, the point actuator and sensor pair may be considered as settled in one of the nodes between two adjacent finite elements. Therefore, taking the derivative of the finite element with respect to that node of the actuator, will give the derivatives of the Finite Element mass and stiffness matrices, which are in turn summed up to obtain the derivative of the global Finite Elements as in summing up all of the element matrices to build the global matrices.

The following strategy is developed to obtain the derivatives of the element matrices. The coordinate of the right node and the coordinate of the left node of the i^{th} element pair is described as x_{i-1} and x_i, respectively, then the length of the i^{th} element can be expressed as (see Figure 5.1)

$$l_i = x_i - x_{i-1}. \tag{5.1}$$

If the coordinate of the left end, x_i, of the beam element is chosen as the design parameter p, the partial derivatives of the element stiffness matrices of all elements must be taken with respect to that node only. For this purpose, consider the stiffness and mass matrix of the element i in Figure 5.1

$$\mathbf{K_e} = \frac{2EI}{l_i^2}\begin{bmatrix} 6 & 3l_i & -6 & 3l_i \\ 3l_i & 2l_i^2 & -3l_i & l_i^2 \\ -6 & -3l_i & 6 & -3l_i \\ 3l_i & l_i^2 & -3l_i & 2l_i^2 \end{bmatrix},$$

$$\mathbf{M_e} = \frac{\rho A l_i}{420}\begin{bmatrix} 156 & 22l_i & 54 & -13l_i \\ 22l_i & 4{l_i}^2 & 13l_i & -3{l_i}^2 \\ 54 & 13l_i & 156 & -22l_i \\ -13l_i & -3{l_i}^2 & -22l_i & 4{l_i}^2 \end{bmatrix}.$$

The partial derivatives of the stiffness and mass matrices with respect to x_i, which is the the design variable p, are

$$\frac{\partial \mathbf{T_e}}{\partial p} = \frac{\partial \mathbf{T_e}}{\partial x_i} = \frac{\partial \mathbf{T_e}}{\partial l_i}\frac{\partial l_i}{\partial x_i},$$

where $\mathbf{T_e}$ is $\mathbf{K_e}$ or $\mathbf{M_e}$, and the partial derivatives of them are

$$\frac{\partial \mathbf{K_e}}{\partial l_i} = \frac{2EI}{{l_i}^4}\begin{bmatrix} -18 & -6l_i & 18 & -6l_i \\ -6l_i & -2{l_i}^2 & 6l_i & -{l_i}^2 \\ 18 & 6l_i & -18 & 6l_i \\ -6l_i & -{l_i}^2 & 6l_i & -2{l_i}^2 \end{bmatrix},$$

$$\frac{\partial \mathbf{M_e}}{\partial l_i} = \frac{\rho A}{420}\begin{bmatrix} 156 & 44l_i & 54 & -26l_i \\ 44l_i & 12{l_i}^2 & 26l_i & -9{l_i}^2 \\ 54 & 26l_i & 156 & -44l_i \\ -26l_i & -9{l_i}^2 & -44l_i & 12\,{l_i}^2 \end{bmatrix}.$$

Since the lengths of the elements can be given in terms of global coordinates x_i from $i = 1$ to N as in Equation (5.1), the partial derivatives with respect to x_i can be expressed as

$$\begin{aligned} \frac{\partial \mathbf{T_e}}{\partial x_i} &= \frac{\partial \mathbf{T_e}}{\partial l_i}\underbrace{\frac{\partial l_i}{\partial x_i}}_{1}, \\ \frac{\partial \mathbf{T}_{\mathbf{e}i+1}}{\partial x_i} &= \frac{\partial \mathbf{T}_{\mathbf{e}i+1}}{\partial l_{i+1}}\underbrace{\frac{\partial l_{i+2}}{\partial x_i}}_{-1}, \\ \frac{\partial \mathbf{T}_{\mathbf{e}i+2}}{\partial x_i} &= \frac{\partial \mathbf{T}_{\mathbf{e}i+2}}{\partial l_{i+2}}\underbrace{\frac{\partial l_{i+2}}{dx_i}}_{0}, \end{aligned}$$

where $\mathbf{T_e}$ is $\mathbf{K_e}$ or $\mathbf{M_e}$. The lengths of the elements i, $i+1$ and $i+2$ are l_i, l_{i+1} and l_{i+2}, respectively.

The i^{th} element with a actuator and sensor pair at its end (right node) and the neighboring $(i+1)^{\text{th}}$ element have partial derivatives with respect to the design variable $p = x_i$. All other elements have no contributions. Hence, for N elements with $N+1$ nodes, the partial derivatives of element lengths l_j with respect to coordinates of each node x_i can be given by (5.2) where the i^{th}-row gives the partial derivatives of the element lengths with respect to the i^{th} node.

After the element matrix derivatives are calculated, the next step is the assembly procedure of the element matrix derivatives. For beams, the partial derivatives with respect to a single coordinate are required. However, for plates, in addition to the partial derivatives with respect to x_i, the derivatives with respect to y_i have to be calculated in the same manner.

$$\frac{\partial l_j}{\partial x_i} = \overbrace{\begin{bmatrix} 0 & 0 & \dots & & & & & 0 \\ 1 & -1 & 0 & \dots & & & & 0 \\ 0 & 1 & -1 & 0 & \dots & & & 0 \\ 0 & 0 & 1 & -1 & 0 & \dots & & 0 \\ \vdots & & & & & & & \vdots \\ 0 & \dots & & & 0 & 1 & -1 & 0 & 0 \\ 0 & \dots & & & 0 & 1 & -1 & 0 \\ 0 & \dots & & & & 0 & 1 & -1 \\ 0 & \dots & & & & & 0 & 0 \end{bmatrix}}^{l_1 \;\; l_2 \;\; \dots \;\; l_j \;\; \dots l_N} \tag{5.2}$$

5.2. Remeshing Policy for Structures with Point Actuator and Sensors

In FEM, a structure is divided into a certain number of elements. However, in the developed optimization algorithm the number, the length and the absolute coordinates of the finite elements may change during iterations since the locations of point forces, which should coincide with the nodes of finite elements, change at each iteration.

One way of achieving this consistency is to accept an initial mesh with finite elements of equal length and to divide an element with forces on it into two or more elements such that the force acts on the node between two adjacent elements during an iteration.

In Figure 5.2 (a), the calculated location of the i^{th} actuator is somewhere between the nodes of the element j. Due to the continuity requirement in FEM, this is not allowed. Hence, to be consistent with the finite element theory, one may simply divide the corresponding element into two elements as in Figure 5.2 (b). The point force is then located at the node between these two neighboring elements, and the number of finite elements is increased by one. In each iteration the positions of the singular forces,

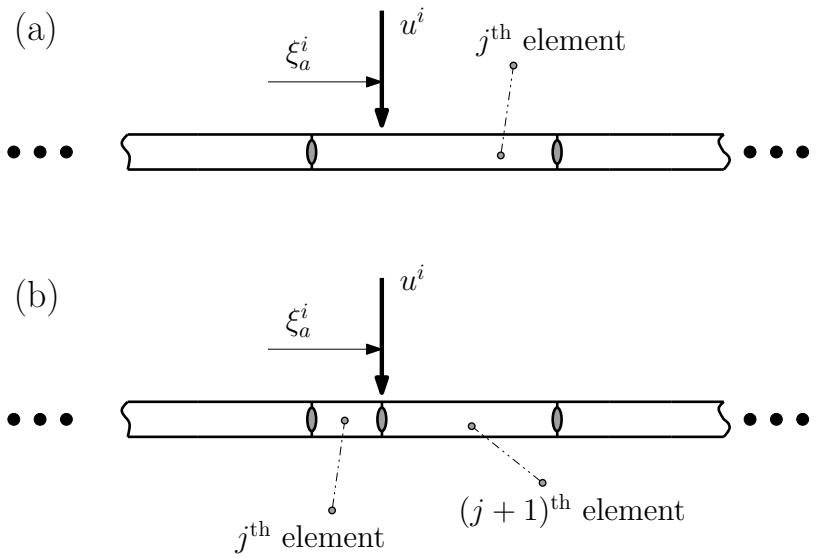

Figure 5.2. Dividing finite elements during an iteration

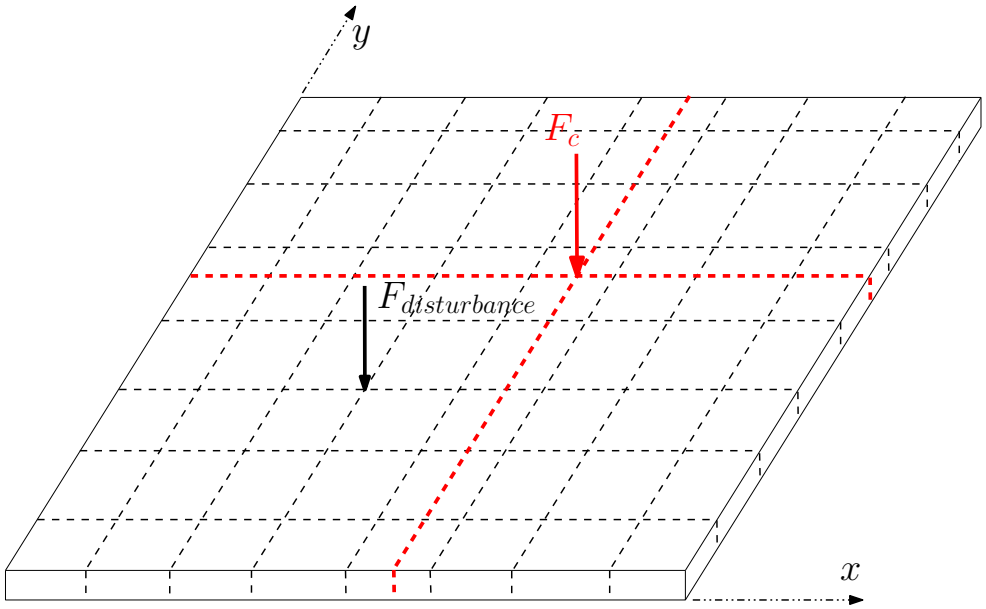

Figure 5.3. Dividing plate finite elements during an iteration

which are either the actuator forces or the disturbances, are checked and the finite element mesh is re-considered. Hence, if one proposes to have N_e number of elements, this number may be increased by the number of the point forces that are acting on the system. The maximum finite elements in some iterations can be $N_e + N_w + 2$, where there are N_w disturbances and two actuators.

In Figure 5.3, the same remeshing strategy is given for plates. The collocated point actuator and sensor pair may not act on an element. Hence, the corresponding

element is divided into four elements.

5.3. Partial Derivatives of FE Matrices for PZT Actuator/Sensor Pairs

For structures combined with PZT patches, the total length of the collocated piezoelectric actuator and sensor pair is constant during iterations, but not the coordinates of the most left and the most right nodes. As the coordinate of the left node of the first piezoelectric patch x_k changes (see Figure 5.4), the lengths L_{k-1}, L_k, L_{k+n} and L_{k+n+1} have partial derivatives with respect to x_k, where the actuator and sensor pair consists of n piezoelectric patches. Hence, similar to the case with point actuators and sensors the partial derivatives of the mass, stiffness and piezoelectric coupling matrices can be given in terms of the partial derivatives of the length of each element with respect to the starting coordinate of PZT pair as

$$\frac{\partial \mathbf{T_e}}{\partial x_i} = \frac{\partial \mathbf{T_e}}{\partial l_i}\frac{\partial l_i}{\partial p},$$

where $\mathbf{T_e}$ can be the element stiffness matrix $\mathbf{K_e}$ or the element mass matrix $\mathbf{M_e}$ or one of the PZT element matrices such as $\mathbf{K_{u\phi}}$, $\mathbf{K_{\phi u}}$ and $\mathbf{K_{\phi\phi}}$.

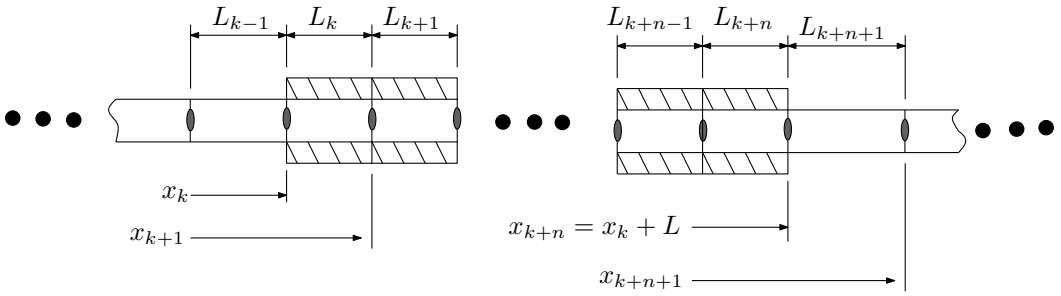

Figure 5.4. Beam finite elements with PZT patches

For PZT patches, $\frac{\partial l_i}{\partial p}$ is replaced by $\mathbf{L}^p$, which is

$$\begin{aligned}
\mathbf{L}^p &= \mathbf{L_i}^p + \mathbf{L_f}^p \\
\mathbf{L_i}^p &= \left[\begin{array}{ccccccccc} 0 & \dots & 0 & \dfrac{\partial}{\partial p}L_{k-1} & \dfrac{\partial}{\partial p}L_{k-1} & 0 & \dots & 0 \end{array}\right] \\
\mathbf{L_f}^p &= \left[\begin{array}{ccccccccc} 0 & \dots & 0 & \dfrac{\partial}{\partial p}L_{k+n} & \dfrac{\partial}{\partial p}L_{k+n+1} & 0 & \dots & 0 \end{array}\right]
\end{aligned}$$

where $\frac{\partial}{\partial p}L_{k-1} = \frac{\partial}{\partial p}L_{k+n} = 1$ and $\frac{\partial}{\partial p}L_{k-1} = \frac{\partial}{\partial p}L_{k+n+1} = -1$. The vectors $\mathbf{L_i}^p$ and $\mathbf{L_f}^p$ are vectors of partial derivatives of individual lengths of elements with respect to the initial and final coordinates of the PZT pairs, respectively, as shown in Figure 5.4. The coordinate of the node, with respect to which the partial derivatives of the FE matrices are to be solved, is given by p. The vector $\mathbf{L}^p$ is an $1 \times N$ vector of the partial derivatives $\dfrac{\partial l_i}{\partial p}$ for $i = 1 : N$. Hence, the partial derivative of an element matrix $\mathbf{T_e}$ with respect to a design variable becomes

$$\frac{\partial \mathbf{T_e}}{\partial x_i} = \frac{\partial \mathbf{T_e}}{\partial l_i} L_i^p.$$

If the element matrix derivatives calculated, the derivatives of global matrices are obtained in the usual assembly procedure.

The overall procedure for calculating the global matrix derivatives for plates is similar. For plates, there is the y-coordinate as the second coordinate, which is independent from the x-coordinate. Hence, repeating the procedure for the y-coordinate of the starting point of the actuator and sensor pair gives the partial derivatives with respect to that coordinate.

5.4. Remeshing Policy for Structures with PZT Actuator/Sensor Pairs

Unlike the case of point actuators and sensors, where the structures are initially divided into elements of equal lengths, the beams with PZT pairs are divided into two regions of PZT parts and non-PZT parts. Before discretizing the structure, the largest allowed sizes of non-PZT and PZT elements are determined (l_n and l_p). All of the non-PZT elements must be smaller than that prescribed size l_n. None of the elements of PZT pairs may be greater than l_p.

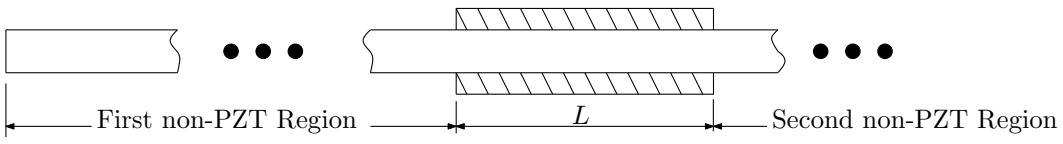

Figure 5.5. Non-PZT and PZT parts of the beam

Then, the non-PZT regions are divided into finite elements. If there are disturbances in that region, the elements around the disturbances may have different lengths as shown in Figure 5.6. After this is repeated for every non-PZT part, the PZT regions are discretized as well.

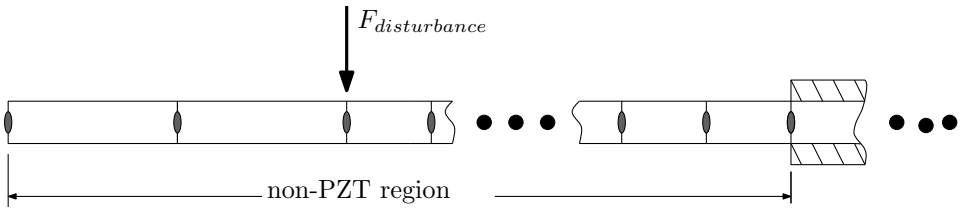

Figure 5.6. Non-PZT part of the beam

To let the point disturbances coincide with the nodes in PZT parts, a strategy is used to better adapt finite elements to the acting disturbances (see Figure 5.7). The parts of the beam with piezoelectric actuator and sensor pair are divided into more finite elements than parts without PZT pairs, and the coordinate of the node, which is closest to the disturbance, is replaced with the coordinate of the disturbance. The main concern is to let the PZT pathes to consist of the same number of finite elements at each iteration.

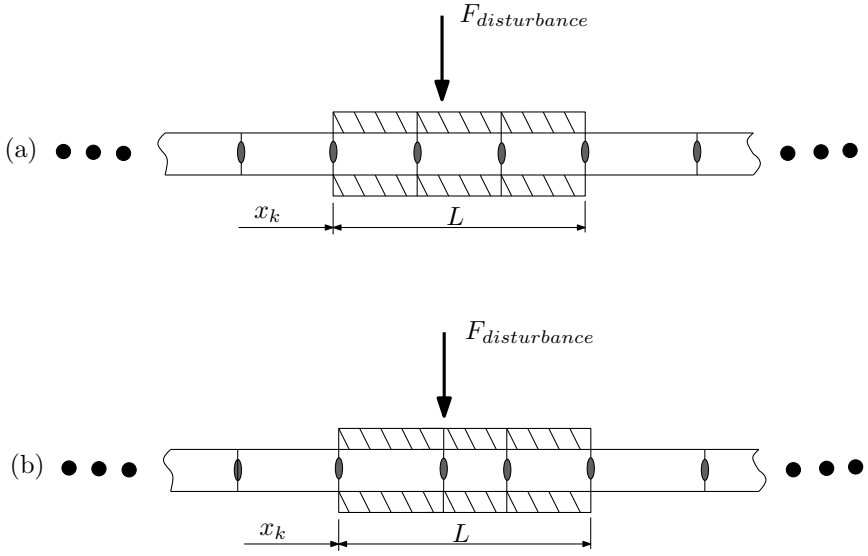

Figure 5.7. Dividing beam finite elements with PZT patches during an iteration

The given discretization procedure can be extended to the plates by simply introducing the y-coordinate.

5.5. Partial Derivatives of Mode Shapes and Natural Frequencies

When the mass matrix $\mathbf{M}$ and the stiffness matrix $\mathbf{K}$ are calculated and the partial derivatives of them with respect to a design parameter p is defined, it is possible to calculate partial derivatives of the mode shapes and of the natural frequencies with respect to the design parameter p. Their partial derivatives are

$$\frac{\partial \omega_r^2}{\partial p} = \mathbf{u}_r^{\mathrm{T}} \left(\frac{\partial \mathbf{K}}{\partial p} - \omega_r^2 \frac{\partial \mathbf{M}}{\partial p} \right) \mathbf{u}_r, \qquad \forall\, r = 1 : n, \tag{5.3}$$

$$\frac{\partial \mathbf{u}_r}{\partial p} = \sum_{j=1}^{m} c_{rj} \mathbf{u}_j, \qquad \forall\, r = 1 : n, \tag{5.4}$$

where $\mathbf{K}$ and $\mathbf{M}$ are global stiffness and mass matices, respectively. The r^{th} eigenvector or mode shape for the eigenvalue problem $(\mathbf{K} - \omega_r^2 \mathbf{M})\, \mathbf{u}_r = 0$ is denoted by $\mathbf{u}_r$. The coefficient c_{rj} is calculated as follows [52, 53, 54, 65, 66]:

$$c_{rj} = \begin{cases} \dfrac{\left(\dfrac{\partial \mathbf{K}}{\partial p} - \omega_r^2 \dfrac{\partial \mathbf{M}}{\partial p} \right)}{\omega_r - \omega_j} & \text{if } r \neq j, \\ -\dfrac{1}{2} \left(\mathbf{u}_r \right)^{\mathrm{T}} \dfrac{\partial \mathbf{M}}{\partial p} \mathbf{u}_r & \text{if } r = j. \end{cases} \tag{5.5}$$

The partial derivatives of natural frequencies and mode shapes defined by Equations (5.3), (5.4) and (5.5) are valid for distinct values of natural frequencies with proportional damping. However, different methodologies are also found in literature for calculating the partial derivatives of natural frequencies and mode shapes of a system with nonproportional damping and/or repeated eigenvalues. Friswell [67] extends the partial derivative calculation to nonproportionally damped system. The papers [68, 69, 70, 71] give different but similar techniques to compute repeated eigenvalue-eigenvectors. The higher order derivatives of natural frequencies and mode shapes can also be calculated according to [72].

5.6. Partial Derivatives of State Space Matrices of Generalized Plant

With the derivatives of the natural frequencies in (5.3) and of the mode shapes in (5.4), it is possible to obtain the partial derivatives of the state matrices of the closed-loop system described in Equations (4.75). The closed-loop system matrices in (4.75) include the open-loop generalized plant in (2.61) and the controller matrices (4.77). Since the controller matrices are functions of the generalized plant in (2.61), the gradient calculation, which is necessary for the optimization part, requires the derivatives of open-loop state space matrices $\mathbf{A}$, $\mathbf{B_1}$, $\mathbf{B_2}$, $\mathbf{C_1}$, $\mathbf{C_2}$, $\mathbf{D_{11}}$, $\mathbf{D_{12}}$, $\mathbf{D_{21}}$ and $\mathbf{D_{22}}$. Their partial derivatives are

$$\frac{\partial \mathbf{A}}{\partial \xi_a^i} = \text{diag}\left(\frac{\partial \mathbf{A_m}}{\partial \xi_a^i}, \frac{\partial \mathbf{A_w}}{\partial \xi_a^i}, \frac{\partial \mathbf{A_z}}{\partial \xi_a^i}, \frac{\partial \mathbf{A_u}}{\partial \xi_a^i}, \frac{\partial \mathbf{A_s}}{\partial \xi_a^i}\right), \tag{5.6}$$

$$\frac{\partial \mathbf{B_1}}{\partial \xi_a^i} = \frac{\partial \mathbf{B_{g1}}}{\partial \xi_a^i}\mathbf{Z} + \mathbf{B_{g1}}\frac{\partial \mathbf{Z}}{\partial \xi_a^i}, \tag{5.7}$$

$$\frac{\partial \mathbf{B_2}}{\partial \xi_a^i} = \frac{\partial \mathbf{B_{g2}}}{\partial \xi_a^i}\mathbf{Z} + \mathbf{B_{g2}}\frac{\partial \mathbf{Z}}{\partial \xi_a^i}, \tag{5.8}$$

$$\frac{\partial \mathbf{C_1}}{\partial \xi_a^i} = \mathbf{Z}^{-1}\frac{\partial \mathbf{C_{g1}}}{\partial \xi_a^i} + \frac{\partial \mathbf{Z}^{-1}}{\partial \xi_a^i}\mathbf{C_{g1}}, \tag{5.9}$$

$$\frac{\partial \mathbf{C_2}}{\partial \xi_a^i} = \mathbf{Z}^{-1}\frac{\partial \mathbf{C_{g2}}}{\partial \xi_a^i} + \frac{\partial \mathbf{Z}^{-1}}{\partial \xi_a^i}\mathbf{C_{g2}}, \tag{5.10}$$

$$\frac{\partial \mathbf{D_{11}}}{\partial \xi_a^i} = \frac{\partial \mathbf{D_{g11}}}{\partial \xi_a^i}, \tag{5.11}$$

$$\frac{\partial \mathbf{D_{12}}}{\partial \xi_a^i} = \frac{\partial \mathbf{D_{g12}}}{\partial \xi_a^i}, \tag{5.12}$$

$$\frac{\partial \mathbf{D_{21}}}{\partial \xi_a^i} = \frac{\partial \mathbf{D_{g21}}}{\partial \xi_a^i}, \tag{5.13}$$

$$\frac{\partial \mathbf{D_{22}}}{\partial \xi_a^i} = \frac{\partial \mathbf{D_{g22}}}{\partial \xi_a^i}, \tag{5.14}$$

where $\dfrac{\partial \mathbf{Z}}{\partial \xi_a^i}$ is the derivative of the coordinate transformation $\mathbf{Z}$ that is used to diagonalize global state matrix $\mathbf{A_g}$ in Equation (2.61) and is given by

$$\frac{\partial \mathbf{Z}}{\partial \xi_a^i} = \frac{\partial \mathbf{X}}{\partial \xi_a^i}\hat{\mathbf{X}}^{-1} + \mathbf{X}\frac{\partial \hat{\mathbf{X}}^{-1}}{\partial \xi_a^i}, \tag{5.15}$$

$$\text{with} \quad \frac{\partial \hat{\mathbf{X}}^{-1}}{\partial \xi_a^i} = -\hat{\mathbf{X}}^{-1}\frac{\partial \mathbf{X}}{\partial \xi_a^i}\hat{\mathbf{X}}^{-1}. \tag{5.16}$$

$\frac{\partial \mathbf{Z}}{\partial \xi_a^i}$ can be assumed to be zero since its contribution to the derivatives to the state space matrices of the generalized plant is of very low level. Hence, matrices from (5.7) to (5.14) can be calculated simpler.

The partial derivatives of the matrices from (5.7) to (5.14) include the derivatives of the state space matrices of the physical plant in the first modal form. Since the nodes of the elements vary, the signal weightings do not change; their contributions to the partial derivatives of the generalized plant vanish. The derivatives of the matrices $\mathbf{A_m}$, $\mathbf{B_{m1}}$, $\mathbf{B_{m2}}$, $\mathbf{C_{m1}}$, $\mathbf{C_{m2}}$, $\mathbf{D_{m11}}$, $\mathbf{D_{m12}}$, $\mathbf{D_{m21}}$ and $\mathbf{D_{m22}}$ of the physical plant are

$$\frac{\partial \mathbf{A_m}}{\partial \xi_a^i} = \operatorname{diag}\left(\begin{pmatrix} 0 & \frac{\partial \omega_i}{\partial \xi_a^i} \\ -\frac{\partial \omega_i}{\partial \xi_a^i} & -2\zeta_i \frac{\partial \omega_i}{\partial \xi_a^i} \end{pmatrix} \right), \tag{5.17}$$

$$\frac{\partial \mathbf{B_{m1}}}{\partial \xi_a^i} = \frac{\partial \hat{\mathbf{B}}_\mathbf{1}}{\partial \xi_a^i}\hat{\mathbf{R}} + \hat{\mathbf{B}}_\mathbf{1}\frac{\partial \hat{\mathbf{R}}}{\partial \xi_a^i}, \tag{5.18}$$

$$\frac{\partial \mathbf{B_{m2}}}{\partial \xi_a^i} = \frac{\partial \hat{\mathbf{B}}_\mathbf{2}}{\partial \xi_a^i}\hat{\mathbf{R}} + \hat{\mathbf{B}}_\mathbf{2}\frac{\partial \hat{\mathbf{R}}}{\partial \xi_a^i}, \tag{5.19}$$

$$\frac{\partial \mathbf{C_{m1}}}{\partial \xi_a^i} = \frac{\partial \hat{\mathbf{R}}^{-1}}{\partial \xi_a^i}\hat{\mathbf{C}}_\mathbf{1} + \hat{\mathbf{R}}^{-1}\frac{\partial \hat{\mathbf{C}}_\mathbf{1}}{\partial \xi_a^i}, \tag{5.20}$$

$$\frac{\partial \mathbf{C_{m2}}}{\partial \xi_a^i} = \frac{\partial \hat{\mathbf{R}}^{-1}}{\partial \xi_a^i}\hat{\mathbf{C}}_\mathbf{2} + \hat{\mathbf{R}}^{-1}\frac{\partial \hat{\mathbf{C}}_\mathbf{2}}{\partial \xi_a^i}, \tag{5.21}$$

$$\frac{\partial \mathbf{D_{m12}}}{\partial \xi_a^i} = \frac{\partial \hat{\mathbf{D}}_\mathbf{12}}{\partial \xi_a^i}, \tag{5.22}$$

where the partial derivative of the coordinate transformation $\hat{\mathbf{R}}$ and of its inverse $\hat{\mathbf{R}}^{-1}$ can be given as

$$\frac{\partial \hat{\mathbf{R}}}{\partial \xi_a^i} = \frac{\partial \mathbf{R_{31}}}{\partial \xi_a^i}\,\mathbf{R}\,. \tag{5.23}$$

In (5.23), $\mathbf{R_{31}}$ and $\mathbf{R}$ are the coordinate transformations given in (2.49) and (2.48), respectively. The partial derivatives of $\mathbf{R_{31}}$ and $\mathbf{R}$ are

$$\frac{\partial \mathbf{R_{31}}}{\partial \xi_a^i} = \operatorname{diag}\left(\begin{pmatrix} 0 & 0 \\ 0 & \frac{\partial \omega_1}{\partial \xi_a^i} \end{pmatrix}, \begin{pmatrix} 0 & 0 \\ 0 & \frac{\partial \omega_2}{\partial \xi_a^i} \end{pmatrix}, \cdots, \begin{pmatrix} 0 & 0 \\ 0 & \frac{\partial \omega_N}{\partial \xi_a^i} \end{pmatrix} \right) \tag{5.24}$$

and

$$\frac{\partial \hat{\mathbf{R}}^{-1}}{\partial \xi_a^i} = -\hat{\mathbf{R}}^{-1}\frac{\partial \hat{\mathbf{R}}}{\partial \xi_a^i}\hat{\mathbf{R}}^{-1}. \tag{5.25}$$

The derivatives of the matrices $\hat{\mathbf{B}}_\mathbf{1}$, $\hat{\mathbf{B}}_\mathbf{2}$, $\hat{\mathbf{C}}_\mathbf{1}$, $\hat{\mathbf{C}}_\mathbf{2}$, $\hat{\mathbf{D}}_\mathbf{12}$ are

$$\begin{aligned}
\frac{\partial \hat{\mathbf{B}}_\mathbf{1}}{\partial \xi_a^i} &= \begin{bmatrix} \mathbf{0} \\ \dfrac{\partial \mathbf{\Phi}^{\mathrm{T}}}{\partial \xi_a^i}\mathbf{L_w} \end{bmatrix}, \qquad \frac{\partial \hat{\mathbf{B}}_\mathbf{2}}{\partial \xi_a^i} = \begin{bmatrix} \mathbf{0} \\ \dfrac{\partial \mathbf{\Phi}^{\mathrm{T}}}{\partial \xi_a^i}\mathbf{L_u} \end{bmatrix}, \\
\frac{\partial \hat{\mathbf{C}}_\mathbf{1}}{\partial \xi_a^i} &= \begin{bmatrix} \mathbf{C_{zq}}\dfrac{\partial \mathbf{\Phi}}{\partial \xi_a^i} & \mathbf{0} \end{bmatrix}, \quad \frac{\partial \hat{\mathbf{C}}_\mathbf{2}}{\partial \xi_a^i} = \begin{bmatrix} \mathbf{0} & \mathbf{C_{yv}}\dfrac{\partial \mathbf{\Phi}}{\partial \xi_a^i} \end{bmatrix}, \\
\frac{\partial \hat{\mathbf{D}}_\mathbf{12}}{\partial \xi_a^i} &= \frac{\partial \mathbf{D_{12}}}{\partial \xi_a^i} = \mathbf{0}.
\end{aligned}$$

5.7. ARE Derivatives for the Improved Coprime Controller

To obtain the gradient of the objective function, the derivatives of the solutions of ARE's (4.9) and (4.10) are also required. The partial derivatives of the solutions of an ARE are calculated by finding the solutions of the derivatives of the ARE with respect to design parameter.

Lemma 5.7.1. *Given the ARE's* (4.9) *and* (4.10)*, and assuming that the partial derivatives of* $\mathbf{S}$ *and* $\mathbf{T}$*, the solutions of* (4.9) *and* (4.10)*, are diagonally dominant as*

$$\begin{aligned}
\frac{\partial \mathbf{S}}{\partial p} &= \operatorname{diag}\left(\frac{\partial s_1}{\partial p}, \ \cdots, \ \frac{\partial s_N}{\partial p} \right), \\
\frac{\partial \mathbf{T}}{\partial p} &= \operatorname{diag}\left(\frac{\partial t_1}{\partial p}, \ \cdots, \ \frac{\partial t_N}{\partial p} \right),
\end{aligned}$$

then the i^{th} *mode's entries* $\frac{\partial s_i}{\partial p}$ *and* $\frac{\partial t_i}{\partial p}$ *are calculated from*

$$\begin{aligned}
&\left(1 + 2\alpha^2 s_i l_{ci}\right) 4\zeta_i \omega_i \frac{\partial s_i}{\partial p} + s_i \frac{\partial}{\partial p}\left(4\zeta_i \omega_i\right) \\
&\qquad + \alpha^2 s_i^2 \frac{\partial}{\partial p}\left(\left(\mathbf{B}_{\mathbf{2}i} \mathbf{B}_{\mathbf{2}\,i}^{\mathrm{T}} \right)_{(2,2)} \right) - \frac{\partial}{\partial p}\left(\left(\mathbf{C}_{\mathbf{2}\,i}^{\mathrm{T}} \mathbf{C}_{\mathbf{2}i} \right)_{(2,2)} \right) = 0,
\end{aligned} \tag{5.26}$$

$$
\begin{aligned}
(1+2t_i l_{oi})4\zeta_i\omega_i\frac{\partial t_i}{\partial p} + t_i\frac{\partial}{\partial p}\left(4\zeta_i\omega_i\right) \\
+ t_i^2\frac{\partial}{\partial p}\left(\left(\mathbf{C}_{\mathbf{2}\,i}^{\mathrm{T}}\mathbf{C}_{\mathbf{2}i}\right)_{(2,2)}\right) - \alpha^2\frac{\partial}{\partial p}\left(\left(\mathbf{B}_{\mathbf{2}i}\mathbf{B}_{\mathbf{2}\,i}^{\mathrm{T}}\right)_{(2,2)}\right) = 0,
\end{aligned}
\tag{5.27}
$$

where the partial derivatives of $\left(\mathbf{B}_{\mathbf{2}i}\mathbf{B}_{\mathbf{2}\,i}^{\mathrm{T}}\right)_{(2,2)}$ *and* $\left(\mathbf{C}_{\mathbf{2}\,i}^{\mathrm{T}}\mathbf{C}_{\mathbf{2}i}\right)_{(2,2)}$ *are*

$$
\begin{aligned}
\frac{\partial}{\partial p}\left(\left(\mathbf{B}_{\mathbf{2}i}\mathbf{B}_{\mathbf{2}\,i}^{\mathrm{T}}\right)_{2,2}\right) =& \frac{\partial}{\partial p}\left\|\mathbf{B}_{\mathbf{2}i}\right\|_2^2 \\
=& 2\left(b_{i1}\frac{\partial b_{i1}}{\partial p} + b_{i2}\frac{\partial b_{i2}}{\partial p} + \cdots + b_{iN_u}\frac{\partial b_{iN_u}}{\partial p}\right),
\end{aligned}
$$

$$
\begin{aligned}
\frac{\partial}{\partial p}\left(\left(\mathbf{C}_{\mathbf{2}\,i}^{\mathrm{T}}\mathbf{C}_{\mathbf{2}i}\right)_{2,2}\right) =& \frac{\partial}{\partial p}\left\|\mathbf{C}_{\mathbf{2}i}\right\|_2^2 \\
=& 2\left(c_{1i}\frac{\partial c_{1i}}{\partial p} + c_{2i}\frac{\partial c_{2i}}{\partial p} + \cdots + b_{iN_u}\frac{\partial c_{N_u i}}{\partial p}\right).
\end{aligned}
$$

Proof. The derivatives of ARE's (4.9) and (4.10) with respect to design parameters p, which are the coordinates of the actuator/sensor pairs $(\xi_a^1 \ldots \xi_a^{N_u})$, are

$$
\left(\mathbf{A}^{\mathrm{T}} - \alpha^2\mathbf{S}\mathbf{B}_{\mathbf{2}}\mathbf{B}_{\mathbf{2}}^{\mathrm{T}}\right)\frac{\partial \mathbf{S}}{\partial p} + \frac{\partial \mathbf{S}}{\partial p}\left(\mathbf{A} - \alpha^2\mathbf{S}\mathbf{B}_{\mathbf{2}}^{\mathrm{T}}\mathbf{B}_{\mathbf{2}}\right) + \mathbf{Q}_{\mathbf{S}} = \mathbf{0}, \tag{5.28}
$$

$$
\left(\mathbf{A} - \mathbf{T}\mathbf{C}_{\mathbf{2}}^{\mathrm{T}}\mathbf{C}_{\mathbf{2}}\right)\frac{\partial \mathbf{T}}{\partial p} + \frac{\partial \mathbf{T}}{\partial p}\left(\mathbf{A}^{\mathrm{T}} - \mathbf{T}\mathbf{C}_{\mathbf{2}}^{\mathrm{T}}\mathbf{C}_{\mathbf{2}}\right) + \mathbf{P}_{\mathbf{T}} = \mathbf{0}, \tag{5.29}
$$

where $\mathbf{Q}_{\mathbf{S}}$ and $\mathbf{P}_{\mathbf{T}}$ are

$$
\begin{aligned}
\mathbf{Q}_{\mathbf{S}} = \frac{\partial \mathbf{A}^{\mathrm{T}}}{\partial p}\mathbf{S} + \mathbf{S}\frac{\partial \mathbf{A}}{\partial p} - \alpha^2\mathbf{S}\frac{\partial \mathbf{B}_{\mathbf{2}}}{\partial p}\mathbf{B}_{\mathbf{2}}^{\mathrm{T}}\mathbf{S} - \alpha^2\mathbf{S}\mathbf{B}_{\mathbf{2}}\frac{\partial \mathbf{B}_{\mathbf{2}}^{\mathrm{T}}}{\partial p}\mathbf{S} \\
+ \frac{\partial \mathbf{C}_{\mathbf{2}}^{\mathrm{T}}}{\partial p}\mathbf{C}_{\mathbf{2}} + \mathbf{C}_{\mathbf{2}}^{\mathrm{T}}\frac{\partial \mathbf{C}_{\mathbf{2}}}{\partial p}
\end{aligned}
$$

and

$$
\begin{aligned}
\mathbf{P}_{\mathbf{T}} = \frac{\partial \mathbf{A}}{\partial p}\mathbf{T} + \mathbf{T}\frac{\partial \mathbf{A}^{\mathrm{T}}}{\partial p} - \mathbf{T}\frac{\partial \mathbf{B}_{\mathbf{2}}}{\partial p}\mathbf{B}_{\mathbf{2}}^{\mathrm{T}}\mathbf{T} - \mathbf{T}\mathbf{B}_{\mathbf{2}}\frac{\partial \mathbf{B}_{\mathbf{2}}^{\mathrm{T}}}{\partial p}\mathbf{T} \\
+ \alpha^2\frac{\partial \mathbf{C}_{\mathbf{2}}^{\mathrm{T}}}{\partial p}\mathbf{C}_{\mathbf{2}} + \alpha^2\mathbf{C}_{\mathbf{2}}^{\mathrm{T}}\frac{\partial \mathbf{C}_{\mathbf{2}}}{\partial p},
\end{aligned}
$$

respectively.

Equations (5.28) and (5.29) are Lyapunov equations and their solutions are obtained in the same manner as in Equations (4.9) and (4.10). Since the system equations of the generalized plant are put into the first modal state space representation, Equations (5.28) and (5.29) can be solved for each mode separately. For the i^{th} mode, they are (5.26) and (5.27). In Equations (5.26) and (5.27), the only unknown quantities are $\frac{\partial s_i}{\partial p}$ and $\frac{\partial t_i}{\partial p}$ and hence can be found immediately. □

5.8. ARE Derivatives for the Low-Authority $\mathcal{H}_\infty$-Controller

Lemma 5.8.1. *If the solutions of ARE's in* (4.23) *and* (4.24) *can be approximated by diagonal solutions as* $\mathbf{X}_\infty = \operatorname{diag}(x_{\infty i})$ *and* $\mathbf{Y}_\infty = \operatorname{diag}(y_{\infty i})$ *so that the partial derivatives of* $\mathbf{X}_\infty$ *and* $\mathbf{Y}_\infty$ *are also diagonally dominant as*

$$\begin{aligned}\frac{\partial \mathbf{X}_\infty}{\partial p} &= \operatorname{diag}\left(\frac{\partial x_{\infty i}}{\partial p}\right), \quad \forall\, i = 1:N,\\ \frac{\partial \mathbf{Y}_\infty}{\partial p} &= \operatorname{diag}\left(\frac{\partial y_{\infty i}}{\partial p}\right), \quad \forall\, i = 1:N,\end{aligned}$$

then for the i^{th} *mode* $\dfrac{\partial x_{\infty i}}{\partial p}$ *and* $\dfrac{\partial y_{\infty i}}{\partial p}$ *are given by*

$$\frac{\partial x_{\infty i}}{\partial p} = \frac{(Q_{X_\infty})_i}{4\zeta_i\omega_i\left[1 + 2x_{\infty i}\left(\gamma^{-2}l_{c1i} + l_{c2i}\right)\right]} \tag{5.30}$$

and

$$\frac{\partial y_{\infty i}}{\partial p} = \frac{(Q_{Y_\infty})_i}{4\zeta_i\omega_i\left[1 + 2y_{\infty i}\left(\gamma^{-2}l_{o1i} + l_{o2i}\right)\right]}, \tag{5.31}$$

where $(Q_{X_\infty})_i$ *and* $(Q_{Y_\infty})_i$ *are*

$$\begin{aligned}(Q_{X_\infty})_i = x_{\infty i}^2 &\left(\frac{\partial}{\partial p}\left(\gamma^{-2}\mathbf{B_1}_i\mathbf{B_1}_i^{\mathrm{T}}\right)_{(2,2)} - \frac{\partial}{\partial p}\left(\mathbf{B_2}_i\mathbf{B_2}_i^{\mathrm{T}}\right)_{(2,2)}\right)\\ &- x_{\infty i}\frac{\partial}{\partial p}\left(4\zeta_i\omega_i\right) + \frac{\partial}{\partial p}\left(\mathbf{C_1}_i^{\mathrm{T}}\mathbf{C_1}_i\right)_{(2,2)}\end{aligned}$$

and

$$(Q_{Y_\infty})_i = {y_\infty}_i^2 \left(\frac{\partial}{\partial p} \left(\gamma^{-2} \mathbf{C_1}_i^{\mathrm{T}} \mathbf{C_1}_i \right)_{(2,2)} - \frac{\partial}{\partial p} \left(\mathbf{C_2}_i^{\mathrm{T}} \mathbf{C_2}_i \right)_{(2,2)} \right) - y_{\infty i} \frac{\partial}{\partial p} \left(4\zeta_i \omega_i \right) + \frac{\partial}{\partial p} \left(\mathbf{B_1}_i \mathbf{B_1}_i^{\mathrm{T}} \right)_{(2,2)},$$

respectively.

Proof. The ARE's in (4.23) and (4.24) have the partial derivatives with respect to a design variable p as

$$\begin{aligned} &\left[\mathbf{A}^{\mathrm{T}} + \mathbf{X}_\infty \left(\gamma^{-2} \mathbf{B_1} \mathbf{B_1}^{\mathrm{T}} - \mathbf{B_2} \mathbf{B_2}^{\mathrm{T}} \right) \right] \frac{\partial \mathbf{X}_\infty}{\partial p} + \\ &\quad \frac{\partial \mathbf{X}_\infty}{\partial p} \left[\mathbf{A} + \left(\gamma^{-2} \mathbf{B_1} \mathbf{B_1}^{\mathrm{T}} - \mathbf{B_2} \mathbf{B_2}^{\mathrm{T}} \right) \mathbf{X}_\infty \right] + \mathbf{Q}_{\mathbf{X}_\infty} = \mathbf{0} \end{aligned} \tag{5.32}$$

and

$$\begin{aligned} &\frac{\partial \mathbf{Y}_\infty}{\partial p} \left[\mathbf{A}^{\mathrm{T}} + \left(\gamma^{-2} \mathbf{C_1}^{\mathrm{T}} \mathbf{C_1} - \mathbf{C_2}^{\mathrm{T}} \mathbf{C_2} \right) \mathbf{Y}_\infty \right] + \\ &\quad \left[\mathbf{A} + \mathbf{Y}_\infty \left(\gamma^{-2} \mathbf{C_1}^{\mathrm{T}} \mathbf{C_1} - \mathbf{C_2}^{\mathrm{T}} \mathbf{C_2} \right) \right] \frac{\partial \mathbf{Y}_\infty}{\partial p} + \mathbf{Q}_{\mathbf{Y}_\infty} = \mathbf{0}, \end{aligned} \tag{5.33}$$

respectively, where $\mathbf{Q}_{\mathbf{X}_\infty}$ and $\mathbf{Q}_{\mathbf{Y}_\infty}$ are

$$\mathbf{Q}_{\mathbf{Y}_\infty} = \frac{\partial \mathbf{A}}{\partial p} \mathbf{Y}_\infty + \mathbf{Y}_\infty \frac{\partial \mathbf{A}^{\mathrm{T}}}{\partial p} + \frac{\partial \mathbf{B_1} \mathbf{B_1}^{\mathrm{T}}}{\partial p} + \mathbf{Y}_\infty \left(\gamma^{-2} \frac{\partial \mathbf{C_1}^{\mathrm{T}} \mathbf{B_1}}{\partial p} - \frac{\partial \mathbf{C_2}^{\mathrm{T}} \mathbf{C_2}}{\partial p} \right) \mathbf{Y}_\infty,$$

$$\mathbf{Q}_{\mathbf{X}_\infty} = \frac{\partial \mathbf{A}^{\mathrm{T}}}{\partial p} \mathbf{X}_\infty + \mathbf{X}_\infty \frac{\partial \mathbf{A}}{\partial p} + \frac{\partial \mathbf{C_1}^{\mathrm{T}} \mathbf{C_1}}{\partial p} + \mathbf{X}_\infty \left(\gamma^{-2} \frac{\partial \mathbf{B_1} \mathbf{B_1}^{\mathrm{T}}}{\partial p} - \frac{\partial \mathbf{B_2} \mathbf{B_2}^{\mathrm{T}}}{\partial p} \right) \mathbf{X}_\infty.$$

Equations (5.32) and (5.33) are Lyapunov equations. Since the generalized plant is given in the first modal state space representation, Equations (5.32) and (5.33) can

be solved for each mode separately. For the i^{th} mode, they become (5.30) and (5.31), from which $\frac{\partial x_{\infty i}}{\partial p}$ and $\frac{\partial y_{\infty i}}{\partial p}$ are to be calculated. □

5.9. Partial Derivative of γ_{min} for the Improved Coprime Controller

For taking the partial derivative of the closed-loop matrix $\mathbf{A_c}$ in Equation (4.75) with respect to the design parameter p, the partial derivative of γ_{min} in Equation (4.77) is also required, which is given as

$$\frac{\partial \gamma_{min}}{\partial p} = \frac{1}{2\sqrt{\mathbf{I} + \lambda_{max}(\mathbf{ST})}} \frac{\partial}{\partial p} \lambda_{max}(\mathbf{ST}),$$

where

$$\frac{\partial}{\partial p} \lambda_{max}(\mathbf{ST}) = \mathbf{u}_k^{\mathrm{T}} \frac{\partial \mathbf{ST}}{\partial p} \mathbf{u}_k,$$

k is the index of the maximum eigenvalue of $\mathbf{ST}$ as

$$\lambda_{max} = \lambda_k = \max_i \lambda_i(\mathbf{ST}), \quad \forall\, i = 1 : N_p,$$

and $\mathbf{u}_k$ is the k^{th} eigenvector of $\mathbf{ST}$.

The distinct eigenvalue derivative of $\frac{\partial}{\partial p} \lambda_{max}(.)$ is taken according to [52, 53], and it is assumed that eigenvalues are always distinct as the design parameter p changes. If this is violated during iterations, the optimization procedure may be stopped.

5.10. Partial Derivatives of the Closed-loop Matrices

When the partial derivatives of the open-loop state space matrices and the controller matrices are obtained, the closed-loop matrices and their partial derivatives

are

$$\left(\begin{array}{c|c} \mathbf{A_{cl}} & \mathbf{B_{cl}} \\ \hline \mathbf{C_{cl}} & \mathbf{D_{cl}} \end{array}\right) = \left(\begin{array}{cc|c} \mathbf{A} & \mathbf{B_2C_K} & \mathbf{B_1 + B_2D_KD_{21}} \\ \mathbf{B_KC_2} & \mathbf{A_K} & \mathbf{B_KD_{21}} \\ \hline \mathbf{C_1 + D_{12}D_KC_2} & \mathbf{D_{12}C_K} & \mathbf{D_{11} + D_{12}D_KD_{21}} \end{array}\right)$$

and

$$\begin{aligned}
\frac{\partial \mathbf{A_{cl}}}{\partial p} &= \begin{bmatrix} \dfrac{\partial \mathbf{A}}{\partial p} & \dfrac{\partial \mathbf{B_2}}{\partial p}\mathbf{C_K} + \mathbf{B_2}\dfrac{\partial \mathbf{C_K}}{\partial p} \\ \dfrac{\partial \mathbf{B_K}}{\partial p}\mathbf{C_2} + \mathbf{B_K}\dfrac{\partial \mathbf{C_2}}{\partial p} & \dfrac{\partial \mathbf{A_K}}{\partial p} \end{bmatrix}, \\
\frac{\partial \mathbf{B_{cl}}}{\partial p} &= \begin{bmatrix} \dfrac{\partial \mathbf{B_1}}{\partial p} + \dfrac{\partial \mathbf{B_2}}{\partial p}\mathbf{D_KD_{21}} + \mathbf{B_2}\dfrac{\partial \mathbf{D_K}}{\partial p}\mathbf{D_{21}} + \mathbf{B_2D_K}\dfrac{\partial \mathbf{D_{21}}}{\partial p} \\ \dfrac{\partial \mathbf{B_K}}{\partial p}\mathbf{D_{21}} + \mathbf{B_K}\dfrac{\partial \mathbf{D_{21}}}{\partial p} \end{bmatrix}, \\
\frac{\partial \mathbf{C_{cl}}}{\partial p} &= \begin{bmatrix} \dfrac{\partial \mathbf{C_1}}{\partial p} + \dfrac{\partial \mathbf{D_{12}}}{\partial p}\mathbf{D_KC_2} + \mathbf{D_{12}}\dfrac{\partial \mathbf{D_K}}{\partial p}\mathbf{C_2} & \\ \qquad + \mathbf{D_{12}D_K}\dfrac{\partial \mathbf{C_2}}{\partial p} & \dfrac{\mathbf{D_{12}}}{\partial p}\mathbf{C_K} + \mathbf{D_{12}}\dfrac{\partial \mathbf{C_K}}{\partial} \end{bmatrix}, \\
\frac{\partial \mathbf{D_{cl}}}{\partial p} &= \begin{bmatrix} \dfrac{\mathbf{D_{11}}}{\partial p} + \dfrac{\mathbf{D_{12}}}{\partial p}\mathbf{D_KD_{21}} + \mathbf{D_{12}}\dfrac{\mathbf{D_K}}{\partial p}\mathbf{D_{21}} + \mathbf{D_{12}D_K}\dfrac{\mathbf{D_{21}}}{\partial p} \end{bmatrix},
\end{aligned}$$

respectively.

Partial derivatives of the open-loop state space matrices are introduced in Section 5.6.

Partial derivatives of the state space matrices for the improved coprime controller and the low-authority $\mathcal{H}_\infty$-controller are given in Subsections 5.10.1 and 5.10.2.

5.10.1. Partial Derivatives of the Improved Coprime Controller Matrices

Partial derivatives of the improved coprime controller matrices with respect to a design variable p are

$$
\begin{aligned}
\frac{\partial \mathbf{A_{K_a}}}{\partial p} &= \frac{\partial \mathbf{A}}{\partial p} - \alpha^2 \left(\frac{\partial}{\partial p}\mathbf{B_2}\mathbf{B_2^T}\mathbf{S} + \mathbf{B_2}\frac{\partial}{\partial p}\mathbf{B_2^T}\mathbf{S} + \mathbf{B_2}\mathbf{B_2^T}\frac{\partial \mathbf{S}}{\partial p} \right) \\
&\quad + 2\beta^2\gamma_{min}\frac{\partial \gamma_{min}}{\partial p}\left(\mathbf{W}^{-1}\right)^{\mathrm{T}}\mathbf{T}\mathbf{C_2^T}\mathbf{C_2} \\
&\quad + \left(\beta\gamma_{min}\right)^2 \left(\frac{\partial \left(\mathbf{W}^{-1}\right)^{\mathrm{T}}}{\partial p}\mathbf{T}\mathbf{C_2^T}\mathbf{C_2} + \left(\mathbf{W}^{-1}\right)^{\mathrm{T}}\frac{\partial \mathbf{T}}{\partial p}\,\mathbf{C_2}^{\mathrm{T}}\mathbf{C_2} \right. \\
&\quad \left. + \left(\mathbf{W}^{-1}\right)^{\mathrm{T}}\mathbf{T}\,\frac{\partial \mathbf{C_2^T}}{\partial p}\,\mathbf{C_2} + \left(\mathbf{W}^{-1}\right)^{\mathrm{T}}\mathbf{T}\mathbf{C_2^T}\,\frac{\partial \mathbf{C_2}}{\partial p} \right), \\
\frac{\partial \mathbf{B_{K_a}}}{\partial p} &= 2\beta^2\gamma_{min}\frac{\partial \gamma_{min}}{\partial p}\left(\mathbf{W}^{-1}\right)^{\mathrm{T}}\mathbf{T}\mathbf{C_2^T} + \left(\beta\gamma_{min}\right)^2 \left(\frac{\partial \left(\mathbf{W}^{-1}\right)^{\mathrm{T}}}{\partial p}\,\mathbf{T}\mathbf{C_2^T} + \right. \\
&\quad \left. \left(\mathbf{W}^{-1}\right)^{\mathrm{T}}\frac{\partial \mathbf{T}}{\partial p}\,\mathbf{C_2}^{\mathrm{T}} + \left(\mathbf{W}^{-1}\right)^{\mathrm{T}}\mathbf{T}\,\frac{\partial \mathbf{C_2^T}}{\partial p} \right), \\
\frac{\partial \mathbf{C_{K_a}}}{\partial p} &= \alpha^2 \left(\frac{\partial \mathbf{B_2^T}}{\partial p}\mathbf{S} + \mathbf{B_2^T}\frac{\partial \mathbf{S}}{\partial p} \right),
\end{aligned}
$$

where

$$
\begin{aligned}
\frac{\partial \mathbf{W}}{\partial p} &= -2\beta^2\gamma_{min}\frac{\partial \gamma_{min}}{\partial p}\,\mathbf{I} + \frac{\partial \mathbf{S}}{\partial p}\mathbf{T} + \mathbf{S}\frac{\partial \mathbf{T}}{\partial p}, \\
\frac{\partial \left(\mathbf{W}^{-1}\right)^{\mathrm{T}}}{\partial p} &= -\left(\mathbf{W}^{-1}\right)^{\mathrm{T}}\left(\frac{\partial \mathbf{W}}{\partial p}\right)^{\mathrm{T}}\left(\mathbf{W}^{-1}\right)^{\mathrm{T}}.
\end{aligned}
$$

The partial derivatives of the ARE solutions $\mathbf{S}$ and $\mathbf{T}$ are given in Subsection 5.7.

5.10.2. Partial Derivatives of the Improved Low-Authority $\mathcal{H}_\infty$-Controller Matrices

The partial derivatives of the low-authority $\mathcal{H}_\infty$-controller matrices are

$$
\begin{aligned}
\frac{\partial \mathbf{A_K}}{\partial p} &= \frac{\partial \tilde{\mathbf{A}}}{\partial p} + \gamma^{-2}\left(\frac{\partial \tilde{\mathbf{B}}_\mathbf{1}}{\partial p}\tilde{\mathbf{B}}_\mathbf{1}^{\mathrm{T}}\mathbf{X}_\infty + \tilde{\mathbf{B}}_\mathbf{1}\frac{\partial \tilde{\mathbf{B}}_\mathbf{1}^{\mathrm{T}}}{\partial p}\mathbf{X}_\infty + \tilde{\mathbf{B}}_\mathbf{1}\tilde{\mathbf{B}}_\mathbf{1}^{\mathrm{T}}\frac{\partial \mathbf{X}_\infty}{\partial p} \right) \\
&\quad + \frac{\partial \tilde{\mathbf{B}}_\mathbf{2}}{\partial p}\tilde{\mathbf{F}}_\infty + \tilde{\mathbf{B}}_\mathbf{2}\frac{\partial \tilde{\mathbf{F}}_\infty}{\partial p} + \frac{\partial \tilde{\mathbf{Z}}_\infty}{\partial p}\tilde{\mathbf{L}}_\infty\tilde{\mathbf{C}}_\mathbf{2} + \tilde{\mathbf{Z}}_\infty\frac{\partial \tilde{\mathbf{L}}_\infty}{\partial p}\tilde{\mathbf{C}}_\mathbf{2} + \tilde{\mathbf{Z}}_\infty\tilde{\mathbf{L}}_\infty\frac{\partial \tilde{\mathbf{C}}_\mathbf{2}}{\partial p}, \\
\frac{\partial \mathbf{B_K}}{\partial p} &= \left[-\frac{\partial \tilde{\mathbf{Z}}_\infty}{\partial p}\tilde{\mathbf{L}}_\infty - \tilde{\mathbf{Z}}_\infty\frac{\partial \tilde{\mathbf{L}}_\infty}{\partial p} \qquad \frac{\partial \tilde{\mathbf{Z}}_\infty}{\partial p}\tilde{\mathbf{B}}_\mathbf{2} + \tilde{\mathbf{Z}}_\infty\frac{\partial \tilde{\mathbf{B}}_\mathbf{2}}{\partial p} \right]\mathbf{S_y},
\end{aligned}
$$

$$\frac{\partial \mathbf{C_K}}{\partial p} = \mathbf{S_u}^{-1} \begin{bmatrix} \dfrac{\partial \tilde{\mathbf{F}}_\infty}{\partial p} \\ -\dfrac{\partial \tilde{\mathbf{C}}_\mathbf{2}}{\partial p} \end{bmatrix}, \tag{5.34}$$

where the partial derivatives of $\tilde{\mathbf{F}}_\infty$, $\tilde{\mathbf{L}}_\infty$ and $\tilde{\mathbf{Z}}_\infty$ are

$$\begin{aligned}
\frac{\partial \tilde{\mathbf{F}}_\infty}{\partial p} &= -\frac{\partial \tilde{\mathbf{B}}_\mathbf{2}^{\mathrm{T}}}{\partial p}\mathbf{X}_\infty - \tilde{\mathbf{B}}_\mathbf{2}^{\mathrm{T}}\frac{\partial \mathbf{X}_\infty}{\partial p}, \\
\frac{\partial \tilde{\mathbf{L}}_\infty}{\partial p} &= -\frac{\partial \mathbf{Y}_\infty}{\partial p}\tilde{\mathbf{C}}_\mathbf{2}^{\mathrm{T}} - \mathbf{Y}_\infty\frac{\partial \tilde{\mathbf{C}}_\mathbf{2}^{\mathrm{T}}}{\partial p}, \\
\frac{\partial \tilde{\mathbf{Z}}_\infty}{\partial p} &= \gamma^{-2}\left(\mathbf{I} - \gamma^{-2}\mathbf{Y}_\infty\mathbf{X}_\infty\right)^{-1}\left(\frac{\partial \mathbf{Y}_\infty}{\partial p}\mathbf{X}_\infty\right. \\
&\qquad \left. + \mathbf{Y}_\infty\frac{\partial \mathbf{X}_\infty}{\partial p}\right)\left(\mathbf{I} - \gamma^{-2}\mathbf{Y}_\infty\mathbf{X}_\infty\right)^{-1}.
\end{aligned} \tag{5.35}$$

The partial derivatives of the generalized plant in (4.82) are

$$\begin{aligned}
&\frac{\partial \tilde{\mathbf{A}}}{\partial p} = \frac{\partial \mathbf{A}}{\partial p}, && \frac{\partial \tilde{\mathbf{B}}_\mathbf{1}}{\partial p} = \frac{\partial \mathbf{B_1}}{\partial p}\mathbf{T_w}^{\mathrm{H}}, && \frac{\partial \tilde{\mathbf{B}}_\mathbf{2}}{\partial p} = \frac{\partial \mathbf{B_2}}{\partial p}\mathbf{S_u}^{-1}, \\
&\frac{\partial \tilde{\mathbf{C}}_\mathbf{1}}{\partial p} = \mathbf{T_z}\frac{\partial \mathbf{C_1}}{\partial p}, && \frac{\partial \tilde{\mathbf{D}}_\mathbf{11}}{\partial p} = \mathbf{T_z}\frac{\partial \mathbf{D_{11}}}{\partial p}\mathbf{T}_\mathbf{w}^{\mathrm{H}}, && \frac{\partial \tilde{\mathbf{D}}_\mathbf{12}}{\partial p} = \mathbf{T_z}\frac{\partial \mathbf{D_{12}}}{\partial p}\mathbf{S_u}^{-1}, \\
&\frac{\partial \tilde{\mathbf{C}}_\mathbf{2}}{\partial p} = \mathbf{S_y}\frac{\partial \mathbf{C_2}}{\partial p}, && \frac{\partial \tilde{\mathbf{D}}_\mathbf{21}}{\partial p} = \mathbf{S_y}\frac{\partial \mathbf{D_{21}}}{\partial p}\mathbf{T}_\mathbf{w}^{\mathrm{H}}, && \frac{\partial \tilde{\mathbf{D}}_\mathbf{22}}{\partial p} = \mathbf{S_y}\frac{\partial \mathbf{D_{22}}}{\partial p}\mathbf{S_u}^{-1}.
\end{aligned} \tag{5.36}$$

The partial derivatives of the CARE and FARE solutions $\mathbf{X}_\infty$ and $\mathbf{Y}_\infty$ in Equations (5.34) and (5.35) are introduced in Section 5.8.

5.11. Partial Derivatives of MNRD-value

The partial derivative of the square of the closed-loop $\mathcal{H}_2$-norm with MNRD-controller can be obtained by differentiating (4.59) or (4.60) as

$$\begin{aligned}
\frac{\partial \left\|\mathbf{T_{zw}}\right\|_2^2}{\partial p} &= \frac{1}{2\pi}\int_{-\infty}^{\infty} \mathrm{trace}\left(\frac{\partial \mathbf{T}_\mathbf{zw}^*(\omega)}{\partial p}\mathbf{T_{zw}}(\omega) + \mathbf{T}_\mathbf{zw}^*(\omega)\frac{\partial \mathbf{T_{zw}}(\omega)}{\partial p}\right)\mathrm{d}\omega, \\
&= \frac{1}{2\pi}\int_{-\infty}^{\infty}\sum_{i=1}^{n} 2\,\sigma_i\left(\mathbf{T_{zw}}(\omega)\right)\frac{\partial \sigma_i\left(\mathbf{T_{zw}}(\omega)\right)}{\partial p}\,\mathrm{d}\omega.
\end{aligned}$$

Similar to the calculation of the optimistic $\mathcal{H}_2$-norm in Subsection 4.1.5, $\frac{\partial \|\mathbf{T_{zw}}\|_2^2}{\partial p}$ can be computed numerically by the MATLAB commands QUADL and QUADGK.

The partial derivative of the i^{th} singular value with respect to p is

$$\frac{\partial}{\partial p}\sigma_i\left(\mathbf{T_{zw}}\right) = \frac{1}{2\sigma_i\left(\mathbf{T_{zw}}\right)}\frac{\partial}{\partial p}\lambda_i\left(\mathbf{T_{zw}^*T_{zw}}\right),$$

where

$$\frac{\partial}{\partial p}\lambda_i\left(\mathbf{T_{zw}^*T_{zw}}\right) = \mathbf{u}_i^{\mathrm{T}}\left(\frac{\partial \mathbf{T_{zw}^*}}{\partial p}\mathbf{T_{zw}} + \mathbf{T_{zw}^*}\frac{\partial \mathbf{T_{zw}}}{\partial p}\right)\mathbf{u}_i,$$

and $\mathbf{u}_i$ is the i^{th} eigenvector of $\mathbf{T_{zw}^*T_{zw}}$. The partial derivative of $\mathbf{T_{zw}}$ is simply defined as

$$\begin{aligned}\frac{\partial \mathbf{T_{zw}}}{\partial p} = \frac{\partial \mathbf{P_{11}}}{\partial p} &- \frac{\partial \mathbf{P_{12}}}{\partial p}\mathbf{P}_{12}^{-\mathrm{L}}\mathbf{P_{11}}\mathbf{P}_{21}^{-\mathrm{R}}\mathbf{P_{21}} - \mathbf{P_{12}}\frac{\partial \mathbf{P}_{12}^{-\mathrm{L}}}{\partial p}\mathbf{P_{11}}\mathbf{P}_{21}^{-\mathrm{R}}\mathbf{P_{21}} \\ &- \mathbf{P_{12}}\mathbf{P}_{12}^{-\mathrm{L}}\frac{\partial \mathbf{P_{11}}}{\partial p}\mathbf{P}_{21}^{-\mathrm{R}}\mathbf{P_{21}} - \mathbf{P_{12}}\mathbf{P}_{12}^{-\mathrm{L}}\mathbf{P_{11}}\frac{\partial \mathbf{P}_{21}^{-\mathrm{R}}}{\partial p}\mathbf{P_{21}} - \mathbf{P_{12}}\mathbf{P}_{12}^{-\mathrm{L}}\mathbf{P_{11}}\mathbf{P}_{21}^{-\mathrm{R}}\frac{\partial \mathbf{P_{21}}}{\partial p}.\end{aligned}$$

By letting $\mathbf{\Theta}$ and $\mathbf{\Xi}$ as

$$\begin{aligned}\mathbf{\Theta} &:= \left(j\omega\mathbf{I} - \mathbf{A_g}\right)^{-1}, \\ \mathbf{\Xi} &:= \left(j\omega\mathbf{I} - \mathbf{A_g^{\mathrm{T}}}\right)^{-1},\end{aligned}$$

the partial derivatives of $\mathbf{P_{11}}$, $\mathbf{P_{12}}$ and $\mathbf{P_{21}}$ become

$$\begin{aligned}\frac{\partial \mathbf{P_{11}}}{\partial p} &= \frac{\partial \mathbf{C_{g1}}}{\partial p}\mathbf{\Theta}\mathbf{B_{g1}} + \mathbf{C_{g1}}\frac{\partial \mathbf{\Theta}}{\partial p}\mathbf{B_{g1}} + \mathbf{C_{1g}}\mathbf{\Theta}\frac{\partial \mathbf{B_{g1}}}{\partial p} + \frac{\partial \mathbf{D_{g11}}}{\partial p}, \\ \frac{\partial \mathbf{P_{12}}}{\partial p} &= \frac{\partial \mathbf{C_{g1}}}{\partial p}\mathbf{\Theta}\mathbf{B_{g2}} + \mathbf{C_{g1}}\frac{\partial \mathbf{\Theta}}{\partial p}\mathbf{B_{g2}} + \mathbf{C_{g1}}\mathbf{\Theta}\frac{\partial \mathbf{B_{g2}}}{\partial p} + \frac{\partial \mathbf{D_{g12}}}{\partial p}, \\ \frac{\partial \mathbf{P_{21}}}{\partial p} &= \frac{\partial \mathbf{C_{g2}}}{\partial p}\mathbf{\Theta}\mathbf{B_{g1}} + \mathbf{C_{g2}}\frac{\partial \mathbf{\Theta}}{\partial p}\mathbf{B_{g1}} + \mathbf{C_{g2}}\mathbf{\Theta}\frac{\partial \mathbf{B_{g1}}}{\partial p} + \frac{\partial \mathbf{D_{g21}}}{\partial p},\end{aligned}$$

where

$$\begin{aligned}\frac{\partial \Xi}{\partial p} &= -\boldsymbol{\Xi}\left(\frac{\partial \mathbf{A}_{\mathbf{g}}^{\mathrm{T}}}{\partial p}\right)\boldsymbol{\Xi},\\ \frac{\partial \boldsymbol{\Theta}}{\partial p} &= -\boldsymbol{\Theta}\left(-\frac{\partial \mathbf{A}_{\mathbf{g}}}{\partial p}\right)\boldsymbol{\Theta}.\end{aligned}$$

By letting $\mathbf{P}_{\mathbf{12}}^{\boldsymbol{\Theta}} := \left(\mathbf{P}_{\mathbf{12}}^{\sim}\mathbf{P}_{\mathbf{12}}\right)^{-1}$ and $\mathbf{P}_{\mathbf{21}}^{\boldsymbol{\Theta}} := \left(\mathbf{P}_{\mathbf{21}}\mathbf{P}_{\mathbf{21}}^{\sim}\right)^{-1}$, the partial derivatives of $\mathbf{P}_{\mathbf{12}}^{-\mathrm{L}}$ and $\mathbf{P}_{\mathbf{21}}^{-\mathrm{R}}$ become

$$\begin{aligned}\frac{\partial \mathbf{P}_{\mathbf{12}}^{-\mathrm{L}}}{\partial p} &= \frac{\partial \mathbf{P}_{\mathbf{12}}^{\boldsymbol{\Theta}}}{\partial p}\mathbf{P}_{\mathbf{12}}^{\sim} + \mathbf{P}_{\mathbf{12}}^{\boldsymbol{\Theta}}\frac{\partial \mathbf{P}_{\mathbf{12}}^{\sim}}{\partial p},\\ \frac{\partial \mathbf{P}_{\mathbf{21}}^{-\mathrm{R}}}{\partial p} &= \frac{\partial \mathbf{P}_{\mathbf{21}}^{\sim}}{\partial p}\mathbf{P}_{\mathbf{21}}^{\boldsymbol{\Theta}} + \mathbf{P}_{\mathbf{21}}^{\sim}\frac{\partial \mathbf{P}_{\mathbf{21}}^{\boldsymbol{\Theta}}}{\partial p},\end{aligned}$$

where

$$\begin{aligned}\frac{\partial \mathbf{P}_{\mathbf{12}}^{\boldsymbol{\Theta}}}{\partial p} &= -\mathbf{P}_{\mathbf{12}}^{\boldsymbol{\Theta}}\left(\frac{\partial \mathbf{P}_{\mathbf{12}}^{\sim}}{\partial p}\mathbf{P}_{\mathbf{12}} + \mathbf{P}_{\mathbf{12}}^{\sim}\frac{\partial \mathbf{P}_{\mathbf{12}}}{\partial p}\right)\mathbf{P}_{\mathbf{12}}^{\boldsymbol{\Theta}},\\ \frac{\partial \mathbf{P}_{\mathbf{21}}^{\boldsymbol{\Theta}}}{\partial p} &= -\mathbf{P}_{\mathbf{21}}^{\boldsymbol{\Theta}}\left(\frac{\partial \mathbf{P}_{\mathbf{21}}}{\partial p}\mathbf{P}_{\mathbf{21}}^{\sim} + \mathbf{P}_{\mathbf{21}}, \frac{\partial \mathbf{P}_{\mathbf{21}}^{\sim}}{\partial p}\right)\mathbf{P}_{\mathbf{21}}^{\boldsymbol{\Theta}},\\ \frac{\partial \mathbf{P}_{\mathbf{12}}^{\sim}}{\partial p} &= -\frac{\partial \mathbf{B}_{\mathbf{g2}}^{\mathrm{T}}}{\partial p}\boldsymbol{\Xi}\mathbf{C}_{\mathbf{g1}}^{\mathrm{T}} - \mathbf{B}_{\mathbf{g2}}^{\mathrm{T}}\frac{\partial \boldsymbol{\Xi}}{\partial p}\mathbf{C}_{\mathbf{g1}}^{\mathrm{T}} - \mathbf{B}_{\mathbf{g2}}^{\mathrm{T}}\boldsymbol{\Xi}\frac{\partial \mathbf{C}_{\mathbf{g1}}^{\mathrm{T}}}{\partial p} + \frac{\partial \mathbf{D}_{12}^{\mathrm{T}}}{\partial p},\\ \frac{\partial \mathbf{P}_{\mathbf{21}}^{\sim}}{\partial p} &= -\frac{\partial \mathbf{B}_{\mathbf{g1}}^{\mathrm{T}}}{\partial p}\boldsymbol{\Xi}\mathbf{C}_{\mathbf{g2}}^{\mathrm{T}} - \mathbf{B}_{\mathbf{g1}}^{\mathrm{T}}\frac{\partial \boldsymbol{\Xi}}{\partial p}\mathbf{C}_{\mathbf{g2}}^{\mathrm{T}} - \mathbf{B}_{\mathbf{g1}}^{\mathrm{T}}\boldsymbol{\Xi}\frac{\partial \mathbf{C}_{\mathbf{g2}}^{\mathrm{T}}}{\partial p} + \frac{\partial \mathbf{D}_{\mathbf{21}}^{\mathrm{T}}}{\partial p}.\end{aligned}$$

6. EXAMPLES FOR OPTIMAL ACTUATOR AND SENSOR LOCATION SELECTION

6.1. Beam Design Example with Point Actuator/Sensor Pairs

Consider the simply supported beam in Figure 6.1, where ξ and ψ are the hor-

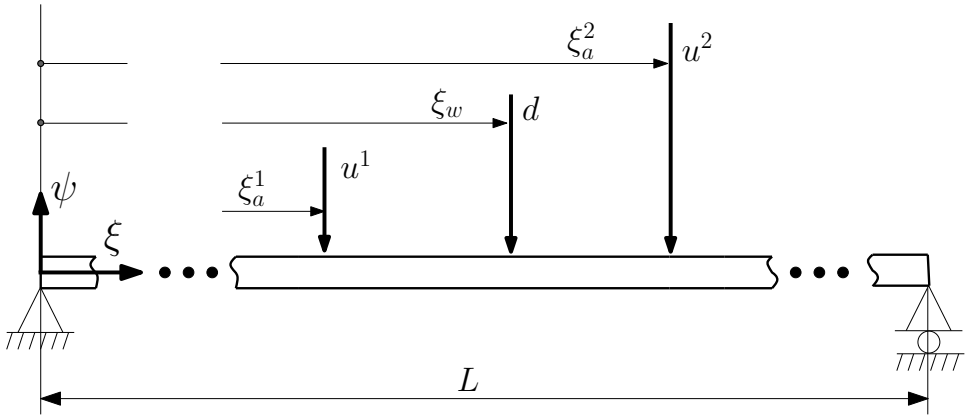

Figure 6.1. Simply supported beam with two point control forces and a single disturbance

izontal coordinate and the vertical deflection, respectively. The inputs $w(t)$ and $u^i(t)$ with $i = 1, 2$ are the single disturbance and the two point actuator forces, respectively. The disturbance is located at ξ_w. The control forces from the first and the second actuators are acting at horizontal positions ξ_a^i for $i = 1, 2$. Since the rate sensors are collocated, they are at the same location as the actuators. The boundary conditions for the simply supported beam are given in Table 6.1.

Table 6.1. The boundary conditions for the simply supported beam

Deflection at the left end	$\psi(0,t) = 0$
Deflection at the right end	$\psi(L,t) = 0$
Moment at the left end	$\dfrac{\partial^2 \psi(0,t)}{\partial \xi^2} = 0$
Moment at the right end	$\dfrac{\partial^2 \psi(L,t)}{\partial \xi^2} = 0$

The terms EI, ρ and S denote the flexural density, the density and cross section

area of the beam respectively. Their values are selected as: $E = 1\,\mathrm{Pa}$, $I = 1\,\mathrm{m}^{-4}$, $\rho = 1\,\mathrm{kg\ m}^{-3}$, $S = 1\,\mathrm{m}^2$. The single disturbance is located at the point $\xi_w = 0.35L$ and the initial places of the actuators are $\xi_a^1 = 0.25L$, $\xi_a^2 = 0.65L$. The parameters required for the controller design step are $\alpha = 100$, $\beta = 1.02$. The performance outputs are described by the vector $\mathbf{z} = [\psi(\xi_a^1), \psi(\xi_a^2), \psi(\xi_w), u^1, u^2]^{\mathrm{T}}$. The damping for each mode is $\zeta = 0.001$.

Assumed modes method is used to discretize the problem. The number of modes are taken as $N = 10$. The equation of motion is

$$EI\frac{\partial^4\psi(\xi,t)}{\partial\xi^4} + \rho S\frac{\partial^2\psi(\xi,t)}{\partial t^2} = w(t)\delta(\xi-\xi_w) + \sum_{i=1}^{2} u^i(t)\delta(\xi-\xi_a^i). \tag{6.1}$$

With the assumed modes approach, Equation (6.1) can be solved by assuming the vertical displacement $\psi(\xi,t)$ to be

$$\psi(\xi,t) = \sum_{i=1}^{N} q_i(t)\ \varphi_i(\xi), \tag{6.2}$$

$$\varphi_i(\xi) = \sqrt{\frac{2}{L}}\sin\frac{i\pi\xi}{L}, \tag{6.3}$$

where $q_i(t)$ and $\varphi_i(\xi)$ are the modal displacements and the normalized mode shapes, respectively.

If (6.2) and (6.3) are inserted in Equation (6.1), and modal analysis is done, the discrete equation is obtained as

$$\ddot{\mathbf{q}}_\mathbf{m} + \mathbf{\Omega^2 q_m} = \mathbf{L_w d} + \mathbf{L_u u}, \tag{6.4}$$

where $\mathbf{q_m}$, $\mathbf{\Omega}$, $\mathbf{w}$, $\mathbf{u}$ are

$$\mathbf{q_m} = [q_1, q_2, \ldots, q_N]^{\mathrm{T}},$$

$$\mathbf{\Omega} = \mathrm{diag}\,(\omega_1, \omega_2, \ldots, \omega_N),$$

$$\begin{aligned}\mathbf{d} &= [w(t)]\,,\\ \mathbf{u} &= \left[u^1(t), u^2(t)\right].^{\mathrm{T}}\end{aligned}$$

The matrices $\mathbf{L_w}$, $\mathbf{L_u}$ and the natural frequencies are

$$\begin{aligned}\mathbf{L_w} &= \left[\begin{array}{cccc}\varphi_1(\xi_w) & \varphi_2(\xi_w) & \dots & \varphi_N(\xi_w)\end{array}\right]^{\mathrm{T}},\\ \mathbf{L_u} &= \left[\begin{array}{cccc}\varphi_1(\xi_a^1) & \varphi_2(\xi_a^1) & \dots & \varphi_N(\xi_a^1)\\ \varphi_1(\xi_a^2) & \varphi_2(\xi_a^2) & \dots & \varphi_N(\xi_a^2)\end{array}\right]^{\mathrm{T}},\\ \omega_i &= (i\pi)^2\sqrt{\frac{EI}{\rho SL^4}}, \quad \forall\, i = 1:N,\end{aligned}$$

respectively.

Equation (6.2) is similar to the first equation in (2.46). If the assumed modal damping of $\zeta = 0.001$ is added, Equation (6.2) includes the term $2\boldsymbol{\Upsilon}\,\boldsymbol{\Omega}\,\dot{\mathbf{q}}_\mathbf{m}$ just as in (2.46), where $\boldsymbol{\Upsilon} = \mathrm{diag}\,(\zeta_1, \zeta_2, \dots \zeta_N)$. Then, $\mathbf{y}$ and $\mathbf{z}$ become

$$\mathbf{y} = \left[\begin{array}{c}\dot\psi(\xi_a^1)\\ \dot\psi(\xi_a^2)\end{array}\right] = \overbrace{\left[\begin{array}{cccc}\phi_1(\xi_a^1) & \phi_1(\xi_a^1) & \dots & \phi_N(\xi_a^1)\\ \phi_1(\xi_a^2) & \phi_1(\xi_a^2) & \dots & \phi_N(\xi_a^2)\end{array}\right]}^{=\mathbf{L_u}} \left[\begin{array}{c}\dot q_1(t)\\ \dot q_1(t)\\ \vdots\\ \dot q_N(t)\end{array}\right], \tag{6.5}$$

$$\begin{aligned}\mathbf{z} = \left[\begin{array}{c}\psi(\xi_a^1)\\ \psi\xi_a^2)\\ \psi\xi_w)\\ u^1\\ u^2\end{array}\right] &= \left[\begin{array}{cccc}\phi_1(\xi_a^1) & \phi_1(\xi_a^1) & \dots & \phi_N(\xi_a^1)\\ \phi_1(\xi_a^2) & \phi_1(\xi_a^2) & \dots & \phi_N(\xi_a^2)\\ \phi_1(\xi_w) & \phi_1(\xi_w) & \dots & \phi_N(\xi_w)\\ 0 & 0 & \dots & 0\\ 0 & 0 & \dots & 0\end{array}\right]\left[\begin{array}{c}q_1(t)\\ q_1(t)\\ q_3(t)\\ \vdots\\ q_N(t)\end{array}\right] +\\ &\qquad \left[\begin{array}{cc}0 & 0\\ 0 & 0\\ 1 & 0\\ 0 & 1\end{array}\right]\left[\begin{array}{c}u^1(t)\\ u^2(t)\end{array}\right].\end{aligned} \tag{6.6}$$

If the state vector is given as $\hat{\mathbf{x}} = \left[\mathbf{q_m}(\mathbf{t})^{\mathrm{T}}\, \dot{\mathbf{q}}_\mathbf{m}(\mathbf{t})^{\mathrm{T}}\right]^{\mathrm{T}}$, the state space representation is obtained as

$$
\begin{aligned}
\dot{\hat{\mathbf{x}}} &= \underbrace{\begin{bmatrix} \mathbf{0} & \mathbf{I} \\ -\mathbf{\Omega}^2 & 2\mathbf{\Upsilon}\,\mathbf{\Omega}\,\dot{\mathbf{q}}_\mathbf{m} \end{bmatrix}}_{\hat{\mathbf{A}}} \hat{\mathbf{x}} + \underbrace{\begin{bmatrix} \mathbf{0} \\ \mathbf{L_w} \end{bmatrix}}_{\hat{\mathbf{B}}_1} \mathbf{d} + \underbrace{\begin{bmatrix} \mathbf{0} \\ \mathbf{L_u} \end{bmatrix}}_{\hat{\mathbf{B}}_2} \mathbf{u}, \\
\mathbf{z} &= \underbrace{\begin{bmatrix} \mathbf{L_u}^{\mathrm{T}} & \mathbf{0} \\ \mathbf{L_w}^{\mathrm{T}} & \mathbf{0} \\ \mathbf{0} & \mathbf{0} \\ \mathbf{0} & \mathbf{0} \end{bmatrix}}_{\hat{\mathbf{C}}_1} \hat{\mathbf{x}} + \underbrace{\begin{bmatrix} \mathbf{0} & \mathbf{0} \\ \mathbf{0} & \mathbf{0} \\ \mathbf{I} & \mathbf{0} \\ \mathbf{0} & \mathbf{I} \end{bmatrix}}_{\hat{\mathbf{D}}_{12}} \mathbf{u}, \\
\mathbf{y} &= \underbrace{\begin{bmatrix} \mathbf{0} & \mathbf{Lu}^{\mathrm{T}} \end{bmatrix}}_{\hat{\mathbf{C}}_2} \hat{\mathbf{x}},
\end{aligned}
\tag{6.7}
$$

which is the same as Equation (2.47). Using the coordinate transformation $\mathbf{x_m} = \mathbf{R_{31}}\mathbf{R}\hat{\mathbf{x}}$ with $\mathbf{R_{31}}$ in (2.49) and $\mathbf{R}$ in (2.48), the state space matrices $\mathbf{A_{m1}}$, $\mathbf{B_{m1}}$, $\mathbf{C_{m1}}$ in the third modal form can be calculated (matrices (6.8)). Using the signal

Table 6.2. Signal weightings for beams with point actuators/sensors

Disturbance Weight	W_{dist}	$\frac{10}{0.03s+1}$
Sensor Noise Weight	W_{sn}	$\frac{1}{10^5}$
Performance Output Weight	W_{er}	1
Control Input Weight	W_{in}	$\frac{1}{25}$

weights in Table 6.2, the generalized plant is obtained. Tables 6.3 and 6.4 give exact and diagonally dominant controllability and observability Gramians of the generalized plant, respectively. Table 6.5 compares the exact CARE and FARE solutions with diagonally dominant ones, which are calculated from Equations (4.71) and (4.72). In Tables 6.3, 6.4 and 6.5, exact Gramians and exact ARE solutions are square matrices. However, since they are diagonally dominant, their diagonal entries are compared with values, which are obtained according to the methods introduced in this study.

$$\text{blockdiag}\left(\overbrace{\begin{pmatrix} 0 & 9.8696 \\ -9.8696 & -0.0197 \\ 0 & 39.4784 \\ -39.4784 & -0.0790 \\ 0 & 88.8264 \\ -88.8264 & -0.1777 \\ 0 & 157.9137 \\ -157.9137 & -0.3158 \\ 0 & 246.7401 \\ -246.7401 & -0.4935 \\ 0 & 355.3058 \\ -355.3058 & -0.7106 \\ 0 & 483.6106 \\ -483.6106 & -0.9672 \\ 0 & 631.6547 \\ -631.6547 & -1.2633 \\ 0 & 799.4380 \\ -799.4380 & -1.5989 \\ 0 & 986.9604 \\ -986.9604 & -1.9739 \end{pmatrix}}^{\mathbf{A_{m1}}\ =}, \overbrace{\left[\begin{array}{ccc|cc} 0 & 0 & 0 & & \\ 0.1277 & 0.1013 & 0.1277 & & \\ 0 & 0 & 0 & & \\ 0.0290 & 0.0358 & -0.0290 & & \\ 0 & 0 & 0 & & \\ -0.0025 & 0.0113 & -0.0025 & & \\ 0 & 0 & 0 & & \\ -0.0085 & 0.0000 & 0.0085 & & \\ 0 & 0 & 0 & & \\ -0.0041 & -0.0041 & -0.0041 & & \\ 0 & 0 & 0 & & \\ 0.0012 & -0.0040 & -0.0012 & & \\ 0 & 0 & 0 & & \\ 0.0029 & -0.0021 & 0.0029 & & \\ 0 & 0 & 0 & & \\ 0.0013 & -0.0000 & -0.0013 & & \\ 0 & 0 & 0 & & \\ -0.0008 & 0.0013 & -0.0008 & & \\ 0 & 0 & 0 & & \\ -0.0014 & 0.0014 & 0.0014 & & \end{array}\right]}^{\left[\ \mathbf{B_{1\,m1}}\ \ \mathbf{B_{2\,m1}}\ \right]=}, \overbrace{\left[\begin{array}{ccc|cc} 1 & 1.2601 & 1.2601 & 0 & 0 \\ 0 & 0 & 0 & 9.8696 & 12.4364 \\ 1.4142 & -1.1441 & 1.1441 & 0 & 0 \\ 0 & 0 & 0 & 55.8309 & -45.1682 \\ 1 & -0.2212 & -0.2212 & 0 & 0 \\ 0 & 0 & 0 & 88.8264 & -19.6512 \\ 0 & 1.3450 & -1.3450 & 0 & 0 \\ 0 & 0 & 0 & 0 & 212.3934 \\ -1 & -1 & -1 & 0 & 0 \\ 0 & 0 & 0 & -246.7401 & -246.7401 \\ -1.4142 & -0.4370 & 0.4370 & 0 & 0 \\ 0 & 0 & 0 & -502.4782 & -155.2743 \\ -1 & 1.3968 & 1.3968 & 0 & 0 \\ 0 & 0 & 0 & -483.6106 & 675.5084 \\ -0 & -0.8313 & 0.8313 & 0 & 0 \\ 0 & 0 & 0 & -0 & -525.0654 \\ 1 & -0.6420 & -0.6420 & 0 & 0 \\ 0 & 0 & 0 & 799.4380 & -513.2708 \\ 1.4142 & 1.4142 & -1.4142 & 0 & 0 \\ 0 & 0 & 0 & 1395.7728 & 1395.7728 \end{array}\right]}^{\left[\ \mathbf{C_{1\,m1}}^{\mathrm{T}}\ \ \mathbf{C_{2\,m1}}^{\mathrm{T}}\ \right]=}\right) \tag{6.8}$$

Table 6.3. Comparison of exact and diagonal controllability Gramians

Controllability Gramians			
for the pair $(\mathbf{A}, \mathbf{B_1})$		for the pair $(\mathbf{A}, \mathbf{B_2})$	
Exact	Diagonal	Exact	Diagonal
Physical Modes from 1 to $2 \times N_p$			
37.960867057	38.002235112	0.672928630	0.672928630
38.002235112	38.002235112	0.672928630	0.672928630
0.221364906	0.221801717	0.013444969	0.013444969
0.221801717	0.221801717	0.013444969	0.013444969
0.000215508	0.000215792	0.000374167	0.000374167
0.000215792	0.000215792	0.000374167	0.000374167
0.000489904	0.000490298	0.000114848	0.000114848
0.000490298	0.000490298	0.000114848	0.000114848
0.000029829	0.000029845	0.000033285	0.000033285
0.000029845	0.000029845	0.000033285	0.000033285
0.000000929	0.000000929	0.000012212	0.000012212
0.000000929	0.000000929	0.000012212	0.000012212
0.000002039	0.000002040	0.000006523	0.000006523
0.000002040	0.000002040	0.000006523	0.000006523
0.000000190	0.000000190	0.000000685	0.000000685
0.000000190	0.000000190	0.000000685	0.000000685
0.000000035	0.000000035	0.000000691	0.000000691
0.000000035	0.000000035	0.000000691	0.000000691
0.000000059	0.000000059	0.000001040	0.000001040
0.000000059	0.000000059	0.000001040	0.000001040
Signal Weight Mode			
5.023035733	5.023035733	0.000000000	0.000000000

Table 6.4. Comparison of exact and diagonal observability Gramians

Observability Gramians			
for the pair $(\mathbf{C_1}, \mathbf{A})$		for the pair $(\mathbf{C_2}, \mathbf{A})$	
Exact	Diagonal	Exact	Diagonal
Physical Modes from 1 to $2 \times N_p$			
105.768859550	105.768436477	6385.104178775	6385.104178775
105.768436477	105.768436477	6385.104178775	6385.104178775
29.244158841	29.244041865	32658.688690963	32658.688690963
29.244041865	29.244041865	32658.688690963	32658.688690963
3.089990333	3.089977973	23293.478752352	23293.478752352
3.089977973	3.089977973	23293.478752352	23293.478752352
5.727889883	5.727866972	71417.128357314	71417.128357314
5.727866972	5.727866972	71417.128357314	71417.128357314
3.039647668	3.039635509	123370.055013618	123370.055013618
3.039635509	3.039635509	123370.055013618	123370.055013618
1.676004035	1.675997331	194617.219635262	194617.219635262
1.675997331	1.675997331	194617.219635262	194617.219635262
2.534132049	2.534121912	356790.564668366	356790.564668366
2.534121912	2.534121912	356790.564668366	356790.564668366
0.546964813	0.546962625	109115.662614320	109115.662614320
0.546962625	0.546962625	109115.662614320	109115.662614320
0.570537331	0.570535049	282244.518007481	282244.518007481
0.570535049	0.570535049	282244.518007481	282244.518007481
1.519823834	1.519817755	986960.440108941	986960.440108942
1.519817755	1.519817755	986960.440108941	986960.440108942
Signal Weight Mode			
0.000034378	0.000034378	0.018009699	0.018009699

Table 6.5. Comparison of exact and diagonal ARE solutions

ARE solutions			
CARE		FARE	
Exact	Diagonal	Exact	Diagonal
Physical Modes from 1 to $2 \times N_p$			
0.973948238	0.974016611	1.026447863	1.026519921
0.964826213	0.974016611	1.016834125	1.026519921
15.549453178	15.581736146	0.064014178	0.064147081
15.386421584	15.581736146	0.063343008	0.064147081
76.037720356	78.767846682	0.012214061	0.012652605
76.503568937	78.767846682	0.012288891	0.012652605
246.864452683	248.932295078	0.003969901	0.004003154
246.903607877	248.932295078	0.003970530	0.004003154
599.812132295	607.306501573	0.001618290	0.001638509
600.491869182	607.306501573	0.001620123	0.001638509
1237.977434456	1258.333989375	0.000776790	0.000789563
1242.017117567	1258.333989375	0.000779325	0.000789563
2307.051272207	2331.139347259	0.000421768	0.000426172
2309.048596506	2331.139347259	0.000422133	0.000426172
3753.984103348	3917.597090254	0.000235816	0.000246094
3764.284656080	3917.597090254	0.000236463	0.000246094
6174.582300492	6319.062558022	0.000151171	0.000154708
6192.361426401	6319.062558022	0.000151606	0.000154708
9609.137563640	9692.958249637	0.000101271	0.000102154
9639.461867987	9692.958249637	0.000101591	0.000102154
Signal Weight Mode			
0.004290010	0.000000000	0.000000000	0.000000000

FEM is also used to model the beam. If the beam is divided into elements as in Figure 6.2, the global mass and stiffness matrices are obtained for the initial locations of the actuator and sensor pairs. After the assembly procedure, the boundary conditions are applied, and the equations of motions are derived. If the state space description in the first modal form and the derivatives of the state space matrices of this representation are achieved, the signal weightings need to be introduced to obtain the generalized plant and its derivatives. The initial number of finite elements is chosen as $N_e = 10$, and similar to the continuous model case first $N = 10$ modes are taken.

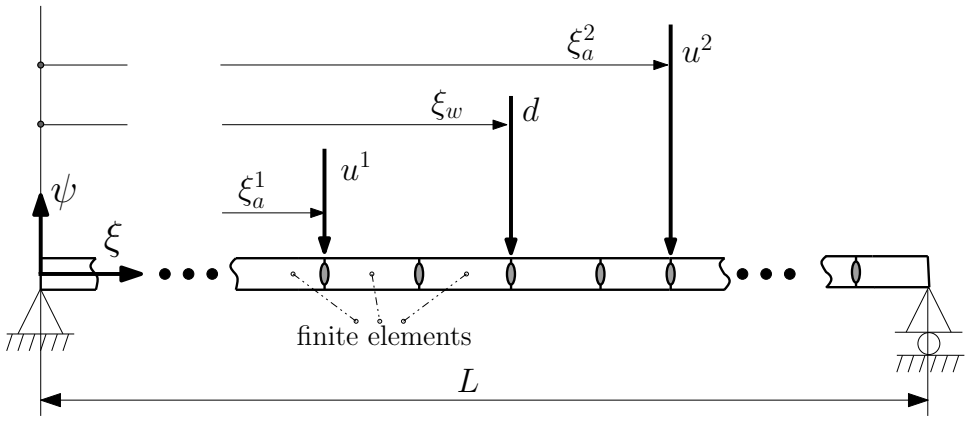

Figure 6.2. Simply supported beam with two point control forces and a single disturbance (FEM)

6.1.1. Optimal Actuator and Sensor Locations for $\xi_w = 0.35L$

The single disturbance is located at the point $\xi_w = 0.35L$, and the initial places of the actuators are $\xi_a^1 = 0.25L$, $\xi_a^2 = 0.65L$.

The signal weightings of the generalized plant (in Figure 2.8) have the transfer functions in Table 6.2.

The resulting optimal actuator and sensor locations can be seen in Figure 6.3. Starting from the initial locations $(0.25L, 0.65L)$, in nearly 55 iterations, the actuator/sensor pairs (ξ_a^1, ξ_a^2) converge to the final locations $(0.35L, 0.35L)$. The objective function $J = \mathcal{H}_2^2$ converges to its minimum also, as can be seen in Figure 6.4.

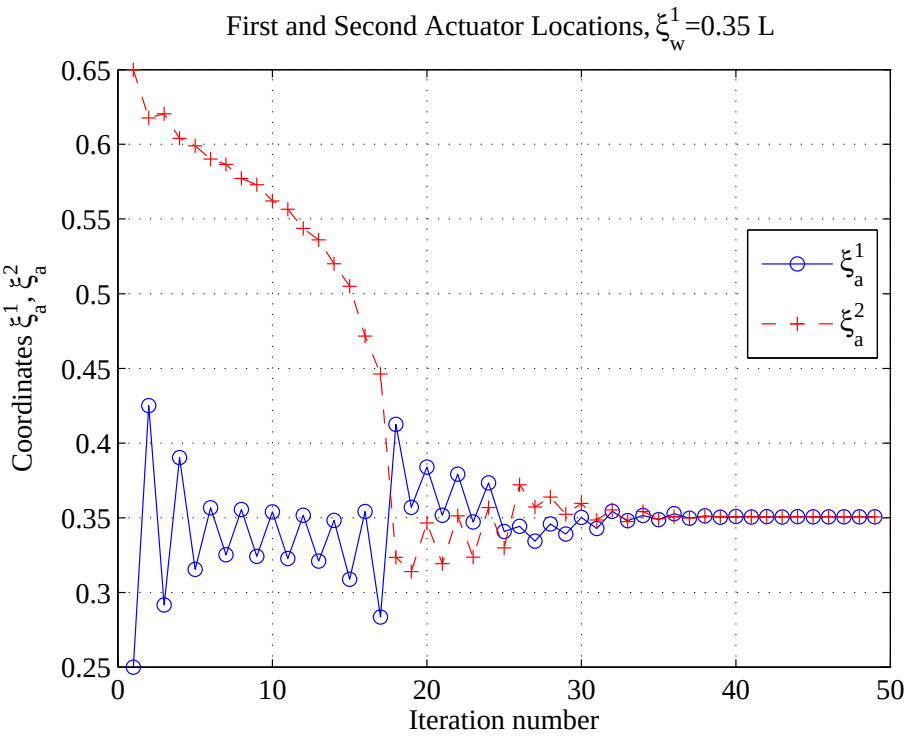

(a) Continuous

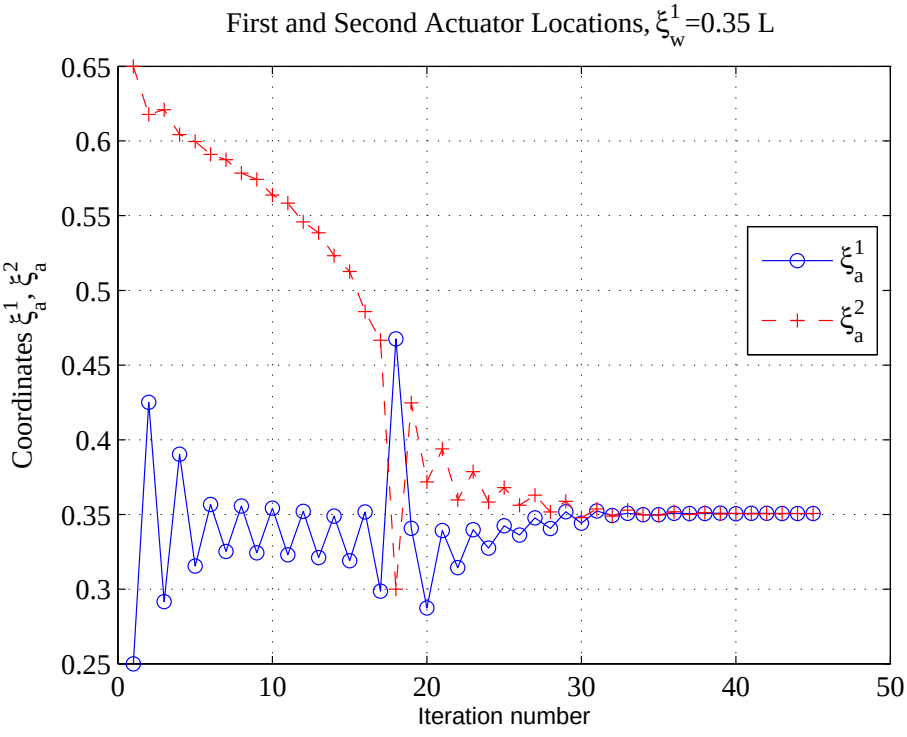

(b) FEM

Figure 6.3. Iterations and convergence to the optimum locations

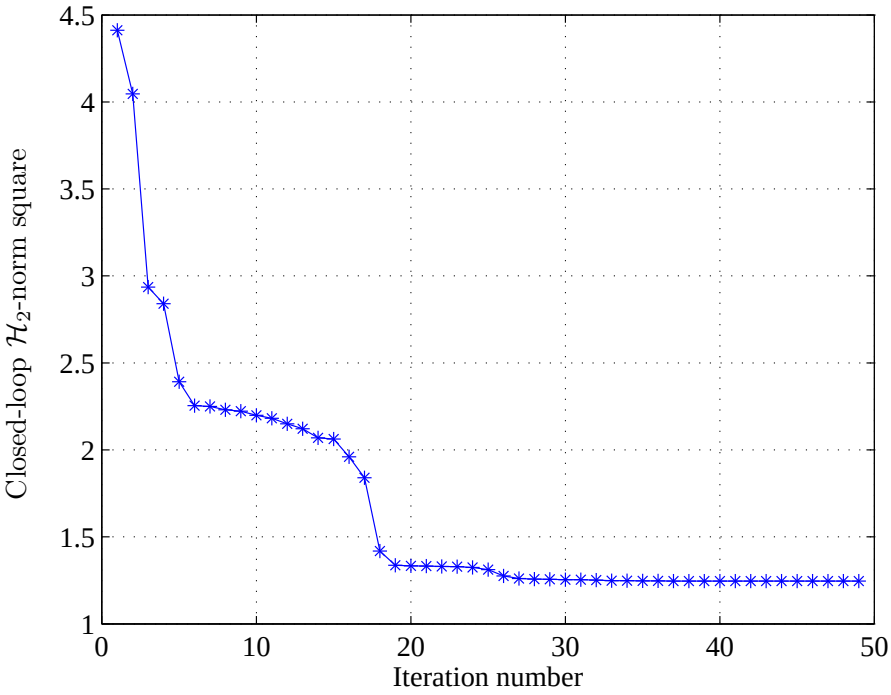

(a) Continuous

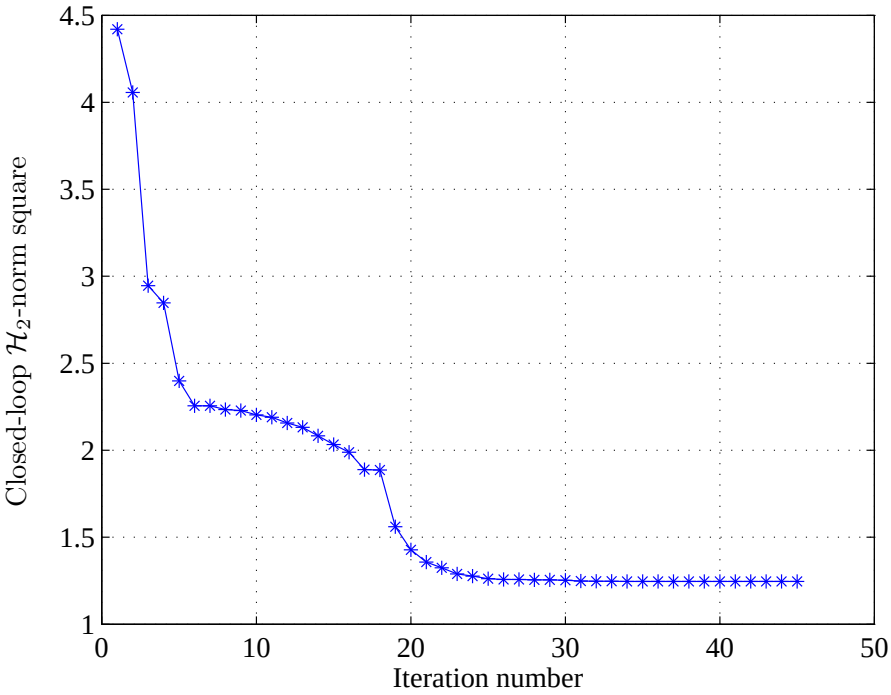

(b) FEM

Figure 6.4. Iterations and the minimized $\mathcal{H}_2^2$

To verify the obtained results, the $\mathcal{H}_2$-norm on the whole domain of the beam is calculated and the variation of J with the change in the actuator coordinates ξ_a^1 and ξ_a^2 is plotted in Figures 6.5 and 6.6. As can be seen in Figures 6.5 and 6.6, there are actuator/sensor locations pairs (ξ_a^1, ξ_a^2)'s, for which the $\mathcal{H}_2$-norms are equivalent or very close.

Figures 6.7 and 6.8 show the results obtained by the formulation given in Hiramoto et al. [1]. That is, the damping is neglected, and the disturbance input and the sensor noise weightings are not present. The optimal locations in Figure 6.7 and the square of the closed-loop $\mathcal{H}_2$-norm in Figure 6.8, which are obtained with the Hiramoto et al. [1]'s formulation, are different than those achieved in Figures 6.3 and 6.4. Because of possibility of including weights and damping in the methods introduced in this thesis, the new methodology should provide more realistic results.

6.1.2. Effect of the Design Parameter α and the Filter Coefficient C_{W_w}

To see the effect of the signal weightings on the resulting optimal actuator/sensor locations, some parametric studies are done. For simulations in Figures 6.9 through 6.12, the initial points are $\xi_a^1 = 0.35L$ and $\xi_a^1 = 0.65L$. The disturbance force is located at $\xi_w = 0.5L$. The signal weigtings and the parameter α, which are used for the simulations in Figures from 6.9 to 6.12, are listed in Table 6.6.

Table 6.6. The signal weigthings used for simulations in Figures 6.9 to 6.12

	Figures 6.9, 6.10	Figures 6.11, 6.12
α	α_c[1]	1
W_{dist}	$\frac{10}{0.03s+1}$	$\frac{10}{C_{Ww}s+1}$[2]
W_{in}	$\frac{1}{25}$	$\frac{1}{25}$
W_{er}	1	1
W_{sn}	$\frac{1}{10^5}$	$\frac{1}{10^5}$

[1] α_c values: 0.015, 0.02, 0.025, 0.03, 0.03, 0.04, 0.045, 0.05, 0.06, 0.075, 0.1, 0.15, 0.2, 0.5, 1.

[2] C_{Ww} values: 0.01, 0.02, 0.03, 0.06, 0.09, 0.12, 0.15, 0.2, 0.3, 0.4, 0.5, 0.6, 0.7, 0.8.

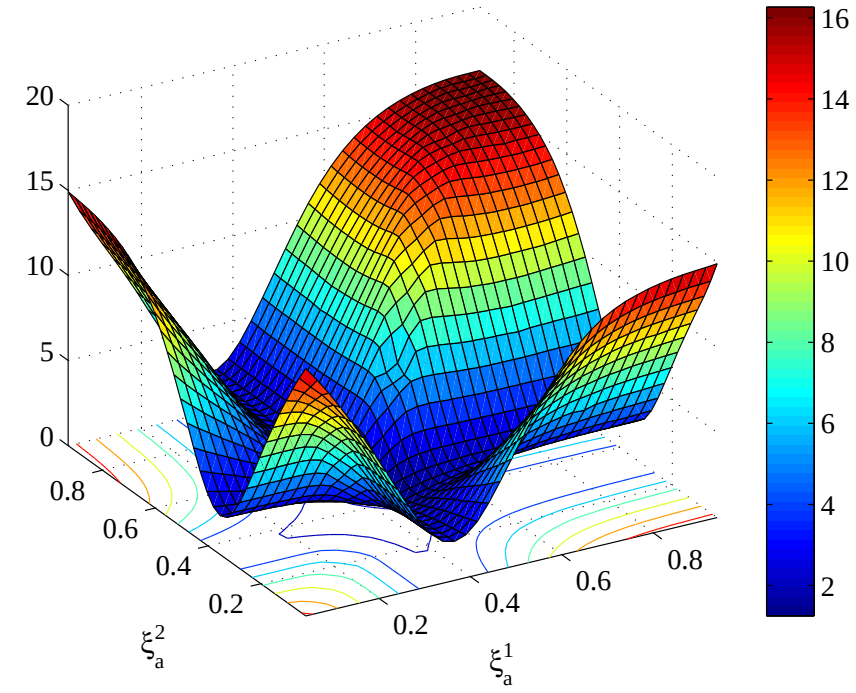

(a) Continuous

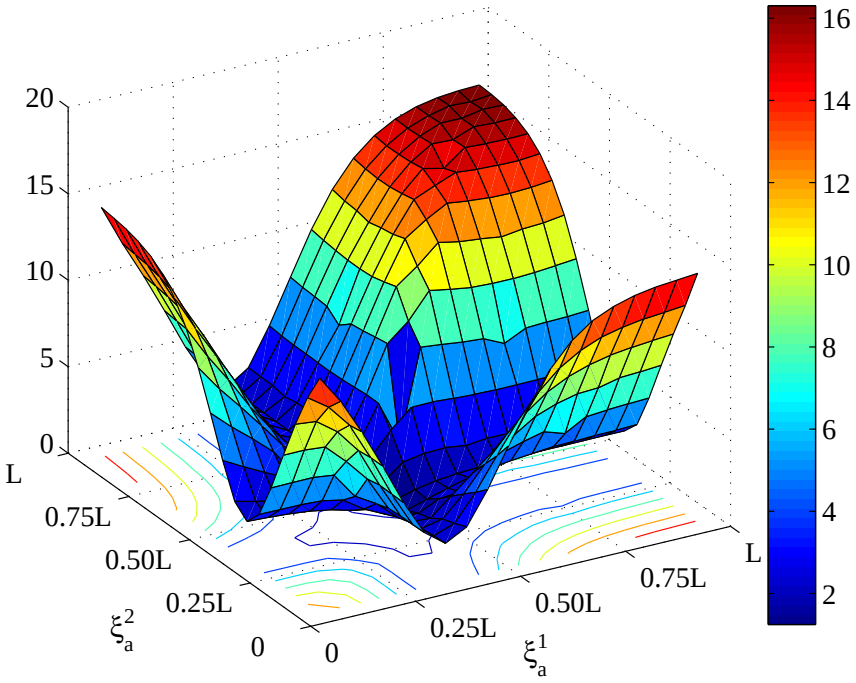

(b) FEM

Figure 6.5. The minimized $J = \mathcal{H}_2^2$ versus actuator locations (surface plot)

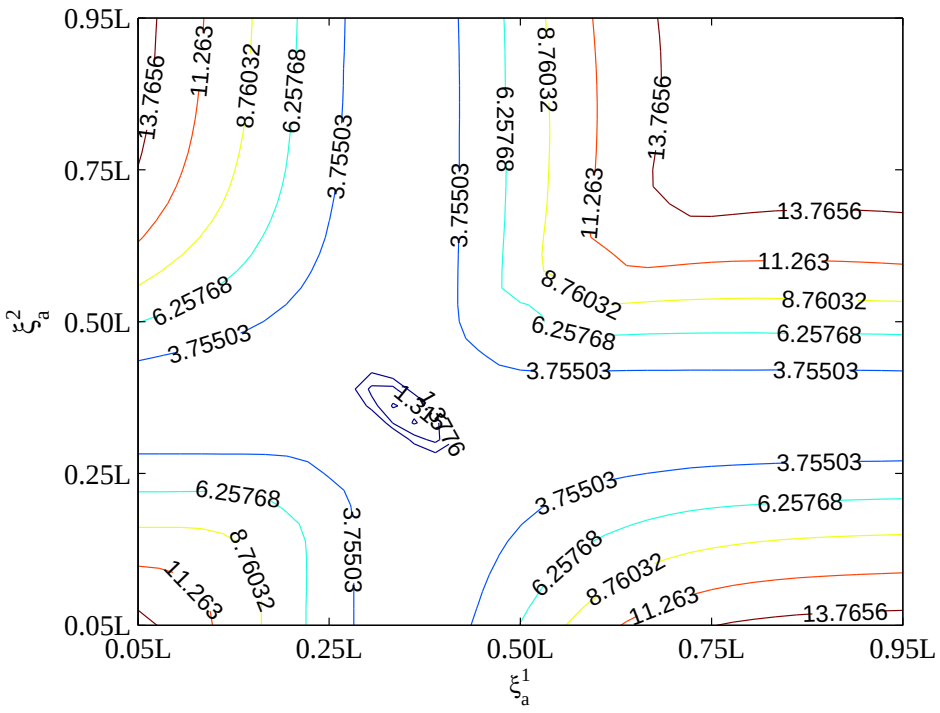

(a) Continuous

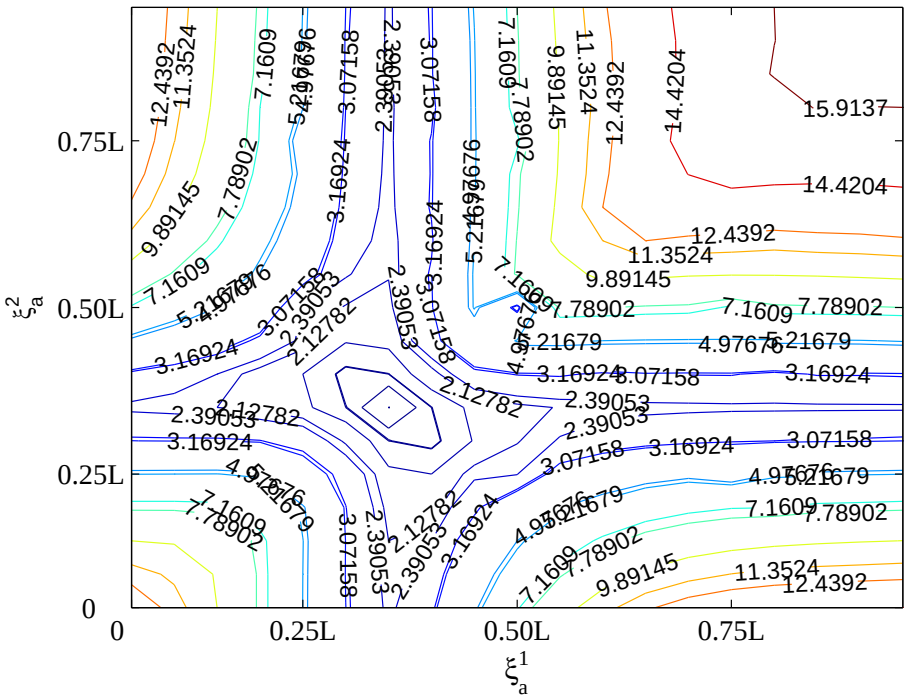

(b) FEM

Figure 6.6. The minimized $J = \mathcal{H}_2^2$ versus actuator locations (contour plot)

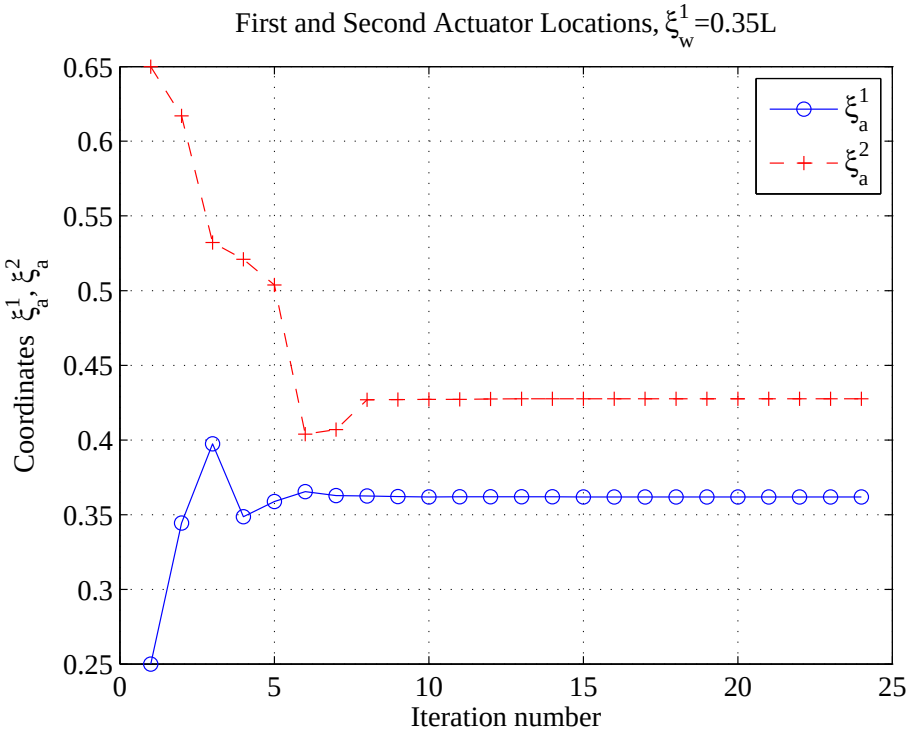

Figure 6.7. Iterations and convergence to the optimum locations with the method of Hiramoto

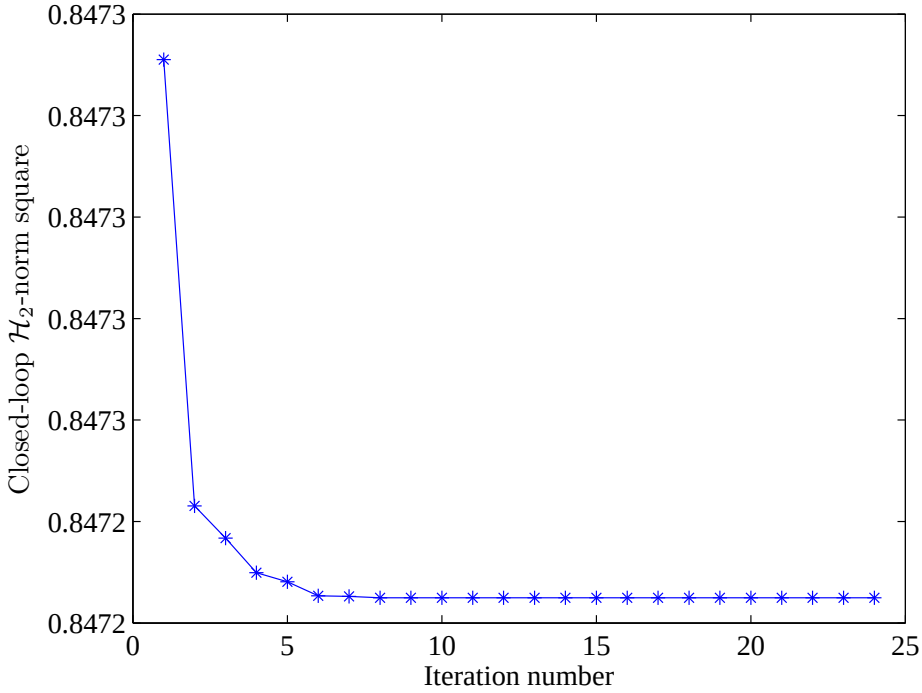

Figure 6.8. Iterations and the minimized $\mathcal{H}_2^2$ with the method of Hiramoto

In Figures 6.9 to 6.12, the minimized optimization metric J and the optimal actuator/sensor locations (ξ_a^1, ξ_a^2) are plotted versus the changing the parameter α and the coefficient C_{Ww} of a low pass filter, which is interconnected to the physical plant.

In Figure 6.9, as α increases, the square of the closed-loop $\mathcal{H}_2$-norm at the optimal actuator and sensor location decreases. Since the $\mathcal{H}_2$-norm is the norm of the closed-loop transfer function between the disturbance inputs and the performance outputs, for disturbance rejection purposes α needs to be selected larger as mentioned in Hiramoto et al. [1]. Figure 6.10 shows the variance of the optimal actuator and sensor location with α.

In Figures 6.11 and 6.12, α is kept constant, but the coefficient C_{Ww} of the disturbance input weight is changed. As C_{Ww} increases, the minimized optimization function decreases. That is, as there are less disturbances acting in higher frequencies, the closed-loop $\mathcal{H}_2$-norm decreases at the optimal actuator and sensor location.

6.1.3. Effect of Disturbance Weights

To further illustrate the effect of signal weights, the bandpass filter

$$W_{dist} = \frac{16s^2}{s^4 + 5.657s^3 + 3125s^2 + 8794s + 2.417^6}$$

is applied as the disturbance input filter. This second order Butterworth filter is shown in Figure 6.17 and is used to stop all modes other than the second one.

If the bandpass filter in Figure 6.17 is selected as the disturbance input filter, the optimal locations converge to the points $(0.25L, 0.25L)$. The location $0.25L$ is one of the antinodes of the second mode of a simply supported beam, as can be seen in Figure 6.18. If the simply supported beam is excited only at its second mode, the maximum deflections occur at the points $0.25L$ and $0.75L$, and the point $0.50L$ becomes a node where the deflections vanish. The optimal locations in the Butterworth filter example seem to reflect this phenomenon correctly, and the optimal locations converge

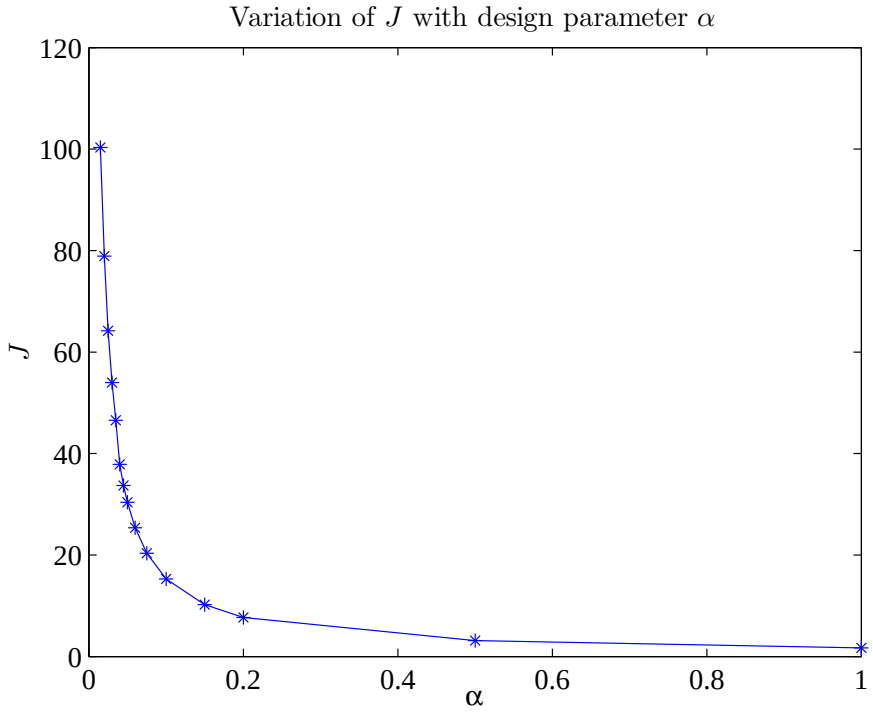

Figure 6.9. The minimized $J = \mathcal{H}_2^2$ versus design parameter α

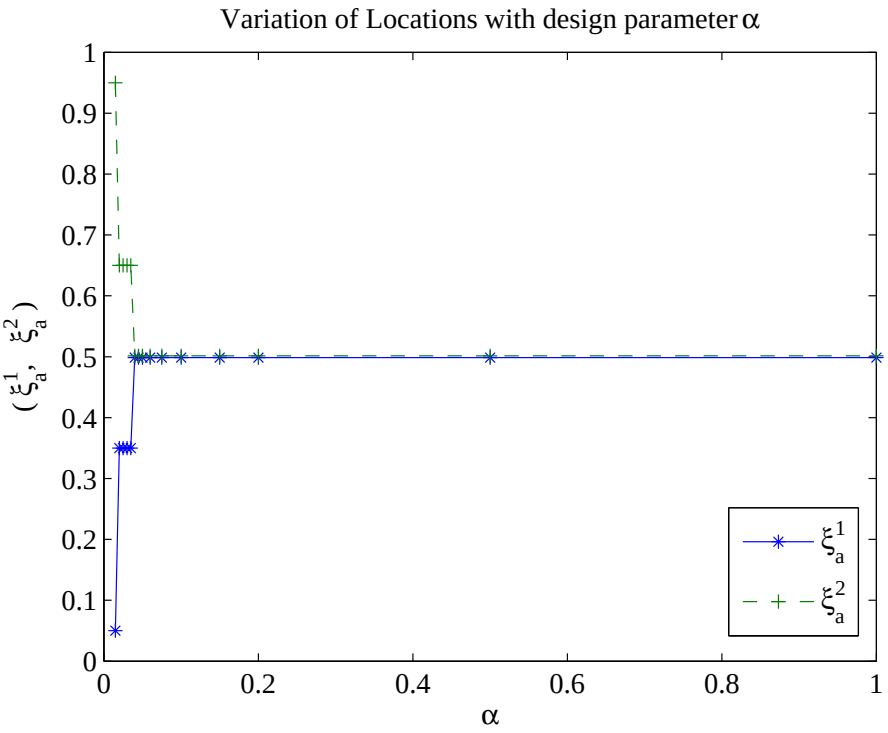

Figure 6.10. The actuator/sensor locations versus design parameter α

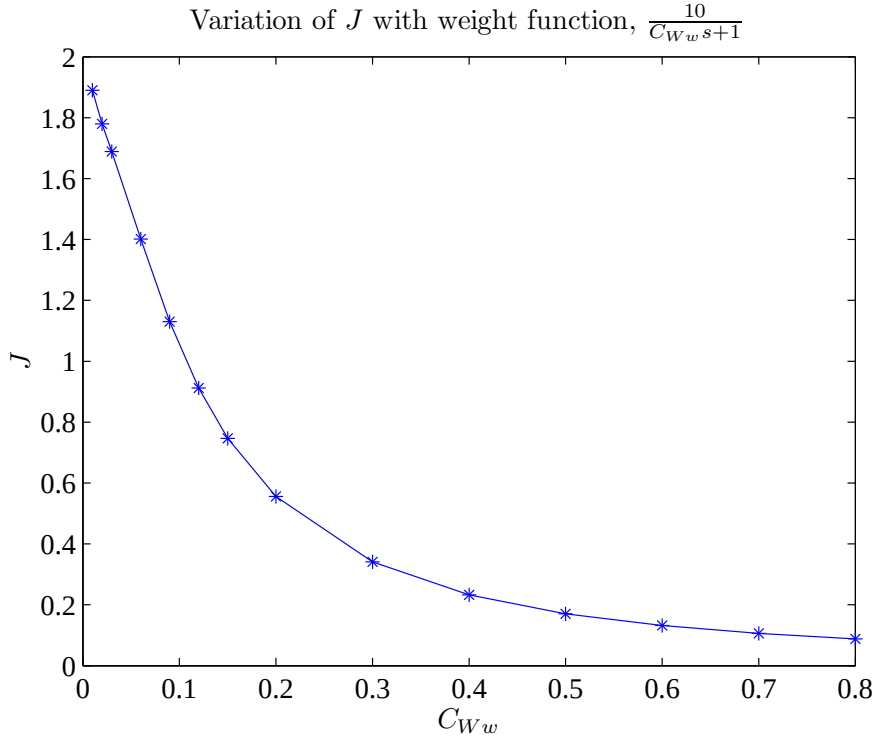

Figure 6.11. The minimized $J = \mathcal{H}_2^2$ versus change in disturbance weight coefficient C_{W_w}

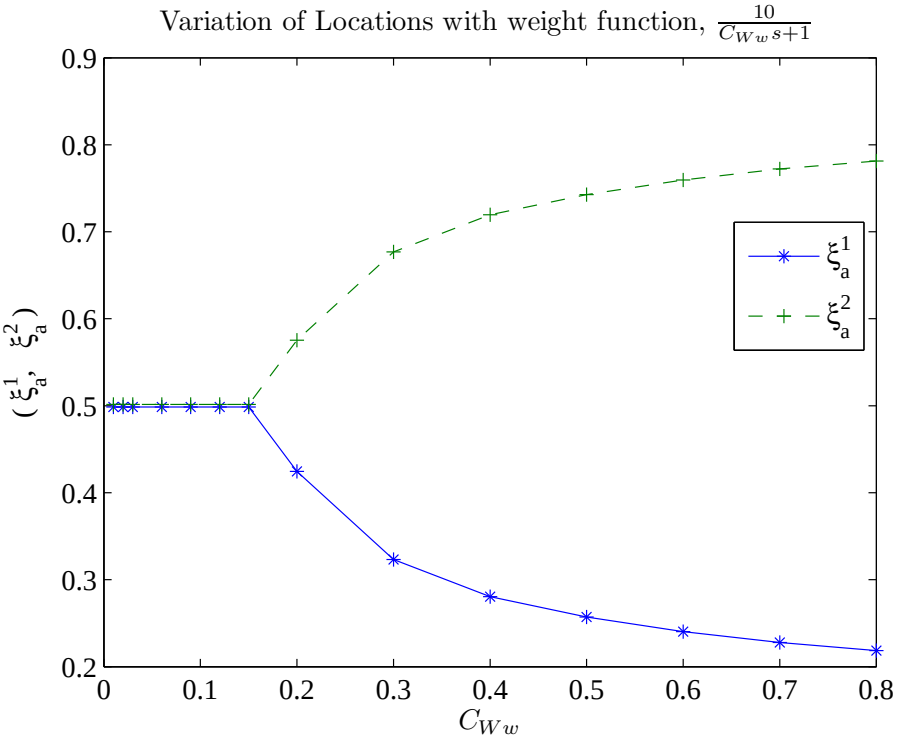

Figure 6.12. The actuator/sensor locations versus change in disturbance weight coefficient C_{W_w}

to points $0.25L$ or $0.75L$, but not the point $0.35L$, where the disturbance is acting. This result shows that the optimization technique introduced in the study can be can effectively handle the plants shaped with different signal weightings. However, the formulation given in Hiramoto et al. [1] does not consider the signal weightings in the controller design stage.

6.1.4. The Optimal Actuator and Sensor Locations for $\xi_w = [0.35L, 0.45L]$

One another advantage of the developed approach is the possibility of using different signal weightings for different channels. This is demonstrated by four cases.

In case one, both of the disturbances are applied the input signal weighting, $W_{dist} = \frac{10}{0.03s+1}$, which is given in Table (6.2). In this case the optimal locations of the collocated actuator and sensor pairs converge to locations where the disturbance inputs act.

In case two, the signal weight for the disturbance input at $\xi_w = 0.35L$ is kept, whereas the bandpass filter in Figure 6.17 is used for the disturbance input at $\xi_w = 0.45L$. The obtained optimal locations are to be seen in Figure 6.22.

In case three, the bandpass filter is applied to the disturbance input at $\xi_w = 0.35L$, and the input at $\xi_w = 0.45L$ is filtered with the low pass filter (see Figure 6.24). In this case, both of the optimal locations converge to the point $0.45L$, whereas the optimal locations approach the point $0.35L$ in case two.

In case four, the bandpass filter is applied to both of the disturbance inputs ($\xi_w = 0.35L$, $\xi_w = 0.45L$). Similar to the example given in Subsection 6.1.3, the optimal locations converge to the first antinode of the second mode of the simply supported beam as can be in Figure 6.26.

If the disturbances act at different frequencies, the improved coprime controller takes this into account, whereas the controller used by Hiramoto et al. [1] cannot.

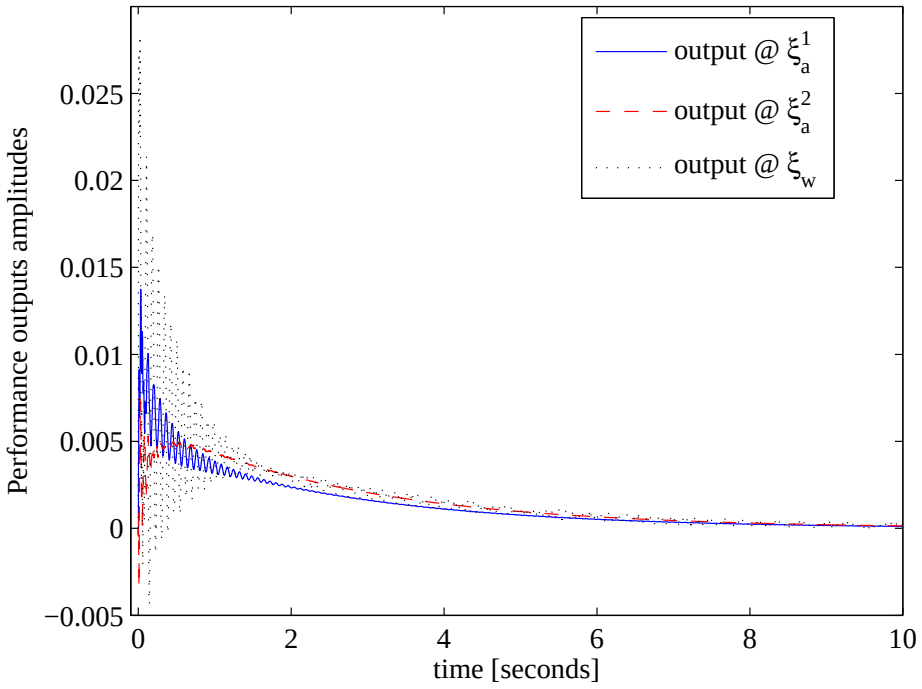

(a) Continuous

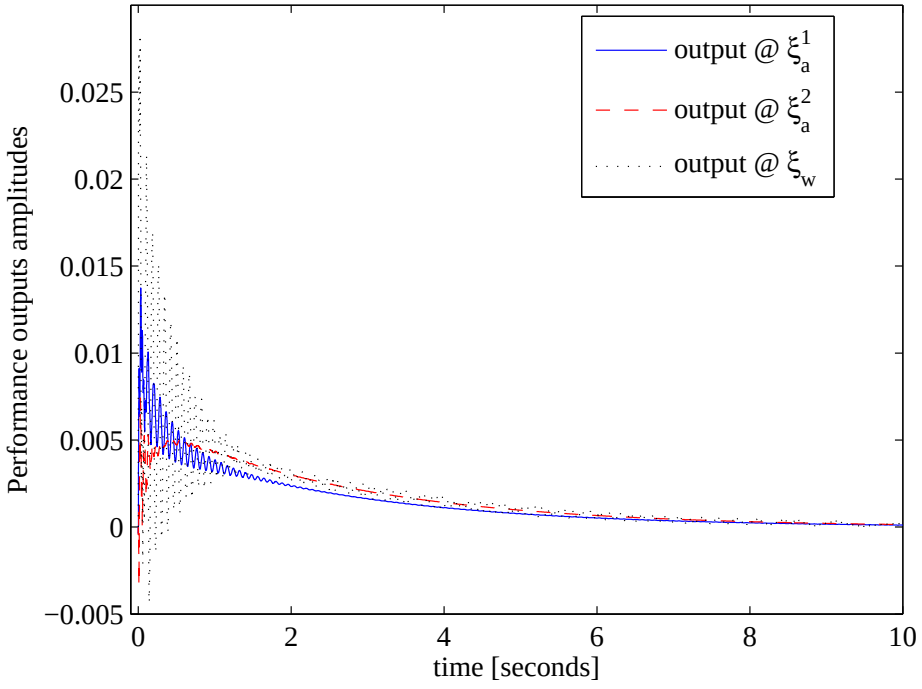

(b) FEM

Figure 6.13. Impulse response of the beam with actuators at initial locations $[\xi_a^1 = 0.25L, \xi_a^1 = 0.65L]$

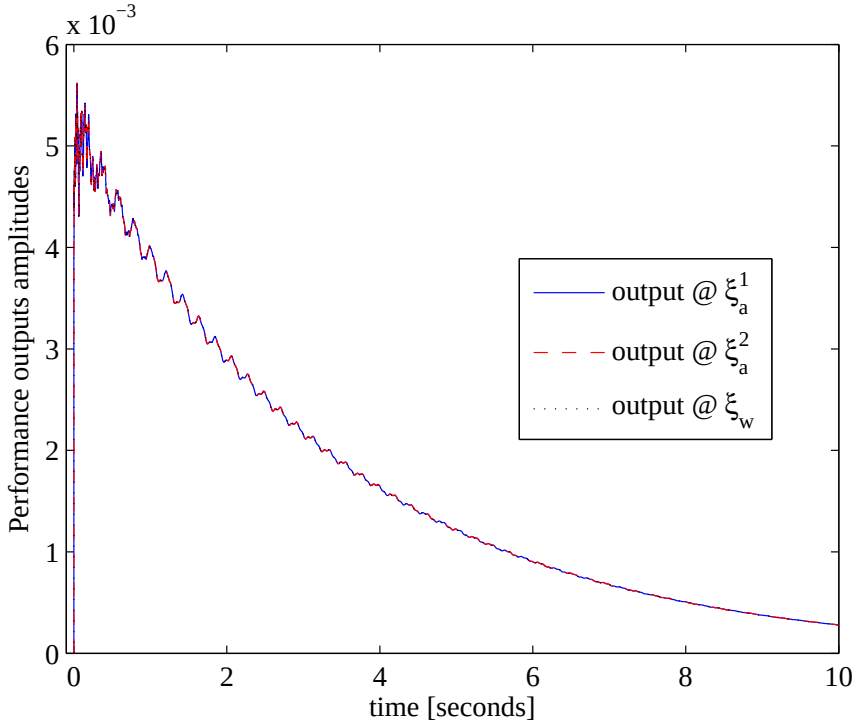

(a) Continuous

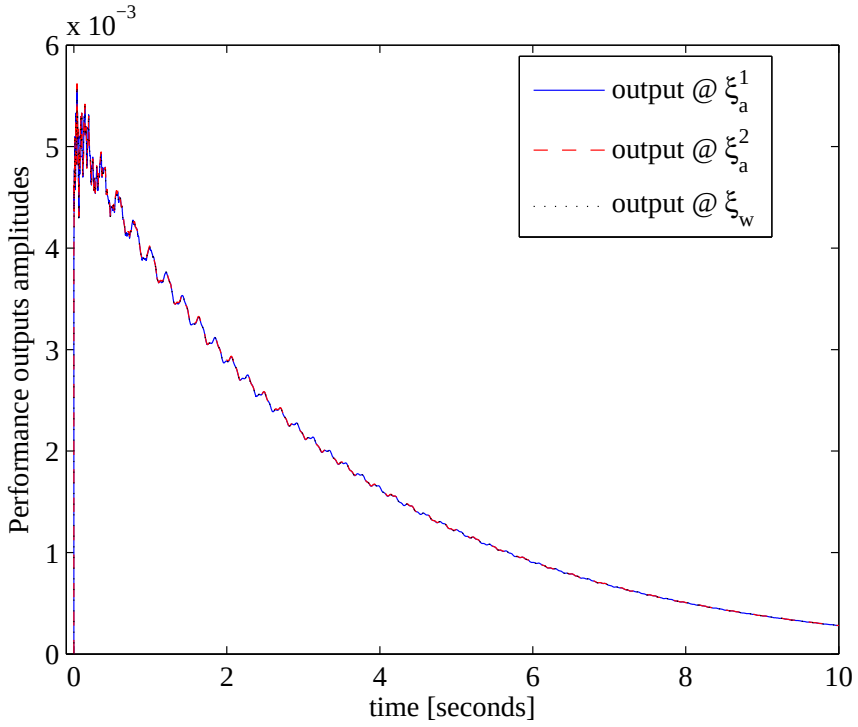

(b) FEM

Figure 6.14. Impulse response of the beam with actuators at final locations $[\xi_a^1 = 0.35L, \xi_a^1 = 0.35L]$

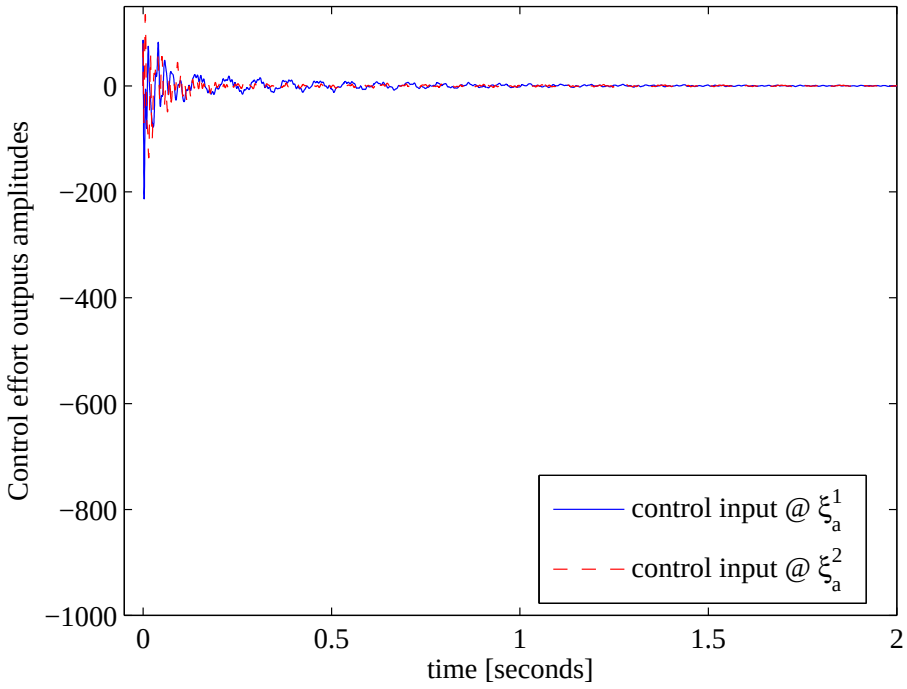

(a) Continuous

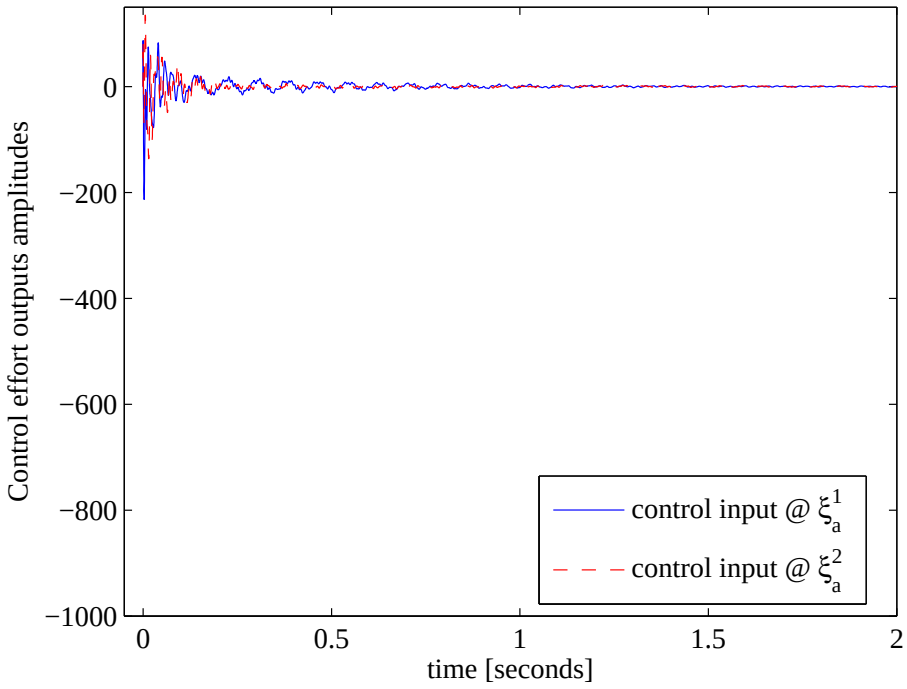

(b) FEM

Figure 6.15. Control effort impulse response of the beam with actuators at initial locations $[\xi_a^1 = 0.25L, \xi_a^1 = 0.65L]$

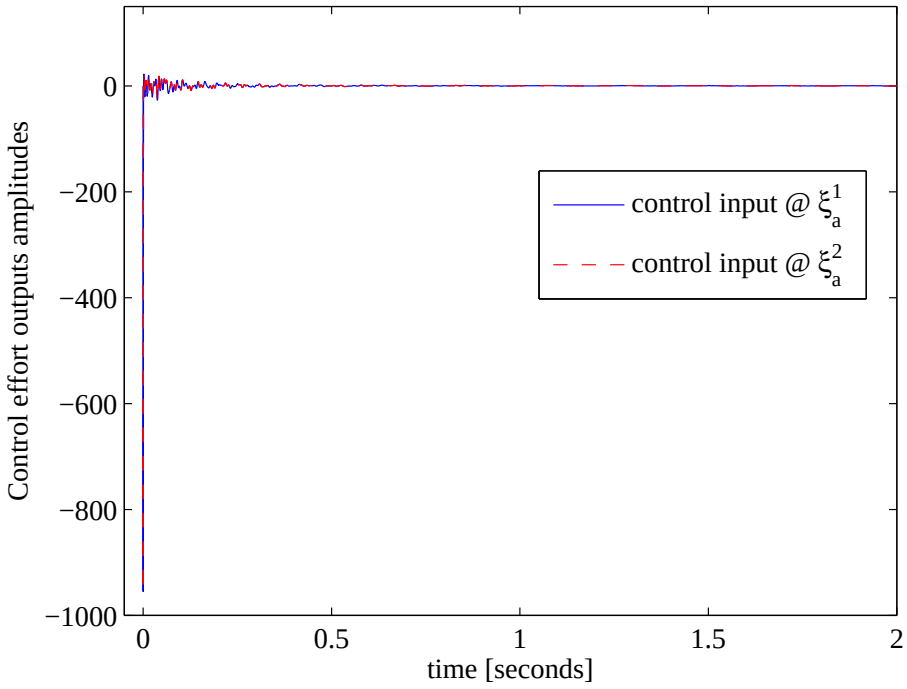

(a) Continuous

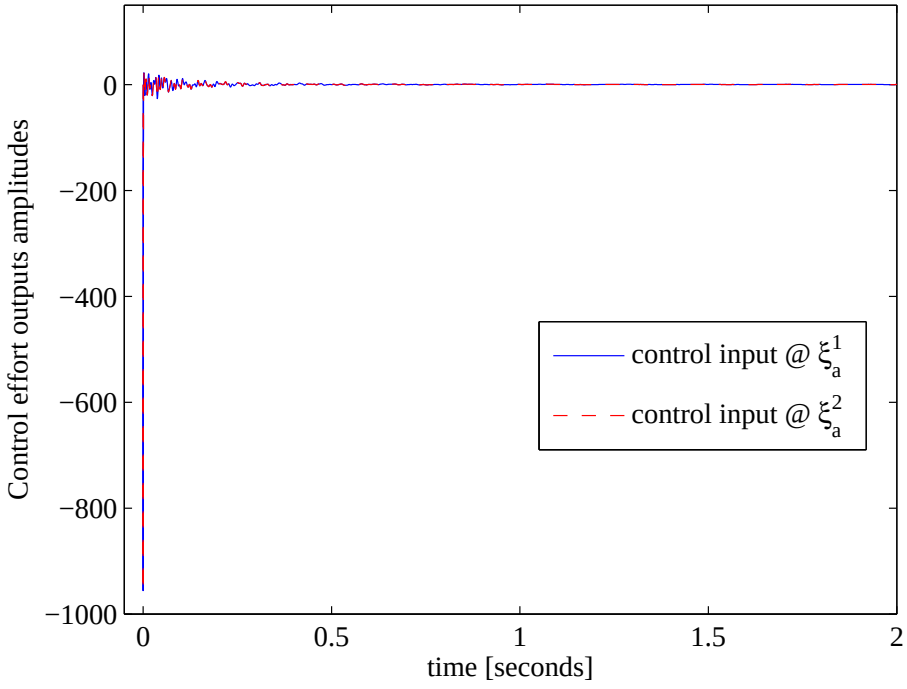

(b) FEM

Figure 6.16. Control effort impulse response of the beam with actuators at final locations $[\xi_a^1 = 0.35L, \xi_a^1 = 0.35L]$

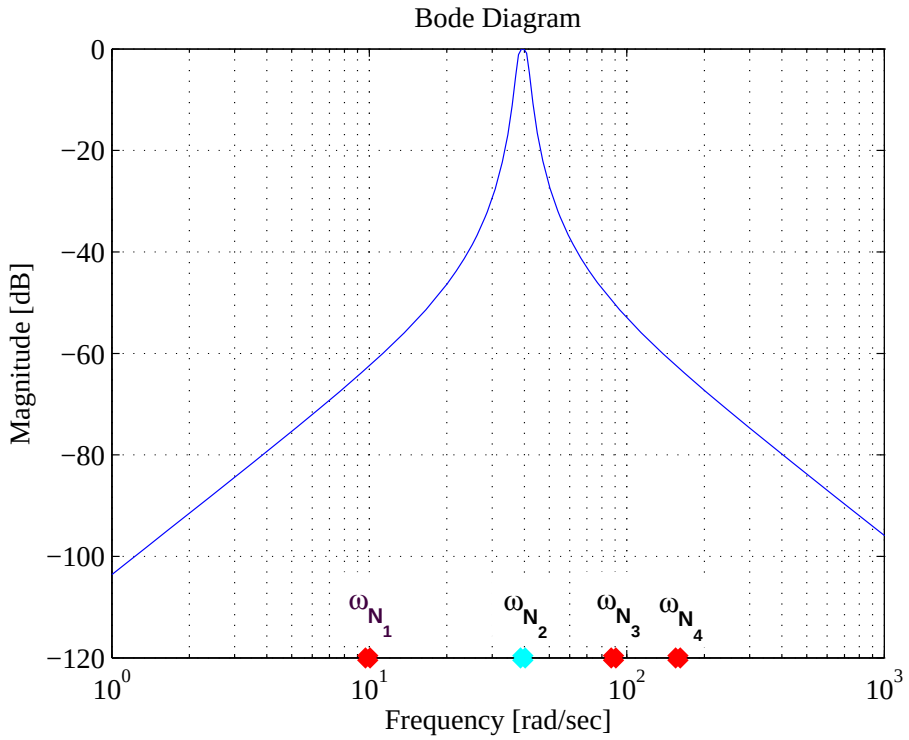

Figure 6.17. The disturbance input filter (ω_{N_i}'s are the natural frequencies of the beam)

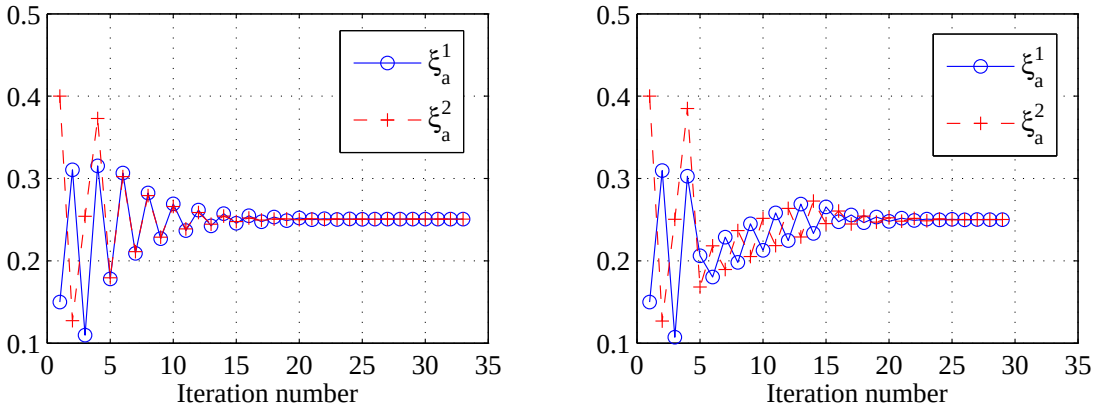

(a) Continuous (b) FEM

Figure 6.18. The actuator/sensor locations with the bandpass filter

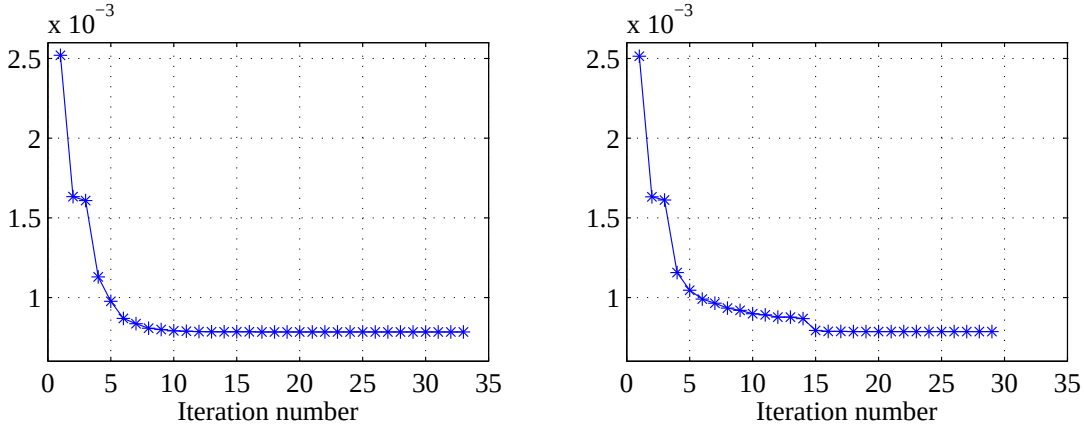

(a) Continuous (b) FEM

Figure 6.19. Iterations and the minimized $\mathcal{H}_2^2$ with the bandpass filter

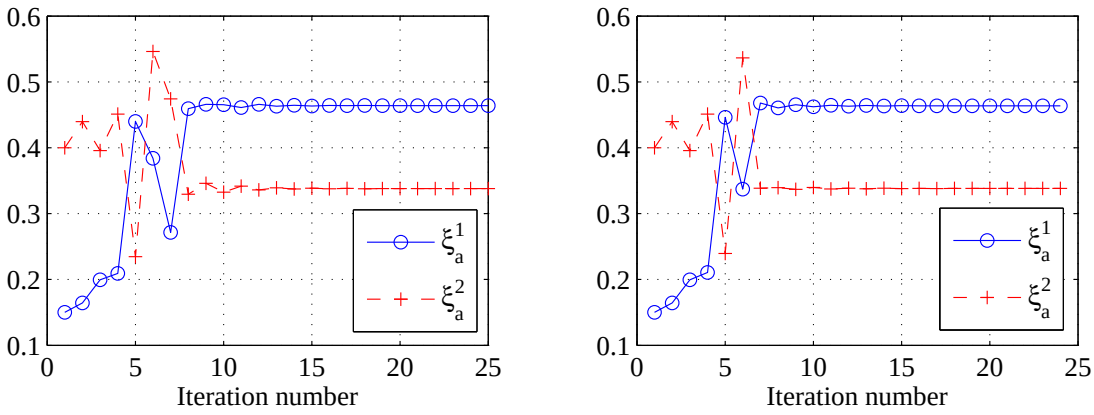

(a) Continuous (b) FEM

Figure 6.20. The actuator/sensor locations (case one)

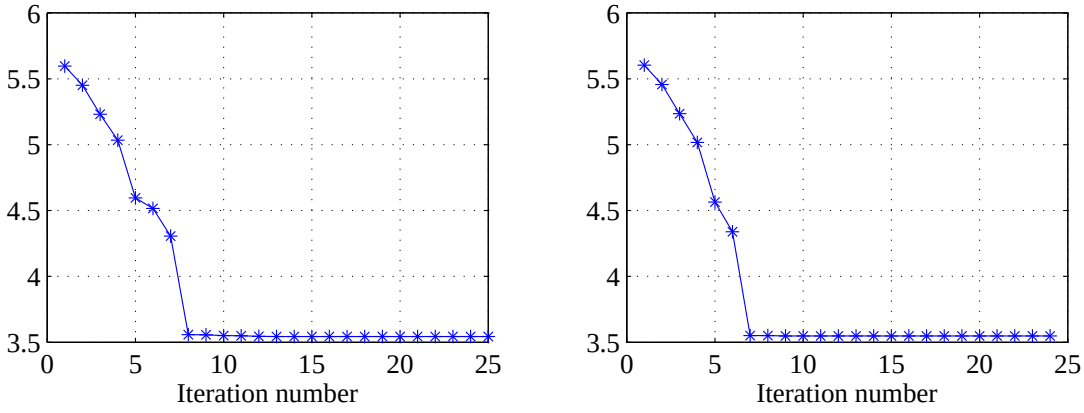

(a) Continuous (b) FEM

Figure 6.21. Iterations and the minimized $\mathcal{H}_2^2$ (case one)

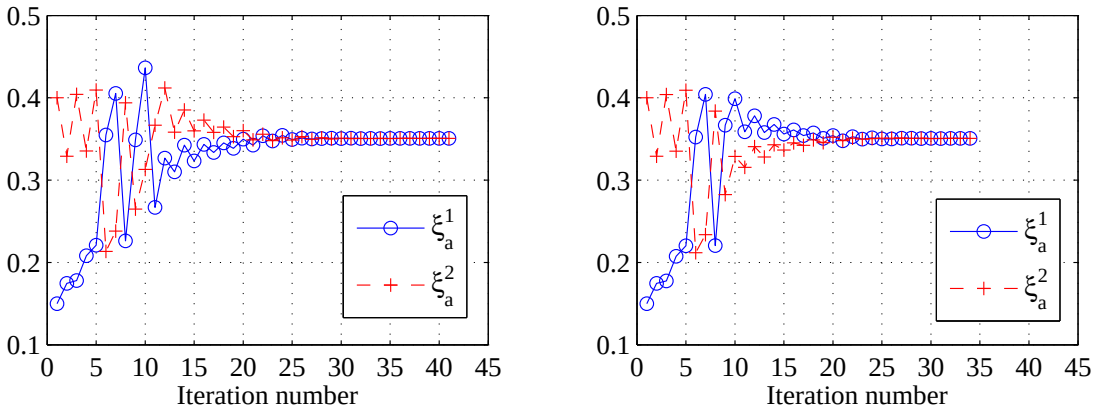

(a) Continuous (b) FEM

Figure 6.22. The actuator/sensor locations (case two)

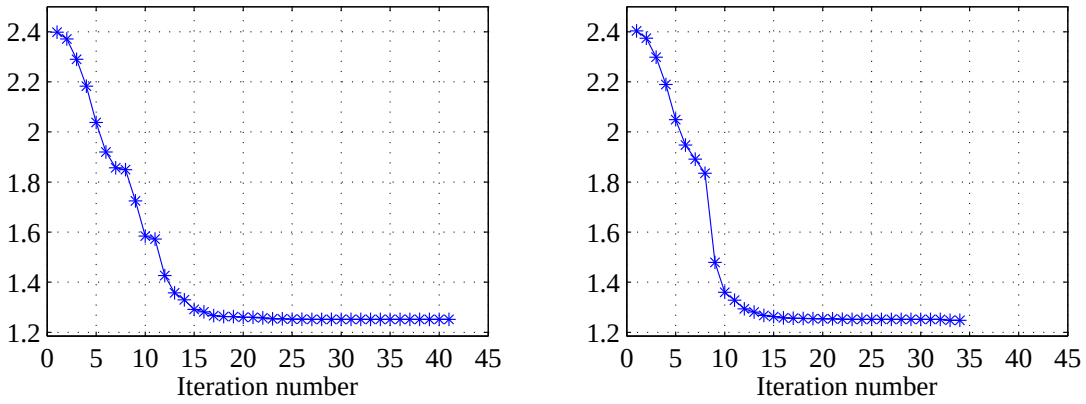

(a) Continuous (b) FEM

Figure 6.23. Iterations and the minimized $\mathcal{H}_2^2$ (case two)

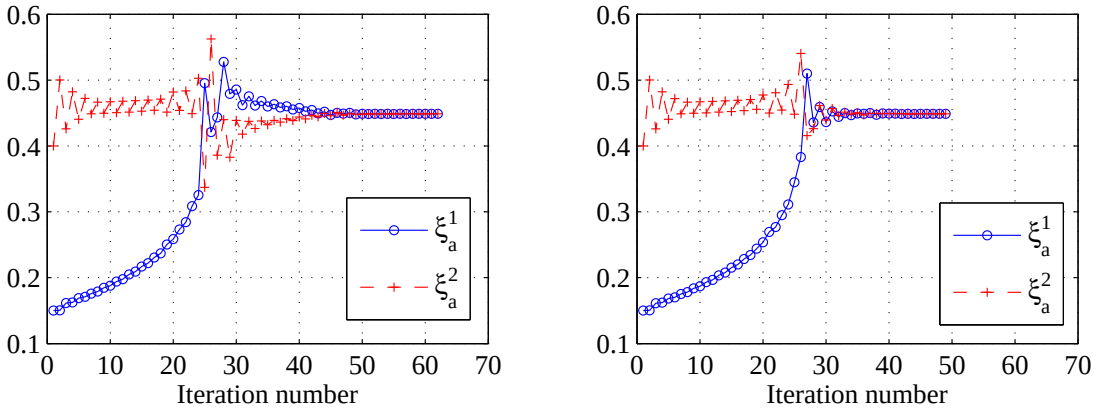

(a) Continuous (b) FEM

Figure 6.24. The actuator/sensor locations (case three)

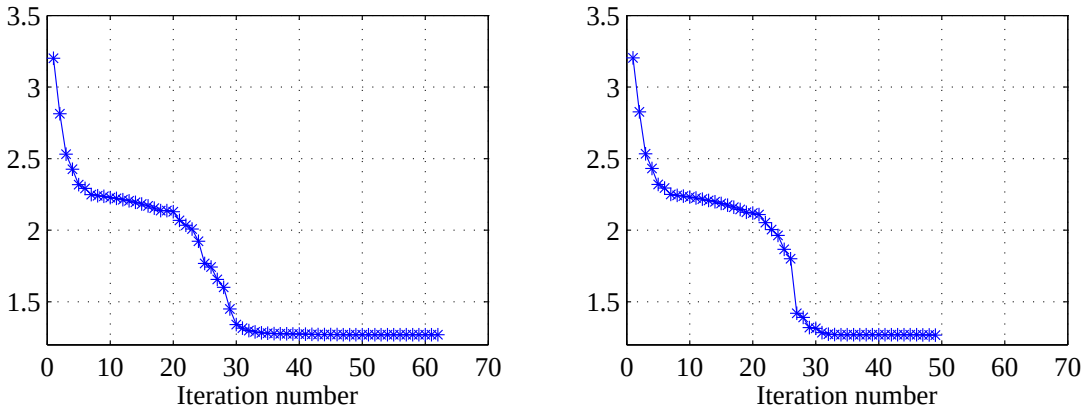

(a) Continuous (b) FEM

Figure 6.25. Iterations and the minimized $\mathcal{H}_2^2$ (case three)

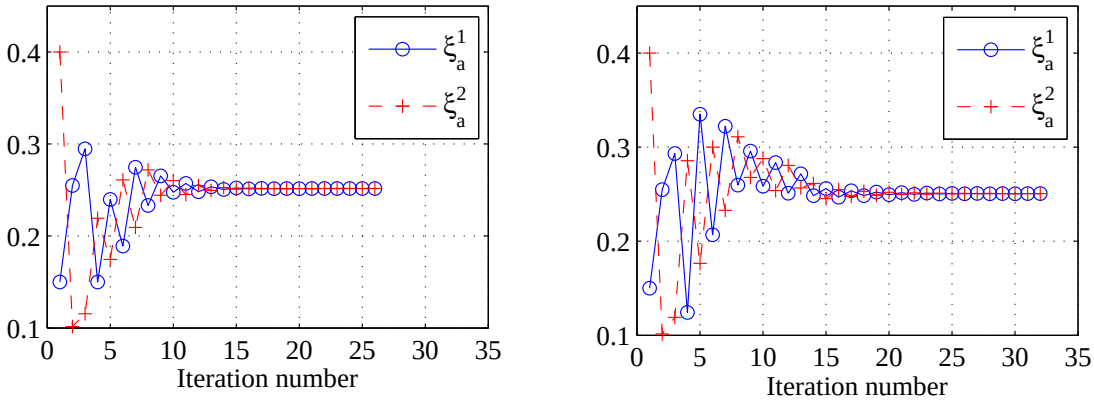

(a) Continuous (b) FEM

Figure 6.26. The actuator/sensor locations (case four)

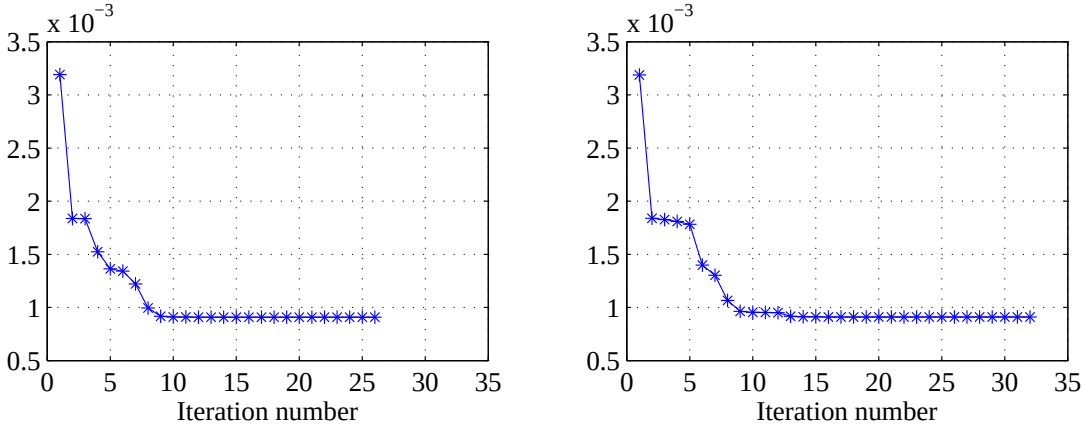

(a) Continuous (b) FEM

Figure 6.27. The actuator/sensor locations (case four)

6.2. Plate Design Example with Point Actuator/Sensor Pair

Another example is a simply supported rectangular plate which is exposed to a single point disturbance located at $\xi_w^x = 0.5L_1$ and $\xi_w^y = 0.8L_2$. The lengths in the x- and y-directions are $L_1 = 2.4\,\mathrm{m}$ and $L_2 = 2.4\,\mathrm{m}$, respectively. The thickness z is $0.005\,\mathrm{m}$. The Young modulus E, the density ρ and the poisson ratio ν are $21 \times 10^{10}\,\mathrm{Pa}$, $7800\,\mathrm{kg\,m^{-3}}$ and 0.3, respectively.

The initial guess for the actuator and sensor location is $\xi_a^x = 0.25L_1$, $\xi_a^y = 0.65L_2$. The parameters required for the controller design step are $\alpha = 10^5$, $\beta = 2$. The performance outputs are described by the vector $\mathbf{z} = [\psi(\xi_a^x, \xi_a^x), \psi(\xi_w^x, \xi_w^x), \mathbf{u}]^{\mathrm{T}}$.

The plate is initially divided into 7×7 finite elements. After the boundary conditions are applied, a system with several hundreds of DOFs results. First 50 modes are taken, and each mode is assumed to have the same damping $\zeta = 0.001$. The signal weightings that are used for the plate are given in Table 6.7.

Table 6.7. Signal weightings for plates with point actuators/sensors

Disturbance Weight	W_{dist}	$\dfrac{10}{0.03s+1}$
Sensor Noise Weight	W_{sn}	$\dfrac{1}{10^5}$
Performance Output Weight	W_{er}	10^5
Control Input Weight	W_{in}	$\dfrac{1}{25}$

Figures 6.28 and 6.29 show the optimal locations (i.e., the coordinates of the point actuator and sensor pair in the x- and y-directions) and the minimized objective function, which is the square of the closed-loop $\mathcal{H}_2$-norm, respectively.

To interpret the results, Figures 6.30 and 6.31 are plotted, which are surface and contour plots, respectively. In those figures, the two axis are the x- and y-coordinates of the point actuator and sensor pairs.

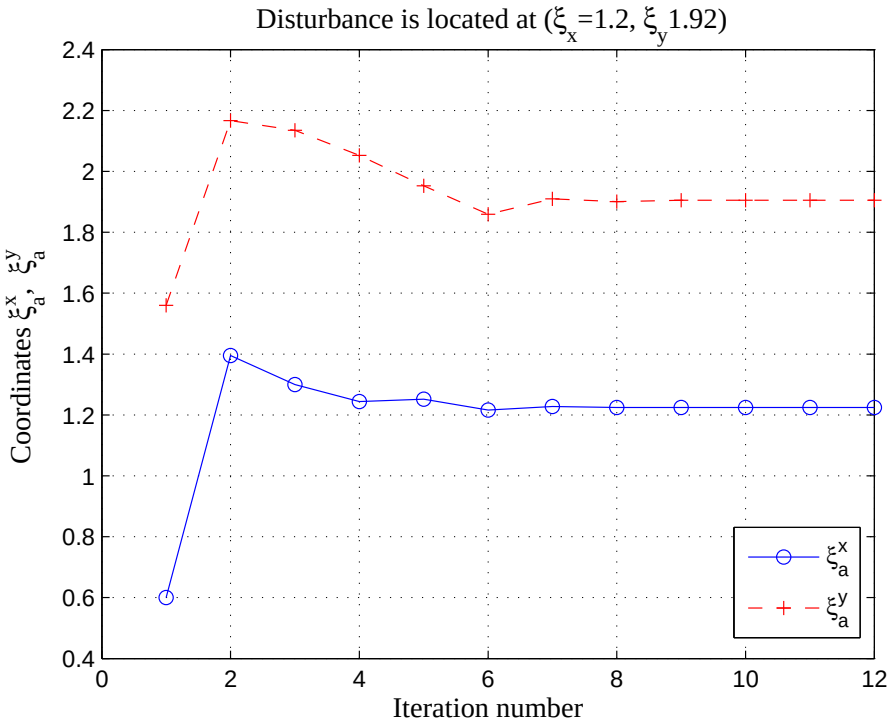

Figure 6.28. Collocated point actuator/sensor locations of a rectangular plate

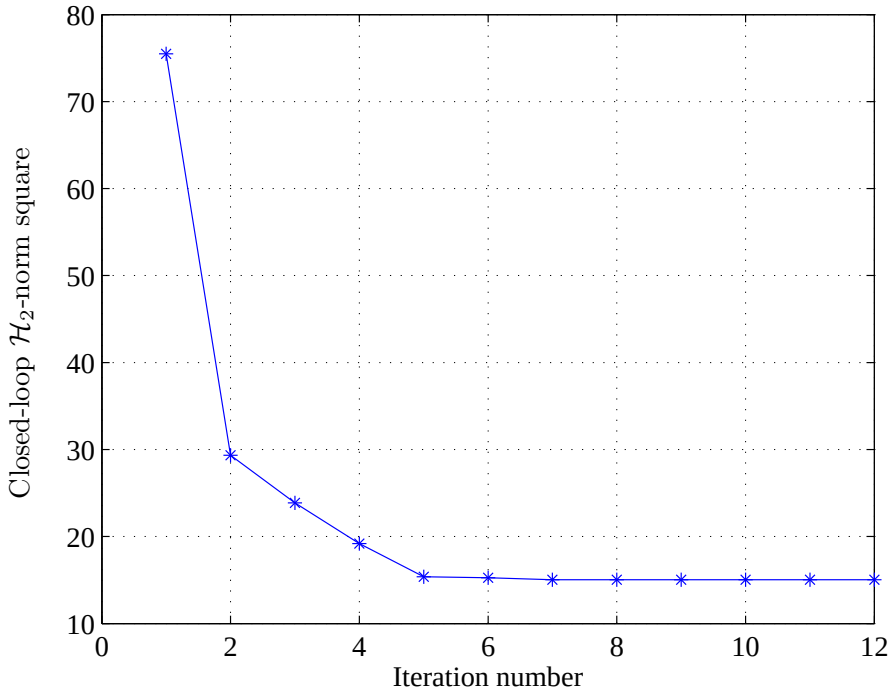

Figure 6.29. The minimized $J = \mathcal{H}_2^2$ values at each iteration

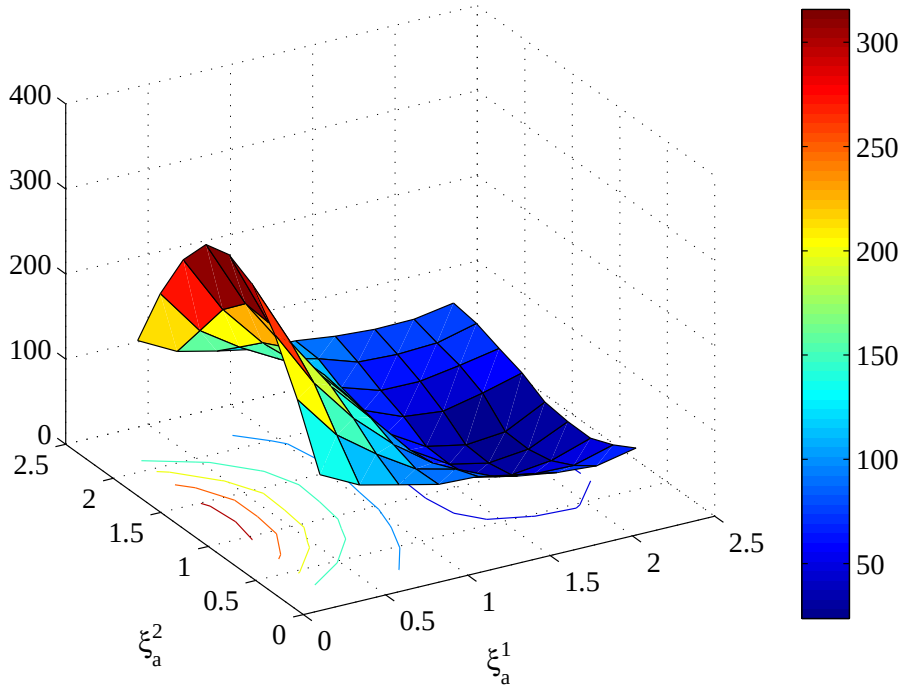

Figure 6.30. The minimized $J = \mathcal{H}_2^2$ versus actuator locations (surface plot)

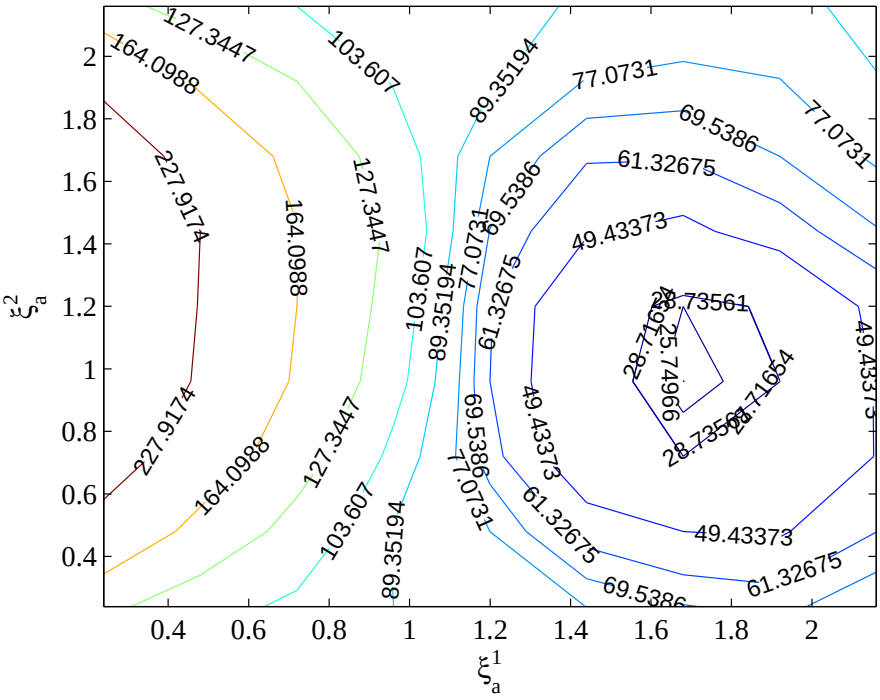

Figure 6.31. The minimized $J = \mathcal{H}_2^2$ versus actuator locations (contour plot)

6.3. Beam with Piezoelectric Actuator/Sensor Pairs

A simply supported beam is exposed to a single disturbance located at $\xi_w = 0.35\,L$. Its length L is 1 m. It is divided into 10 finite elements initially, and the piezoelectric actuator/sensor pairs are about 0.1 m long. The Young modulus E, the density ρ, the thickness and the width of the beam are 7×10^{10} Pa, 7850 kg m^{-3}, 0.010 m and 0.005 m, respectively.

The piezoelectric actuator and sensors pairs have a thickness of 0.002 m and posses the following material properties: $E = 6.3 \times 10^9$ Pa, $\rho = 7500$ kg m^{-3}, $e_{31} = -12$, $\epsilon_{33} = 0.7$. As design parameter $\alpha = 10^4$ and $\beta = 2$ are chosen.

Figures 6.32 and 6.33 show the optimal locations (i.e., the x-coordinates of the two actuator and sensor pairs) and the minimized objective function, which is the square of the closed-loop $\mathcal{H}_2$-norm, respectively.

Figures 6.30 and 6.31 are surface and contour plots, respectively, at which the two axes describe the coordinates of the two actuator and sensor pairs.

Table 6.8. Signal weightings for beams with PZT pairs

Disturbance Weight	W_{dist}	$\dfrac{10}{0.03s+1}$
Sensor Noise Weight	W_{sn}	$\dfrac{1}{10^5}$
Performance Output Weight	W_{er}	10^3
Control Input Weight	W_{in}	$\dfrac{1}{25}$

As the signal weightings, the values in Table 6.8 are selected. The optimal locations obtained using these signal weigthings are given in Figures 6.36 and 6.37.

If one compares Figure 6.32 with Figure 6.36 and Figure 6.33 with Figure 6.37, the effects of the signal weigthings are to be seen. The values of the minimized objective functions are different, and the obtained optimal locations are not the same.

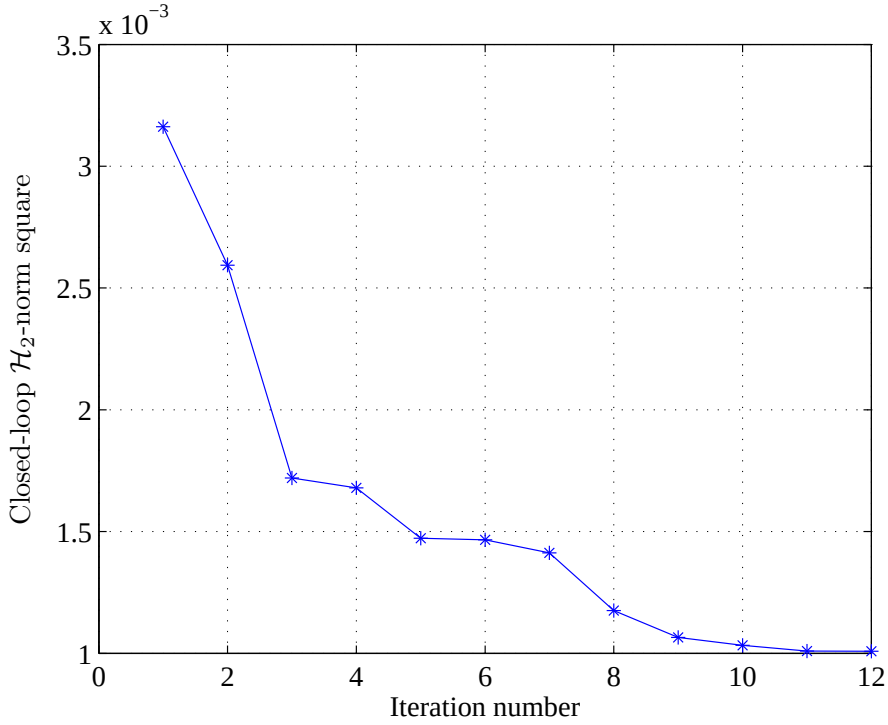

Figure 6.32. Square of the closed-loop $\mathcal{H}_2$-norm of the beam vs iterations

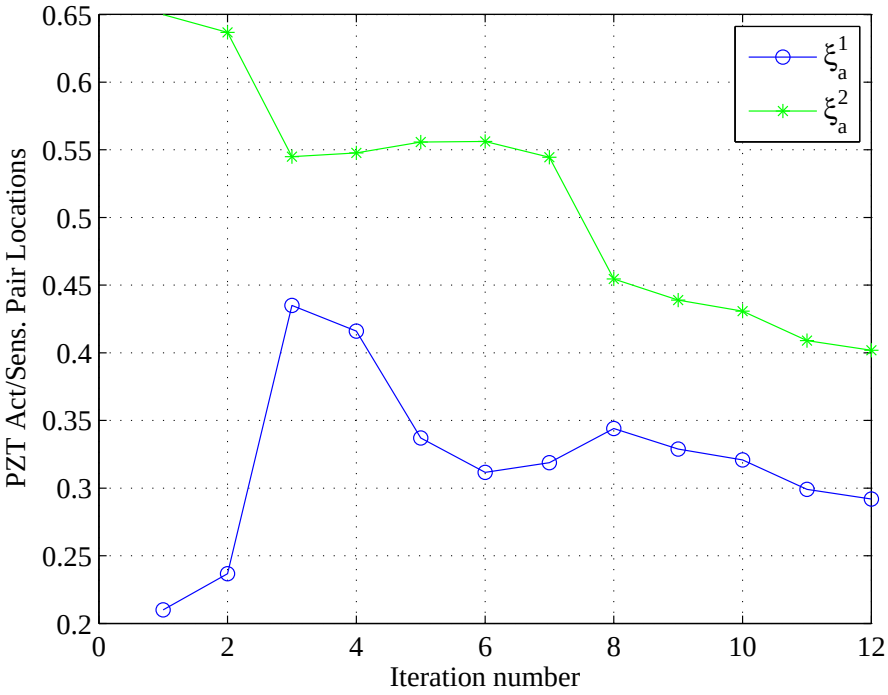

Figure 6.33. Collocated PZT actuator/sensor locations of a simply supported beam vs iterations

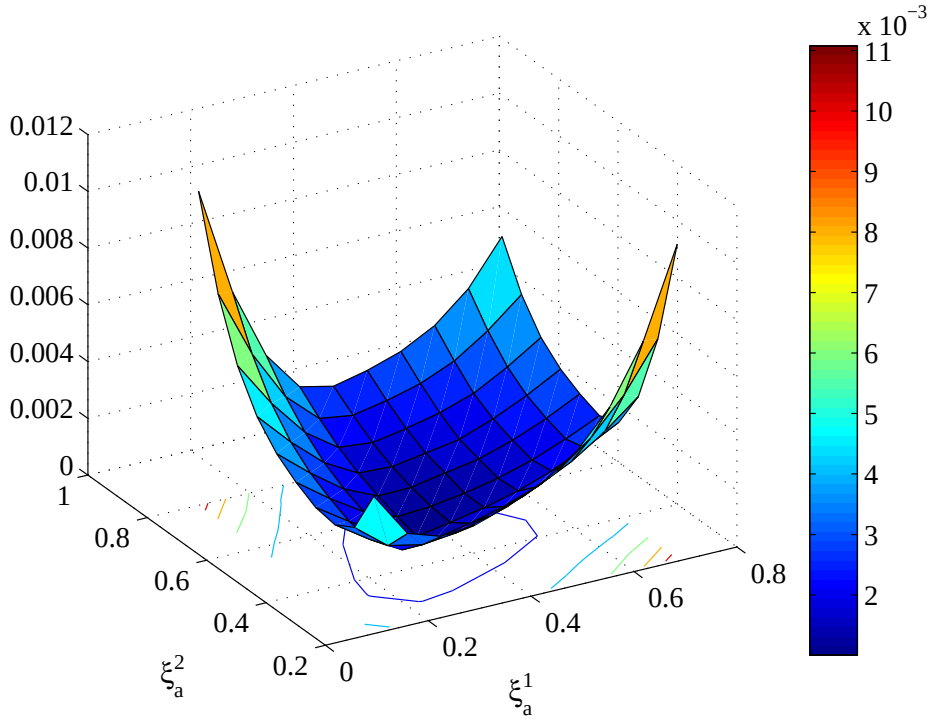

Figure 6.34. The minimized $J = \mathcal{H}_2^2$ versus PZT actuator locations (surface plot)

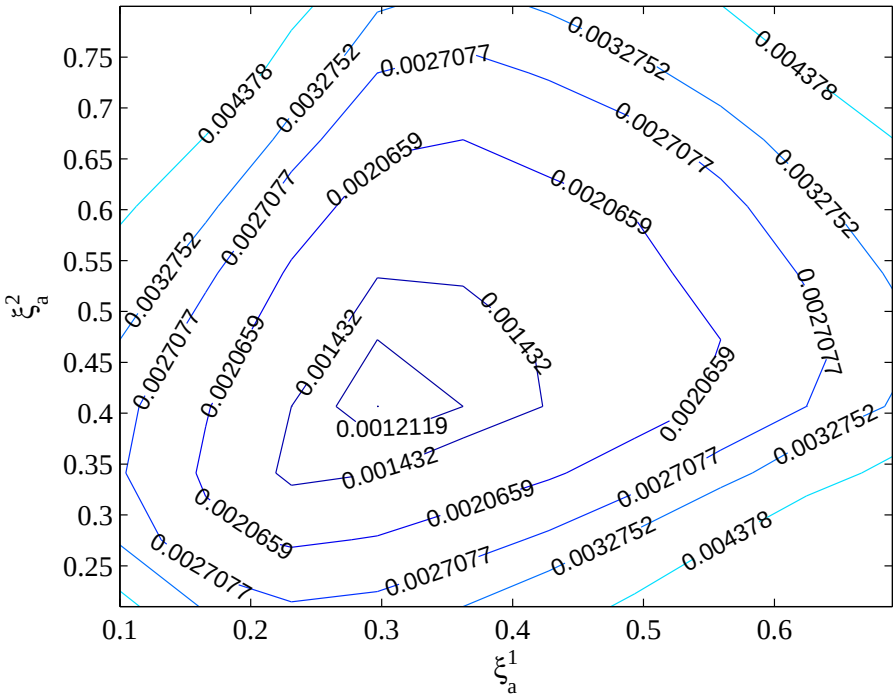

Figure 6.35. The minimized $J = \mathcal{H}_2^2$ versus PZT actuator locations (contour plot)

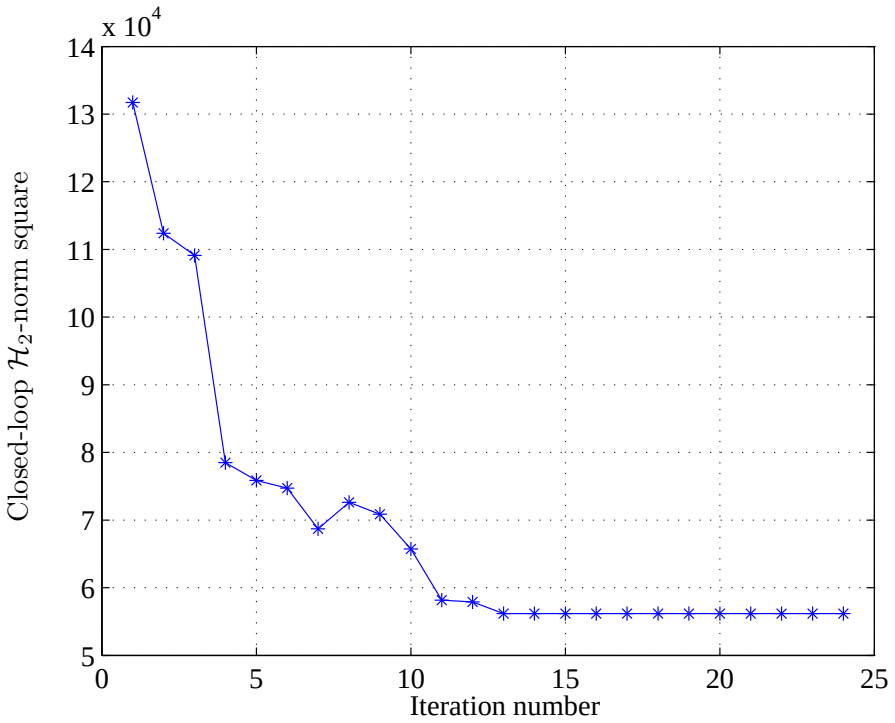

Figure 6.36. Square of the closed-loop $\mathcal{H}_2$-norm of the beam vs iterations (with signal weights)

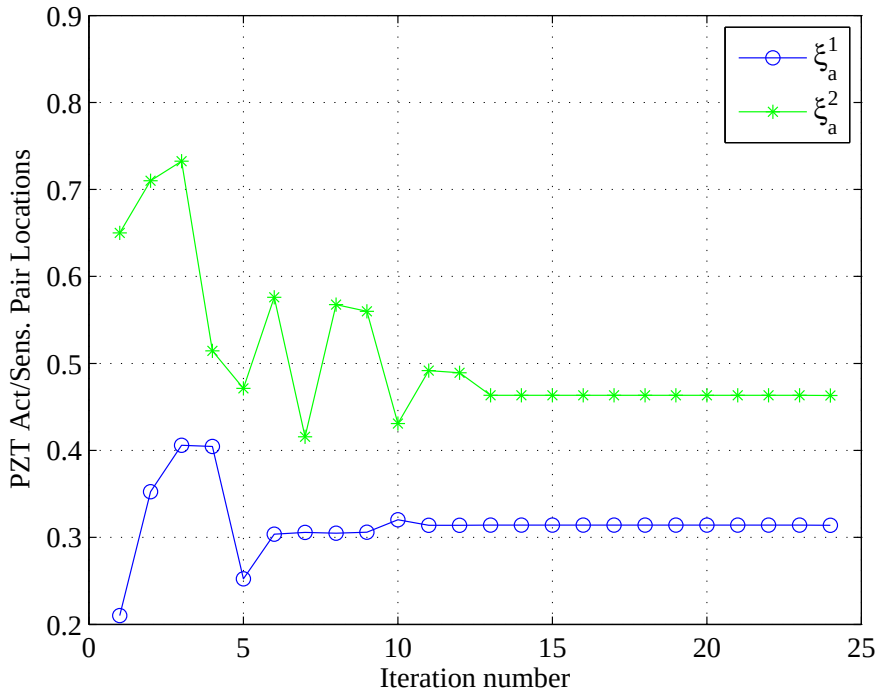

Figure 6.37. Collocated PZT actuator/Sensor locations of a simply supported beam vs iterations (with signal weights)

6.4. Plate with a Single PZT Pair

To further illustrate the optimization methods, consider a simply supported plate combined with a single collocated piezoelectric actuator and sensor pair. The material properties and dimensions of both the plate and its piezoelectric patch are given in Tables 6.9 and 6.10.

Table 6.9. Material properties and the dimensions of the plate

Dimensions	
Length in x-direction	2.4 m
Length in y-direction	2.4 m
Thickness	5 mm
Material properties	
Young modulus	$21 \times 10^{10}\,\mathrm{N\,m^{-2}}$
Density	$7800\,\mathrm{kg\,m^{-3}}$
Poisson ratio	0.3

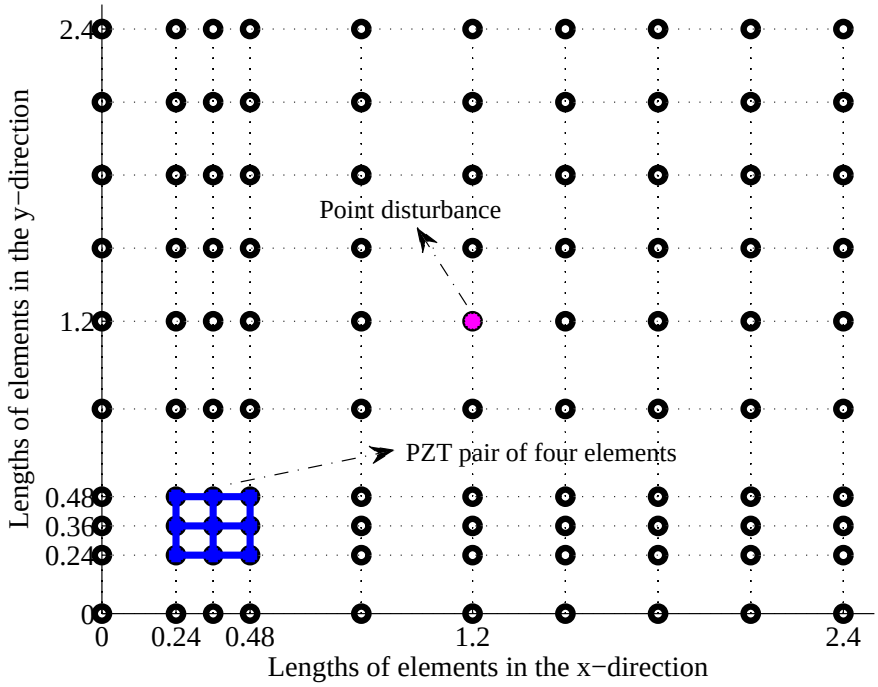

Figure 6.38. Dimensions of the plate with PZT actuator and sensor pair

Table 6.10. Material properties and the dimensions of the PZT patches

Dimensions	
$2a$ (length in x-direction)	$0.24\,\mathrm{m}$
$2b$ (length in y-direction)	$0.24\,\mathrm{m}$
Thickness	$3\,\mathrm{mm}$
Material properties	
Young modulus	$9 \times 10^{10}\,\mathrm{N\,m^{-2}}$
Density	$7500\,\mathrm{kg\,m^{-3}}$
e_{31}	-5.2
e_{32}	5.2
c_{11}	$1.4 \times 10^{11}\,\mathrm{N\,m^{-2}}$
c_{12}	$7.8 \times 10^{10}\,\mathrm{N\,m^{-2}}$
c_{22}	$1.4 \times 10^{11}\,\mathrm{N\,m^{-2}}$
c_{66}	$3.9 \times 10^{9}\,\mathrm{N\,m^{-2}}$
ϵ_{11}	0.7
ϵ_{22}	0.6
ϵ_{33}	0.75

The plate model is restricted to consist of minimum six finite elements in both directions. That is, the length of any element in x-direction may not be larger than $\frac{2.4}{6}$ m. The same argument is valid also for the y-direction. Another restriction is made about the number of the PZT elements. At each iteration, PZT patch should consist of $2 \times 2 = 4$ elements as shown in Figure 6.38. The modal damping for both piezoelectric and plate material is taken as 0.001. Since the physical plant is given in modal state space description, first 10 modes are considered. The plate is simply supported at the line $\xi^x = 0\,\mathrm{m}$ and $\xi^x = 2.4\,\mathrm{m}$.

For the controller design or MNRD calculations the frequency weights in Table 6.11 are used. The single disturbance is located at the point $\xi_w^x = 0.5\,L$, $\xi_w^y = 0.5\,L$, and the initial places of the actuators are $\xi_a^x = 0.25\,L$, $\xi_a^y = 0.25\,L$, where $L = 2.4\,\mathrm{m}$. The performance outputs are described by the vector $\mathbf{z} = [\psi(\xi_a^x, \xi_a^y),\ \psi(\xi_w^x, \xi_w^y),\ \mathbf{u}]^{\mathrm{T}}$.

Table 6.11. Signal weightings for plates with PZT patches

Disturbance Weight	W_{dist}	$\frac{10}{0.02s+1}$
Sensor Noise Weight	W_{sn}	$\frac{1}{10^5}$
Performance Output Weight	W_{er}	10
Control Input Weight	W_{in}	$\frac{1}{25}$

The bound constraints for the example are given as

$$\begin{aligned} g_1^b(\boldsymbol{x}) &= -\xi_a^x + 0.01\,L < 0, \\ g_2^b(\boldsymbol{x}) &= +\xi_a^x + 0.89\,L < 0, \\ g_3^b(\boldsymbol{x}) &= -\xi_a^y + 0.01\,L < 0, \\ g_4^b(\boldsymbol{x}) &= +\xi_a^y + 0.89\,L < 0, \end{aligned}$$

where $\mathbf{x} = [\xi_a^x, \xi_a^y]^{\mathrm{T}}$, $g_1^b(\boldsymbol{x})$ and $g_3^b(\boldsymbol{x})$ are lower bounds on ξ_a^x and ξ_a^y, respectively. The constraints $g_2^b(\boldsymbol{x})$ and $g_4^b(\boldsymbol{x})$ are upper bounds on ξ_a^x and ξ_a^y, respectively. In addition to the upper and lower limits, conditional constraints of the first type, which are described in Section 3.4, are used. These constraints prevent the disturbance to act at a point, which is too close to a side or corner of an element. They are

$$\begin{aligned} g_1^d(\boldsymbol{x}) &= \xi_a^x - \xi_w^x + \frac{2a}{3} < 0, \\ g_2^d(\boldsymbol{x}) &= -\xi_a^x + \xi_w^x - \frac{2a}{3} < 0, \\ g_3^d(\boldsymbol{x}) &= \xi_a^x - \xi_w^x + \frac{2a}{3} + 2a < 0, \\ g_4^d(\boldsymbol{x}) &= -\xi_a^x + \xi_w^x + \frac{2a}{3} < 0, \\ g_5^d(\boldsymbol{x}) &= \xi_a^y - \xi_w^y + \frac{2b}{3} < 0, \\ g_6^d(\boldsymbol{x}) &= -\xi_a^y + \xi_w^y - \frac{2b}{3} < 0, \\ g_7^d(\boldsymbol{x}) &= \xi_a^y - \xi_w^y + \frac{2b}{3} + 2b < 0, \\ g_8^d(\boldsymbol{x}) &= -\xi_a^y + \xi_w^y + \frac{2b}{3} < 0. \end{aligned}$$

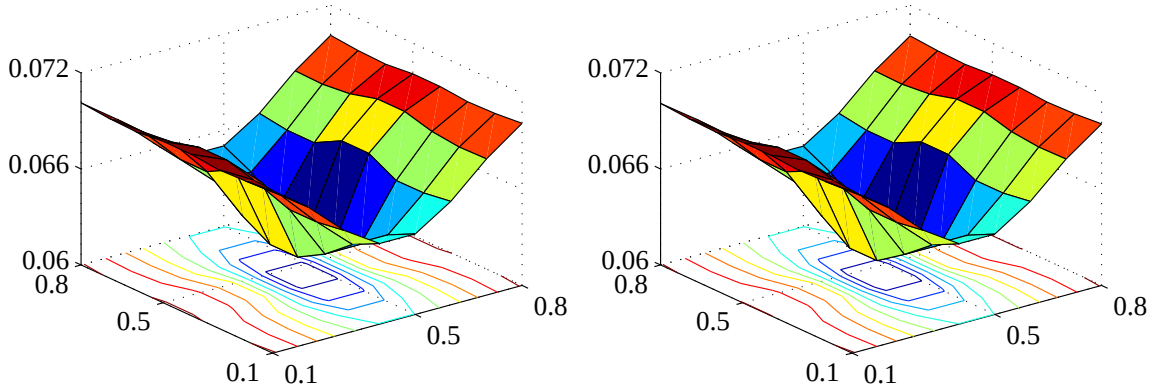

(a) with improved coprime controller (b) with low-authority $\mathcal{H}_\infty$-controller

Figure 6.39. Closed-loop $\mathcal{H}_2$-norm

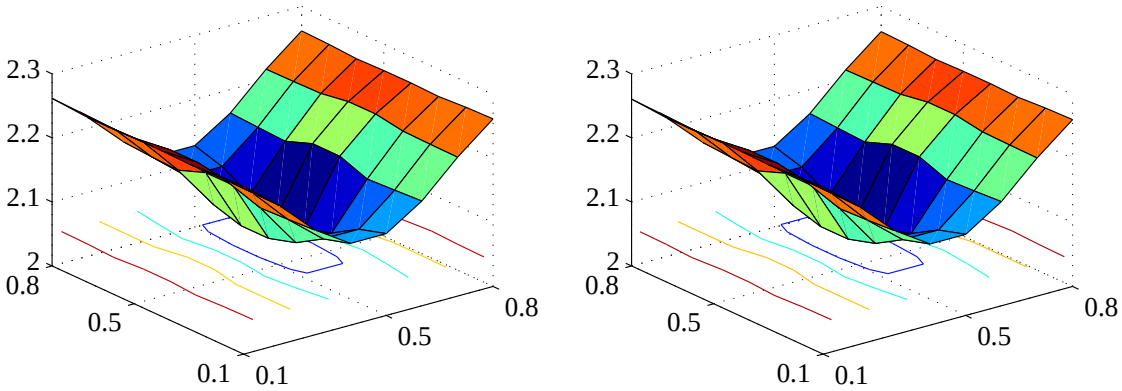

(a) with bisection (b) by frequency-domain calculation

Figure 6.40. Closed-loop $\mathcal{H}_\infty$-norm with low-authority $\mathcal{H}_\infty$-controller

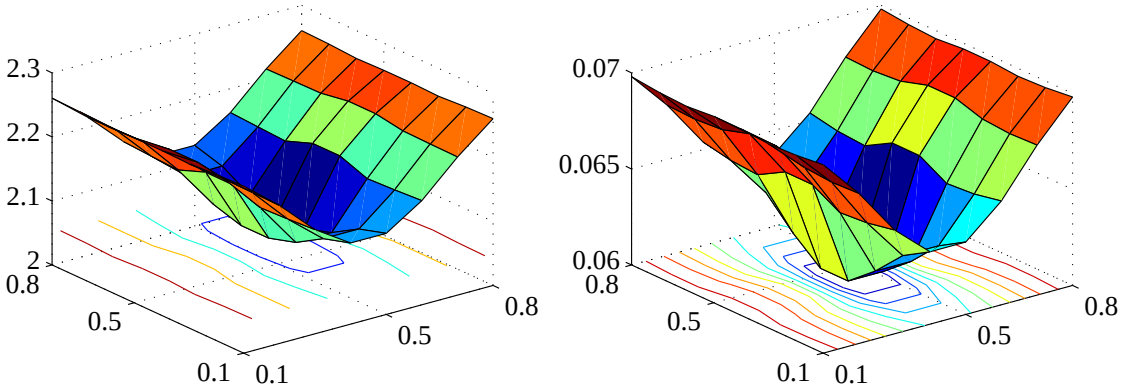

(a) Optimistic $\mathcal{H}_\infty$-norm (b) Optimistic $\mathcal{H}_2$-norm

Figure 6.41. Minimizing the optimistic norms

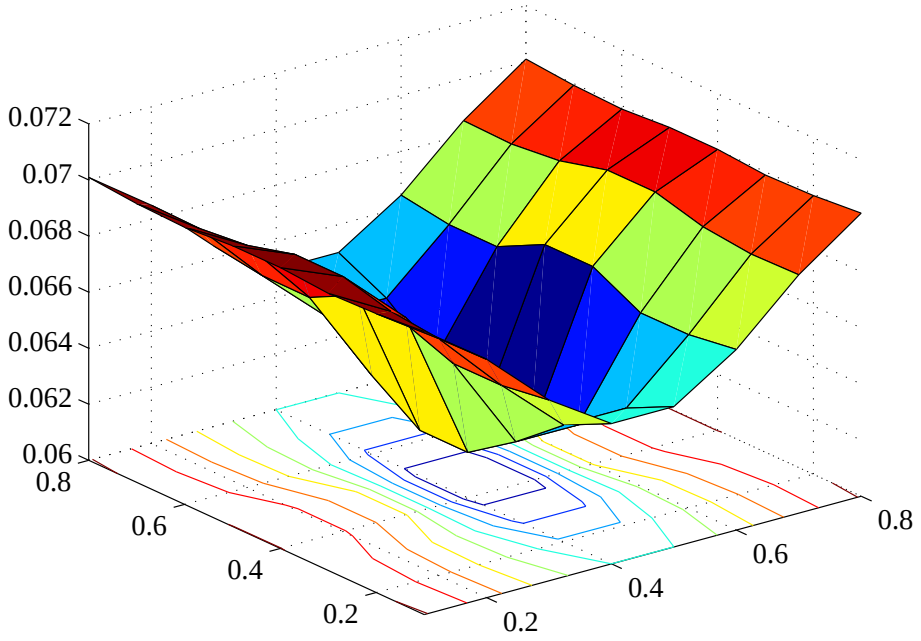

Figure 6.42. Closed-loop $\mathcal{H}_2$-norm with $\mathcal{H}_\infty$-controller (calculated by MATLAB)

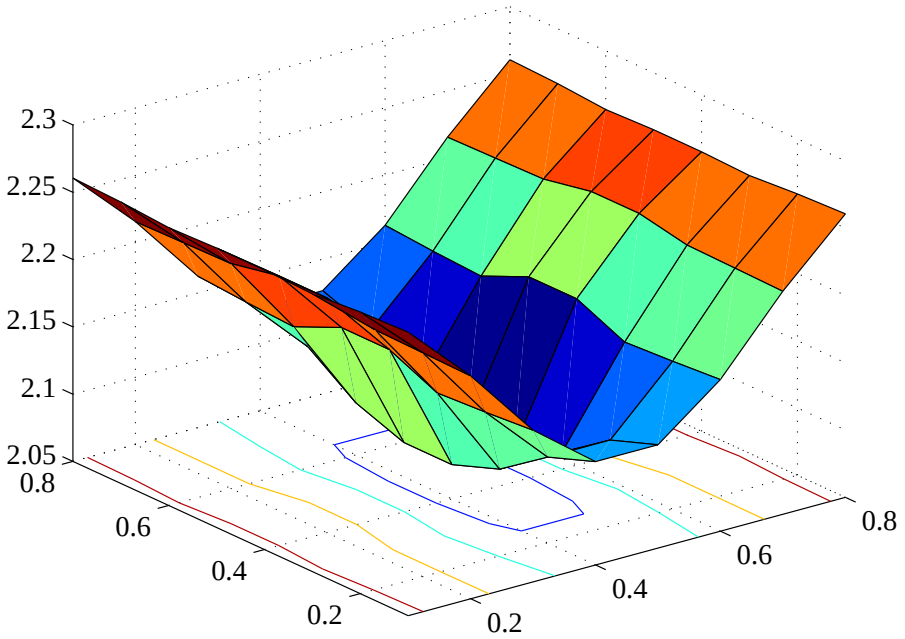

Figure 6.43. Closed-loop $\mathcal{H}_\infty$-norm with $\mathcal{H}_\infty$-controller (calculated by MATLAB)

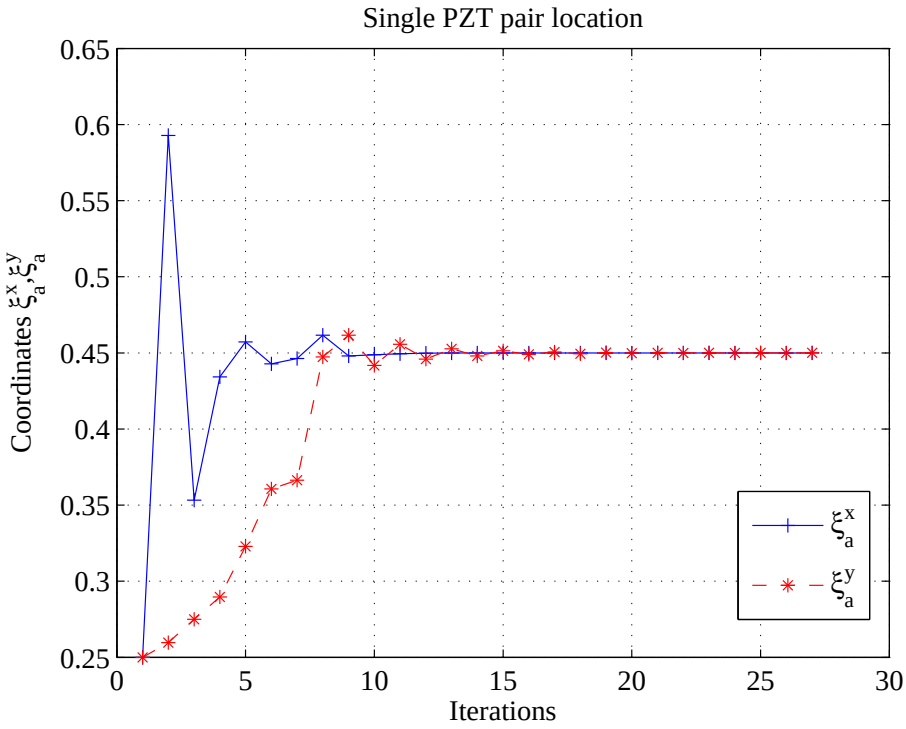

Figure 6.44. Iterations and optimal PZT pair locations with improved coprime controller

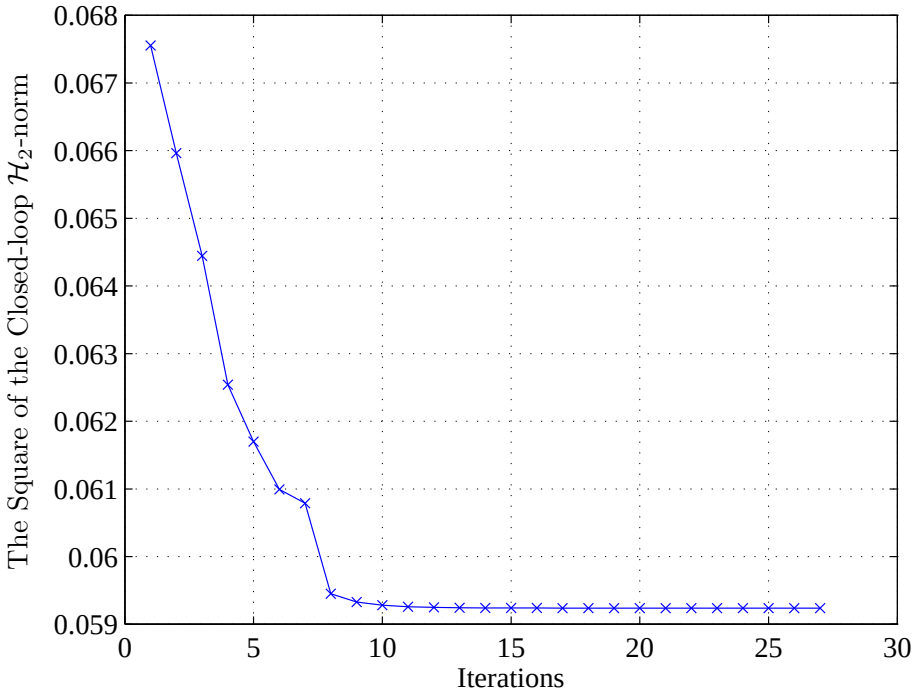

Figure 6.45. The Square of the closed-loop $\mathcal{H}_2$-norm with improved coprime controller

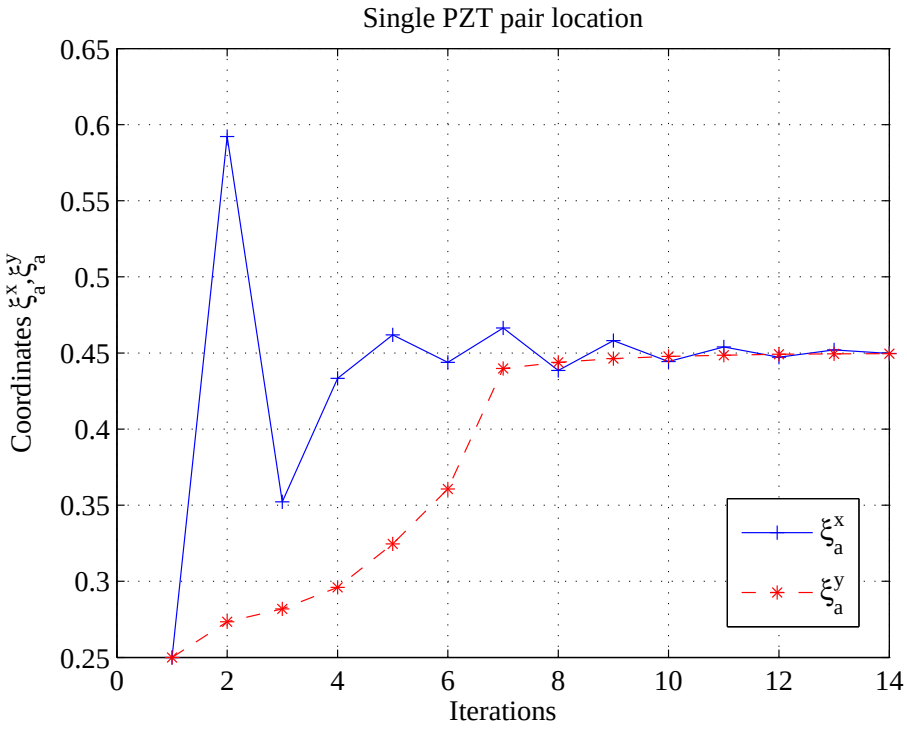

Figure 6.46. Iterations and optimal PZT pair locations with low-authority $\mathcal{H}_\infty$-controller, J=$\mathcal{H}_2^2$-norm

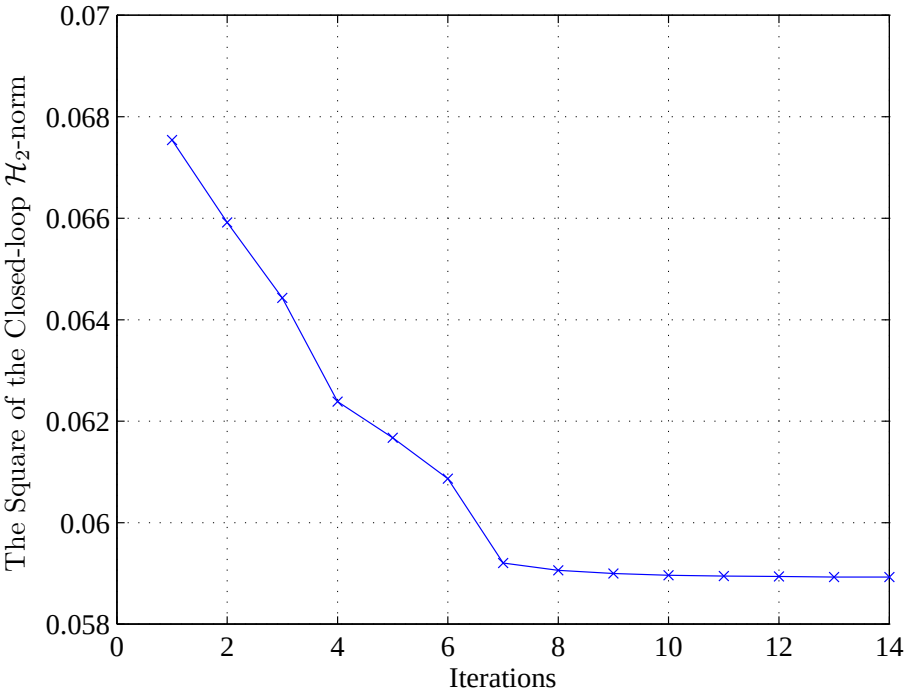

Figure 6.47. The square of the closed-loop $\mathcal{H}_2$-norm with low-authority $\mathcal{H}_\infty$-controller

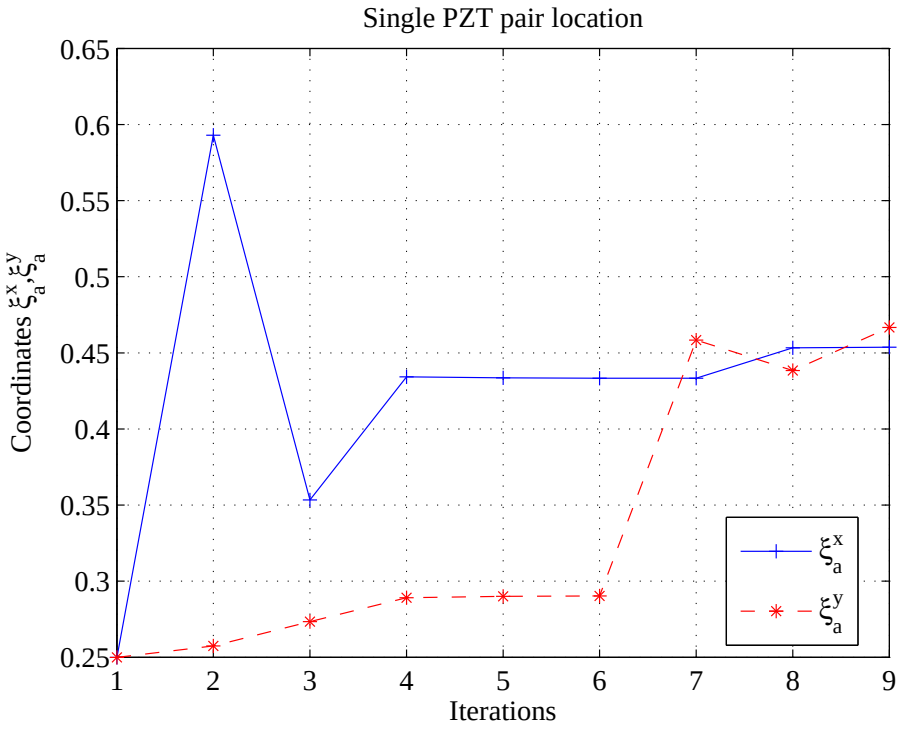

(a) Optimal PZT pair locations

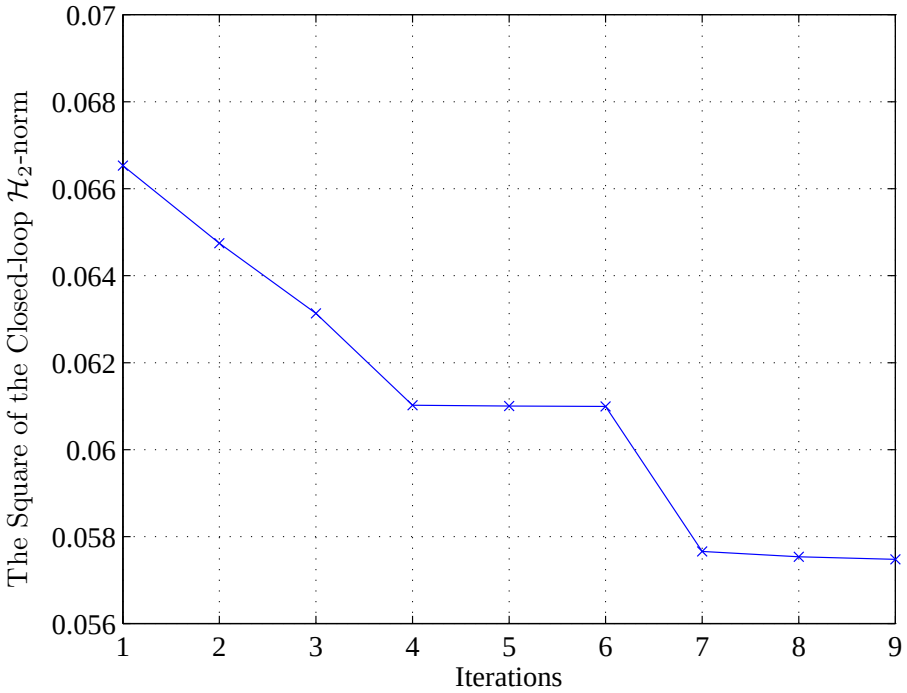

(b) The square of the closed-loop $\mathcal{H}_2$-norm

Figure 6.48. Optimization with optimistic $\mathcal{H}_2$-norm

6.5. Plate with Double PZT Pairs

Another piezoelectric actuator and sensor pair is added to the simply supported plate, which is shown in Figure 6.38. The dimensions and material properties of the plate and the piezoelectric patches are given as in Tables 6.9 and 6.10. As filters, the signal weightings in Table 6.11 are used.

The bound constraints for this example with two pair of actuators and sensors are given as

$$\begin{aligned}
g_1^b(\boldsymbol{x}) &= -\xi_{a_1}^x + 0.01\,L < 0,\\
g_2^b(\boldsymbol{x}) &= +\xi_{a_1}^x + 0.89\,L < 0,\\
g_3^b(\boldsymbol{x}) &= -\xi_{a_1}^y + 0.01\,L < 0,\\
g_4^b(\boldsymbol{x}) &= +\xi_{a_1}^y + 0.89\,L < 0,\\
g_5^b(\boldsymbol{x}) &= -\xi_{a_2}^x + 0.01\,L < 0,\\
g_6^b(\boldsymbol{x}) &= +\xi_{a_2}^x + 0.89\,L < 0,\\
g_7^b(\boldsymbol{x}) &= -\xi_{a_2}^y + 0.01\,L < 0,\\
g_8^b(\boldsymbol{x}) &= +\xi_{a_1}^y + 0.89\,L < 0,
\end{aligned}$$

where $\mathbf{x} = \left[\xi_{a_1}^x, \xi_{a_1}^y, \xi_{a_2}^x, \xi_{a_2}^y\right]^{\mathrm{T}}$ and $g_1^b(\boldsymbol{x})$ and $g_3^b(\boldsymbol{x})$ are lower bounds on $\xi_{a_1}^x$ and $\xi_{a_1}^y$, respectively. The constraints $g_5^b(\boldsymbol{x})$ and $g_7^b(\boldsymbol{x})$ are lower bounds on $\xi_{a_2}^x$ and $\xi_{a_2}^y$, respectively. The constraints $g_2^b(\boldsymbol{x})$ and $g_4^b(\boldsymbol{x})$ are upper bounds on $\xi_{a_1}^x$ and $\xi_{a_1}^y$, respectively. The constraints $g_6^b(\boldsymbol{x})$ and $g_8^b(\boldsymbol{x})$ are upper bounds on $\xi_{a_2}^x$ and $\xi_{a_2}^y$, respectively.

In addition to the upper and lower bounds on optimization variables, the first, second and third types of conditional constraints, which are described in Section 3.4, are applied to this example. The second and third type of conditional constraints are required whenever there are more than one PZT patch.

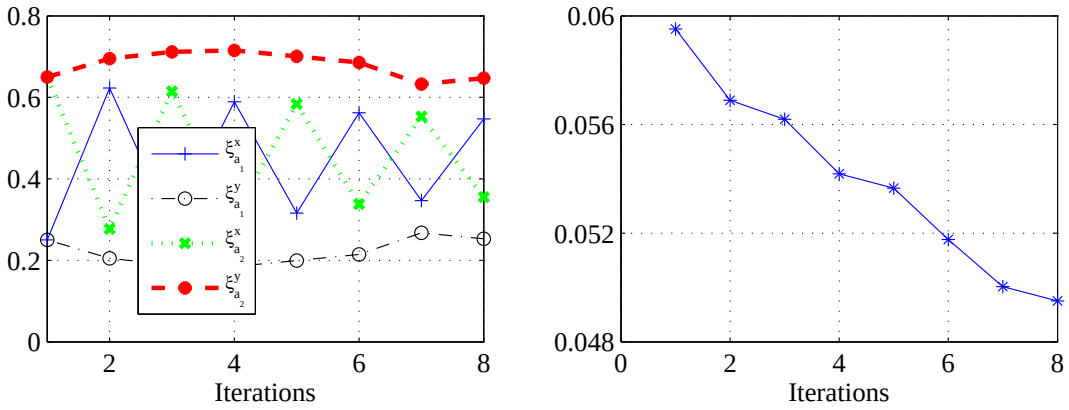

(a) Optimal PZT pair locations (b) The closed-loop $\mathcal{H}_2$-norm square

Figure 6.49. Optimization with improved coprime controller

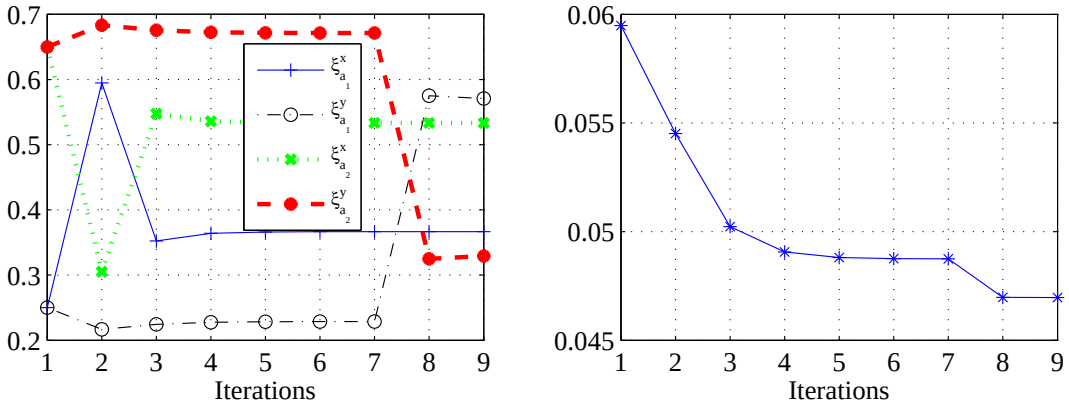

(a) Optimal PZT pair locations (b) The closed-loop $\mathcal{H}_2$-norm square

Figure 6.50. Optimization with low-authority $\mathcal{H}_\infty$-controller, $J = \mathcal{H}_2^2$

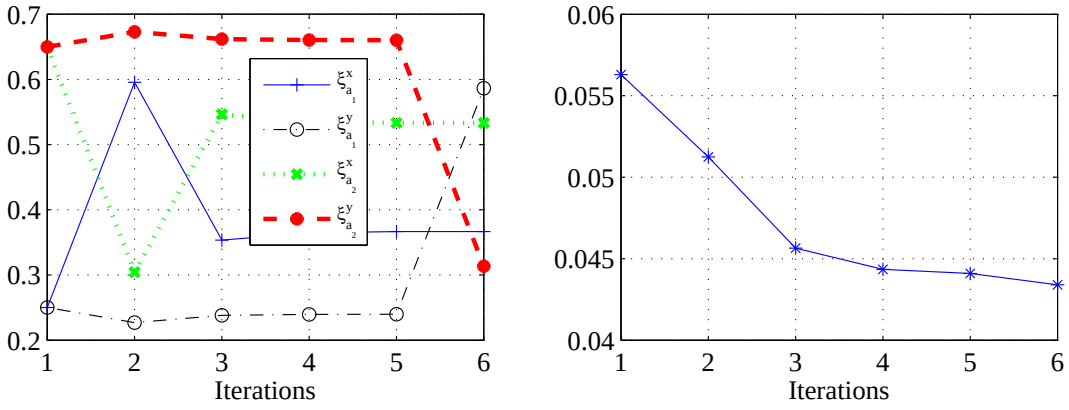

(a) Optimal PZT pair locations (b) The closed-loop $\mathcal{H}_2$-norm square

Figure 6.51. Optimistic $\mathcal{H}_2$-norm (double actuator/sensor case)

7. CONCLUSIONS AND FUTURE WORK

In this thesis, closed-loop optimal location selection methods are developed for actuator and sensor pairs in flexible structures. Either improved coprime controllers or low-authority $\mathcal{H}_\infty$-controllers are used. Therefore, the optimal location selection strategy is said to be closed-loop. Alternatively, MNRD method is utilized for a quasi closed-loop selection criterion. Examples for simply supported beams and plates with point and piezoelectric actuator/sensor pairs are given to demonstrate the effectiveness of the developed approach. The closed-loop $\mathcal{H}_2$-norm is successfully being used as the optimization metric.

Simple diagonally dominant ARE solutions are introduced that reduce the computation time of the optimization pertaining to the design of the controller. Using a coordinate transformation, the state matrix of the generalized plant is block diagonalized so that each mode can be dealt individually. This enables one to assume that the solutions of the generalized algebraic Riccati equations are in the diagonal form. Then, it becomes possible to solve the ARE's in closed form based on quadratic equations.

By resorting to the approach introduced in Hiramoto et al. [1], a coprime $\mathcal{H}_\infty$ controller is designed. However, in contrast to Hiramoto et al. [1], modal dampings are not neglected, and the signal weights are incorporated into ARE solutions. Partial derivatives of the closed-loop system are derived for a gradient based optimization procedure. The derivatives of the closed-loop system include not only the derivatives of the open-loop system, but also the derivatives of the ARE's. Hence, differentiating the ARE's, Lyapunov equations are obtained. Approximate solutions of the Lyapunov equations are calculated in the same fashion as those of the ARE's. When the necessary derivatives are available, the gradient of the optimization metric is obtained, the optimal actuator and sensor locations are found through an unconstrained nonlinear optimization algorithm.

The developed unconstrained optimization technique with improved coprime con-

troller has several advantages over the methods in literature:

- It uses the generalized plant with signal weights.
- The control and filter ARE's and their derivatives are solved approximately by reducing them to simple quadratic equations. In the iterations of the optimal locations selection procedure, solving these quadratic equations consumes less time compared to solving the ARE's fully.
- Hiramoto et al. [1] neglect the damping altogether, whereas the developed technique uses modal dampings.
- The optimization is done using a closed-loop selection criterion. That is, the objective function is the square of the $\mathcal{H}_2$-norm of the closed-loop generalized plant with the designed controller.
- Closed-loop objectives are incorporated to actuator/sensor location procedure, through addition of signal weights and formation of a generalized plant.
- Signal weights are not limited to smooth filters as in the case of generalized plant with modal coordinates in [3, 24]. Gawronski [3, 24] use simple smooth filter to keep the modal diagonal form of the plant. However, in the developed technique, it is possible to use more sophisticated and less smooth filters.

Besides the improved coprime controller, a low-authority $\mathcal{H}_\infty$-controller design procedure is developed. Using the same diagonalization technique for the generalized plant, the central and filter ARE's are solved approximately. Their partial derivatives with respect to design parameters are obtained approximately as well. Since the simulation results in the given examples are promising, the low-authority $\mathcal{H}_\infty$-controller design which takes less computation time for optimization might be a preferable option.

As another alternative to coprime and $\mathcal{H}_\infty$-controllers, MNRD is used, which makes it possible to compute the closed-loop norms approximately without designing a controller. MNRD may give results closer to those obtained with improved coprime and $\mathcal{H}_\infty$-controllers. Hence, it is useful for showing the closed-loop behavior of a generalized plant. Although disturbance attenuation factors achieved by MNRD are in general smaller than those achieved by $\mathcal{H}_\infty$-controllers, for moderate action and low-

authority control cases, where the control inputs are for vibration suppression and not for reference tracking, the MNRD values ($\mathcal{H}_2$-norms of closed-loop system with MNRD-controllers) are quite close to the values obtained by the coprime and $\mathcal{H}_\infty$-controllers.

FEM has been used to model the flexible structures with collocated point and piezoelectric actuator and sensor pairs. To obtain the gradient of the objective function with respect to design parameters, the partial derivatives of the FE matrices are defined, sensitivity analysis and eigenvalue-eigenvector perturbation theory are used, and the partial derivatives of the closed-loop state space matrices are derived.

In the case of piezoelectric actuator and sensor pairs, method of feasible directions has been utilized and some conditional constraints are defined so that any overlap of PZT patches or badly scaled finite elements are prevented. The constrained optimization technique makes it possible to find the best locations of the piezoelectric actuator and sensor pairs in plates. This technique is useful for applying multiple piezoelectric patches on beams and plates.

The following points are worth to investigating as future work:

- Approximate low-authority $\mathcal{H}_\infty$-controllers for nominal plant are designed. The next step could be to develop the controller design strategy for robust control. An optimal location selection with robust controllers might invoke interests more.
- Approximate CARE and FARE solutions are introduced for the generalized plant with signal weights. Different types of uncertainties may be incorporated into the generalized plant and approximate ARE solutions for that plant can be calculated.
- For the minimization, only first derivative information is used throughout the thesis. If second derivatives of closed-loop state space matrices are calculated, it is possible to apply optimization techniques with second order derivatives.
- In the thesis, a singular value based strategy in frequency domain is suggested to take the partial derivative of closed-loop $\mathcal{H}_\infty$-norm. However, methodologies that are frequency independent can be developed to calculate the sensitivities of the closed-loop $\mathcal{H}_\infty$-norm, since calculation of values for each frequency may increase

computation time.

- In this thesis, the ARE solutions in diagonal form are successfully used for selecting the best actuator and sensor locations. To further exercise the suggested controller designs with approximate diagonal ARE solutions, improved coprime controllers and low-authority $\mathcal{H}_\infty$-controllers can be designed for the Feedback Twin Rotor MIMO system (TRMS) [73].
- Although only the optimal actuator and sensor locations are considered in the thesis, structures have different parameters and dimensions which might need to be optimized. The developed technique can be applied for selection of different parameters such as thicknesses, diameters, weights, material constants, etc. as well.
- Since the introduced best I/O location selection technique does not guarantee that the results are globally optimum, it may need to be repeated with different initial points to validate that the obtained results are the global minima. However, it can be utilized as a sub-search algorithm of a global optimization technique or developed into a global optimization technique.
- During iterations of the optimal location selection the FE part of the code discretizes the flexible structure automatically. Although as elements, usual beam and plate elements are selected, different types of finite elements and different meshing policies can also be used and structures of more complicated geometries can be handled.
- Using implicit function theorem, Giesy and Lim [74, 75] has taken the partial derivatives of the closed-loop $\mathcal{H}_\infty$-norm using singular value perturbations based on the works of [76] and [77]. Pandey et al. [78] has developed a technique for computing the optimal $\mathcal{H}_\infty$-norm faster, which uses the gradient of the $\mathcal{H}_\infty$-norm. Burchett and Costello [79] calculate the first and second partial derivatives of the closed-loop $\mathcal{H}_\infty$-norm with respect to feedback gains and design iteratively a PID controller for the Feedback TRMS. The eigenvalue-eigenvector perturbation theory can be used to calculate partial derivatives of $\mathcal{H}_\infty$-norms with respect to actuator and sensor locations if appropriate assumptions and limitations are given correctly.

REFERENCES

1. Hiramoto, K., H. Doki and G. Obinata, "Optimal Sensor Actuator Placement For Active Vibration Control Using Explicit Solution Of Algebraic Riccati Equation", *Journal of Sound Vibration*, Vol. 229(5), pp. 1057–1075, 2000.

2. Arabyan, A., S. Chemishkian and E. Meroyan, "Limits of Vibration Suppression in Flexible Structures", *Dynamics and Control*, Vol. 9, pp. 223–246, 1999.

3. Gawronski, W. K., *Dynamics and Control of Structures: A Model Approach*, Springer-Verlag, 1998.

4. Irschik, H., "A review on static and dynamic shape control of structures by piezoelectric actuation", *Engineering Structures*, Vol. 24, pp. 5–11, 2002.

5. Ikeda, T., *Fundamentals of Piezoelectricity*, Oxford University Press, Great Britain, 1996.

6. Blitz, J., *Fundamentals of Ultrasonics*, Butterworths, Inc., London, 1967.

7. Frederick, J., *Ultrasonic Engineering*, John Wiley, New York, 1965.

8. Mason, W. P., *Physical Acoustics: Principles and Methods*, Academic Press, New York and London, 1964.

9. Kinsler, L. E. and A. R. Frey, *Fundamentals of Acoustics*, John Wiley and Sons, Inc., New York, 1950.

10. C.Z. Rosen, B. H. and R. Newnham, *Piezoelectricity*, American Institute of Physics, New York, 1992.

11. Güney, M., *Dynamic Modelling and Performance Analyis of Ultrasonic Welding Machines*, M.S. Thesis, Boğaziçi University, 2002.

12. Eric B. Becker, J. T. O., Graham F. Carey, *Finite elements an introductions*, Vol. 1, Texas Institute for Computational Mechanics, The University of Texas Austin, 1981.

13. Chandrupatla, T. R. and A. D. Belegundu, *Introduction to finite elements in engineering*, Prentice Hall, 2 edn., 1997.

14. Petyt, M., *Introduction to finite element vibration analysis*, Cambridge University Press, Avon, Great Britain, 1990.

15. O. C. Zienkiewicz, R. L. T., *The finite element method*, Vol. 1, Butterworth-Heinemann, Oxford, Boston, 5 edn., 2000.

16. O. C. Zienkiewicz, R. L. T., *The finite element method*, Vol. 2, Butterworth-Heinemann, Oxford, Boston, 5 edn., 2000.

17. Irving H. Shames, C. L. D., *Energy and finite element methods in structural mechanics*, Taylor and Francis, New York, 1991.

18. Özgül, O., *Active Vibration Control of Beams and Plates Using Piezoelectric Transducers*, M.S. Thesis, Boğaziçi University, 2003.

19. C. Chang-qing, W. X.-m. and S. Ya-peng, "Finite element approach of vibration control using self-sensing piezoelectric actuators", *Computers and Structures*, Vol. 60, pp. 505–512, 1996.

20. Skogestad, S. and I. Postlethwaite, *Multivariable Feedback Control*, John Wiley & Sons, 1996.

21. Zhou, K., J. C. Doyle and K. Glover, *Robust and Optimal Control*, Prentice Hall, 1996.

22. Zhou, K. and J. C. Doyle, *Essentials of Robust Control*, Prentice Hall, 1998.

23. Green, M. and D. J. Limebeer, *Linear Robust Control*, Prentice Hall, 1996.

24. Gawronki, W. K., *Advanced Structural Dynamics and Active Control of Structures*, Springer, New Year, 2004.

25. van de Wal, M. and B. de Jager, "A review of methods for input/output selection", *Automatica*, Vol. 37, pp. 487–510, 2001.

26. Geroges, D., "The use of Observability and Controllability Gramians or Functions for Optimal Sensor and Aactuator Location in Finite-Dimensional Systems", *Proceedings of the 34th IEEE Conference on Decision and Control*, Vol. 4, pp. 3319–3324, December 1995.

27. Hać, A. and L. Liu, "Sensor and Actuator Location in Motion Control of Flexible Structures", *Journal of Sound and Vibration*, Vol. 167(2), pp. 239–261, 1993.

28. Meirovitch, L., *Analytical Methods in Vibrations*, New York: Macmillan, 1967.

29. Gawronski, W. and K. Lim, "Balanced Actuator and Sensor Placement for Flexible Structures", *International Journal of Control*, Vol. 65(1), pp. 131–145, 1999.

30. Maciejowski, J., *Multivariable Feedback Design*, Addison-Wesley, 1989.

31. Morari, M. and E. Zafiriou, *Robust Process Control*, Prentice Hall, United State of America, 1989.

32. Freudenberg, J. S. and D. P. Looze, "Right half plane poles and zeros and design tradeoffs in feedback systems", *IEEE Transactions on Automatic Control*, Vol. 30(6), pp. 555–565, 1985.

33. Sidi, M., "Gain-bandwidth limitations of feedback systems with non-minimum-phase plants", *International Journal of Control*, Vol. 67(5), pp. 731–743, 1997.

34. Havre, K. and S. Skogestad, "Effect of RHP zeros and poles on performance in

multivariable systems", *Proceedings of UKACC International Conference on CONTROL*, Vol. 2, pp. 930–935, 1996.

35. Holt, B. R. and M. Morari, "Design of resilient processing plants-VI: The effect of right-half-plane zeros on dynamic resilience", *Chemical Engineering Science*, Vol. 40(1), pp. 59–74, 1985.

36. Morari, M., E. Zafiriou and B. R. Holt, "Design of resilient processing plants-VI: The effect of right-half-plane zeros on dynamic resilience", *Chemical Engineering Science*, Vol. 40(1), pp. 59–74, 1985.

37. Hovd, M. and S. Skogestad, "Procedure for regulatory control structure selection with application to the FCC process", *A.I.Ch.E. Journal*, Vol. 39(12), pp. 1938–1953, 1993.

38. Maghami, P. G. and S. M. Joshi, "Sensor/Actuator Placement for Flexible Space Structure", *IEEE Transactions on Areospace and Electronic Systems*, Vol. 29(2), pp. 345–352, 1993.

39. Morari, M., "Design of resilient processing plants*III: A general framework for the assessment of dynamic resilience", *Chemical Engineering Science*, Vol. 38(11), pp. 1881–1891, 1983.

40. Skogestad, S. and M. Morari, "Effect of disturbance directions on closed-loop performance", *Industrial and Engineering Chemistry Research*, Vol. 26(10), pp. 2029–2035, 1987.

41. Cao, Y. and D. Rossiter, "Input screening method for disturbance rejection", *UKACC International Conference on CONTROL*, Vol. 1, pp. 497–502, 1996.

42. Bristol, E. H., "On a new measure of interaction for multivariable process control", *IEEE Transactions on Automatic Control*, Vol. 11, pp. 133–134, 1966.

43. Hovd, M. and S. Skogestad, "Simple frequency-dependent tools for control system

analysis, structure selection and design", *Automatica*, Vol. 28(5), pp. 989–996, 1992.

44. Skogestad, S. and M. Morari, "Implications of large RGA elements on control performance", *Industrial and Engineering Chemistry*, Vol. 26(11), pp. 2323–2330, 1987.

45. Al-Sulaiman and S. Zaman, "Actuator placement in lumped parameter systems subjected to disturbance", *Computers and Structures*, Vol. 52(1), pp. 41–47, 1994.

46. Cao, Y., D. Biss and J. Perkins, "Assessment of input-output controllability in the presence of control constraints", *Computers and Chemical Engineering*, Vol. 20(4), pp. 337–346, 1996.

47. Morari, M. and G. Stephanopulos, "Studies in the synthesis of control structures for chemical processes*Part III: Optimal selection of secondary measurements within the framework of state estimation in the presence of persistent unknown disturbances", *A.I.Ch.E. Journal*, Vol. 26(2), pp. 247–260, 1980.

48. Norris, G. A. and R. Skelton, "Selection of dynamic sensors and actuators in the control of linear systems", *Journal of Dynamic Systems, Measurement, and Control*, Vol. 111(3), pp. 389–397, 1989.

49. Mellefont, D. J. and R. W. H. Sargent, "Optimal measurement policies for control purposes", *International Journal of Control*, Vol. 26(4), pp. 595–602, 1977.

50. Boyd, S. and L. Vandenberghe, *Convex Optimization*, Campbidge University Press, 1 edn., 2004.

51. Rao, S. S., *Engineering Optimization*, A Wiley-Interscience Publication, third edn., 1996.

52. Haftka, R. T. and Z. Gürdal, *Elements of Structural Optimization*, Kluver Academic Publishers, Netherlends, 1992.

53. Kirsch, U., *Optimum Structural Design*, A McGraw-Hill, Inc., 1981.

54. Pike, R. W., *Optimization For Engineering System*, Van Nostrand Reinhold Company, Inc., 1986.

55. Arabyan, A. and S. Chemiskian, "Lower Limits of Deformation Suppression in Flexible Structures", *Proceedings of the 30th IEEE Symposium on System Theory*, pp. 271–274, 1998.

56. McFarlane, D. and K. Glover, *Robust Controller Design Using Normalized Coprime Factor Pl ant Descriptions*, Vol. 138 of *Lecture Notes in Control and Information Sciences*, Springer Verlag, Berlin, 1990.

57. Kailath, T., *Linear Systems*, Prentice Hall,Englewood Cliffs,NJ, 1980.

58. Arabyan, A. and S. Chemiskian, "$\mathcal{H}_\infty$-Optimal Mapping of Actuators and Sensors in Flexible Structures", *Proceedings of the 37th IEEE Conference on Decisioin and Control*, pp. 821–826, 1998.

59. Chemiskian, S. and A. Arabyan, "$\mathcal{H}_\infty$-Optimal Mapping of Actuators and Sensors in Flexible Structures", *Proceedings of the American Control Conference San Diego, California*, pp. 1812–1816, 1999.

60. Güney, M., O. Özgül and E. Eşkinat, "An Integrated Structural Modelling, Optimal Placement and Control Approach Using Piezoelectric Transducers", *Proceedings of the 9th International Mechatronics Conference*, September 2004.

61. Gander, W. and W. Gautschi, "Adaptive Quadrature - Revisited", *BIT - Linkoping University*, Vol. 40, pp. 84–101, 200.

62. Shampine, L. F., "Vectorized adaptive quadrature in MATLAB", *J. Comput. Appl. Math.*, Vol. 211, No. 2, 2008.

63. Güney, M. and E. Eşkinat, "Optimal Actuator and Sensor Placement in Flexible

Structures using Closed-loop Criteria", *Journal of Sound and Vibration*, Vol. 312, No. 1-2, pp. 210–233, April 2008.

64. Doyle, J. C., K. Glover, P. P. Khargonekar and B. A. Francis, "State-Space Solution to Standard $\mathcal{H}_2$ and $\mathcal{H}_\infty$ Control Problems", *IEEE Transactions on Automatic Control*, Vol. 34, No. 8, pp. 831–847, August 1988.

65. Bruant, I., G. Coffignal and F. Lene, "A Methodology for Determination of Piezoelectric Actuator and Sensor Location on a Beam Structure", *Journal of Sound Vibration*, Vol. 243(5), pp. 861–882, 2001.

66. Nelson, R. B., "Simplified Calculation of Eigenvector Derivatives", *AIAA Journal*, Vol. 14, No. 9, pp. 1201–1205, September 1976.

67. Friswell, M. I., "Derivatives of Complex Eigenvectors Using Nelson's Method", *AIAA Journal*, Vol. 38, No. 12, pp. 2355–2357, 2000.

68. Mills-Curran, W. C., "Calculation of Eigenvector Derivatives for Structures with Repeated Eigenvalues", *AIAA Journal*, Vol. 26, No. 7, pp. 867–871, 1988.

69. Friswell, M. I., "The Derivatives of Repeated Eigenvalues and Their Asscociated Eigenvectors", *Transactions on ASME*, Vol. 118, pp. 390–397, 1996.

70. Prells, U. and M. I. Friswell, "Partial Derivatives of Repeated Eigenvalues and Their Eigenvectors", *AIAA Journal*, Vol. 35, No. 8, pp. 1363–1368, 1997.

71. Prells, U. and M. I. Friswell, "Calculating Derivatives of Repeated and Nonrepeated Eigenvectors Without Explicit Use of Eigenvectors", *AIAA Journal*, Vol. 38, No. 8, pp. 1426–1436, 2000.

72. Friswell, M. I., "Calculation of Second and Higher Order Eigenvector Derivatives", *Journal of Guidance, Control and Dynamics*, Vol. 18, No. 4, pp. 919–921, 1994.

73. Feedback Incorporated, Address: Park Road, Crowborough, East Sussex, TN6

2QR, UK, *Twin Rotor MIMO System*.

74. Giesy, D. P. and K. B. Lim, "An analytic formula for $\mathcal{H}_\infty$ norm sensitivity with applications to control system design", Vol. 2, pp. 874–884, AIAA Guidance, Navigation and Control Conference, American Institute of Aeronautics and Astronautics, Hilton Head Island, Aug 10-12 1992.

75. Giesy, D. P. and K. B. Lim, "$\mathcal{H}_\infty$ norm sensitivity formula with control system design applications", *Journal of Guidance, Control, and Dynamics*, Vol. 16, No. 6, pp. 1138–1145, 1993.

76. Ji-Guang, S., "A Note On Simple Non-zero Singular Values", *Journal of Computational Mathematics*, Vol. 6, No. 3, pp. 259–266, 1988.

77. Freudenberg, J. S., D. P. Looze and J. B. Cruz, "Robustness analysis using singular value sensitivities", *Internatioanal Journal of Control*, Vol. 35, No. 1, pp. 95–116, 1982.

78. Pandey, P., C. Kenney, A. J. Laub and A. Packerd, "Algorithms for computing the optimal $\mathcal{H}_\infty$ norm", pp. 2584–2588, Proceedings of the 29th Conference on Decisicion Control Conference, Honolulu, Hawaii, December 1990.

79. Burchett, B. T. and M. F. Costello, "An Algorithm for $\mathcal{H}_\infty$ Optimization of a Linear Time Invariant System Using Singular Value Decomposition", pp. 2584–2588, Proceedings of the American Control Conference, Philadelphia, Pennsylvania, June 1998.